Quantum Control of Optomechanical Systems

Von der Fakultät für Mathematik und Physik
der Gottfried Wilhelm Leibniz Universität Hannover
zur Erlangung des Grades

Doktor der Naturwissenschaften
Dr. rer. nat.

genehmigte Dissertation
von

Mag. rer. nat. Sebastian Hofer

geboren am 22. Januar 1984 in Rum in Tirol, Österreich

2015

DISSERTATION

im Rahmen einer Cotutelle

Titel der Dissertation

"Quantum Control of Optomechanical Systems"

Verfasser

Mag. rer. nat. Sebastian Hofer

angestrebter akademischer Grad

Doktor der Naturwissenschaften (Dr. rer. nat.)

Wien, 2015

To my parents.

❧

ACKNOWLEDGEMENTS

Composing the acknowledgements section of a doctoral thesis gives the author time to review the previous years. It is the time to sit back and think about who to be grateful to, and what to be grateful for. For me it is an emotional task; and it is also a task not to be taken lightly.

My greatest and truly heartfelt thanks belong to my supervisors Klemens Hammerer and Markus Aspelmeyer, who guided me through our mutual scientific endeavours over the last five-odd years.

Klemens and I have known each other for nearly a decade now, and thus for the best part of my life in science. Back when I was a undergraduate student at the University of Innsbruck he taught me about basic quantum optics, and later about optomechanics during my diploma thesis. I always enjoyed learning *from* him in the many insightful discussions we had, but also learning *with* him, as we ventured into unknown territory together.

Markus gave me the opportunity to join a band of experimental physicists as a theorist. I could also say: he posed me a challenge; as some people reading these lines will know, those two groups of people don't always think alike. However, Markus was always there to support me, and always kept an open mind, considering my opinion or objections. His ever-positive attitude and his seemingly perpetual energy to tackle new scientific problems have been a source of motivation over the years and continue to amaze me to this day.

Both Klemens and Markus are great mentors to me in all matters scientific, and I always felt that I could fully rely on them. I wouldn't be where I am today without either of them, and I cannot thank them enough.

As the life of a PhD student is very university-centric, I'm thankful to have fellow students and coworkers, who always provided a friendly environment that is fun to work in. I thank Jason and Witti, my closest collaborators within the group, for putting up with my sometimes-impatient self, and Claus, David, Florian, Jonas, Josh, Nikolai, Philipp, Rainer, Ralf, Sungkun, and Uros just for being there to have fun with. People whom I have outlived in the group in Vienna but I'm always looking forward to meeting in various locations around the world are Garrett, Michael and Simon. Many thanks also go out to all CoQuS members, especially to Magdalena, who was the best flatmate one could wish for, Igor, Adrien, Nadine, Philipp, Stefan and Peter. I always enjoyed spending retreats, conferences and conference dinners, and sharing hotel rooms and tram tickets with

you guys. All this would not have been possible without the care and love of Markus Arndt and Christiane, who are constantly looking out for the wellbeing of us students.

As a part-time PhD student in Hannover, I had the pleasure to make friends there too. Thanks to Henning, Stefan and Melanie, Heather, Oli and Ramon, who made me feel welcome in a new city, and for sometimes providing me with a place to stay, occasionally even for extended periods of time. I'm also always happy to look back to many lively discussions with other members of my group in Hannover, which—more often than not—ended in someone (often me) storming back to the office annoyed, possibly slamming a door on the way; thank you André, Denis and Niels (but especially André), it was always fun.

Most importantly, I want to thank all the people outside of academia who accompanied and supported me for all my life. On the one hand my family: my parents Brigitta and Georg; my uncle, aunt and cousin Klaus, Irmgard and Felix; and my grandmother Bertha, who was always there to take care of Felix and me, cooked for and played with us when our parents couldn't. On the other hand, I'm fortunate to have many dear friends in Innsbruck and in Vienna, who provide me strength, love and shelter, and who I know I can always turn to, no matter how long I've been away. You will always have a very special place in my life.

ABSTRACT

This thesis explores the prospects of entanglement-enhanced quantum control of optomechanical systems. We first discuss several pulsed schemes in which the radiation-pressure interaction is used to generate Einstein–Podolsky–Rosen entanglement between the mechanical mode of a cavity-optomechanical system and a travelling-wave light pulse. The entanglement created in this way can be used as a resource for mechanical state preparation. On the basis of this protocol, we introduce an optomechanical teleportation scheme to transfer an arbitrary light state onto the mechanical system. Furthermore, we describe how one can create a mechanical non-classical state (i. e., a state with a negative Wigner function) by single-photon detection, and, in a similar protocol, how optomechanical systems can be used to demonstrate the violation of a Bell inequality.

The second part of the thesis is dedicated to time-continuous quantum control protocols. Making use of optimal-control techniques, we analyse measurement-based feedback cooling of a mechanical oscillator and demonstrate that ground-state cooling is achievable in the sideband-resolved, blue-detuned regime. We then extend this homodyne-detection based setup and introduce the notion of a time-continuous Bell measurement—a generalisation of the standard continuous variable Bell measurement to a continuous measurement setting. Combining this concept with continuous feedback we analyse the generation of a squeezed mechanical steady state via time-continuous teleportation, and the creation of bipartite mechanical entanglement by entanglement swapping. Finally we discuss an experiment demonstrating the evaluation of the conditional optomechanical quantum state by Kalman filtering, constituting a important step towards time-continuous quantum control of optomechanical systems and the possible realisation of the protocols presented in this thesis.

quantum optomechanics, quantum control, quantum entanglement

ZUSAMMENFASSUNG

Diese Arbeit befasst sich mit der Verwendung von Quantenverschränkung um die Kontrolle über optomechanische Systeme zu verbessern. Wir beschäftigen uns als erstes mit gepulsten Protokollen, in denen die Strahlungsdruckwechselwirkung ausgenutzt wird um Einstein–Podolsky–Rosen Verschränkung zwischen einem mechanischen Oszillator und einem Lichtpuls zu erzeugen. Diese kann dazu genutzt werden um auf Basis eines Teleportationsprotokolles einen beliebigen Quantenzustand eines Lichtpulses auf den mechanischen Oszillator zu übertragen. Wir untersuchen weiters wie man mit Hilfe der Detektion einzelner Photonen einen nichtklassischen mechanischen Zustand, d.h. einen Quantenzustand mit negativer Wignerfunktion, zu präparieren. Auf ähnliche Weise ist es außerdem möglich ein optomechanisches System zur Verletzung einer Bellschen Ungleichung zu benutzen.

Der zweite Teil des Manuskriptes ist der zeitkontinuierlichen Kontrolle optomechanischer Quantensysteme gewidmet. Unter Verwendung von optimalen Steuerungstechniken kann ein mechanisches System durch kontinuierliche Messung und Rückkoppelung in seinen Bewegungsgrundzustand gebracht werden—dies ist auch möglich im seitenbandaufgelösten, blauverstimmten Regime. Anschließend diskutieren wir eine Erweiterung dieses Protokolls auf eine sogenannte zeitkontinuierliche Bellmessung, die eine Generalisierung der standard Bellmessung kontinuierlicher Variablen darstellt. Dieses Konzept ermöglicht es, einen mechanischen Oszillator in einem gequetschten stationären Zustand zu präparieren, oder stationäre Verschränkung zweier mechanische Resonatoren zu erzeugen. Abschließend diskutieren wir ein Experiment, das die Rekonstruktion des sogenannten konditionalen Quantenzustand eines optomechanischen Systems demonstriert. Dieses Experiment stellt einen wichtigen ersten Schritt in Richtung der möglichen Durchführung der in dieser Arbeit diskutierten Protokolle dar.

Quantenoptomechanik, Quantenkontrolle, Quantenverschränkung

NOTATION

GENERAL REMARKS

In this thesis vectors are printed in a bold, slanted font, e.g., $\boldsymbol{M}$, while matrices, such as $\mathbf{M}$, are denoted by bold, upright letters. The corresponding transposed quantities are written as $\boldsymbol{M}^{\mathrm{T}}$ and $\mathbf{M}^{\mathrm{T}}$ respectively. The complex conjugate of a complex number z is denoted by z^{*}, the Hermitian conjugate of an operator c is $c^{\dagger}$. For tuples of operators we use the convention $(c_1, c_2, \dots)^{\dagger} = (c_1^{\dagger}, c_2^{\dagger}, \dots)$ which is different from $(c_1^{\dagger}, c_2^{\dagger}, \dots)^{\mathrm{T}}$. The same symbol is used to denote the Hermitian conjugate of complex matrices (or vectors), i.e., $\mathbf{M}^{\dagger} = (\mathbf{M}^{*})^{\mathrm{T}}$ for $\mathbf{M} \in \mathbb{C}^{n \times m}$. Quantum mechanical mean values with respect to the initial state of a system are written as $\langle c \rangle$. A time dependence is indicated in a Heisenberg-type notation, such as $\langle c(t) \rangle$. The symbol $\mathbb{1}$ is used to denote both the identity operator in a Hilbert space or the identity matrix. In the former case a subscript identifies the (sub)system the operator acts on, in the latter case a numerical subscript denotes the matrix dimension.

Also note that that we use the convention $\hbar = 1$, except in chapter 1, where the explicit usage of $\hbar$ is convenient for discussing the physics underlying our optomechanical models.

OPTOMECHANICAL PARAMETERS

ω_c cavity resonance frequency, p 9

C optomechanical cooperativity, p 15

Δ_c effective detuning, p 20

g_0 single-photon coupling strength, p 12

g linear coupling strength, p 20

γ_m mechanical damping, p 8

κ cavity decay rate (FWHM), p 10

ω_0 laser frequency, p 10

$\bar{n}$ mean bath occupation number, p 8

n_0 initial mechanical occupation number, p 41

ω_m mechanical resonance frequency, p 8

Q_m Q-factor, p 8

SYMBOLS

n_B Bose–Einstein distribution, p 8

f Brownian stochastic force, p 17

Σ covariance matrix of X, p 25

D displacement operator, p 20

$\mathcal{F}$ Fourier transform, p 70

$\hbar$ reduced Planck constant, p 8

θ Heaviside step function, p 35

H_{eff} effective Hamiltonian, p 124

$\mathbb{1}$ identity operator/matrix, p 20

$\mathcal{J}$ Jacobian matrix, p 18

j_t quantum flow, p 124

k_B Boltzmann constant, p 8

$\mathcal{D}$ Linblad operator, p 24

$\mathcal{L}$ Liouvillian, p 24

$E_{\mathcal{N}}$ logarithmic negativity, p 28

$\mathcal{H}$ measurement operator, p 25

$\mathcal{N}$ normal distribution

π_t quantum filter, p 134

X vector of quadrature operators, p 25

$\mathcal{T}_{\pm}$ time-ordering operator, p 73

BS	beam splitter, p 14
CDF	cumulative distribution function, p 111
CHSH	Clauser–Horne–Shimony–Holt, p 64
CV	continuous variables, p 42
EPR	Einstein–Podolsky–Rosen, p 37
FME	feedback master equation, p 92
FWHM	full width at half maximum, p 8
JPA	Josephson parametric amplifier, p 52
LC	inductor–capacitor, p 2
LO	local oscillator, p 24
LQG	linear–quadratic–Gaussian, p 82
MEQ	master equation, p 15
PDF	probability density function, p 112
POVM	positive-operator valued measure, p 64
QLE	quantum Langevin equation, p 15
QND	quantum non-demolition, p 14
QSDE	quantum stochastic differential equation, p 122
RWA	rotating-wave approximation, p 15
SME	stochastic master equation, p 25
SSE	stochastic Schrödinger equation, p 89
TMS	two-mode squeezing, p 14

CONTENTS

INTRODUCTION

Conducting any kind of quantum experiment requires, in a general sense, excellent control over the physical system and the experimental setup. On the one hand this means that the system under study must be, to a large degree, decoupled from the environment and all classical noise sources—or from all sources of decoherence in general—, in order for genuine quantum effects to emerge. On the other hand one must be able to manipulate the system's dynamics and quantum state very precisely. In the quantum branch of atomic, molecular and optical physics excellent control has been attained over many systems, in particular over atoms [Chu02] and ions [Win13]. The achievements in these fields led, for example, to the first creation of a Bose–Einstein condensate [AK02] and the generation of Schrödinger cat states of microwave fields in cavity quantum electrodynamics [HR06].

In order to make optimal use of this high level of control a multitude of techniques have been developed. *Quantum control theory* combines concepts from classical control theory with concepts from quantum physics, exploiting inherently non-classical features such as coherent superpositions and entanglement. It is nowadays an active research field that plays a crucial role in modern quantum experiments across different fields [DP10; Gou12]. Prominent examples of successful application of quantum control protocols are spin squeezing [KMB00] and steady-state entanglement generation in atomic ensembles [Kra+11], or come from the field of quantum metrology, such as nuclear magnetic resonance [Ger+03] and atomic clocks [BJW01]. Strongly connected (and partly overlapping) fields are those of *quantum filtering* [BVJ07; BG08] and *quantum estimation theory* [Hel69; Par09], which concern themselves with the estimation of the quantum state itself [Bel80; GJM13], or the estimation of classical parameters (or classical signals) from the measurements of quantum systems [Tsa09; TWC11]. Quantum estimation techniques have also been successfully applied in optomechanics [Szo+12; Ang+13; Iwa+13]. Another successful experiment in the same direction—optimal estimation of the optomechanical quantum state—comprises part this thesis (see section 3.5).

Although radiation-pressure effects on mechanical oscillators have already been analysed theoretically in the late 1960s [BM67], and experimentally demonstrated using microwaves [BMT70] and optical fields [Dor+83] several years later, in its modern form cavity optomechanics is a relatively young field within the quantum sciences. First theoretical studies of quantum effects in optomechanical systems concerned squeezing of light [Fab+94; MMT97], and the

generation of optomechanical entanglement and non-classical states [BJK97; MMT97]. Feedback cooling of vibrational modes via radiation pressure was first analysed theoretically in [MVT98] and later implemented experimentally [CHP99] to cool a Fabry–Pérot cavity's macroscopic end mirror. Today, highly advanced microfabrication techniques allow for the fabrication of high-quality (both optical and mechanical) cavity optomechanical systems, which has then led to the demonstration of passive radiation-pressure cooling [Gig+06; Arc+06; Sch+06]. Since then, cavity optomechanical systems have been implemented in various forms, such as micromembranes in cavities [Tho+08], microtoroids [Kip+05], microdiscs featuring optical whispering gallery modes [Jia+09], and photonic crystals [Eic+09].

In parallel a different—and very successful—approach to observe the same physics has been developed in the form of so-called *electromechanical* systems, which employ inductor–capacitor (LC) resonators in lieu of optical cavities, and make use of capacitive coupling between mechanical resonators and microwave fields [RL11]. Even more approaches to demonstrate optomechanical interaction include levitating nano-objects in cavities [Kie+13; Ase+13; Mil+15], and coupling the collective motion of a cold atomic cloud to the electromagnetic field of a cavity [Mur+08; Bre+08; Sch+11].

Despite these advancements, control of optomechanical systems has not yet been developed to the high degree attained in more mature branches of quantum physics; however, during the last years several experiments in the quantum regime have been conducted using these systems. These include quantum state transfer [OCo+10; Pal+13], ground-state cooling of the mechanical mode [Teu+11; Cha+11], ponderomotive squeezing [Bro+12; Saf+13; Pur+13], and observation of back-action noise in position sensing [Mur+08; PPR13]. Many of these experiments rely on the fact that the employed systems can be operated in the strong-cooperativity regime, in which the coherent (linearized) optomechanical coupling rate exceeds the effective decoherence rates of the optical and the mechanical mode. These developments lay the foundation for quantum limited (feedback) control of optomechanical systems.

Applications of quantum control theory in optomechanics range from feedback cooling of the mechanical motion [CHP99], mechanical squeezing [CMJ08; Woo+08], and two-mode squeezing [WC13] to back-action elimination [Wis95; CHP03] with possible applications in gravitational-wave detection. Importantly for quantum information processing and communication, it can also be used to robustly generate entanglement between remote quantum systems, as has been demonstrated recently for spin qubits [Dol+14]. At the same time entanglement itself can be an essential component to facilitate control of quantum systems, e. g., as a resource for teleportation [Ben+93], when employed as a means for remote state preparation. In optomechanics,

pulsed entanglement between a mechanical oscillator and the electro-magnetic field has recently been demonstrated in an electromechanical setup [Pal+13], using the protocol developed in this thesis (see section 2.1); state preparation (and verification) of an arbitrary mechanical quantum state (e. g., a Fock state) has yet to be accomplished (see, however, [OC0+10], which suffered from a too low mechanical quality factor to perform quantum state tomography). Quantum control protocols are often operated in a time-continuous fashion and rely on continuous measurements that are capable of tracking the quantum state of the controlled system. The resulting measurement record—and the so-called conditional quantum state inferred from it—is then used as a basis for the applied feedback [WM09]. Thus, the control protocol's success critically depends on the precision of the employed measurements. Recently, monitoring a mechanical oscillator with a measurement strength matching its thermal decoherence rate (equivalent to a cooperativity above 1) and measurement-based feedback cooling to an occupation number of several phonons (limited by residual absorption) has been demonstrated in [Wil+14].

Outline of the Thesis

In this thesis we discuss different approaches to control optomechanical systems on the quantum level. One central topic is the generation of optomechanical entanglement, but also its application as a resource to implement quantum control of these systems. The presented protocols can therefore be described as *entanglement-enhanced quantum control*. The thesis is divided into three chapters.

- Chapter 1 provides an introduction to the physics of cavity-optomechanical systems, as well as to their description we use throughout this work. We review the quantum theoretic models of the mechanical and the optical resonator, and their interaction. We then introduce the total system's description as an open quantum system in terms of (stochastic) master equations and quantum Langevin equations, as well as a phase-space description. Finally we discuss characteristic features of the optomechanical steady state.

- Chapter 2 is devoted to pulsed optomechanical quantum control and quantum information protocols. In section 2.1 we discuss a protocol to create and verify continuous-variable entanglement between a mechanical oscillator and a light pulse, including an extension to a teleportation scheme. First the protocol is analysed in a perturbative approach to build intuition for the process; in a second step the full fledged optomechanical model is solved, and the physical parameters are optimized. This section is based on

  'Quantum entanglement and teleportation in pulsed cavity op-tomechanics'

S. G. Hofer, W. Wieczorek, M. Aspelmeyer & K. Hammerer
Physical Review A 84, 052327 (2011)

for which the author of this thesis did the majority of the analytical and all numerical calculations, and prepared the larger share of the published manuscript.

In section 2.2 we analyse the creation of non-classical mechanical quantum states building on the protocol in section 2.1. We discuss how a mechanical state with a negative Wigner function close to a phononic Fock state can be prepared by coupling to a qubit and tomographically reconstructed from measurements of light. This work has not previously been published. The protocol was devised together with Konrad Lehnert, Tauno Palomaki, and Klemens Hammerer during a visit at the University of Colorado, Boulder. The author of this thesis did a substantial part of the analytical and all numerical calculations.

Section 2.3 discusses the violation of a Bell inequality using optomechanical entanglement. The author worked out the details of the optomechanical implementation and did all numerical calculations. This work has been published as:

'Violation of Bell's inequality in Electromechanics'
S. G. Hofer, K. W. Lehnert & K. Hammerer
arXiv:1506.08097 [quant-ph] (2015)

• Chapter 3 discusses time-continuous control protocols, analysing in detail measurement-based feedback schemes to control general and optomechanical systems. First, we analyse homodyne-detection based feedback cooling in section 3.1. We then introduce the notion of a time-continuous Bell measurement, and discuss its application for time-continuous teleportation and entanglement swapping protocols [both for generic (section 3.2) and optomechanical systems (sections 3.3 and 3.4)]. The presented protocols are based on work published in two articles. For

'Time-Continuous Bell Measurements'
S. G. Hofer, D. V. Vasilyev, M. Aspelmeyer & K. Hammerer
Physical Review Letters 111, 170404 (2013)

the author was involved in the development of the generic formalism of time-continuous Bell measurements, worked out the optomechanical implementation (in terms of analytical and numerical calculations) and wrote substantial parts of the manuscript. For the additional material presented in

'Entanglement-enhanced time-continuous quantum control in optomechanics'
S. G. Hofer & K. Hammerer
Physical Review A 91, 033822 (2014)

he did most of the analytical and numerical work and wrote most of the manuscript.

Finally we discuss in section 3.5 first steps towards experimental time-continuous quantum control of (Gaussian) optomechanical systems. The theoretical basis is formed by the so-called Kalman filter, which extracts the conditional quantum state from a measurement trajectory. We show the implementation of a Kalman filter for an existing optomechanical experiment. This work has been published in

'Optimal state estimation for cavity optomechanical systems'
W. Wieczorek, S. G. Hofer, J. Hölscher-Obermaier, R. Riedinger, K. Hammerer & M. Aspelmeyer
Physical Review Letters 114, 223601 (2015).

The author developed the code for the data analysis and the statistical analysis of the filter consistency, was involved in modelling of the experiment and statistical analysis, and wrote parts of the manuscript.

CAVITY-OPTOMECHANICAL SYSTEMS

1.1 THE PHYSICAL SYSTEM

Although optomechanical systems exist in many different physical implementations, many of them can be described by the same simple physical model [AKM14]. To exemplify the most important features of a cavity-optomechanical system, we will use as our toy-model a Fabry–Pérot cavity with one oscillating mirror (see fig. 1). On the most basic level this simple system consist of two coupled harmonic oscillators. In this section we will introduce its main constituents— the optical and mechanical resonator—, and the physical background of the optomechanical interaction.

In this thesis we are mostly interested in optomechanical setups, working with optical photons, but the description as well applies to *electromechanical* systems, where an LC resonator driven by a microwave field takes the role of the optical cavity (see fig. 2).

1.1.1 *Mechanical Oscillators*

Due to their size and high number of degrees of freedom, experimentally employed mechanical oscillators in general posses a multitude of mechanical eigenmodes, whose spectral features are determined by the oscillator's geometry, material properties, and the coupling to its support. For general geometries, the spatial mechanical mode shape can be arbitrarily complex and can be described by a displacement field $u(r,t)$ [PHH99]. We can expand $u(r,t)$ in terms of the oscillator's eigenmodes $u_n(r)$,

$$u(r,t) = \sum_n X_n(t) u_n(r), \tag{1.1}$$

with the corresponding time-dependent amplitudes $X_n(t)$. Two examples of different eigenmodes of a doubly-clamped oscillating mirror pad are shown in fig. 3. While mechanical oscillators are in general not linear (in terms of their response to applied forces), linearity poses a good approximation for the small displacements typically attained in normal operation. We therefore model the amplitudes $X_n(t)$ to follow the damped harmonic evolution given by

$$\ddot{X}_n(t) + \gamma_n \dot{X}_n(t) + \omega_n^2 X_n(t) = \frac{F_{\text{ext}}}{m_{\text{eff}}^{(n)}}. \tag{1.2}$$

Here ω_n and γ_n are the angular resonance frequency and the damping constant of the n-th eigenmode and $m_{\text{eff}}^{(n)}$ denotes the correspond-
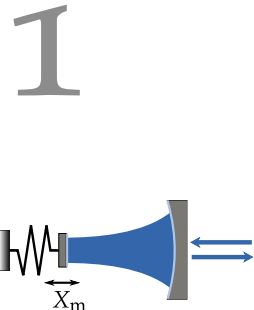

FIG 1. Schematics of an optomechanical setup. The cavity length $L(X_{\text{m}})$ is modulated by the mechanical motion.
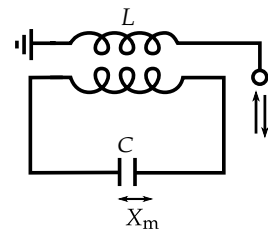

FIG 2. Schematics of an electromechanical setup. The capacitance $C(X_{\text{m}})$ of the LC resonator is modulated by the mechanical motion.

7

ing effective mass determined by the mode volume of $\boldsymbol{u}_n$. F_{ext} denotes the sum of all external forces acting on the specific mechanical mode, e. g., radiation pressure or fluctuating Langevin forces.
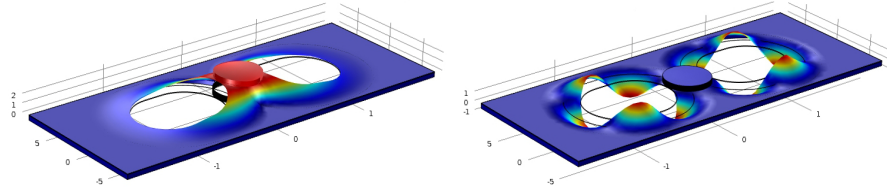

FIGURE 3. Finite-element simulation of the fundamental (right) and a higher-order mode (left) of a doubly-clamped oscillating mirror as has been used in [Grö+09] (courtesy of Witlef Wieczorek, University of Vienna).

In this thesis we will consider the single-mode case only, where we assume that we can experimentally address a single one of the mechanical eigenmodes. This mode is assumed to have no significant spectral overlap with its neighbouring modes. In the following we will denote this mode's resonance frequency by ω_{m}, and the energy damping rate as γ_{m} [the full width at half maximum (FWHM) of the corresponding spectral peak]. The corresponding amplitude of *mechanical res-* the oscillation we will call $X_{\text{m}}(t)$. In our toy-model, the Fabry–Pérot *onance frequency* cavity, the centre-of-mass oscillation is the only available eigenmode, *and damping rate* and the amplitude $X_{\text{m}}(t)$ is simply the mirror's displacement from its equilibrium position. The effective mass m_{eff} is then approximately given by the total mass of the mirror (not accounting for the finite mass of the supporting spring).

The viscous damping term in eq. (1.2) is due to the coupling of the mechanical oscillator to its support, which at the same time also acts as a thermal environment (commonly also referred to as heat bath), and represents a noise source for the mechanical oscillator. Customary this heat bath is modelled as a collection of an infinite number of harmonic oscillators in a thermal state at a temperature T, as first introduced by Caldeira and Leggett [CL83]. The mean bath occupation number follows a Bose–Einstein distribution and we thus have $n_{\text{B}}(\omega) = [\exp(\hbar\omega/k_{\text{B}}T) - 1]^{-1}$ (with the reduced Planck constant $\hbar$ and the Boltzmann constant k_{B}). Later an important figure for us will be the mean bath occupation at the mechanical frequency, i. e., $\bar{n} = n_{\text{B}}(\omega_{\text{m}})$. In the high-temperature limit we can approximate $n_{\text{B}}(\omega_{\text{m}}) \approx k_{\text{B}}T/\hbar\omega_{\text{m}}$. We will see in section 1.3.1 that the effective *Q-factor and thermal* decoherence rate (often called thermal decoherence rate) is given by *decoherence rate* $\bar{n}\gamma_{\text{m}} \approx k_{\text{B}}T/\hbar Q_{\text{m}}$, where we defined the mechanical quality factor (Q-factor) $Q_{\text{m}} = \omega_{\text{m}}/\gamma_{\text{m}}$. One thus sees that in order to have low thermal decoherence we need a high-Q mechanical oscillator and a low-temperature bath, which can be obtained by cryogenic cooling of the experimental setup. Apart from the Caldeira–Leggett approach above, another (phenomenological) model takes into account internal

friction effects [Sau90]; additionally, more realistic microscopic models and experimental studies of system–bath coupling exist [Col+11; Grö+15].

For the quantum treatment of the mechanical oscillator we introduce position and momentum operators X_m, P_m, which fulfil canonical commutation relations $[X_m, P_m] = i\hbar$. As is customary in quantum optics, we also introduce the dimensionless quadratures x_m, p_m with $[x_m, p_m] = i$. We express them in terms of creation and annihilation operators $c_m^\dagger$, c_m ($[c_m, c_m^\dagger] = 1$)

$$x_m = \frac{c_m + c_m^\dagger}{\sqrt{2}}, \qquad\qquad p_m = \frac{c_m - c_m^\dagger}{\sqrt{2}i}. \qquad (1.3)$$

We can convert them to $X_m = \sqrt{2}x_0 x_m$ and $P_m = \sqrt{2}m_{\text{eff}}\omega_m x_0 p_m$ by rescaling with the oscillator's ground state extension

ground-state extension

$$x_0 = \sqrt{\hbar/2m_{\text{eff}}\omega_m}. \qquad (1.4)$$

1.1.2 Optical Resonators

The second constituent of a cavity-optomechanical system is the optical cavity which forms a resonator for photons. A simple Fabry–Pérot cavity consists of two highly reflecting mirrors separated by a distance L. Such a cavity contains a sequence of equally-spaced modes with resonance frequencies $\nu_n = n\Delta\nu$ ($n \in \mathbb{N}$) [VW06], which are separated by a frequency $\Delta\nu$, the so-called free spectral range. *free spectral range* The free spectral range is determined by the cavity length, and—in the absence of an optical medium—is given by

$$\Delta\nu = \frac{c}{2L}. \qquad (1.5)$$

Again, in this work we will focus on the case of the mechanical oscillator interacting with a single cavity mode with a central angular frequency $\omega_c = 2\pi\nu_c$ only. In nano- and micro-optomechanical setups this situation can easily be created experimentally, as the free spectral range is many orders of magnitude larger than any frequency scale of the mechanical system. Thus different cavity modes do not interact via coupling to the mirror. There are systems, however, where coupling between different optical modes can occur (deliberately or as a perturbative effect) [FSW14].

Due to finite mirror reflectivity, absorption in the mirror substrate, or photon scattering out of the cavity mode the lifetime of photons in the cavity is limited to a finite number of round trips. This number is called the optical finesse $\mathcal{F}_{\text{cav}}$ and is connected to the cavity decay rate κ by

finesse and cavity decay rate

$$\mathcal{F}_{\text{cav}} = \frac{2\pi\Delta\nu}{\kappa} = \frac{\pi c}{\kappa L}. \qquad (1.6)$$
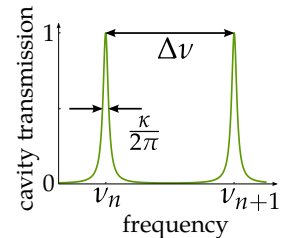
FIG 4. Cavity transmission (power) for $\mathcal{F}_{\text{cav}} = 20$

Throughout this thesis we denote by κ the energy (FWHM) decay rate, i.e., the number of photons leaving the cavity per unit time. As we need to monitor the output light of the cavity in virtually every experiment we need to discriminate between pure photon losses (absorption, scattering) and transmission into the external field which we can eventually measure. The total decay rate is thus $\kappa = \kappa_{in} + \tilde{\kappa}$, where κ_{in} is associated with the input-coupler of the cavity (i.e., the decay channel we can measure), whereas $\tilde{\kappa}$ collects all other loss mechanisms we cannot measure.

Let us assume we drive an optical cavity by a constant coherent laser field with a central frequency ω_0 and a (appropriately rescaled) complex amplitude ε. This amplitude is connected to the input power P_{in} by $|\varepsilon| = \sqrt{P_{in}/\hbar\omega_0}$, and therefore describes the square root of the driving laser's photon-flux. The mean intracavity field α_c then follows the equation of motion

$$\dot{\alpha}_c = -\left(i\omega_c + \frac{\kappa}{2}\right)\alpha_c + \sqrt{\kappa_{in}}\,\varepsilon\,e^{-i\omega_0 t}\,. \tag{1.7}$$

We can get rid of the (trivial) evolution at optical frequencies by introducing $\tilde{\alpha}_c(t) = \alpha_c(t)\,e^{i\omega_0 t}$. After a transient period $\tilde{\alpha}_c$ will assume a constant steady-state amplitude $\tilde{\alpha}_c^{ss} = \lim_{t\to\infty} \tilde{\alpha}_c(t)$ given by

$$\tilde{\alpha}_c^{ss} = \frac{\sqrt{\kappa_{in}}\varepsilon}{i\Delta_0 - \frac{\kappa}{2}}, \tag{1.8}$$

with the detuning $\Delta_0 = \omega_0 - \omega_c$ of the laser with respect to the cavity resonance frequency. Note the distinction between the total decay rate κ and the input-coupling rate κ_{in}, which leads to a decreased intracavity photon number $|\alpha_c|^2$ for increasing losses $\tilde{\kappa}$.

Taking the Fourier transform of eq. (1.7) we obtain the cavity's susceptibility $\chi(\omega_0)$, i.e., its linear response function. The value $\chi(\omega_0)$ determines the response of the system for a constant input at a frequency ω_0. It is given by the Lorentzian

$$\chi(\omega) = \frac{\sqrt{\kappa_{in}}}{\frac{\kappa}{2} - i(\omega - \omega_c)}. \tag{1.9}$$

Its modulus and its argument give the amplitude and phase response of the intracavity field respectively.

Quantum-mechanically the intracavity field can be described as a damped harmonic oscillator [WM08]. In analogy to section 1.1.1 we introduce creation and annihilation operators $c_c^\dagger$, c_c, and the corresponding (dimensionless) quadrature operators

$$x_c = \frac{c_c + c_c^\dagger}{\sqrt{2}}, \qquad\qquad p_c = \frac{c_c - c_c^\dagger}{\sqrt{2}i}. \tag{1.10}$$

We call x_c the amplitude quadrature and p_c the phase quadrature of the electromagnetic field. Their equations of motion we will discuss in detail in section 1.3.1.

1.1.3 *Cavity-Optomechanical Interaction*

In cavity-optomechanical systems the interaction between the optical and the mechanical mode typically manifests itself in the form of a dispersive coupling, which means that the cavity resonance frequency experiences a shift depending on the mechanical oscillator's position. Physically, the interaction is mediated by radiation pressure [Ein09] in the form of momentum transfer due to reflection (Fabry–Pérot type setups, microtoroids) [BM67; BMT70] or gradient forces (membrane in the middle setups [Tho+08], levitated micro-objects [Cha+10; BS10; Rom+10]). In addition to the dispersive regime there exists a dissipative optomechanical coupling where the cavity decay rate is dependent on the mechanical position [EGC09; XSH11; Saw+15]. We will not consider this kind of coupling in this thesis, however.

For photons impinging on a single mirror the radiation pressure is just proportional to the incoming photon flux. As this force exerted by photons on a massive object is typically very weak, cavity-optomechanical experiments employ a resonator for the photons—an optical cavity—in order to enhance the effective photon flux and therefore the radiation pressure coupling. Conversely, the intracavity photon flux now very sensitively depends on the mirror's position, as the mirror parametrically changes the cavity resonance frequency. This can be nicely illustrated by plotting the modified susceptibility of the cavity as a function of the mirror position X_m, which can be obtained from eq. (1.9) by letting the resonance frequency depend linearly on the mirror position, i.e., $\omega_c = \omega_c(X_m)$ (see also the discussion of the radiation pressure Hamiltonian in the next section). Figure 5 shows that moving the mirror modulates the intracavity-field amplitude [shown in (a)], as well as its phase [shown in (b)]. For resonant driving (as depicted in the figure) the amplitude stays constant to second order in X_m, while the phase is changed linearly. Hence, mechanical displacement sensing is typically operated on resonance as there the sensitivity on the mechanical displacement $\Delta\theta/\Delta X_m$ is maximal [AKM14].

FIG 5. Optical response to mechanical modulation

The finite decay time of the cavity (i.e., the average time it takes photons to leave the cavity) leads to a time-lag in the radiation pressure force on the mirror. This leads to so-called *dynamical back-action effects*, most notably the optical-spring effect and back-action cooling (or heating) of the mechanical motion, both of which we will again encounter again below. A classical picture of optomechanical cooling can be given by considering the cavity's susceptibility (see fig. 6) [MG09]: As the mirror oscillates and therefore sweeps the cavity's resonance profile, it modulates the number of photons inside the cavity and thus also the radiation pressure. However, due to the time-delay associated with the cavity bandwidth, the radiation pressure is increased in one half-cycle, while it is decreased in the other half-cycle
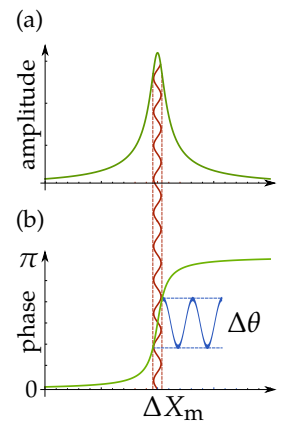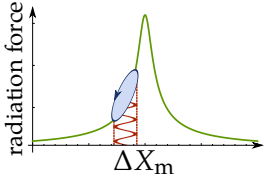
dynamical back-action effects

FIG 6. Radiation pressure (proportional to the intracavity amplitude) as a function of the mechanical motion for a red detuned drive

(schematically depicted by the blue ellipse in fig. 6). Depending on the relative phase between the radiation-pressure cycle and the mechanical oscillation this leads to additional damping for a red-detuned laser drive or amplification for a blue-detuned drive.

1.2 HAMILTONIAN

Here we restrict ourselves to the case where a single mechanical mode interacts with a single optical mode. The generalization to a multi-mode scenario is straightforward. We give a simple derivation of the cavity-optomechanical Hamiltonian; a rigorous version was given by [Law95]. We start from the Hamiltonian of two uncoupled harmonic oscillators

$$H_0 = \hbar\omega_{\mathrm{m}}c_{\mathrm{m}}^\dagger c_{\mathrm{m}} + \hbar\omega_{\mathrm{c}}c_{\mathrm{c}}^\dagger c_{\mathrm{c}}, \tag{1.11}$$

where ω_{m} and ω_{c} denote the mechanical and (nominal) cavity resonance frequency respectively, and we have $[c_i, c_j^\dagger] = \delta_{ij}$ for $i, j \in \{\mathrm{m}, \mathrm{c}\}$. The optical resonance frequency ω_{c} is determined by the round-trip time of photons in the cavity and thus by the effective cavity length L, i.e., $\omega_{\mathrm{c}}/2\pi = 2c/L$. In the case of a cavity with a moving mirror, the effective length $L(X_{\mathrm{m}})$ depends on the (dimensionful) position of the mechanical oscillator X_{m}. Moving the mirror thus shifts the resonance frequency and therefore changes the energy stored inside the cavity mode. For small displacements $X_{\mathrm{m}}/L \ll 1$ [assuming that $X_{\mathrm{m}} = 0$ is the rest position and hence $\omega_{\mathrm{c}} := \omega_{\mathrm{c}}(0)$ the nominal cavity frequency] we can expand $\omega_{\mathrm{c}}(X_{\mathrm{m}})$ in a Taylor series around $X_{\mathrm{m}} = 0$,

$$\omega_{\mathrm{c}}(X_{\mathrm{m}}) = \omega_{\mathrm{c}} + \frac{\partial\omega_{\mathrm{c}}}{\partial X_{\mathrm{m}}}X_{\mathrm{m}} + \mathcal{O}(X_{\mathrm{m}})^2. \tag{1.12}$$

Using that $X_{\mathrm{m}} = x_0(c_{\mathrm{m}} + c_{\mathrm{m}}^\dagger) = \sqrt{2}x_0 x_{\mathrm{m}}$, the Hamiltonian for the optomechanical system is (to first order in X_{m})

$$H'_{\mathrm{nl}} = \hbar\omega_{\mathrm{m}}c_{\mathrm{m}}^\dagger c_{\mathrm{m}} + \hbar\omega_{\mathrm{c}}c_{\mathrm{c}}^\dagger c_{\mathrm{c}} + \hbar g_0 x_{\mathrm{m}}c_{\mathrm{c}}^\dagger c_{\mathrm{c}}. \tag{1.13}$$

single-photon coupling strength

The last term is the sought-after radiation pressure interaction with the so-called single-photon optomechanical coupling strength

$$g_0 = \sqrt{2}x_0\frac{\partial\omega_{\mathrm{c}}}{\partial X_{\mathrm{m}}}, \tag{1.14}$$

which quantifies the interaction between the mechanical oscillator and a single photon in the cavity. For the Fabry–Pérot case we find $g_0 = \sqrt{2}x_0\omega_{\mathrm{c}}/L$. Note that by using these definitions a positive value for the displacement $X_{\mathrm{m}} > 0$ increases the energy in the cavity, which means that the cavity length decreases.

Expression (1.13) shows that the radiation-pressure coupling is non-linear in the amplitudes c_i, $c_i^\dagger$ and depends on the number of photons

in the cavity. However, as g_0 is very small in many current optomechanical systems, the generated non-linear dynamics—and optomechanical effects on the single-photon level in general—are hard to observe. To enhance the radiation pressure one can drive the optomechanical cavity by a strong laser beam with a large coherent (time-dependent) amplitude $\varepsilon(t)$. Such a drive with a centre frequency ω_0 can be described by adding an additional driving term

$$H_{\mathrm{drive}} = -i\hbar \left[E^*(t)\, e^{i\omega_0 t}\, c_{\mathrm{c}} - E(t)\, e^{-i\omega_0 t}\, c_{\mathrm{c}}^\dagger \right] \tag{1.15}$$

to eq. (1.13), where $E(t) = \sqrt{\kappa_{\mathrm{in}}}\varepsilon(t)$ describes the driving strength and $\varepsilon(t) \in \mathbb{C}$ is the complex amplitude of the input field. This Hamiltonian basically arises from a beam-splitter like interaction, where photons are scattered into the cavity mode from the external coherent field. In order to get rid of the explicit time dependence in (1.15) we typically go to a frame rotating at the optical frequency ω_0, which prompts us to introduce the detuning $\Delta_0 = \omega_0 - \omega_{\mathrm{c}}$. The complete optomechanical Hamiltonian including the non-linear radiation-pressure interaction then takes the form

non-linear optomechanical Hamiltonian

$$H_{\mathrm{nl}} = \frac{1}{2}\hbar\omega_{\mathrm{m}}(x_{\mathrm{m}}^2 + p_{\mathrm{m}}^2) - \hbar\Delta_0 c_{\mathrm{c}}^\dagger c_{\mathrm{c}} + \hbar g_0 x_{\mathrm{m}} c_{\mathrm{c}}^\dagger c_{\mathrm{c}}$$
$$- i\hbar \left[E^*(t) c_{\mathrm{c}} - E(t) c_{\mathrm{c}}^\dagger \right]. \tag{1.16}$$

We will discuss below that driving the optomechanical cavity in such a way has two effects: (i) The mirror is shifted to a new equilibrium position, and (ii) the radiation-pressure interaction is enhanced by the classical intracavity amplitude α_{c} created by the laser drive, effectively linearizing[1] it given that we have $|\alpha_{\mathrm{c}}| \gg 1$. For a full description of these effects one needs to account for the open-system dynamics of our system as will be discussed in detail in the next section. Here we want to focus on the dynamics generated by the linearized Hamiltonian, as understanding their effects will be important throughout the whole thesis.

1. By 'linear' we refer to the oscillator's response function or, equivalently, its equations of motion. The corresponding Hamiltonian can be quadratic in the oscillators amplitude.

We will see in section 1.3.1 that for a high-finesse cavity or a strong enough laser drive the optomechanical Hamiltonian (1.16) can be approximated by

linearized optomechanical Hamiltonian

$$H_{\mathrm{lin}} = \hbar\omega_{\mathrm{m}} c_{\mathrm{m}}^\dagger c_{\mathrm{m}} - \hbar\Delta_{\mathrm{c}} c_{\mathrm{c}}^\dagger c_{\mathrm{c}} + \hbar \frac{g_0 \alpha_{\mathrm{c}}}{\sqrt{2}} (c_{\mathrm{m}} + c_{\mathrm{m}}^\dagger)(c_{\mathrm{c}} + c_{\mathrm{c}}^\dagger), \tag{1.17}$$

where we introduced an effective detuning Δ_{c} which is shifted with respect to Δ_0 due to the shifted equilibrium position of the mirror. We can see that the coupling strength $g = g_0\alpha_{\mathrm{c}}/\sqrt{2}$ of the linear interaction is enhanced by α_{c}, which in the present case is the square-root of the intracavity photon number. (Here we assumed $\alpha_{\mathrm{c}} \in \mathbb{R}$ without loss of generality.) For a high-finesse cavity or a strong laser drive the mean number of photons in the cavity can be large, and the interaction strength can be enhanced by several orders of magnitude.

Depending on the chosen detuning Δ_c we can identify different types of interactions which are realized by the linearized radiation-pressure Hamiltonian. Expanding the interaction part of (1.17) we can identify two contributions: The so-called *beam-splitter* (BS) Hamiltonian

$$H_{bs} = \hbar g(c_m c_c^\dagger + c_m^\dagger c_c) \tag{1.18}$$

is resonant for $\Delta_c = -\omega_m$ and describes coherent exchange of energy between the mechanical oscillator and the cavity mode. This term is relevant for cooling the mechanical motion via sideband cooling [Mar+07; Wil+07] (see also section 1.4) and can be employed to generate a state swap between the two modes. The so-called two-mode squeezing (TMS) interaction

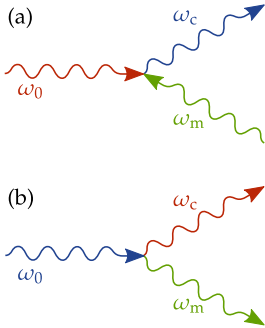$$H_{tms} = \hbar g(c_m c_c + c_m^\dagger c_c^\dagger), \tag{1.19}$$

(a)

(b)

FIG 7. Scattering processes corresponding to (a) the BS and (b) the TMS Hamiltonian

on the other hand, is resonant for $\Delta_c = \omega_m$, and describes simultaneous creation and annihilation of excitations in both modes, and is the optomechanical analogue to the optical down-conversion process. It is known to create optomechanical correlations and entanglement. Customarily we call the $\Delta_c > 0$ "blue detuned" and $\Delta_c < 0$ "red detuned".

Both terms can be interpreted in terms of three-mode scattering processes involving the incoming laser beam (see fig. 7). In the beam splitter process a phonon is annihilated in order to up-scatter a laser photon into the cavity mode (resonant for $\omega_0 = \omega_c - \omega_m$). In the two-mode squeezing process a fraction $\hbar\omega_m$ of a laser photon's energy is transferred to the mechanical motion creating a phonon, while the photon is down-scattered into the cavity mode (resonant for $\omega_0 = \omega_c + \omega_m$).

In the case of zero detuning $\Delta_c = 0$ both processes contribute equally and the full interaction Hamiltonian proportional to $x_m x_c$ is retained. This interaction is often referred to as quantum non-demolition (QND) interaction[2] [Tho+78; BVT80] and can be used to produce squeezed light, as demonstrated in [Bro+12; Saf+13; Pur+13]. Additionally, a resonant drive is commonly employed to measure position changes of the mechanical oscillator via phase shifts of the light field; these measurements can in turn be used to cool the mechanical motion by active feedback [CHP01; Vit+02; Gen+08a].

The resonance conditions for the listed processes can be illustrated by going into an interaction picture with $\hbar\omega_m c_m^\dagger c_m - \hbar\Delta_c c_c^\dagger c_c$ which leads to

$$\tilde{H}_{int} = \hbar g\left[c_m c_c^\dagger e^{-i(\omega_m + \Delta_c)t} + \text{H.c.}\right] + \hbar g\left[c_m c_c e^{-i(\omega_m - \Delta_c)t} + \text{H.c.}\right].$$

Tuning the laser to one of the mechanical sidebands, i.e., choosing $\Delta_c = \pm\omega_m$, makes one of the terms in $\tilde{H}_{int}$ resonant while the second

2. Note that in the resonant case x_c is a QND-variables as $[x_c, H_{lin}] = 0$ [BK96], while x_m does not commute with the full Hamiltonian.

14

term is oscillating rapidly at a frequency $\pm 2\omega_{\mathrm{m}}$. Invoking a rotating-wave approximation (RWA), which is equivalent to taking a temporal average, then allows us to neglect the corresponding off-resonant term. The RWA is a good approximation in the sideband-resolved weak-coupling regime $g < \kappa \ll \omega_{\mathrm{m}}$, where the off-resonant scattering terms are strongly suppressed by the cavity's density of states which is strongly peaked in this regime (see fig. 8).

One of the most important optomechanical parameters for us in this thesis will be the *optomechanical cooperativity*

optomechanical cooperativity

$$C = \frac{4g^2}{\kappa \gamma_{\mathrm{m}}(\bar{n} + 1)},$$ (1.20)

which quantifies the strength of the unitary optomechanical interaction compared to electromagnetic and mechanical decoherence rates. Intuitively, the coherent interaction should be stronger then the decohering dynamics in order to observe quantum effects. Indeed we will see later that all discussed protocols need to be operated in the strong-cooperativity regime of $C > 1$.

1.3 OPEN SYSTEM DYNAMICS

A cavity-optomechanical system couples to two different kinds of environments: On the one hand the mechanical oscillator couples to a mechanical heat bath through its support;[3] on the other hand, photons can leak out of the cavity into the electromagnetic environment in a finite time. Due to this interaction with the environment, cavity-optomechanical systems inherently are open quantum systems and a Hamiltonian description does not suffice to describe their full dynamics. In quantum optics, powerful methods have been developed to describe open quantum systems [GZ04]. In the following sections we will show how to describe the dynamics of optomechanical systems in the master equation (MEQ) and the quantum Langevin equations (QLEs) approach. As is customary we will call the optomechanical system simply "system", while we will refer to the external electromagnetic field and the mechanical environment as "bath" or "environment".

1.3.1 *Quantum Langevin Equations*

The non-linear open-system dynamics of optomechanical systems can be described in the Heisenberg picture by the (Stratonovich) quan-
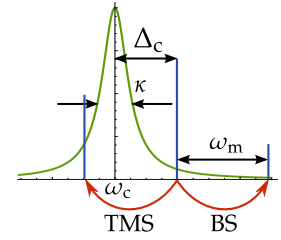

FIG 8. Spectral illustration of scattering processes into mechanical sidebands (here the blue detuned case)

3. Theoretically this type of coupling is mostly eliminated for levitated systems [AKM14].

tum Langevin equations [GC85] written in the frame rotating at the driving-laser frequency ω_0

$$\dot{x}_{\mathrm{m}} = \omega_{\mathrm{m}} p_{\mathrm{m}}, \tag{1.21a}$$

$$\dot{p}_{\mathrm{m}} = -\omega_{\mathrm{m}} x_{\mathrm{m}} - \gamma_{\mathrm{m}} p_{\mathrm{m}} - g_0 c_{\mathrm{c}}^{\dagger} c_{\mathrm{c}} + \sqrt{2\gamma_{\mathrm{m}}} f, \tag{1.21b}$$

$$\dot{c}_{\mathrm{c}} = -(\tfrac{\kappa}{2} - \mathrm{i}\Delta_0) c_{\mathrm{c}} - \mathrm{i} g_0 x_{\mathrm{m}} c_{\mathrm{c}} + E + \sqrt{\kappa} a_{\mathrm{in}}, \tag{1.21c}$$

where $\Delta_0 = \omega_0 - \omega_{\mathrm{c}}$ is the detuning of the laser with respect to the cavity resonance, and $E(t) \in \mathbb{C}$ describes the laser drive (as discussed in section 1.1.2).

The input from the external electromagnetic field to the cavity mode is described by the field operators a_{in} and $a_{\mathrm{in}}^{\dagger}$ (see appendix A). In a Markov approximation they obey the commutation relations[4]

$$[a_{\mathrm{in}}(t), a_{\mathrm{in}}^{\dagger}(t')] = \delta(t - t'), \tag{1.22a}$$

$$[a_{\mathrm{in}}(t), a_{\mathrm{in}}(t')] = [a_{\mathrm{in}}^{\dagger}(t), a_{\mathrm{in}}^{\dagger}(t')] = 0. \tag{1.22b}$$

Due to the Markov approximation the input fields are modelled as a white-noise fields and are therefore δ-correlated. For optical systems the electromagnetic bath is normally assumed to be in the vacuum state, which is due to the fact that at room temperature the mean occupation number of the bath at relevant frequencies is negligible, i. e., $n_{\mathrm{B}}(\omega_{\mathrm{c}}) \approx n_{\mathrm{B}}(\omega_0) \approx 0$.[5] We thus have

$$\langle a_{\mathrm{in}}(t) \rangle = 0, \qquad \langle a_{\mathrm{in}}^{\dagger}(t) \rangle = 0, \tag{1.23a}$$

$$\langle a_{\mathrm{in}}^{\dagger}(t) a_{\mathrm{in}}(t') \rangle = 0, \qquad \langle a_{\mathrm{in}}(t) a_{\mathrm{in}}^{\dagger}(t') \rangle = \delta(t - t'). \tag{1.23b}$$

Note, however, that in electromechanical systems where ω_{c} is in the microwave regime one might have a finite thermal occupation, i. e., $n_{\mathrm{B}}(\omega_{\mathrm{c}}) > 0$. The same description can also be valid if the laser drive of an optomechanical system exhibits broadband amplitude or phase noise that can be approximated by classical white noise. When the external field is in vacuum, we will often refer to the noise contribution

optical shot noise $\qquad$ a_{in} as *shot noise*, which is a purely quantum-mechanical contribution. In the experiment one typically has full access to the cavity input and the corresponding output field. This means that we can (at least in principle) engineer the input state [which modifies equations (1.23)] and monitor the state of the outgoing field. The output of the cavity is given by the input–output relation [GC85] (also see appendix A.3 for a more detailed discussion)

$$a_{\mathrm{out}}(t) = \sqrt{\kappa} c_{\mathrm{c}}(t) - a_{\mathrm{in}}(t). \tag{1.24}$$

This shows that by measuring quadrature operators x_{out}, p_{out} (e. g., by homodyne detection) of the output light we can directly monitor the intracavity field quadratures x_{c} and p_{c} (plus a noise contribution).

In contrast to the treatment of the electromagnetic field, no single accepted model exists for the coupling of the mechanical oscillator

to its thermal environment [Vac00]. A common approach is to model it in the form of Brownian motion damping [CL83; GV01], where f denotes the corresponding Gaussian, Hermitian noise operator. In general f does not describe a white-noise process, but rather has a correlation function [GZ04; GV01]

Brownian noise

$$\langle f(t)f(t') + f(t')f(t)\rangle = \frac{1}{\omega_{\mathrm{m}}}\int_0^\infty \frac{\mathrm{d}\omega}{\pi}\omega \coth\left(\frac{\hbar\omega}{2k_{\mathrm{B}}T}\right)\cos(\omega(t-t')).$$

(1.25)

Here we adopt a quantum-optical stance and treat f in a Markov approximation, which is known to be valid in the high-temperature limit where $k_B T/\hbar\omega_{\mathrm{m}} \gg 1$ [GV01] and for high-Q oscillators [BK81]. For small arguments we can expand $\coth x = x^{-1} + \mathcal{O}(x)$ and thus approximate f as a zero-mean white-noise field which is δ-correlated,[6]

$$\langle f(t)\rangle = 0,$$ (1.26a)

$$\langle f(t)f(t') + f(t')f(t)\rangle \approx (2\bar{n}+1)\delta(t-t').$$ (1.26b)

6. Under this approximation eq. (1.21) do not describe a completely-positive map. These effects are very small, however.

In contrast to the optical input fields the commutator of f at different times is given by [GZ04, p 49]

$$[f(t),f(t')] = \frac{\mathrm{i}}{\omega_{\mathrm{m}}}\delta'(t-t'),$$ (1.27)

where δ' denotes the first derivative of the Dirac δ-function.

Classical Dynamics

The quantum Langevin equations (1.21) allow us to study the classical non-linear dynamics of optomechanical systems. After introducing the mean amplitudes $\alpha_{\mathrm{m}}(t) = \langle c_{\mathrm{m}}(t)\rangle \in \mathbb{C}$ and $\alpha_{\mathrm{c}}(t) = \langle c_{\mathrm{c}}(t)\rangle \in \mathbb{C}$, and the semi-classical approximation that the correlation function $\langle c_{\mathrm{c}}^\dagger c_{\mathrm{c}}\rangle \approx |\alpha_{\mathrm{c}}|^2$ factorizes, we obtain the set of equations

$$\dot{\alpha}_{\mathrm{m}} = -\mathrm{i}\omega_{\mathrm{m}}\alpha_{\mathrm{m}} - \mathrm{i}\frac{g_0}{\sqrt{2}}|\alpha_{\mathrm{c}}|^2,$$ (1.28a)

$$\dot{\alpha}_{\mathrm{c}} = \left\{\mathrm{i}\left[\Delta_0 - \frac{g_0}{\sqrt{2}}(\alpha_{\mathrm{m}} + \alpha_{\mathrm{m}}^*)\right] - \frac{\kappa}{2}\right\}\alpha_{\mathrm{c}} + E.$$ (1.28b)

By defining the vector $\boldsymbol{\alpha} = (\alpha_{\mathrm{m}}, \alpha_{\mathrm{m}}^*, \alpha_{\mathrm{c}}, \alpha_{\mathrm{c}}^*)$ we can write equations (1.28) in compact form as $\dot{\boldsymbol{\alpha}} = \boldsymbol{G}(\boldsymbol{\alpha})$.

Let us first analyse the possible steady-solutions of equations (1.28) for constant driving field $E(t) \equiv E_0$. Steady-state solutions which we denote by $\boldsymbol{\alpha}^{\mathrm{ss}}$ are given by the fixed points of $\boldsymbol{G}$, i.e., $\boldsymbol{G}(\boldsymbol{\alpha}^{\mathrm{ss}}) = 0$.

classical steady-state

They are thus determined by the solutions of the third-order algebraic equations

$$\alpha_{\mathrm{m}}^{\mathrm{ss}} = -\frac{g_0}{\sqrt{2}\omega_{\mathrm{m}}}|\alpha_{\mathrm{c}}^{\mathrm{ss}}|^2, \tag{1.29a}$$

$$\alpha_{\mathrm{c}}^{\mathrm{ss}} = \frac{E_0}{\mathrm{i}[\Delta_0 - \frac{g_0}{\sqrt{2}}(\alpha_{\mathrm{m}}^{\mathrm{ss}} + \alpha_{\mathrm{m}}^{\mathrm{ss}*})] - \frac{\kappa}{2}}. \tag{1.29b}$$

We thus see that while the mechanical mode in equilibrium has zero momentum (i.e., $\mathrm{Im}\,\alpha_{\mathrm{m}}^{\mathrm{ss}} = 0$) it is displaced from its original position by a finite value $u_{\mathrm{m}}^{\mathrm{ss}} = \sqrt{2}\,\mathrm{Re}\,\alpha_{\mathrm{m}}^{\mathrm{ss}}$ that in particular depends on the driving strength E_0. At the same time the cavity resonance is shifted, leading to an effective detuning $\Delta_0 - g_0 u_{\mathrm{m}}^{\mathrm{ss}}$, which in turn leads to a steady-state mean intracavity amplitude depending on $u_{\mathrm{m}}^{\mathrm{ss}}$.

bistability　　Depending on the specific system parameters, equations (1.29) may allow for multiple steady-state solutions. This situation is called bistability [Dor+83; Mey+85]. It is easy to show that a necessary condition for bistability is given by $|\Delta_0| \geq \sqrt{3/4}\kappa$. Assuming this condition is fulfilled, we find that the driving strength must be chosen in a certain interval $E_0 \in [E_-, E_+]$ in order to observe bistable behaviour. Possible solutions of equations (1.29) are shown in fig. 9 for $\Delta_0 = 1.3\kappa$ (solid line)—showing a bistable region— and $\Delta_0 = 0.7\kappa$ (dashed line)—with a single steady-state solution—as a function of the driving strength E_0. The black dashed lines indicate the values of $E_\pm$ which mark the boundaries of the bistable region. The three dots mark three possible steady-state solutions $u_{\mathrm{m}}^{\mathrm{ss}}$ for a fixed driving E_0.
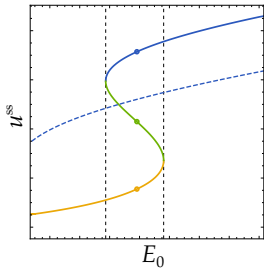

FIG 9. Mean steady-state displacement $u_{\mathrm{m}}^{\mathrm{ss}}$ for $\Delta_0 = 1.3\kappa$ ($\Delta_0 = 0.7\kappa$) [solid (dashed) line] against E_0

In the bistable regime the stability of the three solutions (shown in different colours) can be analysed by applying linear stability theory [Tab89, p 20]. We hence expand G around a chosen fixed point α^{ss} to first order in small fluctuations $\delta\alpha$. Denoting the Jacobian matrix of G by $(\mathcal{J}_G)_{ij} = \partial G_i/\partial u_j$ and defining $\alpha = \alpha^{\mathrm{ss}} + \delta\alpha$ we can write

$$\dot{\alpha} = G(\alpha) = G(\alpha^{\mathrm{ss}}) + \mathcal{J}_G(\alpha^{\mathrm{ss}})\delta\alpha + \mathcal{O}(\delta\alpha)^2. \tag{1.30}$$

Due to the fixed-point condition $G(\alpha^{\mathrm{ss}})$ vanishes. The system is then stable if all eigenvalues of $\mathcal{J}_G(\alpha^{\mathrm{ss}})$ have negative real parts, which means that all deviations from the fixed point will decay exponentially. Linear stability can be most conveniently analysed by using the *Routh–Hurwitz criterion* (see appendix B.4) [Ii07], which eliminates the need to explicitly calculate the eigenvalues of the Jacobian. Applying this to the situation depicted in fig. 9 we can show that the blue and the yellow branch correspond to stable steady-state solutions, while green shows an unstable solution. Which of the two possible stable solutions is assumed in steady state depends on the system's initial conditions, and is determined by the solution's *basin of attraction* (see, e.g., [Stro8]).

We now turn to the analysis of time-dependent solutions of equations (1.28). Due to their non-linear nature no closed-form solution exist in general and we seek approximate solutions under

the resolved-sideband assumption $\kappa \ll \omega_{\mathrm{m}}$. Additionally, we can simplify the analysis considerably if we assume that the effective detuning $\Delta_0 - g_0(\alpha_{\mathrm{m}} + \alpha_{\mathrm{m}})/\sqrt{2}$ is kept constant by appropriately tuning the laser frequency. This means that $\Delta_0(t)$ obtains a time-dependence to counteract the motion of the mirror and consequently that eq. (1.28a) decouples from (1.28b). (Additionally this precludes any bistable behaviour.) This is a reasonable assumption as in almost every optomechanical experiment working in a continuous-wave regime the laser will be locked to the cavity frequency. We can then integrate equations (1.28) formally and find [using the initial conditions $\alpha_{\mathrm{m}}(0) = \alpha_{\mathrm{c}}(0) = 0$]

$$\alpha_{\mathrm{c}}(t) = \int_0^t e^{(i\Delta_{\mathrm{c}} - \frac{\kappa}{2})\tau} E(t-\tau)\,d\tau, \tag{1.31a}$$

$$\alpha_{\mathrm{m}}(t) = -i\frac{g_0}{\sqrt{2}} \int_0^t e^{-i\omega_{\mathrm{m}}\tau} |\alpha_{\mathrm{c}}(t-\tau)|^2\,d\tau. \tag{1.31b}$$

Integrating eq. (1.31a) by parts we find the solution

$$\alpha_{\mathrm{c}}(t) = -\frac{1 - e^{(i\Delta_{\mathrm{c}} - \frac{\kappa}{2})t}}{i\Delta_{\mathrm{c}} - \frac{\kappa}{2}} E(t)(1+\delta) \approx -\frac{E(t)}{i\Delta_{\mathrm{c}} - \frac{\kappa}{2}}, \tag{1.32}$$

where δ is a correction, which is small if $E(t)$ varies slowly on a timescale of $1/\kappa$. More precisely, one can show that a rough upper bound is given by $|\delta(t)| < \sup_{s \in (0,t)} \frac{1}{\kappa} \frac{|\dot{E}(s)|}{|E(t)|}$, which must be much smaller than unity. Also, in the second step we neglected transient terms which only contribute on timescales $t \lesssim 1/\kappa$. Plugging this into (1.31b) and using $\kappa \ll \omega_{\mathrm{m}}$ we find under the same assumptions as above

$$\alpha_{\mathrm{m}}(t) \approx -\frac{g_0}{\sqrt{2}\omega_{\mathrm{m}}} |\alpha_{\mathrm{c}}(t)|^2. \tag{1.33}$$

Comparing eqs. (1.32) and (1.33) to the steady-state solutions above shows that in the sideband-resolved regime and for a slowly varying drive amplitude the system at all times is in a quasi steady state that follows the driving field $E(t)$.

Finally note that the frequency shift of the cavity due to the mean displacement of the mirror is typically small (for $g_0 \ll \omega_{\mathrm{m}}$). Assuming Δ_{c} to be constant will therefore often be a good approximation, even without assuming it to be fixed explicitly.

Linearized Langevin Equations

The semi-classical analysis from the previous section shows that for a strong laser drive $E(t)$ and a high-finesse cavity the intracavity field will have a large coherent mean value $\alpha_{\mathrm{c}}(t)$. Due to the radiation pressure caused by this mean field the mirror will be displaced accordingly by an amplitude $\alpha_{\mathrm{m}}(t)$. Effectively α_{c} and α_{m} define a

new (quasi-)equilibrium point for the optomechanical system, around which the dynamics can be linearized for certain parameter regimes. The discussion of this procedure follows the standard treatment as given in [Fab+94; MT94]. We first define the operator-valued vectors

$$c = (c_{\mathrm{m}}, c_{\mathrm{m}}^{\dagger}, c_{\mathrm{c}}, c_{\mathrm{c}}^{\dagger})^{\mathsf{T}}, \tag{1.34a}$$

$$f = (\sqrt{\gamma_{\mathrm{m}}}\mathrm{i}f, -\sqrt{\gamma_{\mathrm{m}}}\mathrm{i}f, \sqrt{2\kappa}a_{\mathrm{in}}, \sqrt{2\kappa}a_{\mathrm{in}}^{\dagger})^{\mathsf{T}}, \tag{1.34b}$$

which allow us to rewrite the Langevin equations (1.21) in vector form as $\dot{c} = G(c) + f$. We then decompose $c = \alpha\mathbb{1} + \delta c$ where α describes the coherent amplitudes as in the previous section and $\mathbb{1}$ is the identity operator. Formally this is achieved by going into a *displacement operator*   displaced frame created by the displacement operator

$$D_i(\alpha) = \exp(\alpha c_i^{\dagger} - \alpha^* c_i), \tag{1.35}$$

defining $\delta c_i = D_i(\alpha_i)c_i D_i^{\dagger}(\alpha_i)$. For δc we then obtain the *exact* equation

$$\delta\dot{c} = \dot{c} - \dot{\alpha}\mathbb{1} = [G(\alpha) - \dot{\alpha}]\mathbb{1} + \mathcal{J}_G(\alpha)\delta c + h(\delta c) + f, \tag{1.36}$$

where h is quadratic in δc. Choosing α such that it fulfils the classical equations (1.28) makes the first term disappear and leaves us with nonlinear equations for δc, which, however, explicitly depend on a classical solution $\alpha(t)$. They read

$$\delta\dot{c}_{\mathrm{m}} = -\mathrm{i}\omega_{\mathrm{m}}\delta c_{\mathrm{m}} - \mathrm{i}\frac{g_0}{\sqrt{2}}(\alpha_{\mathrm{c}}^*\delta c_{\mathrm{c}} + \alpha_{\mathrm{c}}\delta c_{\mathrm{c}}^{\dagger})$$
$$\qquad - \frac{\gamma_{\mathrm{m}}}{2}(\delta c_{\mathrm{m}} - \delta c_{\mathrm{m}}^{\dagger}) - \mathrm{i}\frac{g_0}{\sqrt{2}}\delta c_{\mathrm{c}}^{\dagger}\delta c_{\mathrm{c}} + \mathrm{i}\sqrt{\gamma_{\mathrm{m}}}f,$$
$$\delta\dot{c}_{\mathrm{c}} = \mathrm{i}[\Delta_0 - \frac{g_0}{\sqrt{2}}(\alpha_{\mathrm{m}} + \alpha_{\mathrm{m}}^*)]\delta c_{\mathrm{c}} - \mathrm{i}\frac{g_0}{\sqrt{2}}\alpha_{\mathrm{c}}(\delta c_{\mathrm{m}} + \delta c_{\mathrm{m}})$$
$$\qquad - \frac{\kappa}{2}\delta c_{\mathrm{c}} - \mathrm{i}\frac{g_0}{\sqrt{2}}\delta c_{\mathrm{c}}(\delta c_{\mathrm{m}} + \delta c_{\mathrm{m}}^{\dagger}) + \sqrt{\kappa}a_{\mathrm{in}}.$$

We can see that the linear interaction terms scale with $g_0\alpha_{\mathrm{c}}$ while all nonlinear terms scale with g_0 only. If we thus work in a regime with a large intracavity amplitude $|\alpha_{\mathrm{c}}(t)| \gg 1$ while on the other hand the single-photon coupling is weak (i. e., $g_0 < \kappa$) we can neglect the nonlinear terms $\delta c_{\mathrm{c}}^{\dagger}\delta c_{\mathrm{c}}$, $\delta c_{\mathrm{c}}\delta c_{\mathrm{m}}$ [AKM14]. For brevity of notation we will in the following drop the prefix δ and use c_i instead of δc_i etc. Additionally we introduce the effective coupling strength g and *effective detuning and*   detuning Δ_{c},
coupling strength

$$g = \frac{\alpha_{\mathrm{c}}g_0}{\sqrt{2}}, \qquad\qquad \Delta_{\mathrm{c}} = \Delta_0 - \frac{g_0}{\sqrt{2}}(\alpha_{\mathrm{m}} + \alpha_{\mathrm{m}}), \tag{1.37}$$

and write the linearized Langevin equations in terms of the quadrature operators as [MT94]

$$\dot{x}_{\mathrm{m}} = \omega_{\mathrm{m}} p_{\mathrm{m}}, \tag{1.38a}$$

$$\dot{p}_{\mathrm{m}} = -\omega_{\mathrm{m}} x_{\mathrm{m}} - \gamma_{\mathrm{m}} p_{\mathrm{m}} - 2g x_{\mathrm{c}} + \sqrt{2\gamma_{\mathrm{m}}} f, \tag{1.38b}$$

$$\dot{x}_{\mathrm{c}} = -\Delta_{\mathrm{c}} p_{\mathrm{c}} - \tfrac{\kappa}{2} x_{\mathrm{c}} + \sqrt{\kappa} x_{\mathrm{in}}, \tag{1.38c}$$

$$\dot{p}_{\mathrm{c}} = \Delta_{\mathrm{c}} x_{\mathrm{c}} - \tfrac{\kappa}{2} p_{\mathrm{c}} - 2g x_{\mathrm{m}} + \sqrt{\kappa} p_{\mathrm{in}}. \tag{1.38d}$$

Note that here we assumed $\alpha_{\mathrm{c}}(t) \in \mathbb{R}$ which can be achieved by appropriately choosing the phase of the input field E [see, e. g., (1.32)]. The Hamiltonian evolution in equations (1.38) is generated by the linearized Hamiltonian (1.17). One should keep in mind that the linearization is only valid if the coherent amplitudes α_i are sufficiently large at all times. Throughout this thesis we will only consider cases where the system is in a (quasi) steady state as discussed in the previous section, and we can thus chose $\boldsymbol{\alpha}(t) \equiv \boldsymbol{\alpha}^{\mathrm{ss}}$. Also we do not account for bistability effects. Note that in the same way as for the classical system, the stability of (1.38) can be analysed using the Routh–Hurwitz criterion [IIo7].

The linearized Langevin equations (1.38), or the corresponding equations for c_i and $c_i^{\dagger}$, will often serve as a starting point for our further analysis.

Mechanical Damping in RWA

Equations (1.38) show an important difference in the treatment of mechanical and optical damping: While for the mechanical mode only the momentum is directly subject to damping, both quadratures of the cavity mode are damped symmetrically. This is an important observation, as (1.38) do not describe a completely positive map, and thus cannot be stated as a Lindblad MEQ (see section 1.3.2). We will now show that the mechanical damping can be cast into a symmetric form by performing a RWA, which effectively constitutes a temporal coarse-graining procedure. We first write the mechanical Langevin equation in the interaction picture with $\hbar\omega_{\mathrm{m}} c_{\mathrm{m}}^{\dagger} c_{\mathrm{m}}$,

$$\dot{\tilde{c}}_{\mathrm{m}} = -\frac{\gamma_{\mathrm{m}}}{2}\left(\tilde{c}_{\mathrm{m}} - \mathrm{e}^{2\mathrm{i}\omega_{\mathrm{m}}t}\,\tilde{c}_{\mathrm{m}}^{\dagger}\right) - \mathrm{i}\sqrt{2}g\,\mathrm{e}^{\mathrm{i}\omega_{\mathrm{m}}t}\,x_{\mathrm{m}} + \mathrm{i}\sqrt{\gamma_{\mathrm{m}}}\,\mathrm{e}^{\mathrm{i}\omega_{\mathrm{m}}t}\,f, \tag{1.39}$$

and introduce a time coarse-graining by averaging the equation over a time δt, which has to be chosen long on the timescale of the mechanical frequency (i. e., $\delta t \gg 1/\omega_{\mathrm{m}}$), but short on all other timescales involved. (See appendix 1.A for a more detailed discussion of this procedure.) This leads us to define the noise operator

$$\bar{f}(t)\,\mathrm{d}t = \mathrm{i}\int_{t}^{t+\delta t}\mathrm{d}\tau\,\mathrm{e}^{\mathrm{i}\omega_{\mathrm{m}}\tau}f(\tau), \tag{1.40}$$

which is not Hermitian and (approximately) obeys

$$\langle \bar{f}(t)\bar{f}^\dagger(t') + \bar{f}^\dagger(t')\bar{f}(t) \rangle = (2\bar{n} + 1)\delta(t - t'), \tag{1.41a}$$

$$\langle \bar{f}(t)\bar{f}(t') \rangle = \langle \bar{f}^\dagger(t)\bar{f}^\dagger(t') \rangle = 0. \tag{1.41b}$$

Note that these relations are only valid on timescales much longer than δt. Due the time average we can drop the fast rotating term $e^{2i\omega_m t}\tilde{c}_m$, which is the gist of the rotating-wave approximation. In this particular approximation we keep the optomechanical coupling term in its original form, but have to keep in mind that the resulting equations are valid only in a narrow bandwidth much smaller than ω_m around ω_m, i.e., in a interval $[\omega_m - \vartheta, \omega_m + \vartheta]$ with $\vartheta \ll \omega_m$; all other frequency components are suppressed by the applied time average. This can be borne out more explicitly in the adiabatic regime, as discussed in appendix 1.A. We can now define Hermitian operators $\bar{f}_x$ and $\bar{f}_p$ by

$$\bar{f} = \frac{1}{\sqrt{2}}(\bar{f}_x + i\bar{f}_p) \tag{1.42}$$

and go back to the original frame; we obtain

$$\dot{x}_m = \omega_m p_m - \frac{\gamma_m}{2}x_m + \sqrt{\gamma_m}\bar{f}_x, \tag{1.43a}$$

$$\dot{p}_m = -\omega_m x_m - \frac{\gamma_m}{2}p_m - 2g x_c + \sqrt{\gamma_m}\bar{f}_p. \tag{1.43b}$$

In this form the QLEs are equivalent to the Lindblad master equation (1.52).

Langevin Equations in the Adiabatic Regime

In the weak coupling regime $g \ll \kappa$ one can significantly simplify the description of the optomechanical dynamics by adiabatically eliminating the cavity mode from the system. This leads to an effective equation for the mechanical oscillator, which then directly couples to the external electromagnetic field. The complete procedure is presented in appendix 1.A; here we summarize the most important expressions.

One can show that the adiabatic solution for the cavity is given by

$$c_c(t) \approx -ig\left[\eta_- c_m(t) + \eta_+ c_m^\dagger(t)\right] + \frac{2}{\sqrt{\kappa}}\xi(t), \tag{1.44}$$

where we introduced the parameters

$$\eta_\pm = \frac{1}{\frac{\kappa}{2} + i(-\Delta_c \pm \omega_m)}, \tag{1.45}$$

which describe the Lorentzian cavity profile. $\xi(t)$ is an electromagnetic vacuum noise term filtered by the cavity [see eq. (1.74)]; in the adiabatic approximation one can set

$$\langle \xi(t)\xi^\dagger(t') \rangle = \delta(t - t') \tag{1.46}$$

for all timescales slow compared to $1/\kappa$. Using the adiabatic solution (1.44) we can derive the effective equation of motion of the mechanical system alone. We first state the result; all terms will be described afterwards. After transforming to a frame rotating with ω_m and introducing a time coarse-grained description (which we indicate by using symbols such as $\bar{c}_m$) we find (see appendix 1.A)

$$\dot{\bar{c}}_m = -i\delta\omega_m\bar{c}_m - \tfrac{1}{2}\left(\gamma_m + \Gamma\right)\bar{c}_m$$
$$- i\sqrt{\Gamma_-}\bar{\xi}_+ - i\sqrt{\Gamma_+}\bar{\xi}_-^\dagger + \sqrt{\gamma_m}\bar{f}. \quad (1.47)$$

This equations nicely illustrates the characteristic dynamical features of optomechanical systems we touched on in section 1.1.3: Firstly we see that the mechanical frequency is shifted by

$$\delta\omega_m = g^2\,\mathrm{Im}(\eta_- + \eta_+) \qquad (1.48)$$

with respect to the nominal value ω_m. This is the *optical-spring effect* [BGK97; BV02; Cor+07], which leads to a softening of the spring for a red-detuned drive ($\Delta_c < 0$) and a hardening for a blue-detuned drive ($\Delta_c > 0$). Secondly we observe a modification of the mechanical damping rate by

optical-spring effect

$$\Gamma = \Gamma_- - \Gamma_+, \qquad (1.49)$$

with

$$\Gamma_\pm = 2g^2\,\mathrm{Re}\,\eta_\pm. \qquad (1.50)$$

This modification leads to sideband cooling for $\Delta_c < 0$, for which we have $\Gamma_- > \Gamma_+$ [Mar+07; Wil+07], while for the case of $\Delta_c > 0$ we find $\Gamma_+ > \Gamma_-$ and thus amplification of the mechanical motion. In the adiabatic approximation the optical mode is treated as an additional bath of the mechanical oscillator. The coupling to this bath introduces the vacuum noise processes $\bar{\xi}_\pm$, which in the given approximation are Markovian and independent. They thus obey

optical cooling and heating

$$\langle \bar{\xi}_\pm(t)\bar{\xi}_\pm^\dagger(t') \rangle = \delta(t - t'), \qquad (1.51a)$$
$$\langle \bar{\xi}_\pm(t)\bar{\xi}_\mp^\dagger(t') \rangle = 0. \qquad (1.51b)$$

Physically $\tilde{\xi}_+$ ($\tilde{\xi}_-$) stems from the process of scattering photons into the upper (lower) mechanical sideband (as discussed in section 1.2) with corresponding scattering rates Γ_- (Γ_+). Hence we see that the parameters $\eta_\pm$ describe the modification of the scattering rates due to the Lorentzian cavity profile. Note that the adiabatic Langevin equation (1.47) is equivalent to the adiabatic master equation (1.55).

1.3.2 *Master Equation and Stochastic Master Equation*

As an alternative to the quantum Langevin equations, which constitute the Heisenberg description of the dynamics, the evolution of the

optomechanical system can also be described in the Schrödinger picture. We denote by ρ the density matrix of the bipartite system consisting of the mechanical and the optical mode. The state ρ evolves according to a Lindblad master equation [Lin76] of the form [Wil+07]

Lindblad master equation

$$
\begin{aligned}
\dot{\rho} &= \mathcal{L}_{H_{\text{lin}}}\rho \\
&= -\frac{\mathrm{i}}{\hbar}[H_{\text{lin}}, \rho] + \kappa\, \mathcal{D}[c_{\text{c}}]\rho + \gamma_{\text{m}}(\bar{n}+1)\, \mathcal{D}[c_{\text{m}}]\rho + \gamma_{\text{m}}\bar{n}\, \mathcal{D}[c_{\text{m}}^{\dagger}]\rho.
\end{aligned}
\tag{1.52}
$$

Its initial condition we typically choose to be $\rho_0 = \rho_{\text{th}}^{(\text{m})} \otimes |0\rangle\langle 0|_{\text{c}}$, where $\rho_{\text{m}}^{(\text{th})}$ denotes a thermal state of the mechanical oscillator given by

$$
\rho_{\text{th}}^{(\text{m})} = \frac{1}{\bar{n}+1}\sum_{n=0}^{\infty}\left(\frac{\bar{n}}{\bar{n}+1}\right)^{n}|n\rangle\langle n|_{\text{m}}
\tag{1.53}
$$

and $|0\rangle\langle 0|_{\text{c}}$ is the ground state of the cavity. The Liouvillian $\mathcal{L}_{H_{\text{lin}}}$ describes the unitary evolution generated by the linearized Hamiltonian H_{lin} [given by eq. (1.17)] together with the dissipative dynamics created by the coupling to the environment. The decoherence effects are captured by the Lindblad terms [GZ04]

Lindblad terms

$$
\mathcal{D}[s]\rho = s\rho s^{\dagger} - \frac{1}{2}\rho s^{\dagger}s - \frac{1}{2}s^{\dagger}s\rho
\tag{1.54a}
$$

$$
= \frac{1}{2}[s\rho, s^{\dagger}] + \frac{1}{2}[s, \rho s^{\dagger}].
\tag{1.54b}
$$

The operator $\mathcal{D}$ is trace-preserving [i.e., $\text{tr}(\mathcal{D}[c]\rho) = 0$], and hence preserves the normalization of the density matrix ρ. In analogy to the treatment in section 1.3.1 we can derive an effective master equation for the mechanical mode from which the cavity is adiabatically eliminated (see appendices 2.C and 3.A.1). We obtain the equation

$$
\dot{\rho}^{(\text{m})} = -\mathrm{i}[\delta\omega_{\text{m}}c_{\text{m}}^{\dagger}c_{\text{m}}, \rho^{(\text{m})}] + \gamma_{-}\,\mathcal{D}[c_{\text{m}}]\rho^{(\text{m})} + \gamma_{+}\,\mathcal{D}[c_{\text{m}}^{\dagger}]\rho^{(\text{m})},
\tag{1.55}
$$

for the mechanical subsystem described by $\rho^{(\text{m})}$ alone, where

$$
\gamma_{-} = \Gamma_{-} + \gamma_{\text{m}}(\bar{n}+1),
\tag{1.56a}
$$

$$
\gamma_{+} = \Gamma_{+} + \gamma_{\text{m}}\bar{n}.
\tag{1.56b}
$$

and $\delta\omega_{\text{m}}$, $\Gamma_{\pm}$ as defined in eqs. (1.48) and (1.50). This equation captures passive cooling and heating effects via the optomechanical interaction, as has been derived before in the quantum theory of sideband cooling [Wil+07; Mar+07].

In this thesis we will often encounter the situation where the optomechanical system is continuously monitored via a homodyne measurement of the output light, realizing a so-called *diffusive* measurement of a given cavity quadrature [set by the local oscillator (LO)

angle ϕ]. The system can then be described by the *conditional quantum state* ρ_c that encodes our knowledge of the system given a specific measurement record $I(t)$. The conditional state's evolution is conveniently described in the Schrödinger picture by the Itō stochastic master equation (SME) [GZ04; WM09]

$$d\rho_c = \mathcal{L}\rho_c\, dt + \sqrt{\eta\kappa}\, \mathcal{H}[e^{i\phi}\, c_c]\rho_c\, dW, \tag{1.57}$$

stochastic master equation

where $0 < \eta < 1$ is the efficiency of the detection. The effect of conditioning is described by the measurement operator

$$\mathcal{H}[s]\rho_c = [s - \text{tr}(s\rho_c)]\rho_c + \rho_c[s - \text{tr}(s\rho_c)]^\dagger. \tag{1.58}$$

$\mathcal{H}$ is thus nonlinear in ρ_c, as is expected for a measurement term. The photo-current $I(t)$ can be expressed as

$$I(t)\, dt = \sqrt{\eta\kappa}\langle c_c(t)\, e^{i\phi} + c_c^\dagger(t)\, e^{-i\phi}\rangle_c\, dt + dW(t), \tag{1.59}$$

where W is a Wiener process with an increment $dW(t) := W(t+dt) - W(t)$, which has zero mean and a variance $dW(t)^2 = dt$. Here and in the following we denote by[7] $\langle A(t)\rangle_c = \text{tr}(A\rho_c(t))$ the expectation value with respect to the conditional state at time t. Equation (1.59) shows that $I(t)$ encodes information about a generalized intracavity quadrature defined by ϕ.

7. This construction is explained in detail in appendix B.1.2.

In contrast to the conditional state ρ_c which solves a SME, we will call the solution of a standard MEQ [such as (1.52)] the *unconditional state*, which we denote by ρ. A general introduction to SMEs is given in appendix B.

1.3.3 *Phase-Space Description*

In the Gaussian regime (i.e., for linearized optomechanical interaction) the system's unconditional state is fully characterized by the first and second moments of the vector $\mathbf{X} = (x_m, p_m, x_c, p_c)^T$, i.e., the mean values $\langle \mathbf{X}(t)\rangle = \text{tr}(\mathbf{X}\rho(t))$ and the symmetric covariance matrix $\mathbf{\Sigma}(t)$ with elements

$$\begin{aligned}\Sigma_{ij}(t) &= \tfrac{1}{2}\langle X_i(t)X_j(t) + X_j(t)X_i(t)\rangle - \langle X_i(t)\rangle\langle X_j(t)\rangle \\ &= \text{Re}\big(\langle X_i(t)X_j(t)\rangle\big) - \langle X_i(t)\rangle\langle X_j(t)\rangle.\end{aligned} \tag{1.60}$$

The linear equations of motion of $\langle \mathbf{X}(t)\rangle$ and $\mathbf{\Sigma}(t)$ are given by (see appendix B.3.2)

$$\frac{d}{dt}\langle \mathbf{X}(t)\rangle = \mathbf{F}\langle \mathbf{X}(t)\rangle, \tag{1.61a}$$

$$\frac{d}{dt}\mathbf{\Sigma}(t) = \mathbf{F}\mathbf{\Sigma}(t) + \mathbf{\Sigma}(t)\mathbf{F}^T + \mathbf{N}. \tag{1.61b}$$

The 4×4 matrices $\mathbf{F}$ and $\mathbf{N}$ describe the system's dynamics and noise properties respectively, and can be deduced directly from the

Langevin equations (1.38) or the corresponding master equation (see appendix B.3.1). For the model used in eq. (1.38) they read

$$
\mathbf{F} = \begin{pmatrix}
0 & \omega_{\mathrm{m}} & 0 & 0 \\
-\omega_{\mathrm{m}} & -\gamma_{\mathrm{m}} & -2g & 0 \\
0 & 0 & -\frac{\kappa}{2} & -\Delta_{\mathrm{c}} \\
-2g & 0 & \Delta_{\mathrm{c}} & -\frac{\kappa}{2}
\end{pmatrix}
\tag{1.62}
$$

and

$$
\mathbf{N} = \frac{1}{2}\,\mathrm{diag}\big(0, 2\gamma_{\mathrm{m}}(2\bar{n}+1), \kappa, \kappa\big).
\tag{1.63}
$$

Equation (1.61b) has an analytic solution given by

$$
\boldsymbol{\Sigma}(t) = \mathrm{e}^{\mathbf{F}t}\,\boldsymbol{\Sigma}(0)\,\mathrm{e}^{\mathbf{F}^{\mathsf{T}}t} + \int_{t_0}^{t} \mathrm{d}\tau\, \mathrm{e}^{\mathbf{F}(t-\tau)}\,\mathbf{N}\,\mathrm{e}^{\mathbf{F}^{\mathsf{T}}(t-\tau)}.
\tag{1.64}
$$

In the limit $t \to \infty$ the steady-state covariance matrix can be written as[8] [Gen+08b]

8. This is obtained by solving the linear Langevin equations in Fourier space.

$$
\boldsymbol{\Sigma}^{\mathrm{ss}} = \int_{-\infty}^{\infty} \mathrm{d}\omega\, (\mathrm{i}\omega\mathbb{1} + \mathbf{F})^{-1}\mathbf{N}(\mathrm{i}\omega\mathbb{1} + \mathbf{F}^{\mathsf{T}})^{-1}.
\tag{1.65}
$$

The integral can be evaluated analytically by a method presented in appendix B.5.

Gaussian conditional quantum states on the other hand are fully described by the mean vector $\hat{X}(t) = \langle \mathbf{X}(t)\rangle_c$ and covariance matrix

$$
\begin{aligned}
\hat{\Sigma}_{ij}(t) &= \tfrac{1}{2}\langle X_i(t)X_j(t) + X_j(t)X_i(t)\rangle_c - \langle X_i(t)\rangle_c\langle X_j(t)\rangle_c \\
&= \mathrm{Re}\big(\langle X_i(t)X_j(t)\rangle_c\big) - \hat{X}_i(t)\hat{X}_j(t),
\end{aligned}
\tag{1.66}
$$

defined with respect to ρ_c [the solution of a stochastic master equation such as (1.57)]. Their equations of motion are given by a linear stochastic differential equation and a (deterministic) matrix Riccati equation respectively [Bel80] (see appendix B.3.1 for a derivation),

$$
\mathrm{d}\hat{X}(t) = \mathbf{F}\hat{X}(t)\,\mathrm{d}t + \mathbf{K}(t)\big[I(t) - \mathbf{H}\hat{X}(t)\big]\,\mathrm{d}t,
\tag{1.67a}
$$

$$
\begin{aligned}
\frac{\mathrm{d}}{\mathrm{d}t}\hat{\boldsymbol{\Sigma}}(t) = {}& \mathbf{F}\hat{\boldsymbol{\Sigma}}(t) + \hat{\boldsymbol{\Sigma}}(t)\mathbf{F}^{\mathsf{T}} + \mathbf{N} \\
& - \big[\hat{\boldsymbol{\Sigma}}(t)\mathbf{H}^{\mathsf{T}} + \mathbf{M}\big]\big[\hat{\boldsymbol{\Sigma}}(t)\mathbf{H}^{\mathsf{T}} + \mathbf{M}\big]^{\mathsf{T}},
\end{aligned}
\tag{1.67b}
$$

where $\mathbf{H}$ describes the homodyne measurement and $\mathbf{M}$ is related to the system's noise properties [see eqs. (B.39b) and (B.41b)]. $\mathbf{K}(t)$ is a time-dependent gain factor

$$
\mathbf{K}(t) = \hat{\boldsymbol{\Sigma}}(t)\mathbf{H}^{\mathsf{T}} + \mathbf{M}.
\tag{1.68}
$$

which itself depends on the state through $\hat{\boldsymbol{\Sigma}}(t)$. In the case of a single homodyne detection with a LO phase ϕ and detection efficiency η [as described by eq. (1.57)], $\mathbf{H}$ and $\mathbf{M}$ are

$$
\mathbf{H} = \sqrt{2\eta\kappa}\,\big(0 \quad 0 \quad \cos(\phi) \quad -\sin(\phi)\big),
\tag{1.69a}
$$

$$
\mathbf{M} = \sqrt{\frac{\eta\kappa}{2}}\,\big(0 \quad 0 \quad -\cos(\phi) \quad \sin(\phi)\big)^{\mathsf{T}}.
\tag{1.69b}
$$

For a one-dimensional system [with a two-dimensional phase space (x, p)] these equations allow us to give a simple graphic interpretation of the SME (1.57) in terms of a phase-space description (see fig. 10): The conditional trajectory $\hat{X}$ (blue line) is determined by the measurements $I(t)$ and therefore follows a random walk in phase space. The covariance matrix $\hat{\Sigma}$ (red ellipse) on the other hand evolves deterministically, independent of the measurement results. Averaging over all possible phase-space trajectories recovers the broad Gaussian distribution described by the standard MEQ (1.52) [or equivalently, equations (1.61)]. For an unstable system (e. g., in the blue detuned regime), the blue line will spiral outwards, leading to a growing unconditional covariance. The conditional covariance matrix $\hat{\Sigma}$, however, may still possess a (finite) steady state. This is due to the fact that the exponential growth is tracked by the conditional mean, with respect to which the covariance matrix is defined. The steady-state conditional covariance matrix $\hat{\Sigma}^{ss}$ can be found in analogy to Σ^{ss} by setting the left-hand side of equation (1.67b) to zero and by solving the resulting algebraic Riccati equation [WM09].
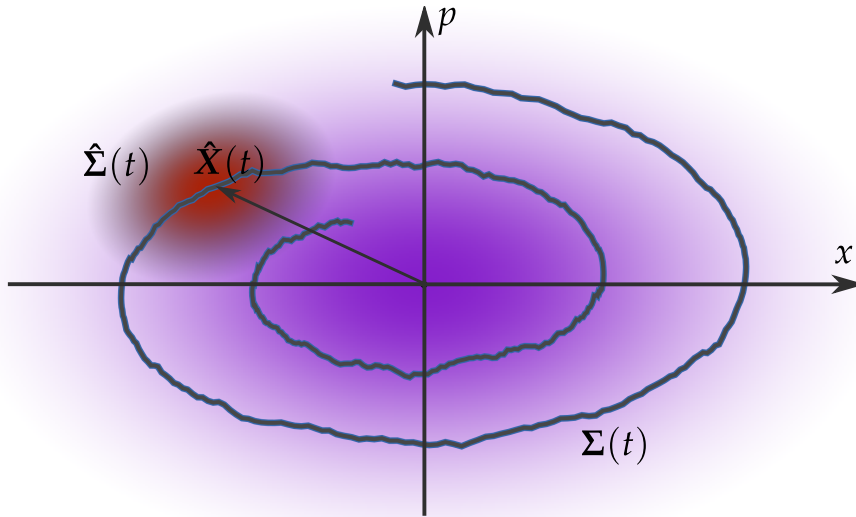

FIGURE 10. Schematic comparison of the master equation (1.52) and the stochastic master equation (1.57) for a single mode Gaussian system in phase space. The conditional state with a covariance $\hat{\Sigma}(t)$, depicted by the red ellipse, moves through phase space on a trajectory given by a realization of $\hat{X}(t)$ (blue line). Averaging over many sample paths recovers the broad, unconditional distribution, determined by $\Sigma(t)$ (violet ellipse).

1.4 THE OPTOMECHANICAL PHASE DIAGRAM

Provided a linear optomechanical system is stable (as determined by the Routh–Hurwitz criterion discussed in section 1.3.1) it will in the long-term assume a steady state, $\lim_{t\to\infty} \rho(t) = \rho^{ss}$, where ρ^{ss} is de-

termined by the condition $\mathcal{L}\rho^{\text{ss}} = 0$. If a stable steady state exists the means $\langle X \rangle^{\text{ss}} := \text{tr}(X\rho^{\text{ss}}) = 0$ vanish, while the steady-state covariance *Lyapunov* matrix $\boldsymbol{\Sigma}^{\text{ss}}$ is given by the solution to the so-called Lyapunov equa-*equation* tion, which is obtained from (1.61b) by setting its left-hand side to zero, i. e., $\mathbf{F}\boldsymbol{\Sigma}^{\text{ss}} + \boldsymbol{\Sigma}^{\text{ss}}\mathbf{F}^{\text{T}} + \mathbf{N} = 0$.

The characteristic features of an optomechanical system's steady state can nicely be illustrated by plotting a phase diagram showing the mechanical steady-state occupation number $n_{\text{m}}^{\text{ss}} = \langle c_{\text{m}}^{\dagger}c_{\text{m}} \rangle^{\text{ss}}$ and optomechanical entanglement between the mechanical resonator and the intracavity field. We quantify the entanglement by the steady-state logarithmic negativity $E_{\mathcal{N}}^{\text{ss}} = E_{\mathcal{N}}(\rho^{\text{ss}})$ [VW02; Ple05], where

$$E_{\mathcal{N}}(\rho) = \log_2(\|\rho^{\text{T}_{\text{m}}}\|_1), \tag{1.70}$$

$\|\cdot\|_1$ is the trace norm, and $\rho^{\text{T}_{\text{m}}}$ is the partial transpose with respect to the mechanical subsystem. Figure 12 shows such a phase diagram of an optomechanical system in the resolved sideband regime ($\kappa < \omega_{\text{m}}$) for a high-Q mechanical oscillator with respect to the laser detuning Δ_{c} and the coupling g. The grey background depicts the regions of instability, where no steady state exists. The first thing to note is that the system is unstable in nearly all the right half-plane, i. e., for blue detuned laser drive, while for red detuning the system becomes unstable only for appreciably high optomechanical coupling. Exactly on resonance $\Delta_{\text{c}} = 0$ the system is unconditionally stable for arbitrary high coupling (as long as $Q_{\text{m}} > 0$). Centred around the first mechanical sideband at $\Delta_{\text{c}} = -\omega_{\text{m}}$, where the beam-splitter part of the optomechanical interaction is resonant, lies the region where $n_{\text{m}}^{\text{ss}} < 1$ (dashed red line) and thus ground-state cooling of the mechanical system through optomechanical sideband cooling is possible. Optomechanical sideband cooling can be understood in analogy to sideband cooling of trapped ions [Cir+92] by looking at the level scheme depicted in fig. 11: Tuning the laser to the lower mechanical sideband resonantly drives the transition $|n\rangle_{\text{m}}|k\rangle_{\text{c}} \rightarrow |n-1\rangle_{\text{m}}|k+1\rangle_{\text{c}}$ with a rate Γ_- (solid red arrow), while in the sideband-resolved regime $\kappa \ll \omega_{\text{m}}$ all other transitions (dashed red arrows) are strongly suppressed. Due to the finite cavity lifetime the systems consecutively decays into $|n-1\rangle_{\text{m}}|k\rangle_{\text{c}}$ and the cycle starts over. Devoid of additional mechanical decoherence (and for $\Gamma_- \gg \Gamma_+$) the mechanical system would thus eventually be driven into the ground state $|0\rangle_{\text{m}}$. Assuming stability we can solve the Lyapunov equation corresponding to eq. (1.55) to obtain the steady-state covariance matrix of the mechanical mode

FIG 11. Illustration of sideband cooling based on the optomechanical level scheme

$$\boldsymbol{\Sigma}_{\text{m}}^{\text{ss}} = \left(\frac{\bar{n}\gamma + \Gamma_+}{\gamma + \Gamma_- - \Gamma_+} + \frac{1}{2} \right) \mathbb{1}_2. \tag{1.71}$$

The first term corresponds to the effective mechanical occupation number n_{eff} in steady state. We can thus see, that in order to achieve
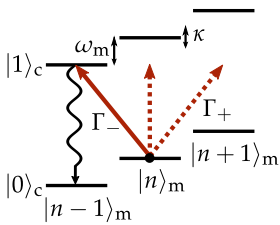
ground state cooling (i. e., $n_{\text{eff}} < 1$) we need $\Gamma_- \gg \gamma, \Gamma_+$ and $\Gamma_- > \bar{n}\gamma$. In leading order we then have $n_{\text{eff}} \approx \bar{n}\gamma/\Gamma_- \approx 1/C$. The region of ground-state cooling thus coincides with the regime of strong cooperativity $C \gtrsim 1$ (clearly visible in the plot).

Right at the border of stability, for a similar detuning, we find regions of large steady-state entanglement between the intracavity field and the mechanical resonator (coloured in green) [Gen+08b]. On the opposite side of the phase diagram, around $\Delta_c = \omega_m$, we also expect to observe optomechanical entanglement due to the effect of the optomechanical two-mode squeezing dynamics. However, there the formation of a steady state is inhibited by the optomechanical instability, which is due to parametric amplification of the amplitude of both the mechanical and the optical mode [AKM14]. The connection of laser cooling, entanglement generation, and the instability region has been analysed in detail in [Gen+08b].

Although no steady state exists for a blue-detuned laser drive, various alternative approaches permit to work with the resonantly enhanced two-mode squeezing dynamics of the optomechanical interaction. In section 2.1 we will analyse in detail a pulsed protocol for entanglement creation, which does not require to be operated in a stable regime. Working with a continuous-wave blue-detuned laser drive on the other hand, is still possible if one employs stabilizing feedback which inhibits the exponential growth of the optomechanical system's quadratures. One possible type of feedback is measurement-based feedback using homodyne detection, which we will consider in chapter 3.

Measurement-based feedback protocols rely on the evaluation of the system's conditional state, whose dynamics are described by a stochastic master equation such as (1.57). For Gaussian systems (such as a linear optomechanical system) the SME is easily integrated, by solving the corresponding Riccati equation. The conditional steady state's mean mechanical occupation number $\langle c_m^\dagger c_m \rangle_c^{\text{ss}}$ is depicted in fig. 12(a) for a measurement of the phase quadrature of the light field, i. e., $\phi = \pi/2$. We find a large region where $\langle c_m^\dagger c_m \rangle_c^{\text{ss}} < 0.4$ for all detunings $-\omega_m \lesssim \Delta_c \lesssim \omega_m$ (blue line). In the region around the red sideband $\Delta_c \approx -\omega_m$ this effect can mainly be attributed to passive sideband cooling of the mirror, which we discussed above. However, we now also find a region of low occupation on the opposite (blue) sideband at $\Delta_c \approx \omega_m$. In this region the reduction of the conditional phonon number, which at the same time means an increase of the mechanical state's purity, is due to correlations between the mechanical oscillator and the light field. These correlations allow us to extract information about the mechanics from the homodyne measurement. We will see in the next section that in the sideband-resolved regime $\kappa < \omega_m$ this effect is strongest for $\Delta_c \approx \omega_m$ where the two-
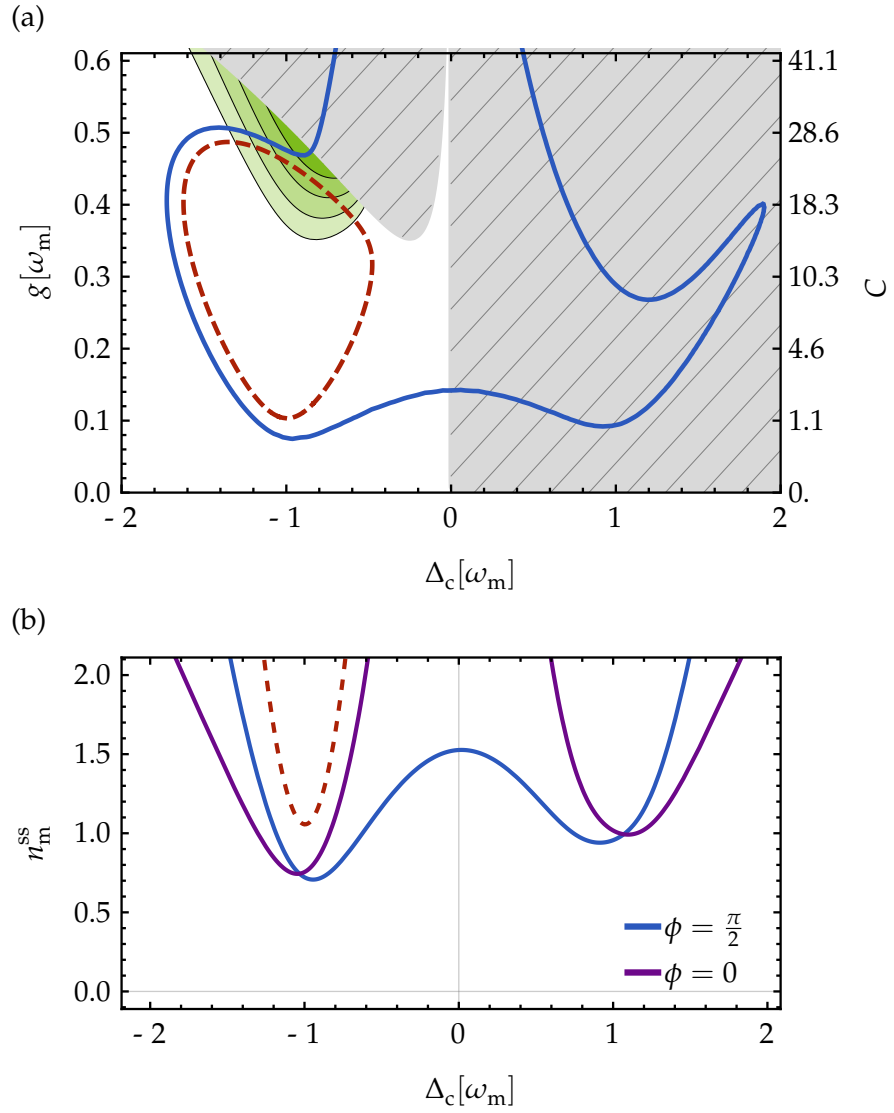
(a)

(b)

FIGURE 12. Upper plot: Steady-state phase diagram of an optomechanical system for $\kappa = \omega_m/4$, $Q_m = 10^7$, $\bar{n} = 3.5 \cdot 10^5$. The grey hatched area depicts unstable regions where no steady-state exists. The dashed red line shows regions of ground state cooling of the mechanical oscillator, here $n_m^{ss} < 1$. The green area shows optomechanical entanglement (logarithmic negativity $E_{\mathcal{N}}^{ss}$), with largest values close to the instability region. The blue line encloses the regions where the conditional mean mechanical occupation number $\langle c_m^\dagger c_m \rangle_c^{ss} < 1$ for a measurement of the optical phase quadrature, i.e., $\phi = \pi/2$. The right axis shows the corresponding optomechanical co-operativity, given by $C = 4g^2/(\bar{n}+1)\gamma_m\kappa$. Lower Plot: Cut through the phase diagram at $g = \omega_m/10$, depicting the conditional phonon number $\langle c_m^\dagger c_m \rangle_c^{ss}$ for LO phases $\phi = \pi/2$ (blue) and $\phi = 0$ (purple). The dashed red line again shows the mean occupation number for the unconditional state for sideband cooling.

mode squeezing, entangling term of the optomechanical Hamiltonian is resonant.

To illustrate how the choice of the LO phase influences the conditional mechanical occupation we plot a cut through fig. 12(a) at a fixed optomechanical coupling $g = \omega_m/10$ in fig. 12(b). If we choose to measure the optical amplitude quadrature we find that on resonance we do not have a reduction of the conditional phonon number. For a detuned laser drive ($|\Delta_c| \gtrsim \omega_m$) however, we again find regions of $\langle c_m^\dagger c_m \rangle_c^{ss} < 1$. This is easily explained by noting that on resonance ($\Delta_c = 0$) only the optical phase quadrature couples to the mechanical oscillator, while the amplitude quadrature contains noise only. Measuring the amplitude quadrature therefore does not allow us to make inferences about the mechanical motion. In general there will be an optimal LO angle, depending on all system parameters (especially g, Δ_c, κ) at which we obtain maximal information about the mechanical motion. Thus, homodyne detection at this particular angle yields the minimal conditional occupation. Typically—especially in the weak-coupling regime where $g < \kappa$—the optimal angle corresponds to the optical quadrature which is *anti*-squeezed by the optomechanical interaction and thus features the best signal-to-noise ratio. We will see later how these features of the optomechanical phase diagram connect to feedback cooling of the mechanical oscillator.

Although no steady state exists in the blue-detuned regime, it is well suited as a working point for optomechanical quantum control protocols. The entanglement created by the two-mode squeezing interaction can be exploited to obtain information about the mechanical system's state, as well as to prepare it in a certain state. We will explore several such protocols in the following sections.

1.A APPENDIX: ADIABATIC ELIMINATION OF THE CAVITY

The goal of adiabatically eliminating the cavity is to find an effective equation of motion for the mechanical mode coupling directly to the external electromagnetic field via a modified interaction. This is possible in the weak-coupling regime $g \ll \kappa$, where the cavity field adiabatically follows the mirror motion. The adiabatic elimination procedure effectively constitutes a perturbative expansion in the small parameter g/κ. We proceed as follows: We first find an adiabatic solution for the cavity mode and then apply a Markov approximation. After a RWA with respect to the optomechanical interaction we obtain an equation which is equivalent to a Lindblad MEQ (see also appendix 2.C).

The author thanks Prof. Gerard Milburn for helpful discussions on this topic during a visit at the University of Queensland, Brisbane.

We start from the QLEs (1.38) which we transform into a rotating frame defined by $c_c(t) = e^{i\Delta_c t} \tilde{c}_c(t)$ and $c_m(t) = e^{-i\omega_m t} \tilde{c}_m(t)$, yielding

$$\dot{\tilde{c}}_m = -\frac{\gamma_m}{2}(\tilde{c}_m - e^{2i\omega_m t} \tilde{c}_m^\dagger) \tag{1.72a}$$
$$- ig\, e^{i\omega_m t}(\tilde{c}_c\, e^{i\Delta_c t} + \text{H.c.}) + i\sqrt{\gamma_m}\, e^{i\omega_m t} f,$$

$$\dot{\tilde{c}}_c = -\frac{\kappa}{2}\tilde{c}_c - ig\, e^{-i\Delta_c t}(\tilde{c}_m\, e^{-i\omega_m t} + \text{H.c.}) + \sqrt{\kappa}\, e^{-i\Delta_c t} a_{in}. \tag{1.72b}$$

We now formally integrate the equation for $\tilde{c}_c$, leading to

$$\tilde{c}_c(t) = -ig \int_{-\infty}^{t} d\tau\, e^{-\frac{\kappa}{2}(t-\tau)}\, e^{-i\Delta_c \tau}[\tilde{c}_m(\tau)\, e^{-i\omega_m \tau} + \text{H.c.}]$$
$$+ \sqrt{\kappa} \int_{-\infty}^{t} d\tau\, e^{-\frac{\kappa}{2}(t-\tau)}\, e^{-i\Delta_c \tau} a_{in}(\tau).$$

Using the fact that $\tilde{c}_m$ is slowly varying on a timescale $1/\kappa$ we can pull it out from under the integral. Additionally, we assume that $\kappa t \gg 1$ and thus neglect transient terms. With that we find the adiabatic solution

$$\tilde{c}_c(t) \approx -ig \left[\eta_- \tilde{c}_m(t)\, e^{-i(\Delta_c + \omega_m)t} + \eta_+ \tilde{c}_m^\dagger(t)\, e^{-i(\Delta_c - \omega_m)t} \right] + \frac{2}{\sqrt{\kappa}}\tilde{\xi}(t), \tag{1.73}$$

with the coefficients $\eta_\pm = [\frac{\kappa}{2} + i(-\Delta_c \pm \omega_m)]^{-1}$. This is the gist of the adiabatic elimination procedure, as the cavity field in this approximation only depends on the mechanical state at the same time. The cavity dynamics give rise to a coloured noise process (white vacuum noise filtered by the cavity mode)

$$\tilde{\xi}(t) = \frac{\kappa}{2} \int_{-\infty}^{t} d\tau\, e^{-\frac{\kappa}{2}(t-\tau)}\, e^{-i\Delta_c \tau} a_{in}(\tau), \tag{1.74}$$

with a two-time correlation function

$$\langle \tilde{\xi}(t)\tilde{\xi}^\dagger(t') \rangle = \tfrac{\kappa}{4}\,\mathrm{e}^{-\frac{\kappa}{2}|t-t'|}. \tag{1.75}$$

For large κ this is a strongly-peaked function that acts as a δ-distribution for functions which vary slowly on a timescale $1/\kappa$, and we can show that $\lim_{\kappa\to\infty}\langle \tilde{\xi}(t)\tilde{\xi}^\dagger(t') \rangle = \delta(t-t')$.

Plugging the adiabatic solution for the cavity into the equation of motion for the mirror [eq. (1.72a)] we find

$$
\begin{aligned}
\dot{\tilde{c}}_\mathrm{m} = {}&-\frac{\gamma_\mathrm{m}}{2}\tilde{c}_\mathrm{m} + \frac{\gamma_\mathrm{m}}{2}\,\mathrm{e}^{2\mathrm{i}\omega_\mathrm{m}t}\,\tilde{c}_\mathrm{m}^\dagger + \mathrm{i}\sqrt{\gamma_\mathrm{m}}\,\mathrm{e}^{\mathrm{i}\omega_\mathrm{m}t}\,f \\
&- g^2 \left[(\eta_- - \eta_+^*)\tilde{c}_\mathrm{m} + (\eta_+ - \eta_-^*)\tilde{c}_\mathrm{m}^\dagger\,\mathrm{e}^{2\mathrm{i}\omega_\mathrm{m}t} \right] \\
&\qquad\qquad + \sqrt{g^2\kappa\frac{|\eta_\pm|}{2}}\left(\tilde{\xi}_+ + \tilde{\xi}_-^\dagger \right),
\end{aligned}
$$

where we defined

$$\tilde{\xi}_\pm(t) = \frac{2}{\kappa|\eta_\mp|}\,\mathrm{e}^{\mathrm{i}(\Delta_\mathrm{c}\pm\omega_\mathrm{m})t}\,\tilde{\xi}(t). \tag{1.76}$$

If we now apply a time coarse-graining by integrating over a time interval $[t, t+\delta t]$ with δt such that $1/g \gg \delta t \gg 1/\kappa$, $1/\omega_\mathrm{m}$, we can make the following approximations:

- As $\tilde{c}_\mathrm{m}$ evolves on a typical timescale $1/g$ which is much longer than δt we approximate $\int_t^{t+\delta t}\mathrm{d}\tau\,\tilde{c}_\mathrm{m}(\tau) \approx \tilde{c}_\mathrm{m}(t)\delta t$, and then formally take the limit $\delta t \to \mathrm{d}t$. To show explicitly that we are working in the coarse-grained picture we denote the corresponding mechanical operators by $\bar{c}_\mathrm{m}$, which can formally be written as

$$\bar{c}_\mathrm{m}(t)\,\mathrm{d}t := \int_t^{t+\delta t}\mathrm{d}\tau\,\tilde{c}_\mathrm{m}(\tau). \tag{1.77}$$

Under the same premiss we write

$$\mathrm{d}\bar{c}_\mathrm{m}(t) := \tilde{c}_\mathrm{m}(t+\delta t) - \tilde{c}_\mathrm{m}(t) = \int_t^{t+\delta t}\mathrm{d}\tilde{c}_\mathrm{m}. \tag{1.78}$$

- In a rotating-wave approximation we can drop the fast oscillating terms proportional to $\mathrm{e}^{2\mathrm{i}\omega_\mathrm{m}t}\,\tilde{c}_\mathrm{m}^\dagger$ in the damping terms produced by the coupling to the mechanical environment and the effective optical environment. This can be justified by observing that

$$
\int_t^{t+\delta t}\mathrm{d}\tau\,\mathrm{e}^{2\mathrm{i}\omega_\mathrm{m}\tau}\,\tilde{c}_\mathrm{m}^\dagger(\tau) \approx \left(\int_t^{t+\delta t}\mathrm{d}\tau\,\mathrm{e}^{2\mathrm{i}\omega_\mathrm{m}\tau} \right)\tilde{c}_\mathrm{m}^\dagger(t)
$$
$$
= \mathcal{O}(\omega_\mathrm{m}\delta t)^{-1}\tilde{c}_\mathrm{m}^\dagger(t)\delta t.
$$

- We introduce the coarse-grained noise processes

$$\bar{\xi}_\pm(t)\,\mathrm{d}t := \int_t^{t+\delta t}\mathrm{d}\tau\,\tilde{\xi}_\pm(\tau), \tag{1.79}$$

which effectively act as white noise at a center frequency $\omega_0 \pm \omega_m$ and are (approximately) independent. To see this we take the limit $\kappa \to \infty$ while keeping Δ_c/κ and ω_m/κ constant such that the condition $g \ll \kappa < \omega_m$ is still fulfiled. In this limit we can analyse the effect of $\langle \tilde{\xi}_\pm(t)\tilde{\xi}_\pm^\dagger(t')\rangle$ and $\langle \tilde{\xi}_\pm(t)\tilde{\xi}_\mp^\dagger(t')\rangle$ on a test function in a distributional sense. We find

$$\int d\tau \langle \tilde{\xi}_\pm(t)\tilde{\xi}_\pm^\dagger(t+\tau)\rangle \varphi(\tau)$$

$$= \frac{1}{\kappa^2|\eta_\mp|^2} \int ds\, e^{-i\frac{\Delta_c \mp \omega_m}{\kappa}s - \frac{1}{2}|s|} \varphi\left(\frac{s}{\kappa}\right)$$

$$\xrightarrow[\kappa \to \infty]{} \frac{1}{\kappa^2|\eta_\mp|^2} \int ds\, e^{-i\frac{\Delta_c \mp \omega_m}{\kappa}s - \frac{1}{2}|s|} \varphi(0) = \varphi(0),$$

and

$$\int d\tau \langle \tilde{\xi}_\pm(t)\tilde{\xi}_\mp^\dagger(t+\tau)\rangle \varphi(\tau)$$

$$= \frac{e^{\pm 2i\omega_m t}}{\kappa^2 \eta_\mp \eta_\pm^*} \int ds\, e^{-i\frac{\Delta_c \mp \omega_m}{\kappa}s - \frac{1}{2}|s|} \varphi\left(\frac{s}{\kappa}\right)$$

$$\xrightarrow[\kappa \to \infty]{} \frac{e^{\pm 2i\omega_m t}}{\kappa^2 \eta_\mp \eta_\pm^*} \int ds\, e^{-i\frac{\Delta_c \mp \omega_m}{\kappa}s - \frac{1}{2}|s|} \varphi(0) = e^{\pm 2i\omega_m t}\frac{\eta_\mp^*}{\eta_\pm^*}\varphi(0).$$

The second term is fast rotating and thus vanishes under the time-average over the timescale $\delta t \gg 1/\kappa,\, 1/\omega_m$, yielding a correction of $\mathcal{O}(\omega_m \delta t)^{-1}$. The correlation functions of the coarse-grained noise processes are thus given by

$$\langle \bar{\xi}_\pm(t)\bar{\xi}_\pm^\dagger(t')\rangle = \delta(t-t'), \tag{1.80a}$$

$$\langle \bar{\xi}_\pm(t)\bar{\xi}_\mp^\dagger(t')\rangle = 0, \tag{1.80b}$$

which is appropriate for timescales much longer than δt (e. g., on the timescale $1/g$). Physically $\bar{\xi}_\pm$ (and $\tilde{\xi}_\pm$) describe scattering of photons into the upper/lower mechanical sideband.

- Finally we introduce the coarse-grained mechanical noise process

$$\bar{f}(t)\, dt := i \int_t^{t+\delta t} d\tau\, e^{i\omega_m \tau} f(\tau), \tag{1.81}$$

which are the same processes already introduced in eq. (1.40). They therefore obey the correlation functions (1.41) in the same limit $\delta t \gg 1/\omega_m$ as above.

Under these approximations the Langevin equation can be written as

$$\dot{\bar{c}}_m = -i\delta\omega_m \bar{c}_m - \tfrac{1}{2}\left(\gamma_m + \Gamma\right)\bar{c}_m$$
$$\qquad\qquad - i\sqrt{\Gamma_-}\bar{\xi}_+ - i\sqrt{\Gamma_+}\bar{\xi}_-^\dagger + \sqrt{\gamma_m}\bar{f}, \tag{1.82}$$

with $\delta\omega_m = g^2 \mathrm{Im}(\eta_- + \eta_+)$ and $\Gamma = 2g^2 \mathrm{Re}(\eta_- - \eta_+) =: \Gamma_- - \Gamma_+$.

Later we will also need the corresponding time-averaged input–output relations. We define the coarse-grained noise operator [with the definition $\tilde{a}_{\text{in}}(t) = e^{-i\Delta_c t} a_{\text{in}}(t)$]

$$\bar{a}_{\text{in}}(t)\, dt := \int_t^{t+\delta t} d\tau\, \tilde{a}_{\text{in}}(\tau), \tag{1.83}$$

and correspondingly $\bar{a}_{\text{out}}$, in the rotating frame of the cavity mode. As above we can show that $\bar{a}_{\text{in}}$ and $\bar{a}_{\text{out}}$ obey the correlation functions

$$\langle \bar{a}_{\text{in}}(t)\bar{a}_{\text{in}}^\dagger(t')\rangle = \langle \bar{a}_{\text{out}}(t)\bar{a}_{\text{out}}^\dagger(t')\rangle = \delta(t - t') \tag{1.84}$$

for timescales longer than δt. If we, in the same way, introduce $\bar{c}_c(t)\, dt = \int_t^{t+\delta t} d\tau\, \tilde{c}_c(\tau)$ we find

$$\bar{a}_{\text{out}}(t) = \sqrt{\kappa}\, \bar{c}_c(t) - \bar{a}_{\text{in}}(t). \tag{1.85}$$

The explicit expression for $\bar{c}_c$ depends on the choice of the detuning Δ_c and cannot be further simplified in general. We can, however, make further simplifications for $\Delta_c = \pm\omega_m$. Using the adiabatic solution for $\tilde{c}_c(t)$ [eq. (1.73)] we find for $\Delta_c = -\omega_m$

$$\bar{c}_c(t) \approx -ig\eta_-\bar{c}_m(t) + \frac{2}{\sqrt{\kappa}}\bar{\xi}(t), \tag{1.86}$$

and for $\Delta_c = \omega_m$

$$\bar{c}_c(t) \approx -ig\eta_+\bar{c}_m^\dagger(t) + \frac{2}{\sqrt{\kappa}}\bar{\xi}(t), \tag{1.87}$$

where in both cases we dropped fast oscillating terms proportional to $\exp(\pm 2i\omega_m t)$ in a RWA. Plugging either (1.86) or (1.87) into (1.85) we obtain a noise operator $2\bar{\xi} - \bar{a}_{\text{in}}$. To find its properties we observe that

$$\langle \tilde{\xi}_-(t)\tilde{a}_{\text{in}}^\dagger(t')\rangle = \frac{\kappa}{2} e^{-\frac{\kappa}{2}(t - t')} \theta(t - t'), \tag{1.88}$$

where we defined the Heaviside step function[9]

$$\theta(t) = \begin{cases} 1 & t > 0 \\ \frac{1}{2} & t = 0 \\ 0 & t < 0 \end{cases}. \tag{1.89}$$

9. Here we used the fact that [EF07]

$$\int_{-\infty}^0 dt\,\delta(t) = \frac{1}{2}.$$

From this follows that $\langle \tilde{\xi}(t)\tilde{\xi}(t')^\dagger\rangle = \frac{1}{2}\langle \tilde{\xi}(t)\tilde{a}_{\text{in}}^\dagger(t')\rangle + \frac{1}{2}\langle \tilde{a}_{\text{in}}(t)\tilde{\xi}^\dagger(t')\rangle$ and thus the *exact* relation

$$\langle [2\tilde{\xi}(t) - \tilde{a}_{\text{in}}(t)][2\tilde{\xi}(t') - \tilde{a}_{\text{in}}(t')]^\dagger\rangle = \langle \tilde{a}_{\text{in}}(t)\tilde{a}_{\text{in}}^\dagger(t')\rangle. \tag{1.90}$$

As by definition we have $\langle \tilde{\xi}(t)\rangle = \langle \tilde{a}_{\text{in}}(t)\rangle = 0$, and $\tilde{\xi}$ and $\tilde{a}_{\text{in}}$ are Gaussian we find that $2\tilde{\xi}_- - \tilde{a}_{\text{in}} = \tilde{a}_{\text{in}}$, and thus also $2\bar{\xi}_- - \bar{a}_{\text{in}} = \bar{a}_{\text{in}}$,

in distribution. We can also show directly, by using the correlation function (1.75), that for $\delta t \gg 1/\kappa$ we have the identity $\bar{\xi} = \bar{a}_{\text{in}}$. Combining these considerations we obtain for $\Delta_{\text{c}} = -\omega_{\text{m}}$

$$\bar{c}_{\text{c}}(t) \approx -ig\eta_{-}\bar{c}_{\text{m}}(t) + \frac{2}{\sqrt{\kappa}}\bar{a}_{\text{in}}(t), \tag{1.91}$$

$$\bar{a}_{\text{out}}(t) \approx -i\sqrt{4g^2/\kappa}\,\bar{c}_{\text{m}}(t) + \bar{a}_{\text{in}}(t), \tag{1.92}$$

and for $\Delta_{\text{c}} = \omega_{\text{m}}$

$$\bar{c}_{\text{c}}(t) \approx -ig\eta_{+}\bar{c}_{\text{m}}^{\dagger}(t) + \frac{2}{\sqrt{\kappa}}\bar{a}_{\text{in}}(t), \tag{1.93}$$

$$\bar{a}_{\text{out}}(t) \approx -i\sqrt{4g^2/\kappa}\,\bar{c}_{\text{m}}^{\dagger}(t) + \bar{a}_{\text{in}}(t). \tag{1.94}$$

Finally note that for $\Delta_{\text{c}} = \pm\omega_{\text{m}}$ we have the identity $\tilde{\xi}_{\mp} = \tilde{\xi}$ [remember the definition of $\tilde{\xi}_{\mp}$, eq. (1.76)].

2.1 PULSED ENTANGLEMENT CREATION AND VERIFICATION

2

Entanglement creation between a mechanical oscillator and light [Pat+07; Gen+08b; MDC10; Vit+07b; GPZ10; Vit+07a; GBS11b; Abd+11; ME09], as well as between two mechanical oscillators [Man+02; ZPB03; Pin+05; Pir+06; HP08; Vac+08; HA09; VMT07; LHM10] has been analysed in a multitude of theoretical studies. These studies are mainly concerned with entanglement in the steady-state regime, where an optomechanical system driven by one or more continuous-wave light modes is prepared in a stationary non-separable multipartite state.

Our discussion of the optomechanical phase diagram showed that creation of steady-state entanglement is limited to a rather small parameter regime: For a blue detuned drive dynamical instability prevents formation of a steady state altogether, while in the red detuned regime entanglement reaches a maximum right at the stability border. Conversely, the amount of achievable entanglement is determined by the conditions guaranteeing the existence of a stationary state. This is of course a consequence of the amplifying two-mode squeezing dynamics [eq. (1.19)] which generate entanglement in the linear regime.

In this section we follow a different approach to generate optomechanical entanglement which circumvents these limitations; entanglement is created and verified by two subsequent pulses of light. Working in such a pulsed regime we do not rely on the existence of a steady state and thus provides us with the benefit of not being limited by any stability requirements. Additionally, the temporal ordering of pulses provides us with an unambiguous way to test light–matter entanglement, ruling out effects such as distribution of entanglement without entanglement [Cub+03; MK09]. As the generated state will exhibit strong Einstein–Podolsky–Rosen (EPR) correlations, the protocol can directly be extended into a continuous-variable teleportation protocol. The employed strategy has first been developed in the context of atomic ensembles [HPC05] and was later considered as a protocol for levitated nanospheres [Rom+11]. Entanglement between a mechanical oscillator and the electromagnetic field has for the first time been created in electromechanical systems [Pal+13] by employing the scheme analysed in this section.
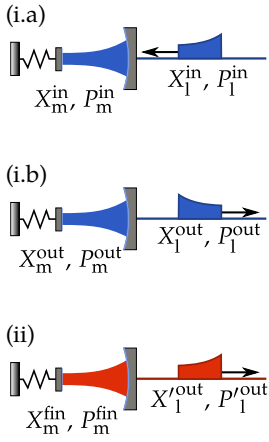
(i.a)

$X_\mathrm{m}^\mathrm{in}, P_\mathrm{m}^\mathrm{in}$ $X_\mathrm{l}^\mathrm{in}, P_\mathrm{l}^\mathrm{in}$

(i.b)

$X_\mathrm{m}^\mathrm{out}, P_\mathrm{m}^\mathrm{out}$ $X_\mathrm{l}^\mathrm{out}, P_\mathrm{l}^\mathrm{out}$

(ii)

$X_\mathrm{m}^\mathrm{fin}, P_\mathrm{m}^\mathrm{fin}$ $X_\mathrm{l}'^\mathrm{out}, P_\mathrm{l}'^\mathrm{out}$

FIG 13. Pulsed entanglement creation

2.1.1 *Protocol Outline and Central Results*

This protocol is operated in a regime of strong driving where we can linearize the dynamics. It is performed in two steps (see fig. 13): First, one drives the cavity with a blue-detuned laser pulse at $\Delta_\mathrm{c} = \omega_\mathrm{m}$ for a duration τ to resonantly enhance the optomechanical two-mode squeezing interaction (1.19) [fig. 13(i.a)]. For a sufficiently strong coupling this generates EPR entanglement between the travelling-wave light pulse and the mechanical oscillator. In a second step a red-detuned light pulse with a detuning $\Delta_\mathrm{c} = -\omega_\mathrm{m}$ is sent onto the cavity [fig. 13(ii)]. This resonantly drives the beam-splitter interaction (1.18) and hence swaps the mechanical state onto the light pulse. Measuring both pulses via homodyne detection and calculating their correlation function then allows us to verify entanglement between the first pulse and the mirror. We will now analyse this procedure in an ideal scenario to illustrate the central results.

In this section we impose the following conditions on the system's parameters: First, we assume to work in the resolved sideband regime ($\kappa \ll \omega_\mathrm{m}$) in order to strongly suppress the off-resonant optomechanical interaction terms (see section 1.2). Secondly, we assume a weak coupling $g \ll \kappa$ such that only first-order interaction of photons with the mechanics contribute. This allows us to adiabatically eliminate the cavity mode and invoke a rotating-wave-approximation in the interaction term. Additionally, we neglect mechanical decoherence effects for the moment. This is justified as long as the pulse duration is short compared to the *effective* mechanical coherence time, i.e., $\tau \ll 1/\gamma_\mathrm{m}\bar{n}$. The pulses are, on the other hand, chosen to be long on the timescale of one mechanical period, i.e., $\omega_\mathrm{m}\tau \gg 1$.[1] The pulses we assume to be flat-top pulses that have a constant amplitude $\varepsilon(t) \approx \sqrt{N_\mathrm{ph}/\tau}$ for the largest part, where N_ph is the total number of photons in the pulse. Their heads and tails are assumed to be short compared to their total duration, but smooth enough to permit the time-dependent linearization outlined in section 1.3.1. We can then model the optomechanical system in a quasi steady state with a coupling constant given by (assuming a one-sided cavity with $\kappa_\mathrm{in} = \kappa$)

$$g = g_0 \left(\frac{\kappa}{\Delta_\mathrm{c}^2 + \frac{\kappa^2}{4}} \frac{N_\mathrm{ph}}{2\tau} \right)^{\frac{1}{2}}. \tag{2.1}$$

Entanglement Creation

In the limit considered here we can use the adiabatic Langevin equation (1.47) which we for now simplify by setting $\Gamma_+ = G := 4g^2/\kappa$, $\Gamma_- = 0$ (rotating-wave approximation for $\Delta_\mathrm{c} = \omega_\mathrm{m}$) and $\gamma_\mathrm{m} = 0$.[2] All the perturbative effects neglected here will be included in the detailed discussion in section 2.1.2. We discuss in appendix 1.A that for

1. This discriminates the scheme at hand from short-pulsed regimes such as [Van+11] where $\omega_\mathrm{m}\tau \ll 1$.

2. Here we also neglect the shift $\delta\omega_\mathrm{m}$, a restriction which can easily be lifted.

$\Delta_c = \omega_m$ we obtain a simple equation of motion for the mechanical mode,

$$\dot{\bar{c}}_m = \frac{1}{2}G\bar{c}_m - i\sqrt{G}\bar{a}_{in}^\dagger, \tag{2.2}$$

where $\bar{a}_{in}$ is a time-coarse-grained noise process averaged over a duration δt [eq. (1.83)]. $\bar{a}_{in}$ is approximately white and thus δ-correlated on timescales much longer than δt. Equation (2.2) can be formally integrated to yield[3]

$$\bar{c}_m^\dagger(t) = e^{\frac{1}{2}Gt}\,\bar{c}_m^\dagger(0) + i\sqrt{G}\,e^{\frac{1}{2}Gt}\int_0^t ds\,e^{-\frac{1}{2}Gs}\,\bar{a}_{in}(s). \tag{2.3}$$

This equation shows that the mirror gets correlated with a light mode with a central frequency ω_c (as $\bar{a}_{in}$ describes the scattering of photons from the laser frequency at ω_0 into the lower mechanical sideband at $\omega_0 - \omega_m = \omega_c$), with an exponentially shaped envelope $\alpha_{in}(t) \propto e^{-\frac{1}{2}Gt}$. In the same manner we simplify the adiabatic solution for the cavity [eq. (1.73)] by setting $\eta_+ = 2/\kappa$ and $\eta_- = 0$, and again applying the coarse-graining procedure. This leaves us with [see eq. (1.87)]

$$\bar{c}_c(t) = -i\frac{2g}{\kappa}\bar{c}_m^\dagger(t) + \frac{2}{\sqrt{\kappa}}\bar{a}_{in}(t). \tag{2.4}$$

Using the input–output relations $\bar{a}_{out} = \sqrt{\kappa}\bar{c}_c - \bar{a}_{in}$ now allows us to define a set of normalized temporal light modes which carry the entanglement to the mirror. We find by using solutions (2.3) and (2.4), that

$$\begin{aligned}\bar{a}_{out}(t) &= -i\sqrt{G}\bar{c}_m^\dagger(t) + \bar{a}_{in}(t)\\ &= -i\sqrt{G}\,e^{\frac{1}{2}Gt}\,c_m^\dagger(0) + G\,e^{\frac{1}{2}Gt}\int_0^t ds\,e^{-\frac{1}{2}Gs}\,\bar{a}_{in}(s) + \bar{a}_{in}(t).\end{aligned} \tag{2.5}$$

Equations (2.3) and (2.5) connect the state of the mirror to the state of the outgoing light field. This prompts us to introduce normalized temporal modes of the field,

$$A_{in} = \int_0^\tau dt\,\alpha_{in}(t)\bar{a}_{in}(t), \qquad \alpha_{in}(t) = \sqrt{\frac{G}{1 - e^{-G\tau}}}\,e^{-\frac{G}{2}Gt} \tag{2.6a}$$

$$A_{out} = \int_0^\tau dt\,\alpha_{out}(t)\bar{a}_{out}(t), \quad \alpha_{out}(t) = \sqrt{\frac{G}{e^{G\tau}-1}}\,e^{\frac{1}{2}Gt} \tag{2.6b}$$

which in our current approximation obey canonical commutation relations $[A_{in}, A_{in}^\dagger] = [A_{out}, A_{out}^\dagger] = 1$. Together with the definitions $B_{in} = \bar{c}_m(0)$ and $B_{out} = \bar{c}_m(\tau)$ we can derive scattering relations which relate the mechanical and optical mode at the end of the pulse $t = \tau$ to their initial state at $t = 0$.

3. The involved integrals over the time-averaged noise processes make sense as $e^{-\frac{1}{2}Gt}$ is slowly varying on a timescale δt.

We plug (2.5) into the definition of A_{out}, and obtain

$$
\begin{aligned}
A_{\text{out}} = &- \mathrm{i} \frac{G}{\sqrt{\mathrm{e}^{G\tau} - 1}} \int_0^\tau \mathrm{d}t \, \mathrm{e}^{Gt} \, \bar{c}_{\text{m}}^\dagger(0) \\
&- \sqrt{\frac{G}{\mathrm{e}^{G\tau} - 1}} \int_0^\tau \mathrm{d}t \left[G \, \mathrm{e}^{Gt} \int_0^t \mathrm{d}s \, \mathrm{e}^{-\frac{1}{2} Gs} \, \bar{a}_{\text{in}}(s) + \mathrm{e}^{\frac{1}{2} Gt} \, \bar{a}_{\text{in}}(t) \right] \\
= &- \mathrm{i} \sqrt{\mathrm{e}^{G\tau} - 1} \, \bar{c}_{\text{m}}^\dagger(0) \\
&- \sqrt{\frac{G}{\mathrm{e}^{G\tau} - 1}} \int_0^\tau \mathrm{d}s \left[G \, \mathrm{e}^{-\frac{1}{2} Gs} \, \bar{a}_{\text{in}}(s) \int_s^\tau \mathrm{d}t \, \mathrm{e}^{Gt} + \mathrm{e}^{\frac{1}{2} Gs} \, \bar{a}_{\text{in}}(t) \right] \\
= &- \mathrm{i} \sqrt{\mathrm{e}^{G\tau} - 1} \, B_{\text{in}}^\dagger + \sqrt{\frac{G}{1 - \mathrm{e}^{-G\tau}}} \int_0^\tau \mathrm{d}s \, \mathrm{e}^{-\frac{1}{2} Gs} \, \bar{a}_{\text{in}}(s),
\end{aligned}
$$

where in the second line we used the identity

$$
\int_0^\tau \mathrm{d}s \int_0^s \mathrm{d}s' h(s, s') = \int_0^\tau \mathrm{d}s' \int_{s'}^\tau \mathrm{d}s \, h(s, s'),
$$

for an integrable function h. Using this and eq. (2.3) we finally obtain

$$
A_{\text{out}} = \mathrm{e}^{\frac{1}{2} G\tau} A_{\text{in}} - \mathrm{i} \sqrt{\mathrm{e}^{G\tau} - 1} B_{\text{in}}^\dagger, \tag{2.7a}
$$

$$
B_{\text{out}} = \mathrm{e}^{\frac{1}{2} G\tau} B_{\text{in}} - \mathrm{i} \sqrt{\mathrm{e}^{G\tau} - 1} A_{\text{in}}^\dagger. \tag{2.7b}
$$

Physically, the rising pulse shape of the output mode is due to the two-mode optomechanical squeezing interaction, which amplifies the mirror motion.[4] The photons scattered into the cavity resonance in this way contribute to the entanglement of the pulse to the mirror.

By expressing equations (2.7) in terms of quadratures $X_{\text{m}}^i = (B_i + B_i^\dagger)/\sqrt{2}$ and $X_{\text{l}}^i = (A_i + A_i^\dagger)/\sqrt{2}$, where $i \in \{\text{in}, \text{out}\}$, and their corresponding conjugate variables, we can calculate the so-called EPR variance Δ_{EPR} of the state after the interaction. For light initially in vacuum $(\Delta X_{\text{l}}^{\text{in}})^2 = (\Delta P_{\text{l}}^{\text{in}})^2 = \frac{1}{2}$ and the mirror in a thermal state $(\Delta X_{\text{m}}^{\text{in}})^2 = (\Delta P_{\text{m}}^{\text{in}})^2 = n_0 + \frac{1}{2}$, the state is entangled if [Dua+00; Simo0][5]

$$
\begin{aligned}
\Delta_{\text{EPR}} &= \left[\Delta(X_{\text{m}}^{\text{out}} + P_{\text{l}}^{\text{out}}) \right]^2 + \left[\Delta(P_{\text{m}}^{\text{out}} + X_{\text{l}}^{\text{out}}) \right]^2 \\
&= 2(n_0 + 1) \left(\mathrm{e}^r - \sqrt{\mathrm{e}^{2r} - 1} \right)^2 < 2,
\end{aligned} \tag{2.8}
$$

where $r = \frac{1}{2} G\tau$ is the *squeezing parameter* and n_0 the initial occupation number of the mechanical oscillator. Note that in the limit of large squeezing $r \gg 1$ we find that the variance $\Delta_{\text{EPR}} \approx (n_0 + 1) \mathrm{e}^{-2r}/2$ is suppressed exponentially, which shows that the created state approximates a two-mode-squeezed state, and thus, asymptotically, an EPR state. Therefore, this state can be readily used to conduct optomechanical teleportation as described in a later section.

4. This is nicely illustrated by the experimental data shown in [Pal+13].

5. Note that in this form this criterion is only sufficient.

squeezing parameter

Rearranging (2.8), we find that the state is entangled as long as

$$r > r_0 = \frac{1}{2} \ln \left(\frac{(n_0 + 2)^2}{4(n_0 + 1)} \right) \overset{n_0 \to \infty}{\sim} \frac{1}{2} \ln n_0. \tag{2.9}$$

This illustrates that in this scheme the requirement on the strength of the effective optomechanical interaction, as quantified by the parameter $r = 2g^2 \tau / \kappa$, scales logarithmically with the initial mechanical occupation number n_0. This scaling eases the protocol's experimental realization, as neither g nor τ can be arbitrarily increased—both for fundamental and technical reasons—, as we will show in section 2.1.2. Note that n_0 need not be equal to the mean bath occupation $\bar{n}$, but may be decreased by laser pre-cooling to improve the protocol's performance.

Entanglement Verification

To verify the successful creation of entanglement a red detuned laser pulse ($\Delta_c = -\omega_m$) is sent to the cavity where it resonantly drives the beam-splitter interaction, and hence generates a state swap between the mechanical and the optical mode.

We now use $\Gamma_- = G = 4g^2 / \kappa$, $\Gamma_+ = 0$ and $\gamma_m = 0$ and repeat the procedure from the previous section. This leaves us with the solutions

$$\bar{c}_m(t) = e^{-\frac{1}{2}Gt} \bar{c}_m(0) - i\sqrt{G} \, e^{-\frac{1}{2}Gt} \int_0^t ds \, e^{\frac{1}{2}Gs} \bar{a}_{in}(s), \tag{2.10a}$$

$$\bar{c}_c(t) = -i\frac{1}{2}G\bar{c}_m(t) + \frac{2}{\sqrt{\kappa}} \bar{a}_{in}(t) \tag{2.10b}$$

By defining modified mode functions $\alpha'_{in(out)} = \alpha_{out(in)}$ and corresponding light modes $A'_{in(out)}$ one obtains scattering relations in analogy the ones in eq. (2.7),

$$A'_{out} = e^{-\frac{1}{2}G\tau} A'_{in} + i\sqrt{1 - e^{-G\tau}} B'_{in}, \tag{2.11a}$$

$$B'_{out} = e^{-\frac{1}{2}G\tau} B'_{in} + i\sqrt{1 - e^{-G\tau}} A'_{in}. \tag{2.11b}$$

Again the pulse shape is determined by the optomechanical interaction, which here dampens the mirror motion (due to the resonant beam-splitter dynamics) and thus leads to an exponentially decreasing scattering into the cavity resonance. As the read out happens directly after the entanglement creation in the protocol we can set $B'_{in} = B_{out} = \bar{c}_m(\tau)$, while $B'_{out} = \bar{c}_m(2\tau)$ is the mirror state after the second pulse. The pulsed state-swapping operation therefore also features an exponential scaling with $G\tau$. For $G\tau \to \infty$ the expressions above reduce to $A'_{out} = iB'_{in}$ and $B'_{out} = iA'_{in}$, which shows that in this case the mechanical state—apart from a phase shift—is perfectly transferred to the optical mode. In the Schrödinger-picture

this amounts to the transformation $|\varphi\rangle_m |\psi\rangle_l \to |\psi\rangle_m |\varphi\rangle_l$, where φ and ψ constitute the initial state of the mechanics and the light pulse, respectively.

The state-swap operation allows us to access mechanical quadratures by measuring quadratures of light and thus to verify the created optomechanical entanglement. This can be achieved in several ways. The most straightforward way is to directly correlate the entangling and the read-out pulse, which gives access to the EPR variance Δ'_{EPR} between both pulses. Note that due to the phase shift introduced by the read-out we have to correlate a different combination of quadratures. We define

$$\Delta'_{\mathrm{EPR}} = \left[\Delta(X_l^{\mathrm{out}'} - X_l^{\mathrm{out}})\right]^2 + \left[\Delta(P_l^{\mathrm{out}'} + P_l^{\mathrm{out}})\right]^2, \tag{2.12}$$

which is constructed such that in the limit of $G\tau \to \infty$ in the read-out we have $\Delta'_{\mathrm{EPR}} \to \Delta_{\mathrm{EPR}}$. Another, however experimentally much more demanding, possibility is to reconstruct the full state of the bipartite system via optical homodyne tomography, as we will discuss in the next section. Having obtained the full quantum state, entanglement can be analysed by various means [AI07], for example, by evaluating its logarithmic negativity $E_{\mathcal{N}}$.

Optomechanical Teleportation Protocol

As we have shown above, pulsed operation allows us to create EPR-type entanglement, which forms the central entanglement resource of many quantum information processing protocols [BL05]. An immediate extension of this scheme is an optomechanical continuous-variables (CV) quantum teleportation protocol. The main idea of quantum state teleportation in this context is to transfer an arbitrary and unknown quantum state $|\psi_{\mathrm{in}}\rangle$ of a travelling-wave light pulse onto the mechanical resonator, without any direct interaction between the two systems, but by making use of optomechanical entanglement instead. The scheme works in full analogy to the continuous-variable teleportation protocol for photons [Vai94; BK98]. Due to its pulsed nature it closely resembles the scheme used in atomic ensembles [HPC05; She+06] and it has also been suggested in the context of levitated microspheres [Rom+11] [see fig. 15(i) for a schematic of the setup and fig. 14 for a phase-space description]: A light pulse (A) is sent to the optomechanical cavity and is entangled with its mechanical mode (B) via the entangling dynamics described above. Meanwhile a second pulse (V) is prepared in the state $|\psi_{\mathrm{in}}\rangle$, which is to be teleported [fig. 14(i)]. This pulse then interferes with A on a beam splitter. In the output ports of the beam splitter, two homodyne detectors measure two joint quadratures $P_l^{\mathrm{out}} + X_v$ and $X_l^{\mathrm{out}} + P_v$, yielding outcomes m_X and m_P, respectively. This constitutes the analogue to the Bell measurement in the case of qubit teleportation and effectively projects previously unrelated systems
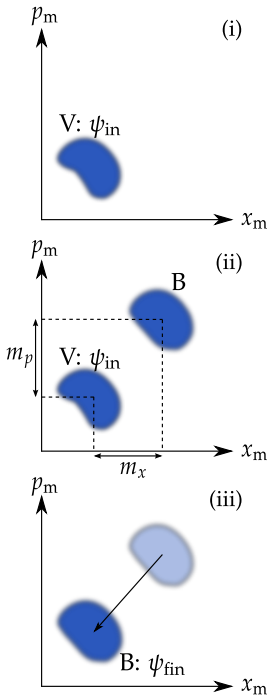

FIG 14. Phase-space description of CV teleportation

A and V onto an EPR state [Bou+97; Fur+98]. The resulting state of mode B is thus displaced in phase-space by (m_x, m_p) [fig. 14(ii)]. Note that both the second pulse and the local oscillator for the homodyne measurements must be mode-matched to A after the interaction; i. e., they must possess the identical carrier frequency as well as the same exponential envelope. The protocol is concluded by displacing the mirror in position and momentum by m_X and m_P according to the outcome of the Bell-measurement [fig. 14(iii)]. This can be achieved by means of short light pulses, applying the methods described in [Van+11; Cer+11]. After the feedback the mirror is then described by [BL05]

$$X_m^{fin} = X_m^{out} + P_l^{out} + X_v,$$
$$= X_v + \left(e^r - \sqrt{e^{2r} - 1}\right)(X_m^{in} - P_l^{in}), \qquad (2.13a)$$

$$P_m^{fin} = P_m^{out} + X_l^{out} + P_v,$$
$$= P_v + \left(e^r - \sqrt{e^{2r} - 1}\right)(P_m^{in} - X_l^{in}), \qquad (2.13b)$$

which shows that its final state corresponds to the input state plus quantum noise contributions. It is obvious from these expressions that the total noise added to both quadratures [second term in (2.13a) and (2.13b), respectively] is equal to the EPR variance. Again, for large squeezing $r \gg 1$ the noise terms are exponentially suppressed and in the limit $r \to \infty$, where the resource state approaches the EPR state, we obtain perfect teleportation fidelity, i. e., $X_m^{fin} = X_v$ and $P_m^{fin} = P_v$. In particular this operator identity means, that *all* moments of X_v, P_v with respect to the input state $|\psi_{in}\rangle$ will be transferred to the mechanical oscillator, and hence its final state will be identically given by $|\psi_{in}\rangle$. To verify the success of the teleportation one has to read out the mirror state after completing the feedback step. This can be achieved by applying tomography on the mechanical state. After the teleportation is completed a second, red detuned pulse is employed to read out the mirror state as described above. It is then sent to a homodyne detection setup where a quadrature $X_l'(\theta) = X_l^{out}\cos(\theta) + P_l^{out}\sin(\theta)$ (θ being the local oscillator phase) is measured. For the case of a perfect state swap this yields the mechanical quadrature $X_l'(\theta) = X_m(\theta + \frac{\pi}{2})$. Here the rotation by $\frac{\pi}{2}$ is due to the phase shift from the swap operation. By repeating this process multiple times for different local-oscillator phases θ_j, the final quantum state of the mechanical system ρ_{out} can be reconstructed. The overlap of the reconstructed state ρ_{out} and a pure input state $|\psi_{in}\rangle$ then gives the teleportation fidelity $F = \langle\psi_{in}|\rho_{out}|\psi_{in}\rangle$. For coherent input states the fidelity is given by

$$F = \left(1 + \frac{\Delta_{EPR}}{2}\right)^{-1}. \qquad (2.14)$$
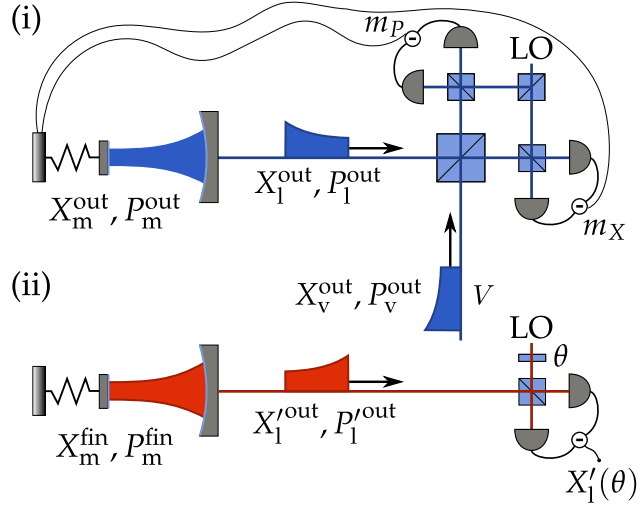
43

FIGURE 15. Setup for the optomechanical teleportation protocol: (i) A CV Bell measurement is used to make a joint measurement on the output light of the optomechanical cavity and a second pulse prepared in the input state. The result (m_X, m_P) is fed back to the mechanical oscillator, displacing it in phase space [see fig. 14]. (ii) Homodyne tomography operated on the red mechanical sideband is used to evaluate the success of the teleportation.

In order to beat the optimal classical strategy for transmission of quantum states (i.e., the optimal measure-and-prepare scheme), the achieved fidelity (averaged over all coherent states) must exceed $F > 1/2$ [Ham+05], which is equivalent to the condition for entanglement, $\Delta_{\mathrm{EPR}} < 2$.

In section 3.3 we will discuss a time-continuous version of the teleportation protocol, which allows us to prepare the mechanical oscillator in a squeezed steady state.

2.1.2 *Full Dynamics*

In the previous section we found that in the ideal scenario the amount of entanglement essentially depends only on the coupling strength (or equivalently on the input laser power) and the duration of the laser pulse, and that it shows an encouraging scaling, growing exponentially with $G\tau$. This in turn means that the minimal amount of two-mode squeezing needed to generate entanglement only grows logarithmically with the initial mechanical occupation n_0. In this section we will develop a more realistic scenario including thermal noise effects and the full system dynamics, both of which will decrease the created entanglement. We will show, however, that one can find an optimal working point such that the significance of these unwanted effects can be suppressed sufficiently strongly.

Perturbative Dynamics

To extend the validity of the previous, simplified model, we now include the following additional dynamics: contributions from the beam-splitter Hamiltonian, higher order interactions beyond the adiabatic approximation, and decoherence effects due to mechanical coupling to a heat bath. Including the above-mentioned perturbations results in a final state that deviates from an EPR-entangled state. To minimize the extent of these deviations, the system parameters must obey the following conditions:

1. Working in the sideband-resolved regime $\kappa \ll \omega_{\mathrm{m}}$ results in a sharply peaked cavity response and implies that the down-conversion dynamics is heavily enhanced with respect to the suppressed beam-splitter interaction.

2. The weak-coupling condition $g \lesssim \kappa$ inhibits multiple interactions of a single photon with the mechanical mode before it leaves the cavity. This suppresses spurious correlations with the intracavity field. It also minimizes pulse distortion which would lead to a mode mismatch with the selected exponential light modes.

3. $g\tau \gg 1$ is needed in order to create sufficiently strong entanglement. This is due to the fact that the squeezing parameter $r = (g/\kappa)g\tau$ should be large, while g/κ needs to be small.

4. The whole protocol needs to be operated within the mechanical coherence time, i.e., $\bar{n}\gamma_{\mathrm{m}}\tau \ll 1$. This assures coherent dynamics over the full duration of the protocol, which is an essential requirement for observing quantum effects. As the thermal occupation of the mechanical bath may be considerably large even at cryogenic temperatures, this poses (for fixed γ_{m} and $\bar{n}$) a very strict upper limit to the pulse duration τ.

Note however that not all of these inequalities have to be fulfilled equally strictly, but there rather exists an optimum which arises from balancing all contributions. It turns out that fulfilling (4) is critical for successful entanglement generation, whereas (1)–(3) only need to be weakly satisfied. Taking the above considerations into account, we find a sequence of parameter inequalities

$$\bar{n}\gamma_{\mathrm{m}} \ll \frac{1}{\tau} \ll g \ll \kappa \ll \omega_{\mathrm{m}}, \tag{2.15}$$

which defines the optimal parameter regime. It is convenient to introduce the following dimensionless parameters: the sideband-resolution parameter η, the adiabaticity parameter ζ, and the ratio of pulse length to mechanical coherence time ϵ. They are given by

$$\eta = \kappa/\omega_{\mathrm{m}}, \qquad \zeta = g/\kappa, \qquad \epsilon = \gamma_{\mathrm{m}}\tau.$$

From (2.15) it follows that $\eta \ll 1$, $\zeta \ll 1$ and $\epsilon \ll 1/\bar{n}$. In section 2.1.1 we assumed all these conditions to be well satisfied and we completely neglected the existence of mechanical decoherence. If we now take into account that the mechanical oscillator couples to a heat bath with an effective decoherence rate $\bar{n}\gamma_{\mathrm{m}}$, we find that increasing the pulse duration to values larger than the mechanical coherence time will drastically decrease entanglement. This results in an upper bound for entanglement, as now both the interaction strength and the pulse duration, and therefore also the squeezing parameter $r = (g/\kappa)g\tau$, are bounded from above.

Dividing (2.15) by γ_{m} and taking a look at the outermost condition $\bar{n} \ll Q_{\mathrm{m}}$, where $Q_{\mathrm{m}} = \omega_{\mathrm{m}}/\gamma_{\mathrm{m}}$ is the mechanical quality factor, we see that the ratio $Q_{\mathrm{m}}/\bar{n}$ defines the range which all the other parameters have to fit into. It is intuitively clear, that a high quality factor and a low bath occupation number—and consequently a low effective mechanical decoherence rate—are favourable for the success of the protocol. Equivalently, we can rewrite the occupation number as $\bar{n} = k_{\mathrm{B}}T_{\mathrm{bath}}/\hbar\omega_{\mathrm{m}}$ and therefore find $k_{\mathrm{B}}T_{\mathrm{bath}}/\hbar \ll Q_{\mathrm{m}} \cdot \omega_{\mathrm{m}}$, where now the Qf-product ($f_{\mathrm{m}} = \omega_{\mathrm{m}}/2\pi$) has to be compared to the thermal frequency of the bath. Let us consider a numerical example for the system employed in [Pal+13]: For a temperature $T_{\mathrm{bath}} \approx 20\,\mathrm{mK}$ the left-hand side gives $k_{\mathrm{B}}T_{\mathrm{bath}}/\hbar \approx 2\pi \cdot 3 \cdot 10^{9}\,\mathrm{Hz}$. The Qf-product consequently has to be several orders of magnitude larger to successfully create entanglement. For the quoted system we find $Q_{\mathrm{m}} \cdot f_{\mathrm{m}} \approx 2\pi \cdot 3 \cdot 10^{12}\mathrm{Hz}$, and other current optomechanical setups feature a Qf-product of up to $10^{14}\,\mathrm{Hz}$ and above [AKM14]. Note that in an experiment T_{bath} will often depend on the input laser power, as scattered light can heat up the cryogenic environment. Hence, for a given bath occupation the coupling strength may be limited for technical reasons.

We can also connect the sequence of inequalities (2.15) to the optomechanical cooperativity C. To do this we first write the squeezing parameter as $r = G\tau/2 \approx \epsilon\bar{n}C/2$. Following the arguments above we require $\epsilon \ll 1/\bar{n}$, which means that we must have $r \ll C$. On the other hand we need a certain amount of squeezing in order to create entanglement, i.e., $r \gg r_0$, where r_0 is a monotonically increasing function of the initial mechanical occupation n_0. Combining these considerations to $r_0 \ll r \ll C$ we see that we can either have a large cooperativity such that we can tolerate a large n_0 (and thus a large r_0), or we prepare an initial state with a low n_0 (and thus a small r_0). The connection between the two situations is given by the pulse length τ. In the former case we work with a high-Q oscillator which allows us to increase the pulse length in order to generate entanglement without suffering from mechanical decoherence; in the latter a short pulse is sufficient to create the required amount of two-mode squeezing. For realistic parameters of r_0 this means that we have to

operate the protocol in the strong-cooperativity regime $C > 1$, as will be illustrated in the discussion of figs. 16 and 17.

In the following we will investigate the effect of the perturbative dynamics discussed above on the protocol and optimize the generated entanglement with respect to the parameters ζ, η and ϵ.

Solving the System

Essentially we have to solve the full (linearized) Langevin equations (1.38) for a chosen classical steady state α^{ss}. We write them in vector form $\dot{X} = FX + X^{in}$, where we collect $X = (x_m, p_m, x_c, p_c)^T$, and $X^{in} = (0, \sqrt{\gamma_m}f, \sqrt{2\kappa}x_{in}, \sqrt{2\kappa}p_{in})^T$ as before. The solutions to this linear set of equations is readily found by variation of constants, yielding

$$X(t) = R(t)X(0) + \int_0^t d\tau R(t - \tau)X^{in}(\tau), \qquad (2.16)$$

where $R(t) = \exp(Ft)$ is the fundamental solution. In order to calculate Δ_{EPR} we decompose R into block form as

$$R = \begin{pmatrix} R_{mm} & R_{ml} \\ R_{lm} & R_{ll} \end{pmatrix}, \qquad (2.17)$$

and define $X_m = (x_m, p_m)^T$ and $X_l = (x_c, p_c)^T$ together with the corresponding vectors X_m^{out}, X_l^{out} and X_l^{in}, X_m^{in}. Setting $t = \tau$ then directly leads to

$$X_m^{out} = R_{mm}(\tau)X_m(0) + R_{ml}(\tau)X_l(0)$$
$$+ \int_0^\tau dt R_{mm}(\tau - t)X_m^{in}(t) + \int_0^\tau dt R_{ml}(\tau - t)X_l^{in}(t). \quad (2.18)$$

Using input–output relations and extracting the output mode α_{out} leads to

$$X_l^{out} = \left[\sqrt{\kappa} \int_0^\tau dt\, \alpha_{out}(t)R_{lm}(t) \right] X_m(0)$$
$$+ \left[\sqrt{\kappa} \int_0^\tau dt\, \alpha_{out}(t)R_{ll}(t) \right] X_l(0)$$
$$+ \int_0^\tau ds \left[\sqrt{\kappa} \int_s^t dt\, \alpha_{out}(t)R_{lm}(t - s) \right] X_m^{in}(s)$$
$$+ \int_0^\tau ds \left\{ \sqrt{\kappa} \int_s^t dt\, \alpha_{out}(t)[R_{ml}(t - s) - \mathbb{1}] \right\} X_l^{in}(s). \quad (2.19)$$

We can therefore express the full scattering relation as ($i \in \{m,l\}$)

$$X_i^{out} = R_{im}^{out}X_m(0) + R_{il}^{out}X_l(0)$$
$$+ \int_0^\tau ds\, \alpha_{im}^{out}(s)X_m^{in}(s) + \int_0^\tau ds\, \alpha_{il}^{out}(s)X_l^{in}(s). \quad (2.20)$$

To make these unwieldy expressions more tractable we simplify them in the following way. First, we drop the mechanical damping from the first term; thus we set $\mathbf{R}_{\mathrm{out}} \approx \mathbf{R}_{\mathrm{out}}|_{\gamma_{\mathrm{m}}=0}$. This amounts to dropping $-\gamma_{\mathrm{m}} p_{\mathrm{m}}$ from eq. (1.38c) and yields corrections of order $\mathcal{O}(\epsilon)$, which will, as discussed above, be smaller than $1/\bar{n}$. Second we approximate the mechanical noise contribution [last term in eq. (2.20)] by only keeping the free, harmonic evolution while neglecting the coupling to the optical mode. The coupling is a second order process and is therefore suppressed by an additional factor of ζ. Note that by doing so we overestimate the effect of mechanical noise, as it contributes to the creation of optomechanical correlations when subject to the coherent dynamics. In this approximation the corresponding mode function simplifies to the diagonal matrix $\boldsymbol{\alpha}_{\mathrm{m}}^{\mathrm{out}}(t) \approx \sqrt{\gamma_{\mathrm{m}}}\mathrm{diag}(\sin(\omega_{\mathrm{m}}t), \cos(\omega_{\mathrm{m}}t), 0, 0)$. This leads us to define (co)sine components $F_{(p),x}$ of the noise input via[6]

$$i\sqrt{\gamma_{\mathrm{m}}} \int_0^{\tau} \mathrm{d}t\, e^{-i\omega_{\mathrm{m}}t} f(t) =: \sqrt{\frac{\gamma_{\mathrm{m}}\tau}{2}}(F_x + iF_p). \tag{2.21}$$

We thus effectively work with weakly perturbed mirror variables

$$X_{\mathrm{m}}^{\mathrm{out}} \approx X_{\mathrm{m}}^{\mathrm{out}}|_{\gamma_{\mathrm{m}}=0} + \sqrt{\epsilon}F_x, \tag{2.22a}$$

$$P_{\mathrm{m}}^{\mathrm{out}} \approx P_{\mathrm{m}}^{\mathrm{out}}|_{\gamma_{\mathrm{m}}=0} + \sqrt{\epsilon}F_p, \tag{2.22b}$$

while we neglect the mechanical noise contribution to the optical mode, i.e., $X_{\mathrm{l}}^{\mathrm{out}} \approx X_{\mathrm{l}}^{\mathrm{out}}|_{\gamma_{\mathrm{m}}=0}$ and $P_{\mathrm{l}}^{\mathrm{out}} \approx P_{\mathrm{l}}^{\mathrm{out}}|_{\gamma_{\mathrm{m}}=0}$. From the commutation relations of the Brownian noise term [eq. (1.27)] it directly follows that

$$[F_x, F_x] = [F_p, F_p] = i + \mathcal{O}(\omega_{\mathrm{m}}\tau)^{-1}, \tag{2.23a}$$

$$[F_x, F_p] = [F_p, F_x] = \mathcal{O}(\omega_{\mathrm{m}}\tau)^{-1}, \tag{2.23b}$$

where the correction $1/\mathcal{O}(\omega_{\mathrm{m}}\tau)$ is small in the long-pulsed regime we are working in. The perturbed variables (2.22) therefore approximately obey canonical commutation relations $[X_{\mathrm{m}}^{\mathrm{out}}, P_{\mathrm{m}}^{\mathrm{out}}] = i(1 + \epsilon)$. From the correlation functions for f (1.26b) we can deduce $\langle F_i F_i \rangle = \bar{n} + \frac{1}{2}$ for $i \in \{c, s\}$. Using this we find for the EPR-variance

$$\Delta_{\mathrm{EPR}} = \left\{[\Delta(X_{\mathrm{m}}^{\mathrm{out}} + P_{\mathrm{m}}^{\mathrm{out}})]^2 + [\Delta(P_{\mathrm{m}}^{\mathrm{out}} + X_{\mathrm{m}}^{\mathrm{out}})]^2\right\}_{\gamma_{\mathrm{m}}=0}$$
$$+ (2\bar{n} + 1)\epsilon, \tag{2.24}$$

which can be evaluated by using eq. (2.20). The resulting expression now includes noise terms from the initial intracavity field and the extra light modes (both assumed to be in vacuum). The latter contributions are given by the overlap of the different light modes, yielding a covariance matrix

$$\frac{1}{2}\int_0^{\tau} \mathrm{d}t\boldsymbol{\alpha}_{\mathrm{ll}}^{\mathrm{out}}(t)[\boldsymbol{\alpha}_{\mathrm{ll}}^{\mathrm{out}}(t)]^{\mathrm{T}}. \tag{2.25}$$

Δ_{EPR} is an involved function of the parameters ϵ, η, ζ and is not presented here; instead we now evaluate the generated entanglement numerically.

Results

As illustrated above, we expect—for fixed values of $\bar{n}$ and Q_{m}—to find optimal values for the remaining parameters ϵ, ζ and η. The maximal possible entanglement will ultimately be set by $\bar{n}$ and Q_{m}, which will also constitute hard boundaries in typical experiments.

Figure 16 shows results of this optimization for different Q-factors, plotted against the thermal occupation number of the mechanical bath. Figure (a) shows the minimal value of Δ_{EPR} for a given Q_{m}, and (b)–(d) show the corresponding optimal values for η_{opt}, ζ_{opt} and ϵ_{opt}. As expected the noise contribution from the mechanical bath is found to be the most critical.

The dashed curves in figure (a) illustrate the noise contribution $(2\bar{n} + 1)\epsilon_{\text{opt}}$ of the thermal bath. As shown above, this quantity is added to the unperturbed EPR variance, and thus the system can only exhibit strong entanglement if its value is far below two. Note that working at the optimal point keeps the fraction of thermal noise in Δ_{EPR} approximately constant over a wide range of $\bar{n}$. This is shown in figure (e), where we defined $\epsilon'_{\text{opt}} = \epsilon_{\text{opt}}/\Delta_{\text{EPR}}$.

As we have seen in the previous section, the EPR variance depends on the occupation number of the oscillator at the initial time $t = 0$. Due to this, the entanglement can be drastically increased by precooling the mechanics by means of laser cooling before starting the actual protocol. Figure 16 shows that it is thus possible to create an entangled state even for a fairly large bath occupation. This works due to short pulse durations, during which the mechanical decoherence is small. Taking a look at figure (c) we note that the sideband-resolution shows rather large optimal values near unity, especially for increasing occupation numbers. This indicates that the beam-splitter dynamics only weakly disturbs the entangling interaction.

As they stand the, optimized parameters from fig. 16 correspond to a very high optomechanical cooperativity. This is, however, not a requirement, as is illustrated in fig. 17. For these plots the EPR-variance is optimized with respect to ϵ for fixed parameters $\eta = 2/100$, $Q_{\text{m}} = 3 \cdot 10^6$ and $\bar{n} = 40$ (which roughly corresponds to the parameters from [Pal+13]). Figure 17(a) shows that entanglement can be produced for $C \gtrsim 1$, depending on the initial mechanical occupation number n_0. As we discussed above a high n_0 requires a large squeezing parameter r to create entanglement, which, for a fixed value of C leads to a large value for ϵ (i. e., a long pulse duration τ) and large contributions from mechanical decoherence effects [yellow curves in fig. 17]. For low initial mechanical occupation short pulses and little squeezing suffice,
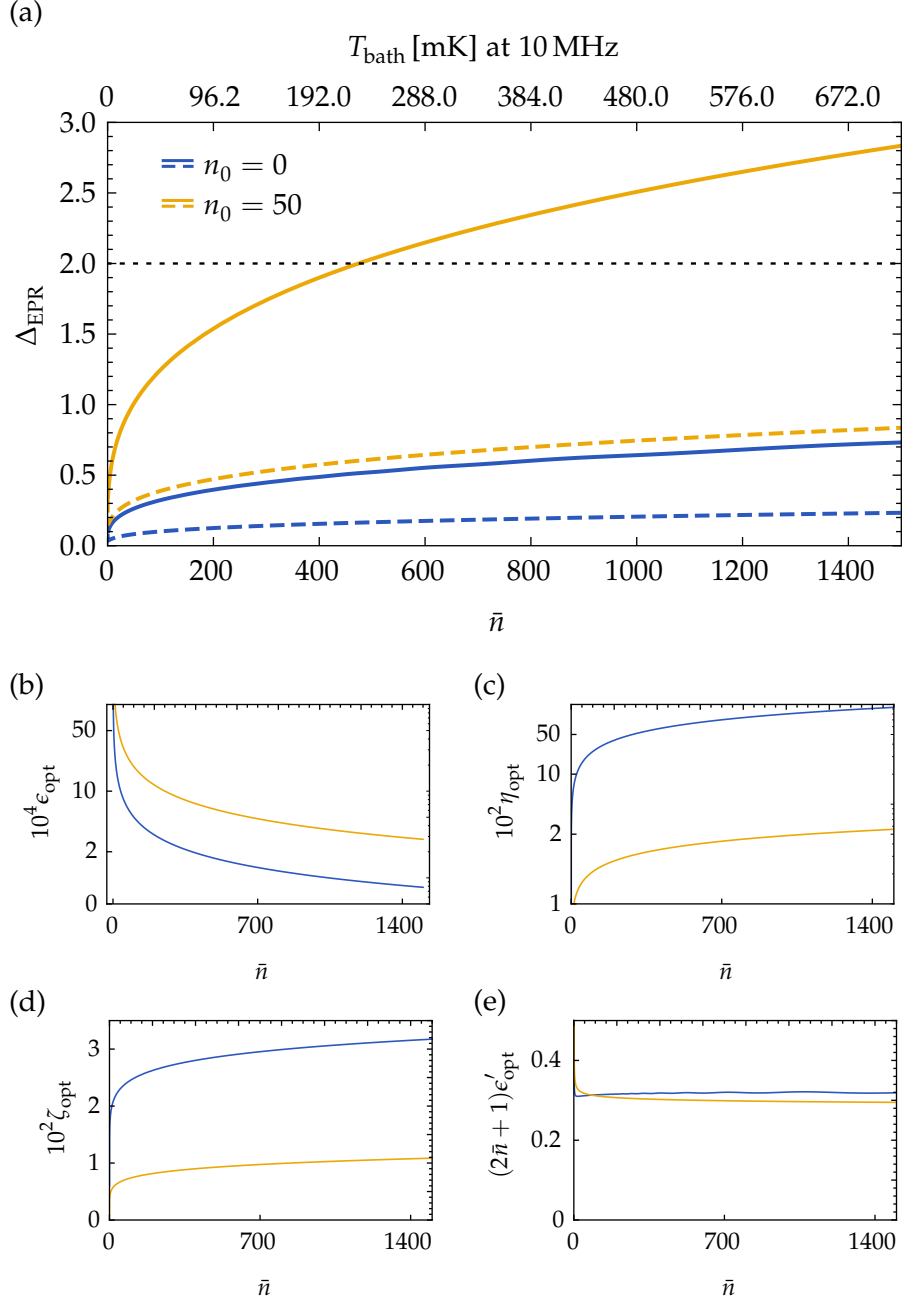
FIGURE 16. Optimized parameters for $Q_m = 10^7$ and $n_0 = 50$ (blue line), and $Q_m = 10^5$ and $n_0 = 0$ (yellow line), where n_0 is the initial mechanical occupation and $\bar{n}$ is the mean bath occupation. This corresponds to the two cases of large Q_m with moderate pre-laser-cooling, and lower Q_m with pre-cooling into the ground state. Clearly, entanglement creation is possible in both cases. (a) Minimal Δ_{EPR} as a function of $\bar{n}$. The upper axis gives the corresponding bath temperature for a oscillator with a resonance frequency of 3.8 MHz. To each point corresponds a triple ϵ_{opt}, η_{opt}, ζ_{opt} [(b)–(d)] for which the minimal value is realized. The dotted, black line shows the upper bound up to which entanglement is present. The dashed lines show the respective thermal noise contribution $(2\bar{n} + 1)\epsilon_{opt}$ to Δ_{EPR} [see eq. (2.24)]. (b)–(d) Values of ϵ, η, ζ which optimize Δ_{EPR} for a given $\bar{n}$. (e) Shows the relative amount of noise induced by the coupling to the mechanical environment ($\epsilon'_{opt} = \epsilon_{opt}/\Delta_{EPR}$).

which also leads to small effects from mechanical decoherence [red curves in fig. 17].

Over and above the fundamental imperfections, technical losses, such as mode-mismatch and detector inefficiencies, additionally decrease entanglement. They can all collectively be described as (passive) beam-splitter losses adding vacuum noise to the optical signal. They will however, never completely break entanglement, as long as the overall loss is smaller than unity. Noise contributions of this type can easily be accounted for by adding appropriate noise terms to eq. (2.24).

(a)

(b)
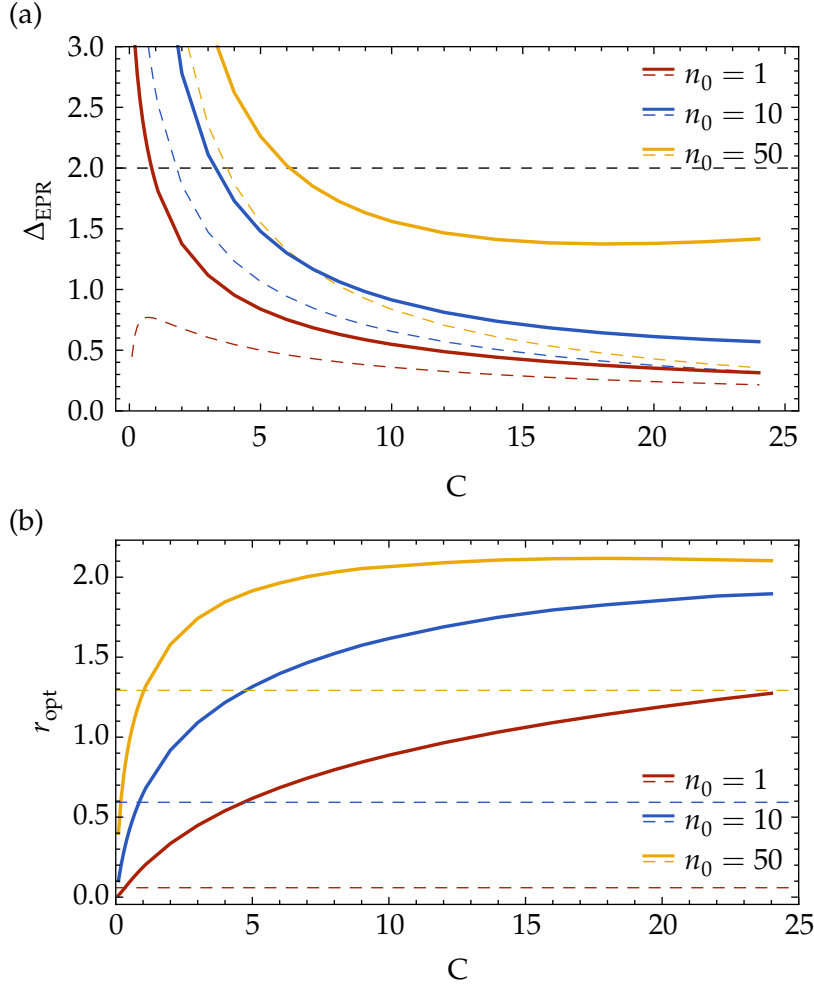
FIGURE 17. (a) Δ_{EPR} against cooperativity for different initial mechanical occupation numbers, optimized with respect to ϵ for fixed values $\eta = 2/100$, $Q_{\text{m}} = 3 \cdot 10^6$, $\bar{n} = 40$. The coloured, dashed lines show the thermal noise contributions $\epsilon_{\text{opt}}(2\bar{n} + 1)$. (b) Squeezing parameter r_{opt} corresponding to the optimal values of ϵ. The dashed lines indicate the different values of the minimally required squeezing $r_0(n_0)$.

2.2 GENERATION OF NON-CLASSICAL MECHANICAL STATES

Up to now the considered optomechanical systems obeyed Gaussian dynamics, i.e., the amplitudes followed linear equations of motion and we assumed all inputs to be Gaussian random processes. Starting our protocols from a (Gaussian) thermal state thus inevitably leads to a Gaussian final state. In this chapter we will explore how one can prepare the mechanical oscillator in a non-Gaussian state, or, more interestingly, in a non-classical state—i.e., a state with a negative Wigner function [KŻo4]. Such states of motional degrees of freedom have been prepared in other systems, e.g., ions [Mee+96] and atoms [KPM97]. Alternative approaches to prepare non-classical mechanical quantum states were presented in [BJK97] (using the nonlinear radiation-pressure interaction), [Kha+10] (by transferring it from an optical field), and in [VAK13] (by phonon addition or subtraction). A protocol similar to the one outlined here has been proposed in [Gal+14]; here we show that based on the protocol developed in chapter 2 we can prepare non-classical quantum states of a mechanical oscillator in existing systems.

The presented scheme was devised together with Konrad Lehnert, Tauno Palomaki, and Klemens Hammerer during a visit at the University of Colorado, Boulder.

2.2.1 *The Cascaded System*

We consider the following generic setup: A mechanical oscillator interacts with a one-dimensional electromagnetic field via a tunable interaction. The outgoing field is unidirectionally coupled into a cavity, whose intracavity field dispersively interacts with a two-level system. The light reflected from this cavity is sent to a phase sensitive detector which measures a single quadrature of the field. The setup can be implemented, e.g., as a cavity-optomechanical system coupling into an optical cavity containing a single atom [fig. 18(b)], or as an electromechanical LC (inductor-capacitor) resonator connected to a microwave cavity containing a superconducting qubit [fig. 18(a)]. The phase sensitive measurement is then either achieved by optical homodyne detection or using a Josephson parametric amplifier (JPA) [Yur87]. Here we will focus on the electromechanical implementation.

We assume that the LC resonator (with a resonance frequency ω_{lc}) is driven by an intense microwave tone at frequency ω_0, which is detuned with respect to ω_{lc} by $\Delta_{lc} = \omega_0 - \omega_{lc}$, such that the electromechanical system in a frame rotating with ω_0 can be described by the standard linearized Hamiltonian

$$H_{em} = \omega_m c_m^\dagger c_m - \Delta_{lc} c_{lc}^\dagger c_{lc} + g(c_{lc} + c_{lc}^\dagger)(c_m + c_m^\dagger), \qquad (2.26)$$

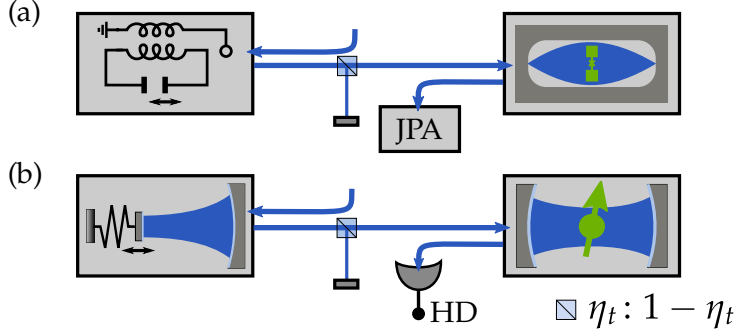where c_{lc} denotes the bosonic annihilation operators of the LC mode.

FIGURE 18. Schematic of the suggested setup. The output field of (a) an electromechanical system, or (b) an optomechanical system couples unidirectionally into a cavity containing a qubit, and is later measured by a phase-sensitive detector. A non-unit transmissivity η_t into the cascaded resonator is modelled by beam splitter losses.

The microwave cavity, which is detuned with respect to the carrier frequency of the microwave pulse by $\Delta_c = \omega_0 - \omega_c$, we describe by creation and annihilation operators $c_c^\dagger$, c_c. The Hilbert space of the superconducting qubit is spanned by $|g\rangle$ and $|e\rangle$, its ground and excited state respectively. We then describe the cavity and the qubit by the Hamiltonians

$$H_{\text{cav}} = -\Delta_c c_c^\dagger c_c, \tag{2.27}$$

$$H_{\text{qb}} = \frac{1}{2}\omega_{\text{eg}}\sigma_z + \chi c_c^\dagger c_c \sigma_z + \Omega(\sigma_+ + \sigma_+^\dagger), \tag{2.28}$$

where $\sigma_z = |e\rangle\langle e| - |g\rangle\langle g|$ is the Pauli z-matrix and $\sigma_+ = |e\rangle\langle g|$. The second term in (2.28) describes the dispersive coupling [Bla+04; Wal+04] between the qubit and the intracavity field with a coupling rate $\chi \propto 1/(\omega_c - \omega_{\text{eg}})$, which can be changed by tuning ω_{eg} in and out of resonance with ω_c. Switchable (i. e., time-dependent coupling) can be achieved by methods demonstrated in [Hof+11; Che+14]. In addition we can directly drive the qubit by an external, classical field, which induces Rabi oscillations at a rate Ω. The dynamics of the cascaded system [Gar93; Car93a] is then described by the master equation (written in a frame rotating at frequency ω_0)

$$\dot{\rho} = -\mathrm{i}\big[H_{\text{em}} + H_{\text{cav}} + H_{\text{qb}}, \rho\big] + \mathcal{L}_{\text{m}}\rho + (1 - \eta_t)\kappa_{\text{lc}}\,\mathcal{D}[c_{\text{lc}}]\rho$$
$$- \sqrt{\eta_t\kappa_{\text{lc}}\kappa_c/4}\big[c_c^\dagger c_{\text{lc}} - c_{\text{lc}}^\dagger c_c, \rho\big] + \mathcal{D}[\sqrt{\eta_t\kappa_{\text{lc}}}c_{\text{lc}} + \sqrt{\kappa_c}c_c]\rho, \tag{2.29}$$

with the mechanical damping term $\mathcal{L}_{\text{m}}\rho = \gamma_{\text{m}}(\bar{n} + 1)\,\mathcal{D}[c_{\text{m}}]\rho + \gamma_{\text{m}}\bar{n}\,\mathcal{D}[c_{\text{m}}^\dagger]\rho$. The last term of the first line describes beam-splitter losses between the LC resonator and the cascaded cavity, where η_t denotes the (power) transmissivity. The second line describes the cascaded dynamics of the LC resonator and the microwave cavity, where κ_{lc} and κ_c describe the FWHM decay rate of both resonators.

2.2.2 *The Protocol*

In order to create a non-classical mechanical state we consider a pulsed protocol operated in three steps:

1 *Entanglement generation*: We drive the electromechanical system on the blue mechanical sideband and couple the output microwave pulse into the cascaded cavity. In the strong-cooperativity regime this effectively generates EPR entanglement between the mechanical oscillator and the intracavity field. This works in full analogy to the scheme described in section 2.1, where now the cascaded cavity defines the shape of the temporal light modes.

2 *Probabilistic Fock state measurement*: By coupling the qubit to the intracavity field and subsequently measuring it [Ris+12a; Ris+12b], we can effect a conditional photon-number measurement of the microwave field. In the presence of EPR entanglement this measurement projects the mechanical mode onto a phononic Fock state—and thus a non-classical state.

3 *Read-out of mechanical state*: The electromechanical system is driven on the red mechanical sideband to generate a state-swap between the mechanical oscillator and the LC circuit. We then use a JPA to do quantum state tomography of the output field which effectively realizes a tomographic reconstruction of the mechanical state.

We will fix the origin of our time-axis such that the Fock state measurement happens at time $t = 0$, while the first and the second pulse interact with the optomechanical system during the intervals $[-\tau_1, 0)$ and $(0, \tau_2]$ respectively.

Entanglement Generation

In this first step the goal is to generate EPR entanglement between the mechanical motion and the intracavity field of the microwave cavity. This is achieved by sending a blue-detuned ($\Delta_{lc} = \omega_m$) flat-top microwave pulse of duration τ_1 into the LC resonator where it interacts with the mechanical oscillator and which subsequently enters the microwave cavity. The electromechanical two-mode squeezing interaction scatters photons into the LC resonator, and generates an exponentially growing pulse in the output field. In the strong cooperativity regime this pulse will be entangled with the mechanical mode. In order to optimally couple it into the microwave cavity, we have to choose (i) its resonance frequency to lie at the carrier frequency of the pulse (i.e., $\Delta_c = \Delta_{lc}$), and (ii) its bandwidth to fit the exponential pulse shape. Assuming the qubit is initially in its ground state, it does not (in the dispersive limit) couple to the microwave field, and factors out from the rest of the system. We will therefore neglect all qubit dynamics for the remainder of this section.

We show in appendix 2.C that in the weak-coupling regime the LC resonator can be adiabatically eliminated and the cascaded evolution of the mechanical oscillator and the microwave cavity, described by $\rho^{(\mathrm{mc})}$, can (in an interaction picture with $\omega_{\mathrm{m}} c_{\mathrm{m}}^{\dagger} c_{\mathrm{m}} - \Delta_{\mathrm{c}} c_{\mathrm{c}}^{\dagger} c_{\mathrm{c}}$) be written as

$$\dot{\rho}^{(\mathrm{mc})} = \mathcal{L}_{\mathrm{m}} \rho^{(\mathrm{mc})} + \epsilon G \, \mathcal{D}[c_{\mathrm{m}}] \rho^{(\mathrm{mc})} + \mathcal{D}[\sqrt{\kappa_{\mathrm{c}}} c_{\mathrm{c}} - \mathrm{i}\sqrt{G} c_{\mathrm{m}}^{\dagger}] \rho^{(\mathrm{mc})}$$
$$+ \, \mathrm{i}\sqrt{G\kappa_{\mathrm{c}}/4} \, [c_{\mathrm{m}} c_{\mathrm{c}} + c_{\mathrm{m}}^{\dagger} c_{\mathrm{c}}^{\dagger}, \rho^{(\mathrm{mc})}]. \quad (2.30)$$

Here we defined $G = 4g^2/\kappa_{\mathrm{lc}}$, which coincides with the exponential envelope of the pulse, and $\epsilon = [1 + (4\omega_{\mathrm{m}}/\kappa_{\mathrm{lc}})^2]^{-1}$, which gives the suppression of the counter-rotating electromechanical interaction terms. If we match the cavity decay rate to the temporal envelope of the light scattered by the mechanical oscillator, i.e., $\kappa_{\mathrm{c}} = G$, and go into the sideband-resolved ($\kappa_{\mathrm{lc}} \ll \omega_{\mathrm{m}}$) strong-cooperativity ($C > 1$) regime, the dominating dynamics are generated by a Lindblad term with a jump operator $c_{\mathrm{c}} - \mathrm{i} c_{\mathrm{m}}^{\dagger}$, and a two-mode squeezing interaction between the mechanical oscillator and the cascaded cavity mode, $H_{\mathrm{tms}} = (G/2)(c_{\mathrm{m}} c_{\mathrm{c}} + c_{\mathrm{m}}^{\dagger} c_{\mathrm{c}}^{\dagger})$ [third and fourth term in eq. (2.30)]. In absence of additional decoherence channels the system would thus be driven to the maximally entangled EPR state

$$|\psi_{\mathrm{epr}}\rangle_{\mathrm{mc}} = \sum_{n} (-\mathrm{i})^{n} |n\rangle_{\mathrm{m}} \otimes |n\rangle_{\mathrm{c}}, \quad (2.31)$$

which at the same time is a dark state of the Lindblad term and a eigenstate of the two-mode-squeezing Hamiltonian, i.e.,

$$(c_{\mathrm{c}} - \mathrm{i} c_{\mathrm{m}}^{\dagger})|\psi_{\mathrm{epr}}\rangle_{\mathrm{mc}} = 0, \quad (2.32a)$$

$$H_{\mathrm{tms}} |\psi_{\mathrm{epr}}\rangle_{\mathrm{mc}} = (G/2)|\psi_{\mathrm{epr}}\rangle_{\mathrm{mc}}. \quad (2.32b)$$

The EPR state possesses infinite energy, reflecting the instability of the amplifying dynamics of the two-mode squeezing interaction, and is thus not physical. These dynamics are counteracted by the additional Lindblad terms in eq. (2.30), which drive the system towards a thermal state. In view of the fact that these perturbative terms are suppressed by the small parameters $\epsilon, 1/C \ll 1$ we expect an appreciable amount of (EPR) entanglement to be created between the mechanical oscillator and the microwave intracavity field. As the dynamics of the mechanical oscillator and the cavity are linear and we assume the initial state of both systems to be Gaussian, their state at a later time—but before the interaction with the qubit—will also be Gaussian. The entanglement between both systems can thus be found by evaluating the covariance matrix Σ of the vector $X = (x_{\mathrm{m}}, p_{\mathrm{m}}, x_{\mathrm{c}}, p_{\mathrm{c}})$. The time evolution of Σ is given by the Lyapunov equation (1.61b)

corresponding to MEQ (2.30), where the matrices $\mathbf{F}$ and $\mathbf{N}$ are given by

$$\mathbf{F} = \frac{1}{2} \begin{pmatrix} (1-\epsilon)G - \gamma_{\mathrm{m}} & 0 & 0 & 0 \\ 0 & (1-\epsilon)G - \gamma_{\mathrm{m}} & 0 & 0 \\ -2\sqrt{\eta_{\mathrm{t}}\kappa_{\mathrm{c}}G} & 0 & -\kappa_{\mathrm{c}} & 0 \\ 0 & 2\sqrt{\eta_{\mathrm{t}}\kappa_{\mathrm{c}}G} & 0 & -\kappa_{\mathrm{c}} \end{pmatrix} \qquad (2.33)$$

and

$$\mathbf{N} = \frac{1}{2} \begin{pmatrix} \tilde{G} & 0 & -\sqrt{\eta_{\mathrm{t}}\kappa_{\mathrm{c}}G} & 0 \\ 0 & \tilde{G} & 0 & \sqrt{\eta_{\mathrm{t}}\kappa_{\mathrm{c}}G} \\ -\sqrt{\eta_{\mathrm{t}}\kappa_{\mathrm{c}}G} & 0 & \kappa_{\mathrm{c}} & 0 \\ 0 & \sqrt{\eta_{\mathrm{t}}\kappa_{\mathrm{c}}G} & 0 & \kappa_{\mathrm{c}} \end{pmatrix}, \qquad (2.34)$$

with $\tilde{G} = (1+\epsilon)G + \gamma_{\mathrm{m}}(2\bar{n}+1)$. As the Lyapunov equation is linear it can readily be integrated for the duration τ_1 of the pulse, assuming the mechanical mode to be initially in thermal equilibrium with the environment and the cavity to be in the vacuum state, i.e., $\boldsymbol{\Sigma}(-\tau_1) = \mathrm{diag}(2\bar{n}+1, 2\bar{n}+1, 1, 1)/2$. From the solution $\boldsymbol{\Sigma}(0)$ (just before the Fock measurement) we then calculate the EPR variance

$$\Delta_{\mathrm{EPR}} = \min_{\phi_{\mathrm{m}}, \phi_{\mathrm{c}}} \left([\Delta(x_{\mathrm{m}}^{\phi_{\mathrm{m}}} - x_{\mathrm{c}}^{\phi_{\mathrm{c}}})]^2 + [\Delta(p_{\mathrm{m}}^{\phi_{\mathrm{m}}} + p_{\mathrm{c}}^{\phi_{\mathrm{c}}})]^2 \right), \qquad (2.35)$$

where $x_i^{\phi} = (c_i\,\mathrm{e}^{-i\phi} + c_i^\dagger\,\mathrm{e}^{+i\phi})/\sqrt{2}$ and $p_i^{\phi} = x_i^{\phi+\pi/2}$ are rotated quadratures. With these definitions the state is necessarily entangled if $\Delta_{\mathrm{EPR}} < 2$ [Dua+00; Sim00]. In the case of non-unit transmissivity between the LC resonator and the microwave cavity, the generated entanglement will be diminished by photon losses. This can be accounted for by introducing a transmissivity parameter $0 \leq \eta_{\mathrm{t}} \leq 1$, as discussed in appendix 2.C. It turns out that it is advantageous to slightly mismatch the cavity decay rate κ_{c} against G in order to maximize entanglement creation, setting $\kappa_{\mathrm{c}} = vG$. This is due to the finite duration of the pulse, which causes a spectral broadening. The cavity's bandwidth thus has to be increased such that it can fit the whole pulse. Figure 19 shows the generated entanglement in terms of the EPR variance (solid lines) and the logarithmic negativity (dashed lines), for optimized values of v. Comparing this to fig. 17, the EPR variance clearly shows a similar behaviour. Note that as the system is prepared in a nearly pure state initially ($n_0 = 1/2$, a value demonstrated in [Pal+13]), a low interaction strength suffices in order to create entanglement.

Mechanical Fock State Preparation

After the first step of the protocol, the bipartite system consisting of the mechanical oscillator and the cavity mode will be in an entangled state resembling the ideal EPR state. It is obvious from the definition
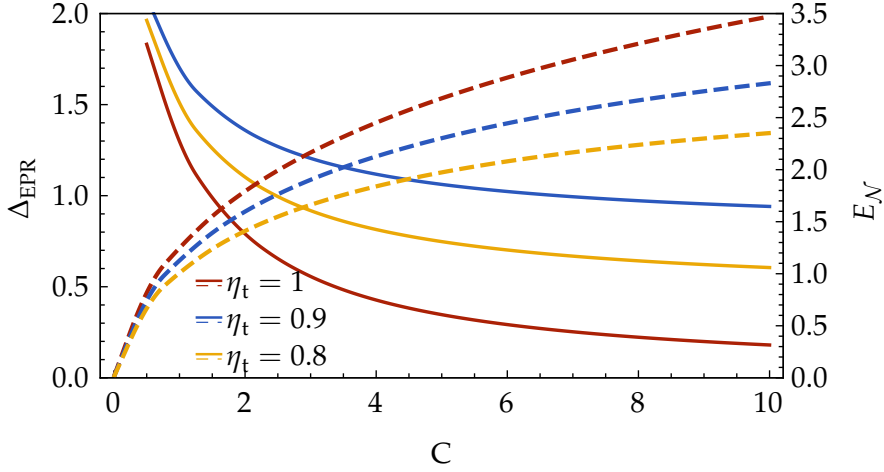
FIGURE 19. Entanglement against cooperativity C for $\epsilon = 1/1000$ and $\bar{n} = 40$. The solid lines show Δ_{EPR} and refer to the left axis, while the dashed lines show $E_{\mathcal{N}}$ and refer to the right axis. Different colours encode different transmissivity values $\eta_{\text{t}} = 1, 0.9, 0.8$ (red, blue, yellow). In all cases we assume pre-cooling of the mechanical oscillator to an initial occupation number $n_0 = 1/2$ and we optimize the linewidth of the microwave cavity κ_{c} for maximal $E_{\mathcal{N}}$ and minimal Δ_{EPR}. (Note that this optimization is done separately for solid and dashed lines)

of this state [eq. (2.31)] that projecting the cavity onto a Fock state $|k\rangle_{\text{c}}$ will also collapse the mechanical oscillator onto the same state $|k\rangle_{\text{m}}$. For our description here we adopt an idealized model for the qubit mediated measurement of the photon number.

The Fock state preparation we will describe below is a probabilistic one; before the measurement we have to choose a natural number k corresponding to the Fock state $|k\rangle_{\text{c}}$ we want to detect. The result of the measurement will then either be 1 if the intracavity field was in state $|k\rangle_{\text{c}}$, or 0 if it was in any other state. Only in the former case on proceeds with the tomography step. A measurement of this form can be achieved in the following way (see fig. 20): Due to the dispersive interaction, the intracavity field shifts the qubit's resonance frequency by $n\chi$, where n is the number of intracavity photons. We start with the qubit in the ground state and apply a π-pulse at a frequency $\omega_{\text{eg}} + 2k\chi$. If the energy levels of the qubit are well resolved, i.e., the frequency shift between adjacent levels χ is larger than the linewidth γ_{q} of the qubit's excited state (this shift approaches values of 1000 times the linewidths of qubit and cavity [Pai+11]), we can describe the unitary evolution generated due to the π-pulse by

FIG 20. Level scheme of a qubit coupled to a microwave cavity

$$U_{\pi}^{(k)} = \mathbb{1}_{\text{m}} \otimes \left(|k,e\rangle\langle k,g|_{\text{cq}} + |k,g\rangle\langle k,e|_{\text{cq}} \right)$$
$$+ \mathbb{1}_{\text{m}} \otimes \sum_{l \neq k} |l\rangle\langle l|_{\text{c}} \otimes \mathbb{1}_{\text{q}}. \quad (2.36)$$
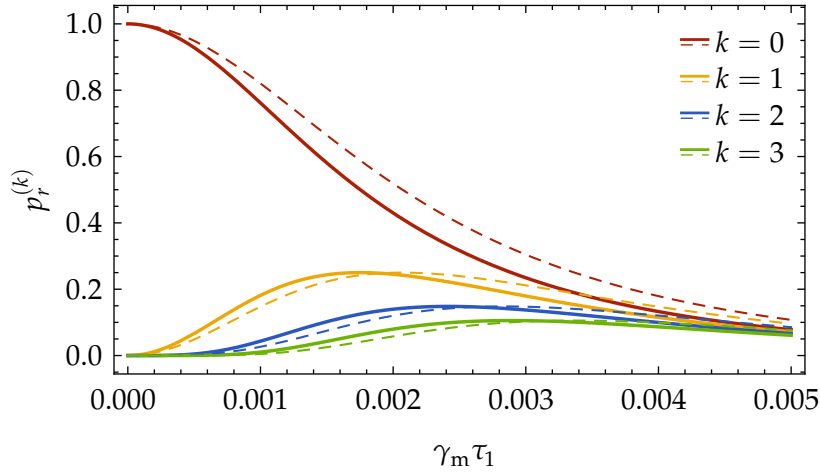
FIGURE 21. Detection probabilities p_k versus the dimensionless pulse length $\gamma_m \tau_1$ for a cooperativity $C = 11$ and total transmissivity $\eta_t = 1, 0.7$ (solid, dashed lines). Different colours encode the number of detected photons $k = 0, 1, 2, 3$ (red, yellow, blue, green). We assume a perfect matching $\kappa_c = G$. Other parameters are $\epsilon = 1/1000$, $\bar{n} = 40$, $n_0 = 1/2$

Measuring the state of the qubit after the π-pulse is then described by the measurement operators $M_r^{(k)} = \langle r | U_\pi^{(k)} | g \rangle$ for possible outcomes $r \in \{g, e\}$. We thus see that measuring the qubit realizes a projective measurement on the cavity field where $M_e^{(k)} = \mathbb{1}_m \otimes |k\rangle\langle k|_c$, $M_g^{(k)} = \mathbb{1}_{mc} - M_e^{(k)}$ correspond to finding the qubit in the excited and ground state respectively. After a measurement with an outcome r the joint state of the mechanical resonator and the cavity mode is

$$\rho_{mc}^{(r,k)}(\tau_1) = \frac{1}{p_r^{(k)}} M_r^{(k)} \rho^{(mc)}(\tau_1) [M_r^{(k)}]^\dagger, \tag{2.37}$$

where the probability of finding the outcome r is

$$p_r^{(k)} = \mathrm{tr}\left([M_r^{(k)}]^\dagger M_r^{(k)} \rho^{(mc)}(\tau_1)\right). \tag{2.38}$$

We are interested only in the case where the qubit after the π-pulse is in the excited state, i.e., $r = e$. The state of the reduced mechanical system conditioned on this outcome is then given by $\rho_m^{(k)} := \mathrm{tr}_c(\rho_{mc}^{(e,k)})$. The corresponding detection probabilities for different values k are depicted in fig. 21. As is intuitively clear, for small pulse lengths τ_1 the cavity will with near-unit probability be in the vacuum state. Only after some time photons start leaking into the cavity to give a non-zero detection probability. The respective Wigner functions $W_m^{(k)}$ we can obtain from the Gaussian Wigner function corresponding to $\Sigma(0)$ as found as the solution of eq. (2.30) and by then using the conditioning procedure described in appendix 2.A.

In the same way we condition the mechanical state on a photon-number measurement, we can additionally condition it on quadrature measurements of the field reflected from the microwave cavity.

To gain some intuition about the effect of this measurement we can rewrite the EPR state in terms of quadrature eigenstates [EPR35]. This yields [BL05]

$$
\begin{aligned}
|\psi_{\mathrm{epr}}\rangle_{\mathrm{mc}} &= \int \mathrm{d}x\, \mathrm{d}p\, \delta(x+p)|x\rangle_{\mathrm{m}} \otimes |p\rangle_{\mathrm{c}} \\
&= \int \mathrm{d}p\, \mathrm{d}x\, \delta(p+x)|p\rangle_{\mathrm{m}} \otimes |x\rangle_{\mathrm{c}},
\end{aligned}
\tag{2.39}
$$

where we denote by $|x\rangle_{\mathrm{m}}$ ($|x\rangle_{\mathrm{c}}$) position (amplitude-quadrature) and by $|p\rangle_{\mathrm{m}}$ ($|p\rangle_{\mathrm{c}}$) momentum (phase-quadrature) eigenstates for the mechanical (cavity) mode. Measuring a quadrature of the cavity field would thus project the mechanical oscillator onto the corresponding quadrature eigenstate, which is again a unphysical state containing infinite energy. In our case, where no ideal EPR state is present, the variance of the mechanical state will instead be decreased in the respective direction. For strong enough squeezing we would expect to generate in this way a distribution with two pronounced peaks at opposite sides in phase space, similar to "Schrödinger kitten" states generated with photons [Our+06; Nee+06]. This situation can be described by a stochastic master equation of the form

$$
\begin{aligned}
\mathrm{d}\rho^{(\mathrm{mc})} &= \mathcal{L}_{\mathrm{m}}\rho^{(\mathrm{mc})}\, \mathrm{d}t + \epsilon G\, \mathcal{D}[c_{\mathrm{m}}]\rho^{(\mathrm{mc})}\, \mathrm{d}t \\
&\quad + \mathcal{D}[\sqrt{\kappa_{\mathrm{c}}}c_{\mathrm{c}} - \mathrm{i}\sqrt{G}c_{\mathrm{m}}^{\dagger}]\rho^{(\mathrm{mc})}\, \mathrm{d}t + \mathrm{i}\sqrt{\kappa_{\mathrm{c}}G/4}[c_{\mathrm{m}}c_{\mathrm{c}} + c_{\mathrm{m}}^{\dagger}c_{\mathrm{c}}^{\dagger}, \rho^{(\mathrm{mc})}]\, \mathrm{d}t \\
&\quad + \mathcal{H}[(\sqrt{\kappa_{\mathrm{c}}}c_{\mathrm{c}} - \mathrm{i}\sqrt{G}c_{\mathrm{m}}^{\dagger})\, \mathrm{e}^{\mathrm{i}\phi}]\rho_{\mathrm{mc}}\, \mathrm{d}W, \quad (2.40)
\end{aligned}
$$

where $\mathrm{d}W$ is a Wiener increment, and ϕ is the measurement phase. The conditional state before the number measurement can then be evaluated by integrating the equation of motion for the covariance matrix Σ. Equation (2.40) gives rise to a Riccati equation such as (1.67b), where $\mathbf{H}$ and $\mathbf{M}$ are given by

$$
\mathbf{H} = \sqrt{2G}\left(\sin(\phi) \quad -\cos(\phi) \quad \sqrt{v}\cos(\phi) \quad -\sqrt{v}\sin(\phi)\right) \quad (2.41)
$$

and

$$
\mathbf{M} = \sqrt{G/2}\left(\sin(\phi) \quad -\cos(\phi) \quad -\sqrt{v}\cos(\phi) \quad \sqrt{v}\sin(\phi)\right)^{\mathrm{T}}.
\tag{2.42}
$$

Finding the Wigner function of the mechanical state conditioned on quadrature and photon-number detection proceeds as before, by first finding the covariance matrix $\hat{\Sigma}(0)$ as a solution to (2.40) and applying the method from appendix 2.A. There is one technical subtlety involved, however. The state conditioned on the quadrature measurement at time τ_2 includes a random displacement of the microwave cavity's intracavity field which cannot easily be undone in the experiment. As this displacement varies between every shot of the tomography, the reconstruction will yield an averaged distribution. This effect can be partly eliminated by postselecting the experiments on

a small interval of results of the homodyne detection. The results presented here are based on the conditional state and the averaging effect is neglected. For a concrete experimental realization, a more detailed treatment should be adopted.

Read-out of the Mechanical State

After preparing the mechanical system in a non-classical state we can transfer it to the microwave field in order to reconstruct it tomographically from phase-sensitive measurements of different microwave quadratures. To this end we again send a flat-top pulse of length τ_2 into the LC resonator, this time red-detuned at $\Delta_{lc} = -\omega_m$ in order to resonantly drive the electromechanical beam-splitter interaction. This generates an exponentially decaying pulse centred at ω_{lc} which carries the read-out mechanical state. Under the same assumptions as before we find after adiabatic elimination of the LC circuit (see appendix 2.C)

$$
\begin{aligned}
\dot{\rho}_{mc} = {}& \mathcal{L}_m \rho^{(mc)} + \epsilon G \, \mathcal{D}[c_m^\dagger] \rho^{(mc)} \\
& + G \, \mathcal{D}[\sqrt{\kappa_c} c_c - i \sqrt{G} c_m] \rho^{(mc)} + i \sqrt{\kappa_c G / 4} [c_m^\dagger c_c + c_m c_c^\dagger, \rho^{(mc)}],
\end{aligned}
\tag{2.43}
$$

where we again neglected the qubit dynamics. To describe the quadrature measurements and to identify the relevant temporal modes in the output field we rewrite the system's evolution in terms of the Langevin equations for the quadrature operators x_m, p_m, x_c, p_c. The relevant matrices [corresponding to the dynamics in eq. (2.43)] are

$$
\mathbf{F} = \frac{1}{2}
\begin{pmatrix}
-(1-\epsilon)G - \gamma_m & 0 & 0 & 0 \\
0 & -(1-\epsilon)G - \gamma_m & 0 & 0 \\
-2\sqrt{\eta_t \kappa_c G} & 0 & -\kappa_c & 0 \\
0 & -2\sqrt{\eta_t \kappa_c G} & 0 & -\kappa_c
\end{pmatrix}
\tag{2.44}
$$

and

$$
\mathbf{N} = \frac{1}{2}
\begin{pmatrix}
\tilde{G} & 0 & \sqrt{\eta_t \kappa_c G} & 0 \\
0 & \tilde{G} & 0 & \sqrt{\eta_t \kappa_c G} \\
\sqrt{\eta_t \kappa_c G} & 0 & \kappa_c & 0 \\
0 & \sqrt{\eta_t \kappa_c G} & 0 & \kappa_c
\end{pmatrix}.
\tag{2.45}
$$

To illustrate the method, we apply a RWA to the electromechanical interaction by setting $\epsilon = 0$ and neglect mechanical decoherence terms. We also choose $\kappa_c = G$ for simplicity. Appendix 2.B shows how to treat the full dynamics. Under these approximations the Langevin equations reduce to

$$
\dot{x}_m = -(G/2)x_m + \sqrt{G} p_{in},
\tag{2.46a}
$$

$$
\dot{p}_c = -(G/2)p_c + G x_m + \sqrt{G} p_{in},
\tag{2.46b}
$$

with similar expressions for $\dot{p}_{\mathrm{m}}$ and $\dot{x}_{\mathrm{c}}$. We formally integrate equations (2.46) and plug them into the input-output relations [GZ04] $p_{\mathrm{out}}(t) = \sqrt{G}(p_{\mathrm{c}} - x_{\mathrm{m}}) - p_{\mathrm{in}}$, which gives

$$p_{\mathrm{out}}(t) = \sqrt{G}\,e^{-\frac{G}{2}t}(Gt-1)x_{\mathrm{m}}(0) + \sqrt{G}\,e^{-\frac{G}{2}t}\,p_{\mathrm{c}}(0) - p_{\mathrm{in}}(t)$$
$$+ G^2 t \int_0^t p_{\mathrm{in}}(s)\,e^{-\frac{G}{2}(t-s)}\,\mathrm{d}s + G \int_0^t p_{\mathrm{in}}(s)Gs\,e^{-\frac{G}{2}(t-s)}\,\mathrm{d}s. \quad (2.47)$$

The goal is to extract from this quantity as much information as possible about the mechanical state [encoded in $x_{\mathrm{m}}(0)$], with minimal contributions from the noise terms. To achieve this we extract from p_{out} a normalized temporal mode with an envelope given by $\alpha_{\mathrm{out}} = e^{-\frac{G}{2}t}(Gt-1)$. We define the normalized mode function $\hat{\alpha}_{\mathrm{out}} = \alpha_{\mathrm{out}}/\|\alpha_{\mathrm{out}}\|$, where $\|\alpha_{\mathrm{out}}\| = \int_0^{\tau_2} |\alpha_{\mathrm{out}}(s)|^2\,\mathrm{d}s$, and the corresponding operator $P_{\mathrm{c}}^{\mathrm{out}} = \int_0^{\tau_2} \hat{\alpha}_{\mathrm{out}}(s)p_{\mathrm{out}}(s)\,\mathrm{d}s$, and find

$$P_{\mathrm{c}}^{\mathrm{out}} = \sqrt{G}\|\alpha_{\mathrm{out}}\|x_{\mathrm{m}}(0) - h_1(G\tau_2)p_{\mathrm{c}}(0) + h_2(G\tau_2)P_{\mathrm{c}}^{\mathrm{aux}}. \quad (2.48)$$

Here, $P_{\mathrm{c}}^{\mathrm{aux}}$ denotes an auxiliary light mode which carries vacuum noise, i.e., $\langle (P_{\mathrm{c}}^{\mathrm{aux}})^2 \rangle = 1/2$. One can show that $\lim_{\tau_2 \to \infty}\|\alpha_{\mathrm{out}}\| = 1/\sqrt{G}$, while the functions h_i obey $\lim_{t \to \infty} h_i(t) = 0$. Thus, in the long-time limit, we have a perfect read-out of the mechanical position via measuring the phase of the output light. If, on the other hand, we want to estimate the momentum p_{m} we measure the amplitude quadrature, $x_{\mathrm{out}} = \sqrt{G}(x_{\mathrm{c}} + p_{\mathrm{m}}) - x_{\mathrm{in}}$. The corresponding temporal output mode $X_{\mathrm{c}}^{\mathrm{out}} = \int_0^{\tau_2} \hat{\alpha}_{\mathrm{out}}(s)x_{\mathrm{out}}(s)\,\mathrm{d}s$ obeys

$$X_{\mathrm{c}}^{\mathrm{out}} = \sqrt{G}\|\alpha_{\mathrm{out}}\|p_{\mathrm{m}}(0) + h_1(G\tau_2)x_{\mathrm{c}}(0) + h_2(G\tau_2)X_{\mathrm{c}}^{\mathrm{aux}}. \quad (2.49)$$

To read-out the non-Gaussian mechanical Wigner function one has to apply homodyne tomography, repeatedly measuring quadratures $X_{\mathrm{c}}^{\mathrm{out}}\sin(\phi) + P_{\mathrm{c}}^{\mathrm{out}}\cos(\phi)$ for a set of different ϕ. This can be described by collecting the output operators into a vector $\boldsymbol{Y}_{\mathrm{out}} = (X_{\mathrm{c}}^{\mathrm{out}}, P_{\mathrm{c}}^{\mathrm{out}})$. Equations (2.48) and (2.49) can then be written as

$$\boldsymbol{Y}_{\mathrm{out}} = \mathbf{S}^{\mathrm{T}}\boldsymbol{Y}_{\mathrm{in}} + \boldsymbol{W}, \quad (2.50)$$

where we defined $\boldsymbol{Y}_{\mathrm{in}} = (x_{\mathrm{m}}(0), p_{\mathrm{m}}(0))$, and $\boldsymbol{W}$ describes all relevant noise processes. Note that $\boldsymbol{Y}_{\mathrm{out}}$ is not a quantity that is directly measurable, as it contains non-commuting operators. We can, however, conveniently use it to find the mechanical Wigner function $W_{\mathrm{out}}^{(k)}$ as reconstructed by homodyne tomography of the microwave field (see appendix 2.A). A non-unit detection efficiency $0 \leq \eta_{\mathrm{d}} \leq 1$ can be modelled by including beam-splitter losses as

$$\boldsymbol{Y}_{\mathrm{out}}' = \sqrt{\eta_{\mathrm{d}}}\mathbf{S}^{\mathrm{T}}\boldsymbol{Y}_{\mathrm{in}} + \sqrt{\eta_{\mathrm{d}}}\boldsymbol{W} + \sqrt{1-\eta_{\mathrm{d}}}\boldsymbol{W}', \quad (2.51)$$

where $\boldsymbol{W}'$ describes additional shot noise, and for the case above has the the diagonal form $\boldsymbol{W}' = \mathrm{diag}(1/2, 1/2)$.

Results

We are now in the position to evaluate the Wigner function $W_m^{(k)}$ of the mechanical state after the qubit measurement, and can compare it to the reconstructed Wigner function $W_{out}^{(k)}$ of the second light pulse. Figure 22 shows cuts through $W_m^{(1)}$ (dashed lines) and $W_{out}^{(1)}$ (solid lines) for a set of current experimental parameters [Pal+13] for different values of transmissivity and detection efficiency. We can nicely see the dip at the origin that is characteristic for the Fock state $|1\rangle$. The depth of the dip is decreased by non-unit transmissivity or detector efficiency, as these effectively lead to incoherent mixing with the Gaussian vacuum state, which has a positive Wigner function at the origin.
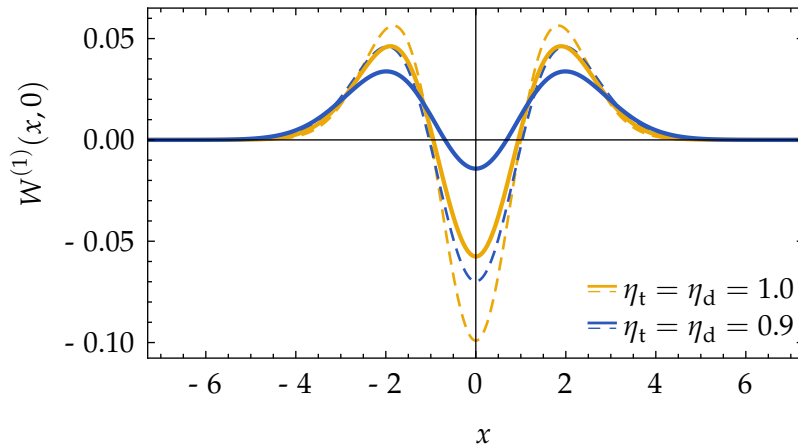

FIGURE 22. Cut through mechanical Wigner function conditioned on the detection of a single photon in the cavity for a cooperativity $C = 11$. Different colours encode different transmissivity values $\eta_t = \eta_d = 1, 0.9$ (yellow, blue). The solid lines correspond to the Wigner function $W_{out}^{(1)}(x,0)$ reconstructed from the output light, while the dashed lines show the mechanical state as prepared by the Fock-state measurement [$W_m^{(1)}(x,0)$]. For the first pulse we assume the microwave cavity's bandwidth to be $\kappa_{c,1} = 1.3G$, while for the second pulse we assume perfect matching $\kappa_{c,2} = G$. Other parameters are $\epsilon = 1/1000$, $\bar{n} = 40$, $n_0 = 1/2$, $\tau_1 = 1/100\,\gamma_m^{-1}$, $\tau_2 = 1/50\,\gamma_m^{-1}$.

If the mechanical state is additionally conditioned on the outcomes of a quadrature measurement of one of the optical quadratures—realizing an effective measurement of a mechanical quadrature—, the Wigner function becomes squeezed in the same direction. This can be seen in fig. 23, depicting cuts through the Wigner function along the x_m (upper row) and p_m direction (lower row) for a homodyne measurement of the optical amplitude quadrature (which extracts information about the mechanical momentum quadrature). The squeezing effect is relatively weak, however, and the overlap with a Schrödinger cat state is rather small.
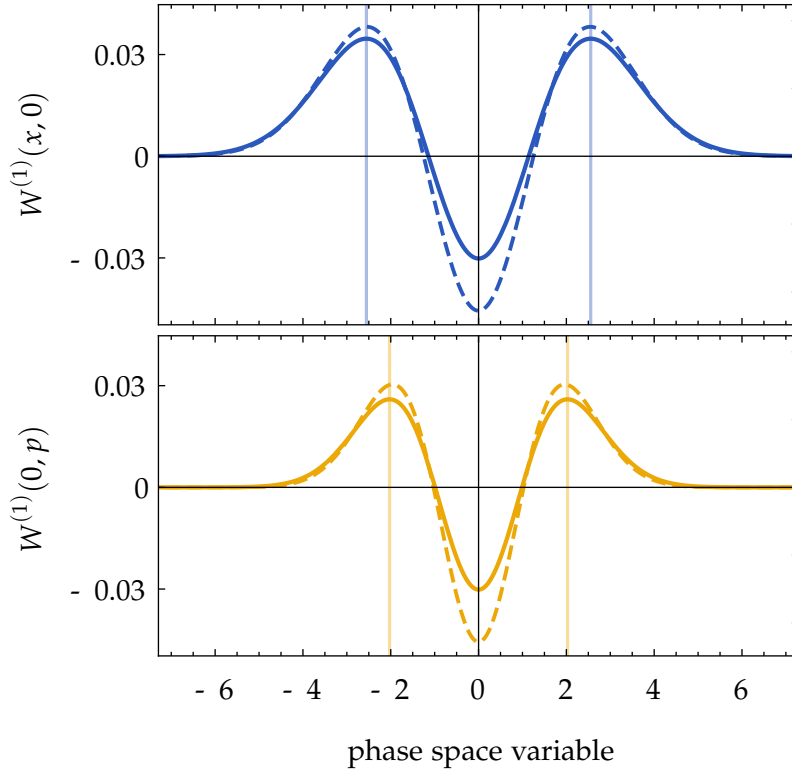
FIGURE 23. Cut through the Wigner function conditioned on a homodyne trajectory and the detection of a single photon. The upper row shows a cut along the x-axis, the lower row along the p-axis. Solid lines correspond to the Wigner function $W_{\text{out}}^{(1)}$ reconstructed from the output light, while the dashed lines show the mechanical state as prepared by the Fock-state measurement $[W_{\text{m}}^{(1)}]$. For the first pulse we assume the microwave cavity's bandwidth to be $\kappa_{\text{c},1} = 0.7G$, while for the second pulse we assume perfect matching $\kappa_{\text{c},2} = G$. Other parameters are $\epsilon = 1/1000$, $\bar{n} = 40$, $n_0 = 1/2$, $\tau_1 = 1/5000\,\gamma_{\text{m}}^{-1}$, $\tau_2 = 1/50\,\gamma_{\text{m}}^{-1}$, $\eta_{\text{t}} = 1$, $\eta_{\text{d}} = 1$.

2.3 BELL INEQUALITY VIOLATION IN OPTOMECHANICS

Since the seminal work of John Bell [Bel64; Bel66] it is well known that the predictions of quantum theory cannot be reproduced by *local hidden-variable theories*. Bell showed that we have to abandon one of the premises of *locality* and *realism*—as originally envisaged by Einstein, Podolsky, and Rosen [EPR35]—for quantum theory. Since its discovery Bell's theorem has been tested in a multitude of experiments using different physical systems, e. g., photons [FC72; ADR82; Wei+98], ions [Row+01], and superconducting qubits [Ans+09]. In this section we will show that the correlations between a mechanical oscillator and a light pulse (or, more specifically, EPR entanglement between the two) can be used to violate a Bell inequality. A Bell test involving nonlinear mechanical oscillators has also been proposed in

[Joh+14]. The presented scheme is similar to the one presented in section 2.2 above, employing a qubit as a photodetector.

We first review briefly the employed Bell inequality [of Clauser–Horne–Shimony–Holt (CHSH) type] and then analyse in detail the optomechanical implementation.

2.3.1 *The CHSH Inequality*

We consider a bipartite quantum system, labelling the parties as A and B. Let $\sigma_A(\alpha)$ and $\sigma_B(\beta)$ be two observables with possible outcomes ± 1, and $\alpha, \beta \in \mathbb{R}$ be measurement settings that can be chosen independently. Given a set of 2×2 detector settings, $\{\alpha_1, \alpha_2, \beta_1, \beta_2\}$, we can evaluate the correlation functions

$$E_{\alpha_i \beta_j} = \langle \sigma_A(\alpha_i) \otimes \sigma_B(\beta_j) \rangle_\rho \tag{2.52}$$

with respect to a state ρ. The CHSH inequality [Cla+69] states that assuming realism and locality, the parameter

$$S = E_{\alpha_1 \beta_1} + E_{\alpha_1 \beta_2} + E_{\alpha_2 \beta_1} - E_{\alpha_2 \beta_2} \tag{2.53}$$

is bounded by

$$-2 \leq S \leq 2. \tag{2.54}$$

The maximum value under the premisses of quantum theory on the other hand is given by $|S| \leq 2\sqrt{2}$ [Cir80].

Here we consider a continuous-variable implementation of the CHSH inequality, first introduced in [TWC91; Har94; BW99] and experimentally realized in [Hes+04]. We use the positive-operator valued measure (POVM) $\{|\alpha\rangle\langle\alpha|_i, \mathbb{1} - |\alpha\rangle\langle\alpha|_i\}$, where $|\alpha\rangle_i$ is a coherent state of one of the subsystems. This measurement can be performed by using a detector that is able to distinguish the vacuum state $|0\rangle_i$ from all other Fock states. For photons this can for example be implemented by using a single-photon counter or a bucket detector. If prior to detection the incoming field is displaced by a coherent amplitude $-\alpha$, a click of the photon counter corresponds to the POVM element $\mathbb{1} - |\alpha\rangle\langle\alpha|$ (which we associate with the measurement result -1), while no click corresponds to $|\alpha\rangle\langle\alpha|$ (associated with $+1$).[7] The corresponding observables σ_i can thus be constructed as

7. This technique is known as weak-field homodyne detection [WV96; Don+14]

$$\sigma_i(\alpha) = |\alpha\rangle\langle\alpha|_i - (\mathbb{1} - |\alpha\rangle\langle\alpha|_i) = 2|\alpha\rangle\langle\alpha| - \mathbb{1}. \tag{2.55}$$

The choice of observables is motivated by the fact that the corresponding Bell inequality can be violated by using Gaussian states [BW98; LJJ09; BC12]. The two-mode squeezed state

$$|\psi_{\mathrm{tms}}\rangle_{AB} = \mathrm{sech}(r) \sum_{n=0}^{\infty} [-\mathrm{e}^{\mathrm{i}\phi} \tanh(r)]^n |n\rangle_A \otimes |n\rangle_B, \tag{2.56}$$

for example, yields a maximal violation of $S \approx 2.45$ for a squeezing parameter $r \approx 0.76$ (squeezing of 6.3 dB) and properly chosen amplitudes α_i, β_j. In terms of entanglement this amount of two-mode squeezing corresponds to a EPR variance of $\Delta_{\mathrm{EPR}} = 2\,\mathrm{e}^{-2r} \approx 0.44$, a value which is comparable to the ones observed in the previous sections (see figs. 17 and 19).

2.3.2 The Protocol

The optomechanical implementation we discuss here is very similar to the scheme presented in section 2.2. The basic idea is the following: We want to apply measurements of the observable σ to the bipartite system formed by the mechanical oscillator and a light pulse. In order to get access to the quantum state of the mechanical subsystem we have to transfer it onto a second light pulse. We thus again consider a protocol operated in three steps:

1 *Entanglement generation:* A blue-detuned light pulse is entangled with the mechanical oscillator. This is achieved in the same way as in the first step in section 2.2 and can therefore be described by the master equation (2.30). We again choose $\kappa_{\mathrm{c}} = vG = v4g^2/\kappa_{\mathrm{lc}}$, where v will be chosen to optimize the transfer of the light pulse into the cascaded cavity.

FIG 24. Abstract depiction of the measurement setup: The input field is displaced by a coherent amplitude $-\alpha$ and sent to a single-photon detector (SPD).

2 *Photodetection:* Before it enters the cascaded cavity we mix the microwave pulse with a coherent field with an amplitude $-\alpha$ (see fig. 24). We then proceed by applying a π-pulse as described in section 2.2.2, selecting the subspace $|0\rangle_{\mathrm{c}}$ (thus choosing $k = 0$; the corresponding level scheme is shown in fig. 25). Looking back at our discussion of the measurement in section 2.2.2, we can see that the displacement $\rho^{(\mathrm{mc})} \to D_{\mathrm{c}}(-\alpha)\rho^{(\mathrm{mc})}D_{\mathrm{c}}(\alpha)$ [with D_{c} as defined in eq. (1.35)] of the field leads to measurement operators $M_r^{(0)} \to M_r^{(0)}D_{\mathrm{c}}(-\alpha)$. The corresponding probabilities are then $p_e^{(0)} = \mathrm{tr}(|\alpha\rangle\langle\alpha|\rho^{(\mathrm{mc})})$ and $p_g^{(0)} = 1 - p_e^{(0)}$ just as required. Reading out the state of the qubit after the π-pulse is thus equivalent to measuring $\sigma_{\mathrm{c}}(\alpha)$.

FIG 25. π-pulse in the $k = 0$ subspace. Detecting the qubit in $|e\rangle$ corresponds to the POVM element $|\alpha\rangle\langle\alpha|$.

3 *Phonon detection:* In order to apply a measurement of the observable $\sigma_{\mathrm{m}}(\beta)$ to the mechanical oscillator, we swap its quantum state into the cascaded cavity and repeat the procedure from step 2. As was already discussed earlier, such a state swap can be achieved by a red-detuned microwave drive, resonantly enhancing the optomechanical beam-splitter interaction. However, the exponentially decaying envelope of the resulting microwave pulse prohibits an efficient transfer into the cavity. This problem can be tackled by simultaneously modulating both the optomechanical coupling $G := G(t)$ and the bandwidth of the cavity $\kappa_{\mathrm{c}} := \kappa_{\mathrm{c}}(t)$ as a function of time. While achieving the former is a simple matter of changing the power $P(t)$ of the mi-
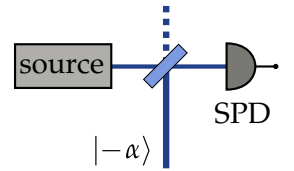
crowave drive, the latter can be accomplished by techniques demonstrated in [Ker+13; Pie+14; Sri+14; Pec+14; Yin+13; Flu+15]. The problem of how to determine the optimal shape of $G(t)$ and $\kappa_c(t)$ is addressed in appendix 2.D. We obtain the solutions

$$G(t) = \frac{M}{1 + e^{M(2t-\tau_2)}}, \tag{2.57a}$$

$$\kappa_c(t) = \frac{M}{1 + e^{-M(2t-\tau_2)}}, \tag{2.57b}$$

which are shown in fig. 26. The parameter M fixes the maximal values $G(\tau_2)$ and $\kappa_c(0)$, and minimal values $G(0)$ and $\kappa_c(\tau_2)$. In the experiment one has to choose a suitable M such that one can satisfy these conditions for both G and κ_c.
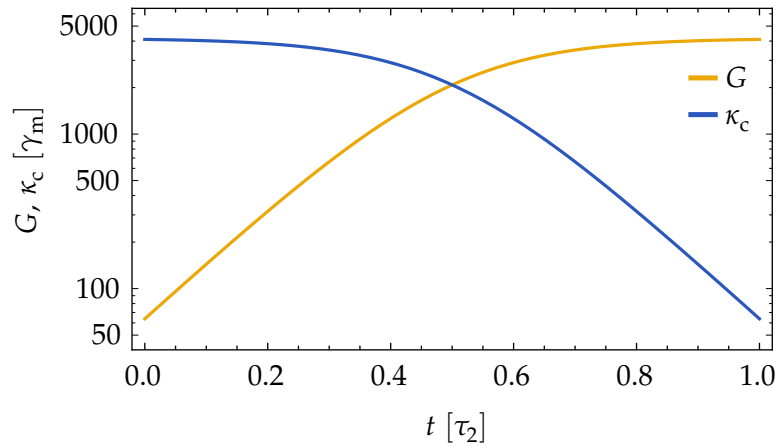
FIGURE 26. Optimal shape of the modulated coupling strength $G(t)$ (yellow line) and the cascaded cavity's decay rate $\kappa_c(t)$ (blue line) in units of the mechanical decay rate γ_m, plotted against time t (in units of the total duration τ_2). Parameters where chosen such that $\kappa_c(0) = G(\tau_2) = 4100\gamma_m$, $\gamma_m = 1/500\tau_2$.

From repeating this protocol for different settings $\{\alpha_i, \beta_j\}$ and collecting the measurement outcomes of steps 2 and 3 we can evaluate the quantity S [eq. (2.53)]. How to evaluate S theoretically is discussed in the next section.

2.3.3 *Evaluating the Bell correlations*

In order to evaluate the quantity S for the bipartite system consisting of the two light pulses, we extend our setup by a virtual, second cascaded cavity (plus a qubit), which acts as the measurement device for the second pulse. We can then model the protocol as follows: The blue-detuned pulse propagates into the first cavity, now constituting our system A. The red-detuned pulse is routed into the second cavity, constituting system B. S can then be conveniently evaluated from the

state of both cavities $(A + B)$, while the mechanical mode is traced out. (In fact the mechanics should nearly factor out from the rest of the system at this point.) Before the measurement all involved dynamics are Gaussian and we can employ the Lyapunov equations corresponding to the master equations (2.30) and (2.43) to model the evolution of the first and the second pulse respectively. Starting from the initial condition that the mechanical mode is in a thermal state with a mean occupation number n_0 and both cavities are in the vacuum state, i. e., $\Sigma_0 = \frac{1}{2}\mathrm{diag}(2n_0 + 1, 2n_0 + 1, 1, 1, 1, 1)$, this allows us to find the covariance matrix for modes A and B before the qubit measurements. To evaluate $E_{\alpha\beta}$ we decompose it as (denoting the Gaussian state of A and B just before the measurement as ρ_{AB})

$$
\begin{aligned}
E_{\alpha\beta} = {}& 4\,\mathrm{tr}\big(\rho_{AB}|\alpha\rangle\langle\alpha|_A \otimes |\beta\rangle\langle\beta|_B\big) \\
& - 2\,\mathrm{tr}\big(\rho_{AB}|\alpha\rangle\langle\alpha|_A \otimes \mathbb{1}_B + \rho_{AB}\mathbb{1}_A \otimes |\beta\rangle\langle\beta|_B\big) + 1. \quad (2.58)
\end{aligned}
$$

$E_{\alpha\beta}$ can thus easily be evaluated by calculating the overlap of two Gaussian states [MM12], and is directly related to the Husimi Q-function (see, for example, [CG69]).

2.3.4 Results

We are now in the position to numerically evaluate the attained Bell correlations. The numerical value of S strongly depends on the choice of $\{\alpha_i, \beta_j\}$, as well as on the electromechanical parameters. In an experiment the parameters $\bar{n}$, n_0, Q_m will be practically fixed—it is clear that $\bar{n}$ and n_0 should be chosen as small as possible, while Q_m should be made as large as possible—, while the pulse duration and the electromechanical coupling strength can be easily tuned (up to a certain maximal value). We therefore optimize S with respect to the parameters τ_1, τ_2, and v (v being optimized for the first pulse only), and the measurement settings $\{\alpha_i, \beta_j\}$. As it turns out, the maximal violation can be obtained for $\alpha_i, \beta_j \in \mathbb{R}$. We show the maximal value of S for different values of the electromechanical cooperativity C, which fixes the constant coupling strength G in the first pulse, and the maximal coupling strength at the end of the second pulse, i. e., $G(\tau_2) = C\gamma_\mathrm{m}(\bar{n} + 1)$ (see fig. 26). [We therefore assume that the minimal cavity decay rate $\kappa_\mathrm{c}(\tau_2)$ can be chosen accordingly.]

The resulting values are shown in fig. 27(a) for different values of the transmissivity η_t and initial mechanical occupation numbers n_0. One can clearly see that both parameters have strong detrimental effects on S, and overall transmissivities clearly exceeding 90% are required. While the required initial occupation numbers n_0 are within reach of current experiments ($n_0 = 0.5$ has been demonstrated in [Pal+13]), satisfying the transmissivity requirements seems a challenging task. The attained values of S are, however, en-par with similar
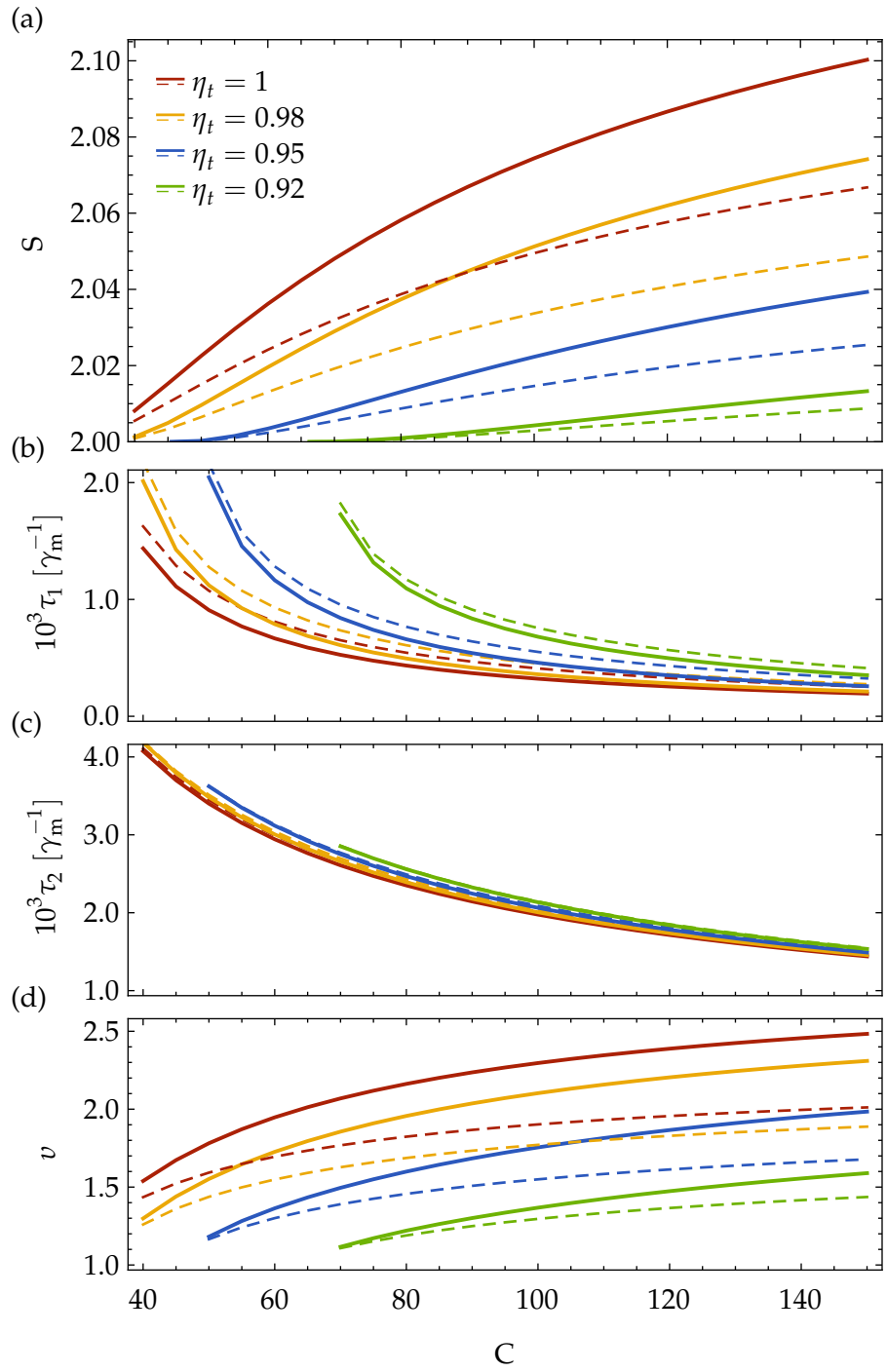
FIGURE 27. (a) Bell correlations against cooperativity optimized with respect to τ_1, τ_2 and v for different transmissivities $\eta_t = 1, 0.98, 0.95, 0.92$ (red, yellow, green, blue), and initial mechanical occupation numbers $n_0 = 0.1, 0.25$ (solid, dashed lines). (b)–(d) Optimal values of τ_1, τ_2, and v for the corresponding values of S in (a). Other parameters are $\bar{n} = 40$ and $\epsilon = 1/1000$ (corresponding to $\kappa_{lc}/\omega_m \approx 1/8$).

Bell tests for photons based on single-photon subtraction and homo-dyne detection [Gar+04; NC04].

Figure 27(b)–(d) show the values of the optimal parameters τ_1, τ_2, v corresponding to the values of S in (a). We can see that for low co-operativity values the pulse length increases for both pulses [plots (a) and (b)]. This is intuitively clear as both the generation of entangle-ment and the state swap depend on the product $G\tau_i = C(\bar{n}+1)\gamma_{\mathrm{m}}\tau_i$. Figure 27(c) shows that as the length of the first pulse increases, the optimal value for κ_{c} approaches G, i.e., we have $v \approx 1$. This is con-sistent with our discussion about mode matching in section 2.2.2.

2.A APPENDIX: PHASE SPACE DESCRIPTION

We use the following conventions for the phase space description of a n-mode bosonic system. We define the Weyl operator [similar to the displacement operator (1.35)] as

$$\mathcal{W}(\boldsymbol{r}) = \exp(-i\boldsymbol{r}^{\mathrm{T}}\boldsymbol{X}) \tag{2.59}$$

where $\boldsymbol{X} = (x_1, p_1, ...)^{\mathrm{T}}$ collects the quadrature operators obeying the commutation relations $[X_i, X_j] = iJ_{ij}$, and $\boldsymbol{r} \in \mathbb{R}^{2n}$. We can then write the characteristic function for a state ρ as

$$\Phi_\rho(\boldsymbol{r}) = \mathrm{tr}(\rho\mathcal{W}(\boldsymbol{r})). \tag{2.60}$$

Fourier transform We define the corresponding Wigner function [Hil+84] to be the symplectic Fourier transform, denoted by the linear operator $\mathcal{F}$, of Φ, i.e.,

$$W_\rho(\boldsymbol{r}) = \mathcal{F}\Phi_\rho(\boldsymbol{r}) := \frac{1}{(2\pi)^{2n}} \int_{\mathbb{R}^{2n}} \mathrm{d}v\, e^{i\boldsymbol{r}^{\mathrm{T}}\boldsymbol{J}v}\, \Phi(v). \tag{2.61}$$

Iff $\Phi(0) = 1$ then W_ρ is normalized, i.e., $\int_{\mathbb{R}^{2n}} \mathrm{d}r\, W\rho(\boldsymbol{r}) = 1$. For a zero-mean Gaussian state with a symmetric covariance matrix $\boldsymbol{\Sigma}$ the *Wigner function* characteristic function and the corresponding Wigner function take the form

$$\Phi_\rho(\boldsymbol{r}) = \exp\left(-\frac{1}{2}\boldsymbol{r}^{\mathrm{T}}\boldsymbol{\Sigma}\boldsymbol{r}\right), \tag{2.62}$$

$$W_\rho(\boldsymbol{r}) = \frac{1}{(2\pi)^n\sqrt{\det\boldsymbol{\Sigma}}} \exp\left(-\frac{1}{2}\boldsymbol{r}^{\mathrm{T}}\boldsymbol{J}^{\mathrm{T}}\boldsymbol{\Sigma}^{-1}\boldsymbol{J}\boldsymbol{r}\right). \tag{2.63}$$

In the main text we need to find the Wigner function for states of the form $\rho_k = \mathrm{tr}_2(P_k\rho_{12})$, where ρ_{12} describes a bipartite Gaussian state and P_k is a projection operator acting on subsystem 2. Using the identity

$$\rho = \frac{1}{\pi} \int_{\mathbb{R}^{2n}} \mathrm{d}v\, \mathcal{W}^\dagger(v)\Phi_\rho(v), \tag{2.64}$$

one can show that

$$\Phi_{\rho_k}(\boldsymbol{r}) = \int_{\mathbb{R}^n} \mathrm{d}v\, \Phi_{\rho_{12}}((\boldsymbol{r}, v))\Phi_{P_k}(-v), \tag{2.65}$$

where the integral is taken over the phase space of the second subsystem. More specifically we need to analyze the case where $\Phi_{\rho_{12}}$ is a zero-mean Gaussian function with a covariance matrix

$$\boldsymbol{\Sigma} = \begin{pmatrix} \sigma_a & \sigma_c \\ \sigma_c^{\mathrm{T}} & \sigma_b \end{pmatrix}, \tag{2.66}$$

and $P_k = \mathbb{1}_1 \otimes |k\rangle\langle k|_2$ projects onto the k-th Fock state. We then find that $\Phi_{\rho_k}(\boldsymbol{r}) = \tilde{\Phi}_{\rho_k}(\boldsymbol{r})/\tilde{\Phi}_{\rho_k}(0)$ with

$$\tilde{\Phi}_{\rho_k}(\boldsymbol{r}) = \frac{\Phi_{\rho_1}(\boldsymbol{r})}{k!} \partial_\lambda^k \left. \frac{\exp[\frac{1}{2}\boldsymbol{r}^\mathrm{T}\sigma_c(\sigma_b + \mu_\lambda)^{-1}\sigma_c^\mathrm{T}\boldsymbol{r}]}{(1-\lambda)|\sigma_b + \mu_\lambda|^{1/2}} \right|_{\lambda=0}, \qquad (2.67)$$

where we defined $\Phi_{\rho_1}(\boldsymbol{r}) = \exp(-\frac{1}{2}\boldsymbol{r}^\mathrm{T}\sigma_a\boldsymbol{r})$ and $\mu_\lambda = (1+\lambda)/2(1-\lambda)$. $\tilde{\Phi}_{\rho_k}$ at the same time determines the probability of finding subsystem 2 in state $|k\rangle_2$, i.e., $p_k = \tilde{\Phi}_{\rho_k}(0)$. To show eq. (2.67) we use the expansion of the thermal state ρ_{th} of a harmonic oscillator (which is a Gaussian state) in terms of Fock states $|k\rangle$. We have [see eq. (1.53)]

$$\rho_{\mathrm{th}} = \sum_{n=0}^{\infty} (1-\lambda)\lambda^n |n\rangle\langle n| \qquad (2.68)$$

where the parameter λ is connected to the mean occupation number by $\bar{n} = \lambda/(1-\lambda)$. We can prove the identity $\partial_\lambda^k \lambda^n|_{\lambda=0} = k!\,\delta_{n,k}$, where $\delta_{n,k}$ denotes the Kronecker delta, and thus

$$|k\rangle\langle k| = (k!)^{-1} \frac{\partial^k}{\partial\lambda^k} \left. \frac{\rho_{\mathrm{th}}}{1-\lambda} \right|_{\lambda=0}. \qquad (2.69)$$

We can then write the corresponding characteristic functions as

$$\Phi_{\mathrm{th}}^\lambda(\boldsymbol{r}) = \exp\left(-\tfrac{1}{2}\mu\boldsymbol{r}^\mathrm{T}\boldsymbol{r}\right), \qquad (2.70\mathrm{a})$$

$$\Phi_{P_k}(\boldsymbol{r}) = \frac{1}{k!} \frac{\partial^k}{\partial\lambda^k} \left. \frac{\Phi_{\mathrm{th}}^\lambda(\boldsymbol{r})}{1-\lambda} \right|_{\lambda=0}. \qquad (2.70\mathrm{b})$$

Using these results together with eq. (2.65) and evaluating the Gaussian integral leads to eq. (2.67).

2.B APPENDIX: INPUT–OUTPUT RELATIONS AS A GAUSSIAN CHANNEL

We consider a linear, Gaussian system of the form

$$\mathrm{d}X(t) = \mathbf{F}X(t)\,\mathrm{d}t + \mathbf{M}\,\mathrm{d}V(t), \qquad (2.71\mathrm{a})$$

$$\mathrm{d}Y(t) = \mathbf{H}X(t)\,\mathrm{d}t + \mathrm{d}V(t), \qquad (2.71\mathrm{b})$$

where the n-vector X contains the phase space operators of the system (e.g., x_{m}, p_{m}, x_{c}, p_{c}), the m-vector Y describes the measurements (e.g., x_{out}, p_{out}), and $\mathrm{d}V$ collects different noise sources (e.g., electromagnetic shot noise or mechanical noise terms). $\mathbf{F}$, $\mathbf{M}$ and $\mathbf{H}$ are real matrices of appropriate dimensions (see appendix 2.A). The formal solution of (2.71) is

$$X(t) = \mathbf{R}(t)X(0) + \int_0^t \mathbf{R}(t-s)\,\mathrm{d}V(t), \qquad (2.72)$$

where $\mathbf{R}(t) = \exp(\mathbf{F}t)$. If we collect a set of temporal modes $\{\alpha_i\}$ in the $n \times n$ matrix $\mathbf{Z}$ we can write

$$Y_{\text{out}} = \int_0^\tau \mathbf{Z}(t)\, \mathrm{d}Y(t) = \mathbf{S}^{\mathsf{T}}X(0) + \tilde{W}, \tag{2.73}$$

where $\mathbf{S}$ and W are given by

$$\mathbf{S} = \int_0^\tau \mathbf{Z}(t)\mathbf{H}\mathbf{R}(t)\, \mathrm{d}t, \tag{2.74a}$$

$$\tilde{W} = \int_0^\tau \left[\int_s^\tau \mathbf{Z}(t)\mathbf{H}\mathbf{R}(t-s)\mathbf{M}\, \mathrm{d}t + \mathbf{Z}(s) \right] \mathrm{d}V(s). \tag{2.74b}$$

In our setup we only want to extract information about the mechanical system while we treat the cavity as an additional bath we trace over. This means that the number of measurements will be smaller than the number of state variables ($m < n$). We therefore decompose $\mathbf{S} = (\mathbf{S}_{\text{m}}^{\mathsf{T}}, \mathbf{S}_{\text{c}}^{\mathsf{T}})^{\mathsf{T}}$ and $X(0) = (X_{\text{m}}^{\mathsf{T}}(0), X_{\text{c}}^{\mathsf{T}}(0))^{\mathsf{T}}$ and write

$$Y_{\text{out}} = \mathbf{S}_{\text{m}}^{\mathsf{T}}X_{\text{m}}(0) + \mathbf{S}_{\text{c}}^{\mathsf{T}}X_{\text{c}}(0) + \tilde{W}, \tag{2.75}$$

which, after setting $Y_{\text{in}} = X_{\text{m}}(0)$ and $W = \mathbf{S}_{\text{c}}^{\mathsf{T}}X_c(0) + \tilde{W}$, yields (2.50).

Let us briefly discuss how the Wigner function of a state ρ transforms under the action of a Gaussian channel of the form (2.50). We first note that under $Y_{\text{in}} \to Y_{\text{out}}$ the Weyl operator transforms as

$$\mathcal{W}(r) \to \mathcal{W}'(r) = \mathcal{W}(\mathbf{S}r)\exp\left(-\tfrac{1}{2}r^{\mathsf{T}}\mathbf{N}_W r\right) \tag{2.76}$$

where $\mathbf{N}_W$ is the symmetric covariance matrix of W. For the characteristic function $\Phi_{\rho'}(r) = \mathrm{tr}(\rho'\mathcal{W}(r)) = \mathrm{tr}(\rho\mathcal{W}'(r))$ of the transformed state ρ' this leads to

$$\Phi_{\rho'}(r) = \Phi_\rho(\mathbf{S}r)\exp\left(-\tfrac{1}{2}r^{\mathsf{T}}\mathbf{N}_W r\right). \tag{2.77}$$

The corresponding Wigner function is then the Fourier transform of $\Phi_{\rho'}$ [see eq. (2.61)], and thus by the convolution theorem [IIo7, p 1118] the convolution of $\Phi_\rho(\mathbf{S}r)$ with a Gaussian of variance $\mathbf{N}_W$. For a zero-mean Gaussian state ρ with a characteristic function of the form (3.17) we can simply add the respective covariance matrices, yielding

$$W_{\rho'}(r) = \exp\left(-\frac{1}{2}r^{\mathsf{T}}\left[(\mathbf{S}^{\mathsf{T}}\Sigma\mathbf{S})^{-1} + \mathbf{N}_W^{-1}\right]r\right). \tag{2.78}$$

2.C APPENDIX: ADIABATIC ELIMINATION IN THE CASCADED SYSTEM

Adiabatic elimination of the cavity mode on the basis of the master equation (1.52) can be achieved through the time-convolutionless projection operator method [CS79]. First we briefly review the basic idea and the most important expressions, and then adapt it to fit the structure of the optomechanical master equation.

2.C.1 *Time-convolutionless Projection Operator Method*

Given a set of linear operators $\mathcal{L}_i$ ($i \in \{0, 1\}$) and a corresponding equation of the form

$$\frac{\mathrm{d}}{\mathrm{d}t}\rho(t) = [\mathcal{L}_0 + \epsilon\mathcal{L}_1(t)]\rho(t), \qquad (2.79)$$

the goal is to find the dynamics of ρ on a subspace defined by the projection $\mathcal{P} = \mathbb{1} - \mathcal{Q}$. We first transform into an interaction picture with $\mathcal{L}_0$ and define

$$\tilde{\rho}(t) = \exp(-\mathcal{L}_0 t)\rho(t), \qquad (2.80a)$$

$$\tilde{\mathcal{L}}_i(t) = \exp(-\mathcal{L}_0 t)\mathcal{L}_i(t)\exp(\mathcal{L}_0 t). \qquad (2.80b)$$

The equation of motion for $\mathcal{P}\rho$ can then be written in the form[8]

$$\frac{\mathrm{d}}{\mathrm{d}t}\mathcal{P}\tilde{\rho}(t) = \mathcal{K}(t)\mathcal{P}\tilde{\rho}(t), \qquad (2.81)$$

where we assumed that $\mathcal{Q}\rho(0) = 0$. The exact expression for $\mathcal{K}$ is [CS79]

$$\mathcal{K}(t) = \epsilon\mathcal{P}\tilde{\mathcal{L}}_1(t)[1 - \Sigma(t)]^{-1}\mathcal{P}, \qquad (2.82a)$$

$$\Sigma(t) = \epsilon\int_0^t \mathcal{G}(t,s)\mathcal{Q}\tilde{\mathcal{L}}_1(s)\mathcal{P}G(t,s), \qquad (2.82b)$$

where G and $\mathcal{G}$ are the forward and backward propagators

$$\mathcal{G}(t,s) = \mathcal{T}_+\exp\left(\epsilon\int_s^t \mathrm{d}\tau\,\mathcal{Q}\tilde{\mathcal{L}}_1(\tau)\right), \qquad (2.83a)$$

$$G(t,s) = \mathcal{T}_-\exp\left(-\epsilon\int_s^t \mathrm{d}\tau\,\tilde{\mathcal{L}}_1(\tau)\right), \qquad (2.83b)$$

and $\mathcal{T}_{(-)+}$ the (anti-)chronological time-ordering operator. We are mainly interested in a expansion of $\mathcal{K}$ in powers of the small parameter ϵ, which we write as $\mathcal{K} = \sum_n \epsilon^n \mathcal{K}_n$. We can show that up to second order the expansion coefficients are given by

$$\mathcal{K}_1(t) = \mathcal{P}\tilde{\mathcal{L}}_1(t)\mathcal{P}, \qquad (2.84a)$$

$$\mathcal{K}_2(t) = \mathcal{P}\tilde{\mathcal{L}}_1(t)\int_0^t \mathrm{d}\tau\,\mathcal{Q}\tilde{\mathcal{L}}_1(\tau)\mathcal{P}. \qquad (2.84b)$$

In order to apply this method for adiabatic elimination we need to identify a suitable subspace $\mathcal{P}$ which describes the relevant dynamics. This subspace must be chosen such that [Gar84]

$$\mathcal{P}\mathcal{L}_0 = \mathcal{L}_0\mathcal{P} = 0, \qquad (2.85a)$$

$$\mathcal{P}\mathcal{L}_1\mathcal{P} = 0, \qquad (2.85b)$$

$$\mathcal{P} = \lim_{t\to 0} e^{\mathcal{L}_0 t}. \qquad (2.85c)$$

8. This form is similar to the Nakajima–Zwanzig equation; however it is local in time [BP02].

Below we will look at a master equation whose generator can be written as $\mathcal{L}(t) = \mathcal{L}_0 + \mathcal{L}_m + \epsilon \mathcal{L}_1(t) + \epsilon^2 \mathcal{L}_2$. $\mathcal{L}_m$ commutes with $\mathcal{L}_0$, i.e., $\mathcal{L}_0 \mathcal{L}_m = \mathcal{L}_m \mathcal{L}_0$, and we thus have

$$\mathcal{L}_m \mathcal{P} = \mathcal{P} \mathcal{L}_m, \tag{2.86a}$$

$$\mathcal{Q} \mathcal{L}_m \mathcal{P} = \mathcal{P} \mathcal{L}_m \mathcal{Q} = 0. \tag{2.86b}$$

Let us explore the expansion of $\mathcal{K}$ for the modified Liouvillian $\mathcal{L}$. We first make the substitution $\mathcal{L}_0 \to \mathcal{L}_0 + \mathcal{L}_m$, under which equations (2.82) then become (denoting the new expressions by $\mathcal{K}'$, etc.)

$$\mathcal{K}'(t) = \mathcal{K}(t) + \mathcal{L}_m \mathcal{P}[\mathbb{1} - \Sigma'(t)]^{-1} \mathcal{P} \tag{2.87a}$$

$$\Sigma'(t) = \epsilon \int_0^t \mathcal{G}'(t,s) \mathcal{Q} \tilde{\mathcal{L}}_1(s) \mathcal{P} G'(t,s). \tag{2.87b}$$

Here we already used relations (2.86). Using $\mathcal{P} \mathcal{G}'(t,s) \mathcal{Q} = 0$ and thus $\mathcal{P} \Sigma' = 0$ leads to $\mathcal{P}[\mathbb{1} - \Sigma']^{-1} \mathcal{P} = \mathcal{P}[\mathbb{1} - \mathcal{P}\Sigma'\mathcal{P}]^{-1} \mathcal{P} = \mathcal{P}$. This shows that

$$\mathcal{K}' = \mathcal{K} + \mathcal{L}_m \mathcal{P}. \tag{2.88}$$

In the next step we can substitute $\mathcal{L}_1(t) \to \mathcal{L}_1(t) + \epsilon \mathcal{L}_2$ into expressions (2.84) and collect the terms of matching order in ϵ. Taking this together the expansion coefficients $\mathcal{K}'_n$ up to second order are

$$\mathcal{K}'_0 = \mathcal{L}_m \mathcal{P}, \tag{2.89a}$$

$$\mathcal{K}'_1(t) = \mathcal{P} \tilde{\mathcal{L}}_1(t) \mathcal{P}, \tag{2.89b}$$

$$\mathcal{K}'_2(t) = \mathcal{P} \tilde{\mathcal{L}}_2(t) \mathcal{P} + \mathcal{P} \tilde{\mathcal{L}}_1(t) \int_0^t \mathrm{d}\tau \mathcal{Q} \tilde{\mathcal{L}}_1(\tau) \mathcal{P}. \tag{2.89c}$$

2.c.2 *Elimination of the Optical Mode*

To eliminate the LC mode we choose $\mathcal{P}\rho = \mathrm{tr}_{lc}(\rho) \otimes \rho_{vac}$ which projects the state ρ onto the cavity's ground state. This is the subspace we are interested in, as in the limit $g \ll \kappa_{lc}$ all photons scattered from the mechanical oscillator into the resonator (typically on a timescale $1/g$) immediately decay from it (on a much shorter timescale $1/\kappa_{lc}$). For the microwave cavity we have $\kappa_c \approx 4g^2/\kappa_{lc}$ and thus $\kappa_c/\kappa_{lc} \approx (2g/\kappa_c)^2$. It is convenient to introduce the parameter $\bar{\kappa} = \sqrt{\kappa_{lc}\kappa_c}$. Consequently we assume a separation of time scales of the form

$$\kappa_c \ll g, \bar{\kappa} \ll \kappa_{lc}, \omega_m, \Delta_c, \Delta_{lc}$$

which reflects the structure of the Liouvillian if we identify ϵ with g/κ_c. By going into an interaction picture with the free Hamiltonian

$\omega_m c_m^\dagger c_m - \Delta_c c_c^\dagger c_c$ we can write the master equation (2.29) in the required form $\dot{\rho} = [\mathcal{L}_0 + \mathcal{L}_m^{th} + \mathcal{L}_1(t) + \mathcal{L}_2]\rho$ with the definitions

$$\mathcal{L}_0\rho = -i\Delta_{lc}[c_{lc}^\dagger c_{lc}, \rho] + \kappa_{lc}\,\mathcal{D}[c_{lc}]\rho, \tag{2.90a}$$

$$\mathcal{L}_1(t) = e^{i\omega_m t}\,\mathcal{L}_{1,m}^+\rho + e^{-i\Delta_c t}\,\mathcal{L}_{1,c}^-\rho + \mathrm{H.c.}, \tag{2.90b}$$

$$\mathcal{L}_2 = \kappa_c\,\mathcal{D}[c_c]\rho, \tag{2.90c}$$

$$\mathcal{L}_m^{th}\rho = \gamma_m(\bar{n}+1)\,\mathcal{D}[c_m]\rho + \gamma_m\bar{n}\,\mathcal{D}[c_m^\dagger]\rho, \tag{2.90d}$$

and

$$\mathcal{L}_m^+\rho = -ig[c_m^\dagger(c_{lc} + c_{lc}^\dagger), \rho], \tag{2.90e}$$

$$\mathcal{L}_m^-\rho = (\mathcal{L}_m^+\rho)^\dagger = -ig[c_m(c_{lc} + c_{lc}^\dagger), \rho], \tag{2.90f}$$

$$\mathcal{L}_c^+\rho = -\sqrt{\eta_t}\bar{\kappa}[c_c^\dagger, c_{lc}\rho], \tag{2.90g}$$

$$\mathcal{L}_c^-\rho = (\mathcal{L}_c^-\rho)^\dagger = \sqrt{\eta_t}\bar{\kappa}[c_c, \rho c_{lc}^\dagger]. \tag{2.90h}$$

We can then show equations (2.85) and additionally find the useful relations

$$\mathcal{Q}\mathcal{L}_0\mathcal{Q} = 0, \tag{2.91a}$$

$$\mathcal{P}\,e^{\mathcal{L}_0 t} = e^{\mathcal{L}_0 t}\,\mathcal{P} = \mathcal{P}, \tag{2.91b}$$

which we can use to evaluate equations (2.89). Additionally it is immediate to show relations (2.86) and we thus separate the mechanical decoherence term $\mathcal{L}_m^{th}$ from the rest of the dynamics and neglect it for the rest of this section. We immediately find $\mathcal{K}_1(t) = \mathcal{P}\tilde{\mathcal{L}}_1(t)\mathcal{P} = \mathcal{P}\mathcal{L}_1(t)\mathcal{P} = 0$ and $\mathcal{P}\tilde{\mathcal{L}}_2\mathcal{P} = \mathcal{L}_2\mathcal{P}$. The second term in eq. (2.89c) is more involved. We find

$$\mathcal{P}\tilde{\mathcal{L}}_1(t)\int_0^t d\tau\,\mathcal{Q}\tilde{\mathcal{L}}_1(\tau)\mathcal{P}\rho(t) = \mathcal{P}\tilde{\mathcal{L}}_1(t)\int_0^t d\tau\tilde{\mathcal{L}}_1(\tau)\mathcal{P}\rho(t)$$

$$= \mathcal{P}\mathcal{L}_1(t)\int_0^t d\tau\,e^{\mathcal{L}_0(t-\tau)}\,\mathcal{L}_1(\tau)\mathcal{P}\rho(t)$$

$$= \mathcal{P}\mathcal{L}_1(t)\int_0^t d\tau\,e^{\mathcal{L}_0\tau}\,\mathcal{L}_1(t-\tau)\mathcal{P}\rho(t)$$

$$= \mathcal{P}\mathcal{L}_1(t)\int_0^t d\tau\,e^{\mathcal{L}_0\tau}[\mathcal{L}_m^+\,e^{i\omega_m(t-\tau)} + \mathcal{L}_m^-\,e^{-i\omega_m(t-\tau)}]\mathcal{P}\rho(t)$$

$$= \mathcal{P}[\mathcal{L}_m^+\,e^{i\omega_m t} + \mathrm{H.c.}]\int_0^t d\tau\,e^{\mathcal{L}_0\tau}[\mathcal{L}_m^+\,e^{i\omega_m(t-\tau)} + \mathrm{H.c.}]\mathcal{P}\rho(t)$$

$$+ \mathcal{P}[\mathcal{L}_c^+\,e^{-i\Delta_c t} + \mathrm{H.c.}]\int_0^t d\tau\,e^{\mathcal{L}_0\tau}[\mathcal{L}_m^+\,e^{i\omega_m(t-\tau)} + \mathrm{H.c.}]\mathcal{P}\rho(t),$$

taking into account that $\mathcal{L}_c^{\pm}\mathcal{P} = 0$. We thus end up with the expanded expression

$$\mathcal{P}\tilde{\mathcal{L}}_1(t)\int_0^t d\tau Q\tilde{\mathcal{L}}_1(\tau)\mathcal{P}\rho(t) = \int_0^t d\tau\, e^{i\omega_m\tau}\,\mathcal{P}\mathcal{L}_m^+ e^{\mathcal{L}_0\tau}\,\mathcal{L}_m^-\mathcal{P}\rho(t) + \mathrm{H.\,c.}$$

$$+ \int_0^t d\tau\, e^{i\omega_m\tau}\,\mathcal{P}\mathcal{L}_m^- e^{\mathcal{L}_0\tau}\,\mathcal{L}_m^-\mathcal{P}\rho(t)\, e^{-2i\omega_m t} + \mathrm{H.\,c.}$$

$$+ \int_0^t d\tau\, e^{i\omega_m\tau}\,\mathcal{P}\mathcal{L}_c^+ e^{\mathcal{L}_0\tau}\,\mathcal{L}_m^-\mathcal{P}\rho(t)\, e^{-i(\Delta_c+\omega_m)t} + \mathrm{H.\,c.}$$

$$+ \int_0^t d\tau\, e^{-i\omega_m\tau}\,\mathcal{P}\mathcal{L}_c^+ e^{\mathcal{L}_0\tau}\,\mathcal{L}_m^+\mathcal{P}\rho(t)\, e^{-i(\Delta_c-\omega_m)t} + \mathrm{H.\,c.}$$

The first term results from the optomechanical interaction alone and will give rise to the familiar heating and cooling terms derived in [Wil+08]. The second term is fast oscillating and will later be dropped in a rotating-wave-approximation. The last two terms correspond to scattering of photons into the cascaded cavity mode. Note that depending on the detuning of the second cavity only one of the mechanical sidebands is resonantly scattered into the second cavity mode. We evaluate the important terms separately, treating the integrand only for the moment. We introduce $\mu(t) = \mathrm{tr}_{lc}(\rho(t))$ and thus have $\mathcal{P}\rho(t) = \mu(t) \otimes \rho_0$. Additionally we here use $x_{lc} = c_{lc} + c_{lc}^\dagger$. The first term gives[9]

$$\mathrm{tr}_{lc}(\mathcal{P}\mathcal{L}_m^+ e^{\mathcal{L}_0\tau}\,\mathcal{L}_m^-\mathcal{P}\rho(t)) = -ig\,\mathrm{tr}_{lc}(\mathcal{L}_m^+ e^{\mathcal{L}_0\tau}[c_m x_{lc}, \mu\otimes\rho_0])$$

$$= -ig\,\mathrm{tr}_{lc}(\mathcal{L}_m^+(c_m\mu\otimes e^{\mathcal{L}_0\tau}x_{lc}\rho_0 - \mu c_m\otimes e^{\mathcal{L}_0\tau}\rho_0 x_{lc}))$$

$$= -g^2\,\mathrm{tr}_{lc}([c_m^\dagger x_{lc}, c_m\mu\otimes e^{\mathcal{L}_0\tau}x_{lc}\rho_0 - \mu c_m\otimes e^{\mathcal{L}_0\tau}\rho_0 x_{lc}])$$

$$= -g^2\big(\mathrm{tr}_{lc}(x_{lc}e^{\mathcal{L}_0\tau}x_{lc}\rho_0)[c_m^\dagger, c_m\mu] - \mathrm{tr}_{lc}(x_{lc}e^{\mathcal{L}_0\tau}\rho_0 x_{lc})[c_m^\dagger, \mu c_m]\big)$$

$$= -g^2\big(\mathrm{tr}_{lc}(c_{lc}(\tau)c_{lc}^\dagger\rho_0)[c_m^\dagger, c_m\mu] - \mathrm{tr}_{lc}(c_{lc}c_{lc}^\dagger(\tau)\rho_0)[c_m^\dagger, \mu c_m]\big).$$

The third and fourth term give respectively

$$\mathrm{tr}_{lc}(\mathcal{P}\mathcal{L}_c^+ e^{\mathcal{L}_0\tau}\,\mathcal{L}_m^-\mathcal{P}\rho(t)) = -ig\,\mathrm{tr}_{lc}(\mathcal{L}_c^+ e^{\mathcal{L}_0\tau}[c_m x_{lc}, \mu\otimes\rho_0])$$

$$= -ig\,\mathrm{tr}_{lc}(\mathcal{L}_c^+(c_m\mu\otimes e^{\mathcal{L}_0\tau}x_{lc}\rho_0 - \mu c_m\otimes e^{\mathcal{L}_0\tau}\rho_0 x_{lc}))$$

$$= ig\sqrt{\eta_t}\bar{\kappa}\,\mathrm{tr}_{lc}([c_c^\dagger, c_m\mu\otimes c_m e^{\mathcal{L}_0\tau}x_{lc}\rho_0 - \mu c_m\otimes c_m e^{\mathcal{L}_0\tau}\rho_0 x_{lc}])$$

$$= ig\sqrt{\eta_t}\bar{\kappa}\big(\mathrm{tr}_{lc}(c_{lc}e^{\mathcal{L}_0\tau}x_{lc}\rho_0)[c_c^\dagger, c_m\mu] - \mathrm{tr}_{lc}(c_{lc}e^{\mathcal{L}_0\tau}\rho_0 x_{lc})[c_c^\dagger, \mu c_m]\big)$$

$$= ig\sqrt{\eta_t}\bar{\kappa}\,\mathrm{tr}_{lc}(c_{lc}(\tau)c_{lc}^\dagger\rho_0)[c_c^\dagger, c_m\mu],$$

and

$$\mathrm{tr}_{lc}(\mathcal{P}\mathcal{L}_c^+ e^{\mathcal{L}_0\tau}\,\mathcal{L}_m^+\mathcal{P}\rho(t)) = -ig\,\mathrm{tr}_{lc}(\mathcal{L}_c^+ e^{\mathcal{L}_0\tau}[c_m^\dagger x_{lc}, \mu\otimes\rho_0])$$

$$= -ig\,\mathrm{tr}_{lc}(\mathcal{L}_c^+(c_m^\dagger\mu\otimes e^{\mathcal{L}_0\tau}x_{lc}\rho_0 - \mu c_m^\dagger\otimes e^{\mathcal{L}_0\tau}\rho_0 x_{lc}))$$

$$= ig\sqrt{\eta_t}\bar{\kappa}\,\mathrm{tr}_{lc}([c_c^\dagger, c_m^\dagger\mu\otimes c_{lc}e^{\mathcal{L}_0\tau}x_{lc}\rho_0 - \mu c_m^\dagger\otimes c_{lc}e^{\mathcal{L}_0\tau}\rho_0 x_{lc}])$$

$$= ig\sqrt{\eta_t}\bar{\kappa}\big(\mathrm{tr}_{lc}(c_{lc}e^{\mathcal{L}_0\tau}x_{lc}\rho_0)[c_c^\dagger, c_m^\dagger\mu] - \mathrm{tr}_{lc}(c_{lc}e^{\mathcal{L}_0\tau}\rho_0 x_{lc})[c_c^\dagger, \mu c_m^\dagger]\big)$$

$$= ig\sqrt{\eta_t}\bar{\kappa}\,\mathrm{tr}_{lc}(c_{lc}(\tau)c_{lc}^\dagger\rho_0)[c_c^\dagger, c_m^\dagger\mu].$$

As we will drop the second term in RWA we do not state the explicit expression here. Next we need to find the correlation functions $\text{tr}_{\text{lc}}(c_{\text{lc}}(t)c_{\text{lc}}^\dagger(0)\rho_0)$ and $\text{tr}_{\text{lc}}(c_{\text{lc}}(0)c_{\text{lc}}^\dagger(t)\rho_0) = \text{tr}_{\text{lc}}(c_{\text{lc}}(t)c_{\text{lc}}^\dagger(0)\rho_0)^*$. These can be calculated by observing that

$$\frac{\text{d}}{\text{d}t}\text{tr}_{\text{lc}}(c_{\text{lc}}(t)c_{\text{lc}}^\dagger(0)\rho_0) = \text{tr}_{\text{lc}}([\mathcal{L}_0^\dagger c_{\text{lc}}(t)]c_{\text{lc}}^\dagger(0)\rho_0) =$$

$$(\text{i}\Delta_{\text{lc}} - \kappa_{\text{lc}}/2)\,\text{tr}_{\text{lc}}(c_{\text{lc}}(t)c_{\text{lc}}^\dagger(0)\rho_0), \quad (2.92)$$

$\mathcal{L}_0^\dagger$ being the adjoint Liouville operator discussed in appendix A.3, and thus

$$\text{tr}_{\text{lc}}(c_{\text{lc}}(t)c_{\text{lc}}^\dagger(0)\rho_0) = \exp\left[(\text{i}\Delta_{\text{lc}} - \kappa_{\text{lc}}/2)t\right], \quad (2.93\text{a})$$

$$\text{tr}_{\text{lc}}(c_{\text{lc}}(0)c_{\text{lc}}^\dagger(t)\rho_0) = \exp\left[-(\text{i}\Delta_{\text{lc}} + \kappa_{\text{lc}}/2)t\right]. \quad (2.93\text{b})$$

If we neglect terms of the form $\exp(-\kappa_{\text{lc}}t)$ we thus find[10]

10. This can be made exact by taking the initial time to $-\infty$.

$$\int_0^t \text{d}\tau\, \text{e}^{\pm\text{i}\omega_{\text{m}}\tau}\,\text{tr}_{\text{lc}}(c_{\text{lc}}(\tau)c_{\text{lc}}^\dagger(0)\rho_0) \approx \eta_\mp, \quad (2.94\text{a})$$

where $\eta_\pm = \left[\frac{\kappa_{\text{lc}}}{2} - \text{i}(-\Delta_{\text{lc}} \pm \omega_{\text{m}})\right]^{-1}$. Taking this all together we neglect fast rotating terms in a RWA,[11] and find

11. This is justified by the time average introduced below.

$$\dot{\mu} = -\text{i}[\delta\omega_{\text{m}}c_{\text{m}}^\dagger c_{\text{m}}, \mu] + \mathcal{L}_{\text{m}}^{\text{th}}\mu$$

$$+ \Gamma_-\,\mathcal{D}[c_{\text{m}}]\mu + \Gamma_+\,\mathcal{D}[c_{\text{m}}^\dagger]\mu + \kappa_{\text{c}}\,\mathcal{D}[c_{\text{c}}]\mu$$

$$- g\sqrt{\eta_{\text{t}}\kappa_{\text{c}}/\kappa_{\text{lc}}}\left\{[c_{\text{c}}^\dagger, s_+\mu]\,\text{e}^{-\text{i}(\Delta_{\text{c}} - \omega_{\text{m}})t} + \text{H.c.}\right\}$$

$$- g\sqrt{\eta_{\text{t}}\kappa_{\text{c}}/\kappa_{\text{lc}}}\left\{[c_{\text{c}}^\dagger, s_-\mu]\,\text{e}^{-\text{i}(\Delta_{\text{c}} + \omega_{\text{m}})t} + \text{H.c.}\right\}, \quad (2.95)$$

where we introduced jump operators $s_+ = -\text{i}\kappa_{\text{lc}}\eta_+ c_{\text{m}}^\dagger$ and $s_- = -\text{i}\kappa_{\text{lc}}\eta_- c_{\text{m}}$. The other parameters are given by eqs. (1.48) and (1.50). To get a time-independent master equation we first go into an interaction picture with $\delta\omega_{\text{m}}c_{\text{m}}^\dagger c_{\text{m}}$, which eliminates the first term in eq. (B.12) and leads to the replacement $\text{e}^{\pm\text{i}\omega_{\text{m}}t} \to \text{e}^{\pm\text{i}\omega_{\text{m}}^{\text{eff}}t}$ (with $\omega_{\text{m}}^{\text{eff}} = \omega_{\text{m}} + \delta\omega_{\text{m}}$). We then introduce an averaged density operator, formally defined by

$$\bar{\mu}(t)\,\text{d}t = \int_t^{t+\delta t}\text{d}\tau\mu(\tau) \quad (2.96)$$

in analogy to the treatment of adiabatic elimination in the Heisenberg picture (appendix 1.A). (See also the treatment of heterodyne detection in appendix B.1.1 for more details on this construction.) δt has to be chosen to be long on the mechanical oscillation frequency, but short on all other timescales. This leads to the inequality $\omega_{\text{m}}^{\text{eff}} \gg 1/\delta t \gg g^2/\kappa_{\text{lc}}, g\sqrt{\kappa_{\text{c}}/\kappa_{\text{lc}}}$. If we now consider the cases $\Delta_{\text{c}} = \pm\omega_{\text{m}}^{\text{eff}}$ and neglect fast rotating terms [which give a correction of

order $\mathcal{O}(1/\omega_{\mathrm{m}}^{\mathrm{eff}}\delta t)]$ we eventually find for $\bar{\mu}$ the coarse-grained master equation

$$\dot{\bar{\mu}} = \mathcal{L}_{\mathrm{m}}^{\mathrm{th}}\bar{\mu} + \Gamma_- \mathcal{D}[c_{\mathrm{m}}]\bar{\mu} + \Gamma_+ \mathcal{D}[c_{\mathrm{m}}^\dagger]\bar{\mu} + \kappa_{\mathrm{c}} \mathcal{D}[c_{\mathrm{c}}]\bar{\mu}$$
$$- g\sqrt{\eta_{\mathrm{t}}\kappa_{\mathrm{c}}/\kappa_{\mathrm{lc}}}([c_{\mathrm{c}}^\dagger, s_\pm\bar{\mu}] + [\bar{\mu}s_\pm^\dagger, c_{\mathrm{c}}]). \quad (2.97)$$

(This procedure is discussed in more detail in appendix 3.A.) Note that dropping the terms involving the cascaded cavity (fourth and fith term) leads to the MEQ (1.55). We can now use the identity

$$\mathcal{D}[a+b]\rho = \mathcal{D}[a]\rho + \mathcal{D}[b]\rho + \frac{1}{2}[a^\dagger b - ab^\dagger, \rho] - ([a^\dagger, b\rho] + [\rho b^\dagger, a])$$

to convert this to explicit Lindblad form. For the two cases $\Delta_{\mathrm{c}} = \pm\omega_{\mathrm{m}}^{\mathrm{eff}}$ we find respectively

$$\dot{\bar{\mu}} = \mathcal{L}_{\mathrm{m}}\bar{\mu} + \mathrm{i}\sqrt{\eta_{\mathrm{t}}\kappa_{\mathrm{c}}\Gamma_+/4}[\mathrm{e}^{-\mathrm{i}\varphi_+}c_{\mathrm{m}}c_{\mathrm{c}} + \mathrm{H.\,c.}, \bar{\mu}] + \Gamma_- \mathcal{D}[c_{\mathrm{m}}]\bar{\mu}$$
$$+ (1-\eta_{\mathrm{t}})\Gamma_+ \mathcal{D}[c_{\mathrm{m}}^\dagger]\bar{\mu} + \mathcal{D}[\sqrt{\kappa_{\mathrm{c}}}c_{\mathrm{c}} - \mathrm{i}\,\mathrm{e}^{\mathrm{i}\varphi_+}\sqrt{\eta_{\mathrm{t}}\Gamma_+}c_{\mathrm{m}}^\dagger]\bar{\mu},$$
$$(2.98\mathrm{a})$$

$$\dot{\bar{\mu}} = \mathcal{L}_{\mathrm{m}}\bar{\mu} + \mathrm{i}\sqrt{\eta_{\mathrm{t}}\kappa_{\mathrm{c}}\Gamma_-/4}[\mathrm{e}^{-\mathrm{i}\varphi_-}c_{\mathrm{m}}^\dagger c_{\mathrm{c}} + \mathrm{H.\,c.}, \bar{\mu}] + \Gamma_+ \mathcal{D}[c_{\mathrm{m}}^\dagger]\bar{\mu}$$
$$+ (1-\eta_{\mathrm{t}})\Gamma_- \mathcal{D}[c_{\mathrm{m}}]\bar{\mu} + \mathcal{D}[\sqrt{\kappa_{\mathrm{c}}}c_{\mathrm{c}} - \mathrm{i}\,\mathrm{e}^{\mathrm{i}\varphi_-}\sqrt{\eta_{\mathrm{t}}\Gamma_-}c_{\mathrm{m}}]\bar{\mu},$$
$$(2.98\mathrm{b})$$

with the definition $\varphi_\pm = \arg(\eta_\pm)$. If we additionally choose $\Delta_{\mathrm{lc}} = \pm\omega_{\mathrm{m}}^{\mathrm{eff}}$ the resonant terms have phases $\varphi_\pm = 0$ and the resonant scattering rates are $\Gamma_\pm = \Gamma := 4g^2/\kappa_{\mathrm{lc}}$, while the off-resonant rates $\Gamma_\mp = \epsilon\Gamma$ with $\epsilon = 1/[1 + (4\omega_{\mathrm{m}}/\kappa_{\mathrm{lc}})^2]$. Equations (2.98) then lead to eqs. (2.30) and (2.43) respectively.

2.D APPENDIX: PULSE SHAPE OPTIMISATION

Here we discuss the optimal-control problem of how to transfer the mechanical quantum state into a cascaded cavity. We use a red-detuned ($\Delta_{\mathrm{c}} = -\omega_{\mathrm{m}}$) light pulse of length τ_2, whose power $P(t)$ can be varied in time [leading to a adiabatic coupling strength $G(t)$]. Additionally we assume we can tune the bandwidth $\kappa_{\mathrm{c}}(t)$ of the cascaded cavity. To identify the relevant temporal shapes we rewrite the system's evolution in terms of Langevin equations [see equations (2.46)]. Here we are only interested in the classical dynamics and we thus introduce the mean values $\beta(t) = \langle c_{\mathrm{m}}(t)\rangle$ and $\xi(t) = \langle c_{\mathrm{c}}(t)\rangle$. Their equations of motion are

$$\dot{\beta}(t) = -\frac{G(t)}{2}\beta(t), \quad (2.99\mathrm{a})$$

$$\dot{\xi}(t) = -\frac{\kappa_{\mathrm{c}}}{2}(t)\xi(t) - \mathrm{i}\sqrt{G(t)\kappa_{\mathrm{c}}(t)}\beta(t). \quad (2.99\mathrm{b})$$

Clearly (2.99a) has the solution

$$\beta(t) = \exp\left(-\frac{1}{2}\int_0^t d\tau G(\tau)\right)\beta(0) \tag{2.100}$$

and we can thus write, after formally integrating (2.99b),

$$\xi(\tau_2) = e^{-\frac{1}{2}\int_0^{\tau_2} dt\kappa_c(t)}\xi(0)$$
$$- i\left[\int_0^{\tau_2} dt\sqrt{G(t)\kappa_c(t)}\, e^{-\frac{1}{2}\int_t^{\tau_2} ds\kappa_c(s)}\, e^{-\frac{1}{2}\int_0^t dsG(s)}\right]\beta(0). \tag{2.101}$$

Our goal now is to maximize the term in brackets in the second line (we call it I) which quantifies the fidelity of the state swap and fulfills $0 \le I \le 1$. We define two functions

$$v(t) = \sqrt{G(t)}\, e^{-\frac{1}{2}\int_0^t dsG(s)}, \tag{2.102a}$$

$$w(t) = \sqrt{\kappa_c(t)}\, e^{-\frac{1}{2}\int_t^{\tau_2} ds\kappa_c(s)}, \tag{2.102b}$$

which we assume to be square integrable. We can thus write the overlap I as a scalar product on the underlying vector space, which obeys the Cauchy–Schwartz inequality

$$I = \langle v, w\rangle^2 \le \langle v, v\rangle\langle w, w\rangle. \tag{2.103}$$

The right-hand side is easily evaluated and we find

$$\langle v, v\rangle = 1 - e^{-K_v},$$
$$\langle w, w\rangle = 1 - e^{-K_w}$$

with $K_v = \int_0^{\tau_2} dsG(s)$ and $K_w = \int_0^{\tau_2} ds\kappa_c(s)$. The inequality (2.103) is saturated for the choice $v \equiv w$, or equivalently (as $v, w \ge 0$) for $v^2 \equiv w^2$. A possible choice for G and κ_c is thus

$$G(t) = N\, e^{-\int_t^{\tau_2} ds\kappa_c(s)}, \tag{2.104a}$$

$$\kappa_c(t) = N\, e^{-\int_0^t dsG(s)}, \tag{2.104b}$$

where N fixes their norm. The set of differential equations corresponding to (2.104) is

$$\dot{G}(t) = \kappa_c(t)G(t), \tag{2.105a}$$
$$\dot{\kappa}_c(t) = -\kappa_c(t)G(t), \tag{2.105b}$$

with the boundary conditions

$$G(\tau_2) = \kappa_c(0) = N. \tag{2.106}$$

Non-singular solutions of these equations are given by

$$G(t) = \frac{M}{1 + e^{M(2t-\tau_2)}}, \tag{2.107a}$$

$$\kappa_c(t) = \frac{M}{1 + e^{-M(2t-\tau_2)}}, \tag{2.107b}$$

where the parameter M is determined by the condition $G(\tau_2) = \kappa_c(0) = M(1 + e^{M\tau_2})^{-1}$. Functions (2.107) are shown in fig. 26.

We discussed in chapter 2 how pulsed protocols can be used to achieve quantum control of optomechanical systems. These schemes do not rely on the existence of a steady state, i. e., they can also be operated in an unstable regime, and thus also in the case of a resonantly driven two-mode squeezing interaction.

In this chapter we explore *continuous-wave* protocols that exploit entanglement as a resource for measurement-based *time-continuous* control of cavity-optomechanical systems, and which allow us to engineer a steady state. Specifically we will discuss feedback cooling of the mechanical oscillator to its ground state for a blue detuned laser drive (section 3.1), preparation of a mechanical oscillator in a general Gaussian (squeezed) state via time-continuous teleportation (section 3.3), and preparation of two remote mechanical systems in an (Einstein–Podolsky–Rosen) entangled state by time-continuous entanglement swapping (section 3.4).

3.1 OPTOMECHANICAL FEEDBACK COOLING

Feedback cooling of mechanical oscillators has been analysed in detail in the literature [MVT98; DJ99; CHP01; Vit+02; Gen+08a; HM13]. The setup typically considered, which is also the basis for the scheme discussed here, is depicted in fig. 28: The output light of an optomechanical cavity is measured by a homodyne detector and the measurement results are fed back to the cavity in a suitable manner, such that the mechanical system is driven to a low-entropy steady state. The regime for feedback cooling discussed in the literature is typically restricted to a resonant drive and the bad-cavity regime $\kappa > \omega_\mathrm{m}$. In this section we will discuss that feedback cooling can also be effectively operated in the sideband-resolved regime $\kappa < \omega_\mathrm{m}$, and even on the blue sideband $\Delta_\mathrm{c} = \omega_\mathrm{m}$, which is normally affiliated with heating. We will show that we can harness the entanglement created by the optomechanical two-mode squeezing interaction for a measurement-based feedback scheme, which enables us to cool the mechanical motion to its ground state.

Feedback control typically consists of two stages: An estimation part that aims to obtain the best possible understanding of the system's state, and a control part that generates a feedback signal from the knowledge obtained in the estimation. We already discussed in section 1.4 how measurement results from homodyne detection can be used to calculate the conditional quantum state of the mechan-
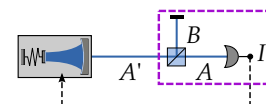

FIG 28. Single homodyne detection for feedback cooling (non-unit efficiency is modelled by a beam-splitter before a perfect detector, marked by the purple box; see appendix B.1.1)

ical system. This state can now be used as a basis for applying a linear–quadratic–Gaussian (LQG) control scheme—a tool from classical control theory that attains the optimal cooling performance for the chosen configuration—in order to prepare a cold mechanical quantum state.

Feedback onto the mechanical system can either be effected by direct driving through a piezoelectric device [Pog+07], or by modulation of the laser input, as we will assume in the following. This type of optical feedback can be described by adding an additional time-dependent term

$$H_{\text{fb}} = -\mathrm{i}\sqrt{\kappa}[\varepsilon(t)^* c_{\text{c}} - \varepsilon(t) c_{\text{c}}^\dagger] = \sqrt{2\kappa}[u_p(t) x_{\text{c}} + u_x(t) p_{\text{c}}] \qquad (3.1)$$

to the Hamiltonian, where $\varepsilon(t) = u_x(t) + \mathrm{i} u_p(t) \in \mathbb{C}$ is the complex amplitude of the feedback signal, and $|\varepsilon(t)|^2$ accordingly is the incoming photon flux. To choose an appropriate feedback strategy we employ quantum LQG control [Bel99], which is designed to minimize a quadratic cost function as described in appendix B.3.2. Applied to feedback cooling the basic working principle is the following: From the measurement results of the homodyne detection we calculate the system's conditional state $\rho_c(t)$, whose evolution is described by eq. (1.57). Based on this state we can then determine the optimal feedback signal $\varepsilon(t)$ that minimizes the steady-state mechanical occupation number $\langle c_{\text{m}}^\dagger c_{\text{m}}\rangle^{\text{ss}} = \frac{1}{2}[\langle x_{\text{m}}^2 + p_{\text{m}}^2\rangle^{\text{ss}} - 1]$. This of course means that the final occupation number depends on the conditional state (more specifically on the covariance matrix $\hat{\Sigma}$), and thus on the chosen LO angle for the homodyne detection as we discussed above. A suitable cost function for this problem is given by

$$h(x_{\text{m}}(t), p_{\text{m}}(t), \varepsilon(t)) = h_{\text{m}} \left[x_{\text{m}}(t)^2 + p_{\text{m}}(t)^2 \right] + |\varepsilon(t)|^2, \qquad (3.2)$$

with $h_{\text{m}} > 0$. Note that h also includes a contribution by the feedback signal ε, which precludes feedback strategies with unrealistically high feedback strength. The parameter h_{m} therefore effects a trade-off between feedback strength and final occupation number n_{m}^{ss}: high values of h_{m} result in low occupation number possibly requiring large $|\varepsilon|$ and vice versa. The mean photon flux in the feedback signal can be calculated as described in appendix B.3.2. For the parameters used in this section we find that on average $|\varepsilon|^2$ is small compared to the overall driving strength in typical experiments. Only in the region of $\kappa \to 0$—where almost no photons enter the cavity—the required $|\varepsilon|^2$ may increase dramatically. We note that in order for LQG control to work correctly, certain observability and controllability conditions need to be satisfied [WM09], which is indeed the case for our system. Additionally, we assume here that the feedback onto the laser field is instantaneous. In practice this means that any feedback delay τ should be small on the typical timescales of the system, i.e., $\tau \ll 1/\omega_{\text{m}}, 1/\kappa$.

(a)

(b)
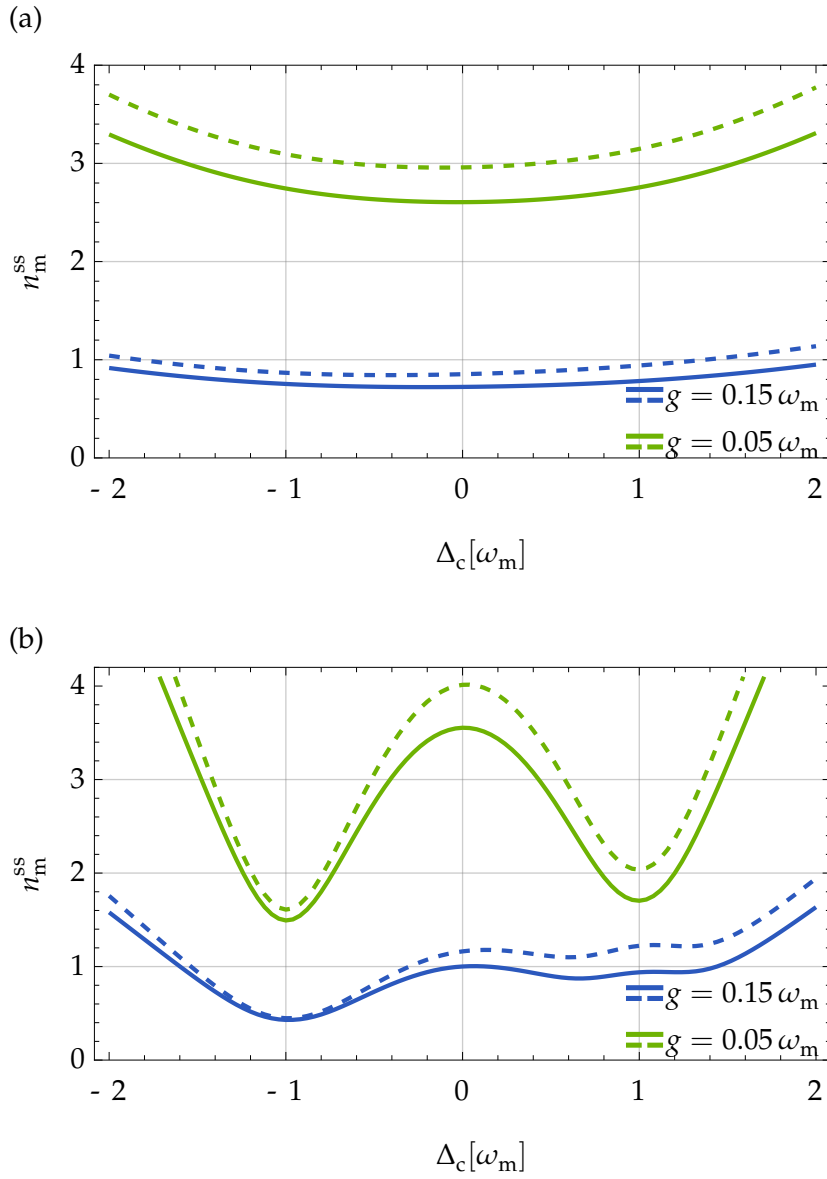
FIGURE 29. Steady-state mechanical occupation number $n_{\mathrm{m}}^{\mathrm{ss}}$ minimized with respect to the LO angle ϕ against detuning of the driving laser Δ_{c} (a) in the bad-cavity regime ($\kappa = 4\omega_{\mathrm{m}}$) and (b) in the sideband-resolved regime ($\kappa = \omega_{\mathrm{m}}/2$), for detection efficiencies $\eta = 1$ (solid lines) and $\eta = 8/10$ (dashed lines). Different colours denote different coupling strengths g. Other parameters: $Q = 5 \cdot 10^6$, $\bar{n} = 3.5 \cdot 10^5$, $h_m = 100$

The final mechanical occupation is found by first calculating the steady-state variances $(\Delta x_m)^2$ and $(\Delta p_m)^2$ for a closed feedback loop as outlined in appendix B.3.2. n_m^{ss} is then given by $n_m^{ss} = \frac{1}{2}[(\Delta x_m)^2 + (\Delta p_m)^2 - 1]$ (for $\langle x_m \rangle^{ss} = \langle p_m \rangle^{ss} = 0$).

In fig. 29 we plot the steady-state occupation numbers of the feedback-cooled mechanical mode against the laser detuning Δ_c, for the bad-cavity regime (upper plot) and the sideband-resolved regime (lower plot), for two different coupling strengths g. For each detuning the homodyne phase ϕ is chosen such, that the occupation number is minimized.[1] Note that we keep g constant while varying Δ_c (or κ). This means that the driving laser power has to be adjusted accordingly. In the bad-cavity regime $\kappa > \omega_m$ we find that driving on resonance is favourable for both values of g. In this case the optimal LO phase is $\phi = \pi/2$, as discussed in the previous section. This is the usual regime for feedback cooling [CHP99; Wil+14].

For micro-mechanical systems, however, the sideband-resolved regime $\kappa < \omega_m$ is typically more relevant. In this regime the picture changes completely. For weak coupling ($g < \kappa$) we find two pronounced dips at *both* mechanical sidebands ($\Delta_c = \pm\omega_m$), where n_m^{ss} is locally minimal and clearly lies below the value on resonance. It is obvious from the figure that cooling works best on the red sideband ($\Delta_c = -\omega_m$), where we have a cumulative effect from passive sideband and feedback cooling (see also fig. 30). However, even on the blue sideband ($\Delta_c = \omega_m$)—which is commonly associated with heating—we find an appreciable reduction of the mechanical occupation by feedback cooling. As we discussed in section 1.4, we can attribute this effect to large optomechanical correlations, which allow for a good read out of the mechanical motion and thus a good feedback performance. If we increase the coupling strength to $g = 0.3\kappa$ we see a peak appearing around the blue sideband (which we attribute to ponderomotive squeezing of the output fields), pushing the occupation number above the value at $\Delta_c = 0$. For both regimes we plot graphs for two different detection efficiencies $\eta = 1$ (lossless detection) and $\eta = 8/10$. Clearly, non-unit detection efficiency leads to a noticeable degradation of feedback-cooling performance. Only at the red sideband and in the sideband-resolved regime, where the effect of sideband cooling dominates, the final occupation number is virtually unaffected.

Figure 30(a) shows the mechanical occupation for three detunings $\Delta_c = 0, \pm\omega_m$ plotted against g. For $\Delta_c = -\omega_m$ we show, additionally to the closed-loop feedback solution (red solid line), the solution for sideband cooling (red dashed line). While for $\Delta_c = 0$ and $\Delta_c = -\omega_m$ the occupation number steadily decreases—in the depicted range— for growing g, for $\Delta_c = \omega_m$ a clear minimum is visible in the weak coupling regime at $g \approx \kappa/10$. This minimum lies well below the value for $\Delta_c = 0$ (but still above the value for the red sideband). This means

1. This can be achieved in a systematic way by finding the "optimal unravelling", see [WM09]. Here we simply use a simplex method for optimization.

(a)

(b)
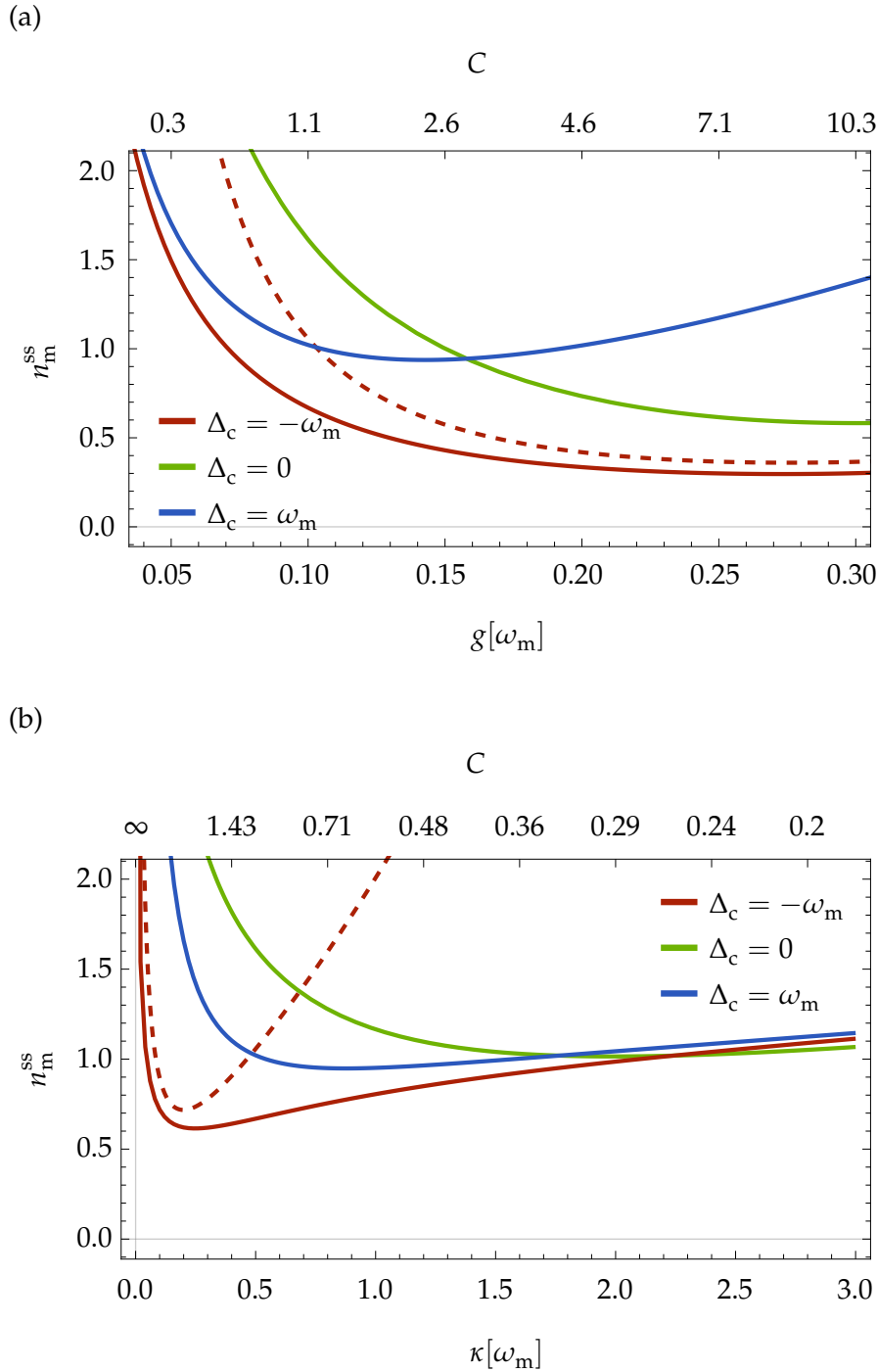
FIGURE 30. Steady-state mechanical occupation number n_m^ss minimized with respect to ϕ for different driving frequencies $\Delta_\mathrm{c} = 0, \pm\omega_\mathrm{m}$, corresponding to a laser drive on the mechanical sidebands and on resonance (represented by different colours). Solid lines represent feedback cooling, while the dashed line (for $\Delta_\mathrm{c} = -\omega_\mathrm{m}$ only) corresponds to sideband cooling without feedback. (a) n_m^ss against coupling g for fixed cavity decay rate $\kappa = \omega_\mathrm{m}/2$ (sideband resolved regime). (b) n_m^ss against κ for $g = \omega_\mathrm{m}/10$ (weak coupling regime). Other parameters for both (a) and (b): $Q = 5 \cdot 10^6$, $\bar{n} = 3.5 \cdot 10^5$, $h_m = 100$, $\eta = 1$

that there exists a considerably large parameter regime where a detuned operation significantly improves the performance of feedback cooling. Note that all curves rise drastically in the strong-coupling regime, where $g/\kappa \gtrsim 1$ (not shown in the plot). In fig. 30(b) we plot $n_{\mathrm{m}}^{\mathrm{ss}}$ against cavity linewidth κ for constant coupling g. Again we find that feedback on the sidebands works best in the sideband-resolved regime, while in the bad cavity regime working on resonance yields (slightly) better performance. Again, the occupation number is minimized with respect to the homodyne phase ϕ at each point in the plot.

In summary we illustrated that feedback cooling in the resolved-sideband regime is a viable option for cooling the mechanical oscillator into its ground state. It turns out that in this regime driving the system on the blue mechanical sideband yields a lower mechanical occupation number than operating on resonance. As an extension of this protocol we will show in section 3.3, that a similar setup operating at the same working point can be used to remotely prepare a squeezed mechanical state via time-continuous teleportation.

3.2 TIME-CONTINUOUS BELL MEASUREMENTS

We discussed in section 2.1 how a continuous-variable Bell measurement can be used to teleport the quantum state of a light pulse onto a mechanical oscillator. In systems which are amenable to strong projective measurements (e. g., photons [Bou+97; She+06] and atoms [Rie+04; Bar+04]), Bell measurements constitute a well established, versatile tool for quantum control and state engineering. However, in many physical systems only weak, indirect, but time-continuous measurements are available. Continuous measurements, described by stochastic Schrödinger and master equations, themselves constitute a corner stone of quantum control. In this section we will combine these important concepts and establish the notion of time-continuous Bell measurements. They are realized via continuous homodyne detection of electromagnetic fields, and can be applied to a great number of systems, including those which cannot be measured projectively. We derive the constitutive equations of motion—the conditional stochastic Schrödinger/master equation and the unconditional feedback master equation—of the monitored systems. In particular we analyse two generic scenarios—*time-continuous quantum teleportation* and *continuous entanglement swapping*. We will first discuss both protocols for generic systems (sections 3.2.1 and 3.2.2); the optomechanical implementation is the subject of sections 3.3 and 3.4.

3.2.1 *Time-continuous Teleportation*

We consider the setup depicted in fig. 31: A one-dimensional electromagnetic field mode A [described by the field operator $a(t)$] couples to a system S via a beam-splitter-like interaction

$$H_{\text{int}} = i[sa^\dagger(t) + s^\dagger a(t)]. \tag{3.3}$$

A is then mixed with a second field B [with a field operator $b(t)$] on a beam-splitter and the resulting fields are sent to two homodyne detection setups which measure the EPR quadratures $x_+ = x_a + x_b$ and $p_- = p_a - p_b$ where x_a, x_b and p_a, p_b are the amplitude and phase quadratures of the respective fields. The field B is prepared in a pure state of Gaussian squeezed white noise, which we denote by $|M\rangle$, where $M \in \mathbb{C}$ characterizes the squeezing; $|M|$ describes the absolute increase (reduction) of the (anti-)squeezed quadrature, while $\arg(M)$ determines the squeezing angle. Provided the system–field interaction creates entanglement between the system and the outgoing light field, the state of B can be teleported to S by applying (instantaneous) feedback proportional to the measurement results of the Bell measurement ($I_\pm$). This effectively generates dissipative dynamics which drive the system into a steady state coinciding with the input light state.
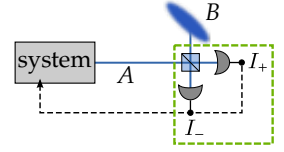
FIG 31. Time-continuous teleportation setup. The green box marks the time-continuous Bell measurement.

Conditional Master Equation

To find the corresponding SME, describing the state of S conditioned on measurements of x_+ and p_-, we apply the same reasoning as in appendix B.1.1 to describe homodyne detection. (The presented results have also been derived in a more formal way in [DG14].) We start from the Schrödinger equation [eq. (A.27)] for the full system (S+A+B)

$$d|\Psi(t)\rangle = [-iH_{\text{eff}}\,dt + s\,dA^\dagger(t) - s^\dagger\,dA(t)]|\Psi(t)\rangle, \tag{3.4}$$

with the initial condition $|\Psi_0\rangle = |\psi_0\rangle_S \otimes |\text{vac}\rangle_A \otimes |M\rangle_B$, $H_{\text{eff}} = H_{\text{sys}} - i\frac{1}{2}s^\dagger s$, and an unspecified system Hamiltonian H_{sys}. As mode A is assumed to be in vacuum, the quantum Wiener increment dA obeys the Itō multiplication table (A.14). As B is prepared in a squeezed state the multiplication table for dB on the other hand is given by

$\times$	dB	$dB^\dagger$	dt
dB	$M\,dt$	$(N+1)\,dt$	0
$dB^\dagger$	$N\,dt$	$M^*\,dt$	0
dt	0	0	0

Due to the Heisenberg uncertainty relation N and M must obey $|M|^2 \leq N(N+1)$, where equality holds for a pure state. The eigenvalue equation for squeezed states can be written as

$$[dB(t) - \alpha\,dB^\dagger(t)]|M\rangle = 0, \tag{3.5}$$

with $\alpha = (N+M)/(N+M^* + 1)$. Using this together with the fact that $dA(t)|\text{vac}\rangle = 0$, we can write

$$\begin{aligned} d|\Psi\rangle &= \left\{ -iH_{\text{eff}}\,dt + s\left[dA^\dagger - \alpha\,dA + dB - \alpha\,dB^\dagger\right] \right\}|\Psi\rangle \\ &= \left\{ -iH_{\text{eff}}\,dt + \sqrt{1/2}\,s\left[\mu\,dX_+ + i\nu\,dP_-\right] \right\}|\Psi\rangle, \end{aligned} \tag{3.6}$$

where $\mu = 1 - \alpha$, $\nu = 1 + \alpha$. We introduced $dX_+(t) = x_+(t)\,dt$, $dP_-(t) = p_-(t)\,dt$ and going from the first to the second line we used the fact that $a^\dagger + b = (x_+ + ip_-)/\sqrt{2}$. We now note that x_+ and p_- commute and can be measured simultaneously.[2] We can thus directly project equation (3.6) onto the EPR state $|I_+ I_-\rangle_{AB}$ defined by $x_+|I_+ I_-\rangle_{AB} = I_+|I_+ I_-\rangle_{AB}$ and $p_-|I_+ I_-\rangle_{AB} = I_-|I_+ I_-\rangle_{AB}$. This yields the linear stochastic Schrödinger equation

$$d|\tilde{\psi}_c\rangle = \left\{ -iH_{\text{eff}}\,dt + \sqrt{1/2}\,s[\mu\,d\widetilde{X}_+ + i\nu\,d\widetilde{P}_-] \right\}|\psi_c\rangle, \tag{3.7}$$

where $d\widetilde{X}_+(t) = I_+(t)\,dt$ and $d\widetilde{P}_-(t) = I_-(t)\,dt$ are classical processes, which possess the same statistical properties as their quantum counterparts. The photo-currents $I_\pm$ (analogous to homodyne detection discussed in section 1.3.2) can be written as

$$I_+\,dt = \sqrt{1/2}\langle s + s^\dagger\rangle_c\,dt + dW_+, \tag{3.8a}$$

$$I_-\,dt = i\sqrt{1/2}\langle s - s^\dagger\rangle_c\,dt + dW_-, \tag{3.8b}$$

with correlated Wiener increments $dW_\pm$. The (co-)variances of $dW_\pm$ are given by

$$w_1\,dt := (dW_+)^2 = [N + 1 + (M + M^*)/2]\,dt, \tag{3.9a}$$

$$w_2\,dt := (dW_-)^2 = [N + 1 - (M + M^*)/2]\,dt, \tag{3.9b}$$

$$w_3\,dt := dW_+\,dW_- = -[i(M - M^*)/2]\,dt, \tag{3.9c}$$

and directly follow from the definition of dX_+, dP_- and the multiplication tables for dA and dB. To find the SME corresponding to eq. (3.7) we first use Itō calculus to find an expression for $d|\tilde{\psi}_c\rangle\langle\tilde{\psi}_c|$, which we can then normalize. (See appendix B.1.1 for a more detailed explanation of this process.) It is convenient to introduce the complex increment

$$dY(t) = \mu\,d\widetilde{X}_+(t) + i\nu\,d\widetilde{P}_-(t), \tag{3.10}$$

which obeys[3]

$$dY^2 = 2\zeta\,dt := -2N/M^*\,dt, \tag{3.11a}$$

$$|dY|^2 = \left[|\mu|^2 w_1 + |\nu|^2 w_2 + 2\,\text{Im}(\mu\nu^*)\right]dt = 2\,dt. \tag{3.11b}$$

With this knowledge we can immediately write the Zakai equation—the equation of motion for the unnormalized state [WM09, p 197]—corresponding to (3.7) as

$$d\tilde{\rho}_c = \mathcal{L}\rho_c\,dt + \sqrt{1/2}\left(s\rho_c\,dY + \rho_c s^\dagger\,dY^*\right), \tag{3.12}$$

with the standard Liouvillian $\mathcal{L}\rho = -\mathrm{i}[H_{\mathrm{sys}}, \rho] + \mathcal{D}[s]\rho$. To normalize this equation we first calculate

$$\mathrm{tr}(\tilde{\rho}_c(t + \mathrm{d}t)) = 1 + \sqrt{1/2}\big[\langle s(t)\rangle_c \, \mathrm{d}Y(t) + \mathrm{H.\,c.}\big], \qquad (3.13)$$

which we use to obtain (by expanding to second order in $\mathrm{d}Y$)

$$\mathrm{tr}(\tilde{\rho}_c(t + \mathrm{d}t))^{-1} = 1 - \sqrt{1/2}\big[\langle s(t)\rangle_c \, \mathrm{d}Y(t) + \mathrm{H.\,c.}\big]$$
$$+ (1/2)\left\{ [\langle s(t)\rangle_c]^2 \zeta + [\langle s^\dagger(t)\rangle_c]^2 \zeta^* + 4|\langle s(t)\rangle_c|^2 \right\} \mathrm{d}t. \quad (3.14)$$

Combining this with (3.12) we find after some algebra

$$\mathrm{d}\rho_c = \mathcal{L}\rho_c \, \mathrm{d}t + \sqrt{1/2}\left[\mu\big(s - \langle s\rangle_c\big)\rho_c + \mathrm{H.\,c.}\right]\rho_c \, \mathrm{d}W_+$$
$$+ \sqrt{1/2}\left[\mathrm{i}\nu\big(s - \langle s\rangle_c\big)\rho_c + \mathrm{H.\,c.}\right]\rho_c \, \mathrm{d}W_- \qquad (3.15)$$
$$= \mathcal{L}\rho_c \, \mathrm{d}t + \sqrt{1/2}\left\{ \mathcal{H}[\mu s]\rho_c \, \mathrm{d}W_+ + \mathcal{H}[\mathrm{i}\nu s]\rho_c \, \mathrm{d}W_- \right\}.$$

It can easily be checked that due to the fact $|\mathrm{d}Y|^2 = 2\,\mathrm{d}t$ this is an equation of the form eq. (B.17) and thus a valid Belavkin equation [Bel92].

To conclude this section let us briefly discuss, as a slight variation of the above setup, the situation where instead of the squeezed state $|M\rangle_B$ we use a displaced squeezed state $|M, \beta\rangle_B = \exp(\beta b^\dagger - \beta^* b)|M\rangle_B = D_B(\beta)|M\rangle_B$ with $\beta \in \mathbb{C}$ as an initial state of mode B, and thus as an input state for teleportation. Transforming the Schrödinger equation (3.4) into a displaced frame with $D_B(\beta)$ shows that the structure of the stochastic Schrödinger equation (SSE) (3.7) and the SME (3.15) remains unchanged, if the measurement processes are replaced by appropriately displaced versions

$$\mathrm{d}\widetilde{X}'_+ = \mathrm{d}\widetilde{X}_+ - \sqrt{1/2}(\beta + \beta^*)\,\mathrm{d}t, \qquad (3.16a)$$
$$\mathrm{d}\widetilde{P}'_- = \mathrm{d}\widetilde{P}_- + \mathrm{i}\sqrt{1/2}(\beta - \beta^*)\,\mathrm{d}t \qquad (3.16b)$$

[which consequently is also the case for the currents $I_\pm$ in equations (3.8)]. Note that due to Itō rules we have $\mathrm{d}\widetilde{X}'^2_- = \mathrm{d}\widetilde{X}^2_-$, $\mathrm{d}\widetilde{P}'^2_- = \mathrm{d}\widetilde{P}^2_-$.

Feedback Master Equation

We follow [Wis94] to apply Markovian (i. e., instantaneous) feedback proportional to the homodyne currents $I_\pm$ to the system S. (The simpler case of homodyne feedback is reviewed in detail in appendix B.2.) We want to add a term

$$(\mathbf{S}) \quad [\mathrm{d}\rho_c]_{\mathrm{fb}} = \sqrt{1/2\eta}(\mathcal{K}_+ I_+ + \mathcal{K}_- I_-)\rho_c \qquad (3.17)$$

describing the feedback to the conditional evolution (where η describes a non-unit detector efficiency, as discussed in appendix B.1.1).

The feedback we model as generalized forces $F_\pm = F_\pm^\dagger$ in the form of additional Hamiltonian terms, which we write as

$$\mathcal{K}_\pm \rho I_\pm = -\mathrm{i}[F_\pm I_\pm, \rho]. \tag{3.18}$$

As $\mathcal{K}$ is linear, eq. (3.17) can easily be converted to Itō form,[4]

$$(\mathbf{I}) \quad [\mathrm{d}\rho_c]_{\text{fb}} = \sqrt{1/2\eta}(\mathcal{K}_+ \, \mathrm{d}\widetilde{X}_+ + \mathcal{K}_- \, \mathrm{d}\widetilde{P}_-)\rho_c +$$
$$(1/4\eta)(\mathcal{K}_+ \, \mathrm{d}\widetilde{X}_+ + \mathcal{K}_- \, \mathrm{d}\widetilde{P}_-)^2 \rho_c. \tag{3.19}$$

We then rewrite the SME (3.15) in terms of the complex Wiener increment

$$\mathrm{d}W_y = \mu \, \mathrm{d}W_+ + \mathrm{i}\nu \, \mathrm{d}W_-. \tag{3.20}$$

Additionally introducing the (non-linear) operators $\mathcal{G}\rho = [s - \mathrm{tr}(s\rho)]\rho$ and $\mathcal{G}'\rho = (\mathcal{G}\rho)^\dagger$ this leads to

$$\mathrm{d}\rho_c = \mathcal{L}\rho_c \, \mathrm{d}t + \sqrt{\frac{\eta}{2}}(\mathcal{G}\rho_c \, \mathrm{d}W_y + \mathcal{G}'\rho_c \, \mathrm{d}W_y^*). \tag{3.21}$$

The evolution under continuous feedback and measurement is then described by [Wis94]

$$\begin{aligned}
\rho_c(t + \mathrm{d}t) = {}& [1 + (1/2\eta)(\mathcal{K}_+ \, \mathrm{d}\widetilde{X}_+ + \mathcal{K}_- \, \mathrm{d}\widetilde{P}_-) \\
& + (1/4\eta)(\mathcal{K}_+ \, \mathrm{d}\widetilde{X}_+ + \mathcal{K}_- \, \mathrm{d}\widetilde{P}_-)^2] \times \\
& [1 + \mathcal{L} \, \mathrm{d}t + \sqrt{\eta/2}(\mathcal{G} \, \mathrm{d}W_y + \mathcal{G}' \, \mathrm{d}W_y^*)]\rho_c(t),
\end{aligned} \tag{3.22}$$

which can be cast into the form

$$\begin{aligned}
\mathrm{d}\rho_c = {}& \mathcal{L}\rho_c + (1/4\eta)(\mathcal{K}_+ \, \mathrm{d}\widetilde{X}_+ + \mathcal{K}_- \, \mathrm{d}\widetilde{P}_-)^2 \rho_c \\
& + (1/2)(\mathcal{K}_+ \, \mathrm{d}\widetilde{X}_+ + \mathcal{K}_- \, \mathrm{d}\widetilde{P}_-)(\mathcal{G} \, \mathrm{d}W_y + \mathcal{G}' \, \mathrm{d}W_y^*)\rho_c \\
& + \sqrt{1/2\eta}(\mathcal{K}_+ \, \mathrm{d}\widetilde{X}_+ + \mathcal{K}_- \, \mathrm{d}\widetilde{P}_-)\rho_c \\
& + \sqrt{\eta/2}(\mathcal{G} \, \mathrm{d}W_y + \mathcal{G}' \, \mathrm{d}W_y^*)\rho_c. \tag{3.23}
\end{aligned}$$

Note that the ordering $\mathcal{K}\mathcal{G}$ ensures that we obtain a trace-preserving master equation [WM93]. We can now average over all possible measurement trajectories (i.e., over all classical processes $\widetilde{X}_+$, $\widetilde{P}_-$) to obtain an unconditional (deterministic) master equation. Expanding the quadratic terms yields,

$$(\mathcal{K}_+ \, \mathrm{d}\widetilde{X}_+ + \mathcal{K}_- \, \mathrm{d}\widetilde{P}_-)^2 = [w_1 \mathcal{K}_+^2 + w_2 \mathcal{K}_-^2 + w_3(\mathcal{K}_+ \mathcal{K}_- + \mathcal{K}_- \mathcal{K}_+)] \, \mathrm{d}t,$$

and

$$\begin{aligned}
(\mathcal{K}_+ \, \mathrm{d}\widetilde{X}_+ &+ \mathcal{K}_- \, \mathrm{d}\widetilde{P}_-)(\mathcal{G} \, \mathrm{d}W_y + \mathcal{G}' \, \mathrm{d}W_y^*)\rho_c \\
&= \mathcal{K}_+(\mathcal{G} + \mathcal{G}')\rho_c \, \mathrm{d}t + \mathcal{K}_-(\mathrm{i}\mathcal{G} - \mathrm{i}\mathcal{G}')\rho_c \, \mathrm{d}t, \\
&= \mathcal{K}_+ \mathcal{H}[s]\rho_c \, \mathrm{d}t + \mathcal{K}_- \mathcal{H}[\mathrm{i}s]\rho_c \, \mathrm{d}t,
\end{aligned}$$

4. For an Stratonovich equation

$$(\mathbf{S}) \; \mathrm{d}\rho = \sum \mathcal{K}_i \rho \, \mathrm{d}W_i$$

with correlated noise processes W_i and linear operators $\mathcal{K}_i$, we find the equivalent Itō equation

$$(\mathbf{I}) \; \mathrm{d}\rho = \sum \mathcal{K}_i \rho \, \mathrm{d}W_i$$
$$+ \tfrac{1}{2} \sum M_{ij} \mathcal{K}_i \mathcal{K}_j \rho \, \mathrm{d}t$$

with $\mathrm{d}W_i \, \mathrm{d}W_j = M_{ij} \, \mathrm{d}t$.

where we used

$$dX_+ \, dW_y = \mu w_1 + i\nu w_3 = 1,$$
$$dP_- \, dW_y = \mu w_3 + i\nu w_2 = i.$$

Taking this all together leads to

$$\dot{\rho} = \mathcal{L}\rho + \frac{1}{2}\left\{\frac{w_1 - w_3}{\eta}\mathcal{D}[F_+] - i[F_+, s\rho + \rho s^\dagger]\right\}$$
$$+ \frac{1}{2}\left\{\frac{w_2 - w_3}{\eta}\mathcal{D}[F_-] - i[F_-, (is)\rho + \rho(is)^\dagger]\right\}$$
$$+ \frac{w_3}{2\eta}\mathcal{D}[F_+ + F_-], \quad (3.24)$$

where we used the fact that $\frac{1}{2}(\mathcal{K}_\pm)^2 = \mathcal{D}[F_\pm]$ and $\frac{1}{2}(\mathcal{K}_+\mathcal{K}_- + \mathcal{K}_-\mathcal{K}_+) = \mathcal{D}[F_+ + F_-] - \mathcal{D}[F_-] - \mathcal{D}[F_\pm]$. Using the identity $\mathcal{D}[s + iF_\pm]\rho = \mathcal{D}[s]\rho + \mathcal{D}[F_\pm]\rho + i[F_\pm, s\rho + \rho s^\dagger] + \frac{i}{2}[\rho, F_\pm s + s^\dagger F_\pm]$ this can be written in the more familiar Lindblad form

$$\dot{\rho} = -i\left[H + \frac{1}{4}\left\{(F_+ + iF_-)s + s^\dagger(F_+ - iF_-)\right\}, \rho\right]$$
$$+ \frac{1}{2}\left\{\mathcal{D}[s - iF_+]\rho + \mathcal{D}[s - F_-]\rho + \frac{w_3}{\eta}\mathcal{D}[F_+ + F_-]\rho\right.$$
$$\left. + \left(\frac{w_1 - w_3}{\eta} - 1\right)\mathcal{D}[F_+]\rho + \left(\frac{w_2 - w_3}{\eta} - 1\right)\mathcal{D}[F_-]\rho\right\}. \quad (3.25)$$

This is the main result of this section. The evolution of the system S thus effectively depends on the state of the field B (via w_i) which has never interacted with S, and which can, in principle, even change (adiabatically) in time. Equation (3.25) can thus be viewed as a continuous "remote preparation" of quantum states.

To illustrate this point we consider the case where the target system S is a bosonic mode. For a system to be amenable to continuous teleportation the system–field interaction must enable entanglement creation. We thus set[5] $s = d^\dagger$, with d a bosonic annihilation operator, and therefore obtain $H_{int} \propto d\, a(t) + d^\dagger a^\dagger(t)$ (which is just a two-mode-squeezing interaction). Additionally we choose $F_+ = i(d - d^\dagger)$ and $F_- = (d + d^\dagger)$, which means that the photocurrents I_+, I_- will be fed back to the $x \propto (d + d^\dagger)$ and $p \propto i(d + d^\dagger)$ quadrature, respectively. The resulting equation can be brought into the form

$$\dot{\rho} = -i[H_{sys}, \rho] + (2N + 1)\mathcal{D}[J]\rho, \quad (3.26)$$

where the jump operator J is determined by

$$J \propto -i(2N + 1 - M - M^*)x + (1 + M - M^*)p \quad (3.27)$$

(with an appropriate normalization). If we define as $U_{\pi/2}$ the local unitary which effects the canonical transformation $x \to p$, $p \to -x$, we find by comparison with the eigenvalue equation for $|M\rangle$,

$$[(1 - M + M^*)x + i(2N + 1 + M + M^*)p]|M\rangle = 0, \quad (3.28)$$

5. Note that the jump operators include an interaction strength. As we choose $H_{sys} = 0$ below we can set it to 1 without loss of generality.

that $U_{\pi/2}^\dagger J U_{\pi/2}|-M\rangle = 0$. Taking into account the relations

$$\langle x^2 \rangle_M = \tfrac{1}{2}(2N + 1 + M + M^*), \tag{3.29a}$$

$$\langle p^2 \rangle_M = \tfrac{1}{2}(2N + 1 - M - M^*), \tag{3.29b}$$

$$\mathrm{Re}(\langle xp \rangle_M) = -\tfrac{i}{2}(M - M^*), \tag{3.29c}$$

one can easily see that $U_{\pi/2}|-M\rangle = |M\rangle$. For $H_{\mathrm{sys}} = 0$ equation (3.26) thus has the steady-state solution $\rho^{\mathrm{ss}} = |M\rangle\langle M|$, where $J|M\rangle = 0$ and hence $\mathcal{D}[J]\rho^{\mathrm{ss}} = 0$. Note that for the vacuum case $N = M = 0$ we find $J = c$, which means that, devoid of other decoherence terms, the system will be driven to its ground state.

Below, we will come back to this scenario, and discuss its implementation on the basis of an optomechanical system in more detail.

If we consider again the situation where we use a displace squeezed state $|M, \beta\rangle_B$ as input, we make the replacements $d\widetilde{X}_+ \to d\widetilde{X}_+'$ and $d\widetilde{P}_- \to d\widetilde{P}_-'$ [see (3.16)] in equation (3.23). This only changes the third line as all products $d\widetilde{X}^2$, $d\widetilde{X}\,dW_y$, etc. are unaffected. After taking the classical average this yields an additional Hamiltonian term

$$H_{\mathrm{coh}} = \sqrt{2}[\mathrm{Re}(\beta)F_+ - \mathrm{Im}(\beta)F_-] \tag{3.30}$$

which has to be incorporated into $\mathcal{L}$ in the feedback master equation (3.24), and effects a displacement of the steady state.

3.2.2 Time-continuous Entanglement Swapping

FIG 32. Schematic of time-continuous entanglement swapping setup (green dashed box marks the time-continuous Bell measurement)

We now replace the Gaussian input state in mode B with a field state emitted by a second system [see fig. 32], which is then, together with field A, sent to a Bell measurement as before. If before the measurement the light fields are entangled to the emitting systems, the bipartite system state will be projected into an EPR-entangled state. As this might lead to unstable system dynamics, we add two homodyne detectors to the setup, which help us to stabilize the systems [VMH13].

Conditional Master Equation

FIG 33. Detail of the additional stabilizing measurements (yellow box).

We assume that the second system S_2 couples to the field B via $H_{\mathrm{int}} = i[s_2 b^\dagger(t) - s_2^\dagger b(t)]$. A and B are combined on a 50:50 beam-splitter to form the combinations $a \pm b$ in the outputs. These outputs are sent to a pair of beam-splitters (with an uneven splitting ratio $v : 1 - v$) and subsequently to a total of four homodyne setups. If we label the modes incident on the homodyne detectors as C_i (described by field operators c_i) for $i = 1 \ldots 4$ [see fig. 33], we find the following relations to modes A and B,

$$a = \sqrt{v/2}(c_1 + c_2) - \sqrt{(1-v)/2}(c_3 + c_4), \tag{3.31a}$$

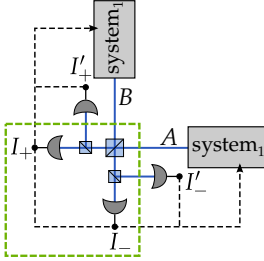$$b = \sqrt{v/2}(c_1 - c_2) - \sqrt{(1-v)/2}(c_3 - c_4). \tag{3.31b}$$

We now choose the LO phases of the four homodyne setups such that they measure $x_+ = c_1 + c_1^\dagger$, $p_- = -i(c_2 - c_2^\dagger)$, $x_- = c_4 + c_4^\dagger$ and $p_+ = -i(c_3 - c_3^\dagger)$. These four measurements allow us to simultaneously monitor both quadratures of both systems (although with reduced efficiency). The measurement of x_+ and p_-, which we choose to have a relative strength v set by the beam-splitting ratio, realize a Bell measurement as before, while the measurement of the conjugate quadratures x_- and p_+, with a strength $1 - v$, we will need for stabilization of S_1 and S_2.

To derive the corresponding SME we apply the same logic as before. We start from the Schrödinger equation for the full system ($S_1 + S_2 +$ field modes),

$$d|\Psi\rangle = \left[-iH_{\text{eff}}\,dt + s_1(dA^\dagger + dA) + s_2(dB^\dagger + dB)\right]|\Psi\rangle, \quad (3.32)$$

with an initial state $|\Psi_0\rangle = |\psi_0\rangle_{S_1 S_2} \otimes |\text{vac}\rangle_{\text{field}}$ and an effective Hamiltonian $H_{\text{eff}} = H_{\text{sys}}^{(1)} + H_{\text{sys}}^{(2)} - \frac{i}{2}\sum_{i=1,2} s_i^\dagger s_i$. We then rewrite this in terms of $dX_\pm$ and $dP_\pm$ [by plugging (3.31) into eq. (3.32)] and project onto eigenstates corresponding to measurement outcomes $I_\pm$, $I_\pm'$. With the definition $s_\pm = s_1 \pm s_2$ we find

$$d|\tilde{\psi}_c\rangle = -iH_{\text{eff}}|\psi_c\rangle\,dt + \sqrt{v/2}[s_+\,d\widetilde{X}_+ + is_-\,d\widetilde{P}_-]|\psi_c\rangle$$
$$+ \sqrt{(1-v)/2}[is_+\,d\widetilde{X}_- + s_-\,d\widetilde{P}_+]|\psi_c\rangle \quad (3.33)$$

where $|\tilde{\psi}_c\rangle$ is unnormalized. As all electromagnetic field modes are assumed to be in vacuum we find that the measurement processes have unit variance, $d\widetilde{X}_\pm(t)^2 = d\widetilde{P}_\pm(t)^2 = dt$, and that they are mutually uncorrelated, i. e., $d\widetilde{X}_+\,d\widetilde{X}_- = d\widetilde{X}_+\,d\widetilde{P}_+ = 0$, etc. This can be shown by expressing c_i in terms of a, b and using Itō rules, where we have to take into account vacuum noise entering through the open ports of the second pair of beam-splitters (not explicitly introduced here). The homodyne currents are given by

$$I_+\,dt = \sqrt{v/2}\,\langle s_+ + s_+^\dagger\rangle_c + dW_+, \quad (3.34a)$$

$$I_-\,dt = i\sqrt{v/2}\,\langle s_- - s_-^\dagger\rangle_c + dW_-, \quad (3.34b)$$

$$I_+'\,dt = i\sqrt{(1-v)/2}\,\langle s_+ - s_+^\dagger\rangle_c + dV_+, \quad (3.34c)$$

$$I_-'\,dt = \sqrt{(1-v)/2}\,\langle s_- + s_-^\dagger\rangle_c + dV_-. \quad (3.34d)$$

where the Wiener increments $dW_\pm$ and $dV_\pm$ obey a multiplication table corresponding to the one of $d\widetilde{X}_\pm$ and $d\widetilde{P}_\pm$. As we now have four uncorrelated homodyne measurements we can directly apply the procedure laid out in appendix B.1.1 and arrive at the SME

$$d\rho_c = \mathcal{L}\rho_c\,dt + \sqrt{v/2}\,\{\mathcal{H}[s_+]\rho_c\,dW_+ + \mathcal{H}[is_-]\rho_c\,dW_-\}$$
$$+ \sqrt{(1-v)/2}\,\{\mathcal{H}[is_+]\rho_c\,dV_+ + \mathcal{H}[s_-]\rho_c\,dV_-\}, \quad (3.35)$$

with $\mathcal{L}\rho = -\mathrm{i}[H_{\mathrm{sys}}^{(1)} + H_{\mathrm{sys}}^{(2)}, \rho] + \mathcal{D}[s_1]\rho + \mathcal{D}[s_2]\rho$. These results can alternatively be derived in a similar spirit but in a more formal way within the framework of quantum networks, as for example presented in [GJ09].

Feedback Master Equation

In this entanglement swapping scheme all four homodyne currents, $I_\pm$ (Bell measurement) and $I'_\pm$ (stabilizing measurements), are fed back to *both* systems. (For convenience we will in the following label the photo-currents by I_i, $i = 1, \ldots, 4$, according to the light modes C_i they correspond to.) We again describe this by the operations $\mathcal{K}[F_i]\rho I_i = -\mathrm{i}[F_i I_i, \rho]$ $(i = 1, \ldots, 4)$, where $F_i = F_i^\dagger$ now act on the combined Hilbert space of $S_1 + S_2$. Using the procedure from before it is straightforward to show that the corresponding FME can be written as

$$\dot{\rho} = -\mathrm{i}[H_{\mathrm{sys}}, \rho] - \frac{\mathrm{i}}{2} \sum_{i=1}^4 [s_i^\dagger F_i + F_i s_i, \rho]$$

$$+ \sum_{i=1}^4 \left\{ \mathcal{D}[s_i - \mathrm{i}F_i] + \frac{1-\eta}{\eta} \mathcal{D}[F_i] \right\}, \quad (3.36)$$

with $(s_i)_{i=1}^4 = (\sqrt{v}s_+, \mathrm{i}\sqrt{v}s_-, \mathrm{i}\sqrt{1-v}s_+, \sqrt{1-v}s_-)$. [Compare this to eq. (B.34)]. Here we assumed that all detectors have the same efficiency η.

Let us again consider the case of bosonic modes, with jump operators (assuming a unity coupling rate) $s_1 = d_1^\dagger$, $s_2 = d_2^\dagger$ ($[d_i, d_j^\dagger] = \delta_{ij}$), not including the stabilizing measurements (i.e., $v = 1$). We thus have $(s_-, s_+) = (d_+^\dagger, d_-^\dagger)$ and choose $(F_1, F_2) = (\mathrm{i}d_+ - \mathrm{i}d_+^\dagger, d_- + d_-^\dagger)$. For $H_{\mathrm{sys}} = 0$ (and $\eta = 1$) this gives the master equation

$$\dot{\rho} = -\frac{\mathrm{i}}{2}[d_+^2 - d_-^2 - \mathrm{H.c.}, \rho] + \mathcal{D}[d_+]\rho + \mathcal{D}[d_-]\rho.$$

The Lindblad terms damp the system, while the Hamiltonian term generates squeezing dynamics in the EPR-modes,[6] which amplifies the system. This becomes clearer when looking at the corresponding Langevin equations for the quadratures corresponding quadratures $x_\pm \propto d_\pm + d_\pm^\dagger$, $p_\pm \propto \mathrm{i}(d_\pm - d_\pm^\dagger)$,

$$\frac{\mathrm{d}}{\mathrm{d}t}x_+ = -\left(\tfrac{1}{2} + 2\right)x_+ + x_+^{\mathrm{in}}, \qquad \frac{\mathrm{d}}{\mathrm{d}t}p_+ = -\left(\tfrac{1}{2} - 2\right)p_+ + p_+^{\mathrm{in}},$$

$$\frac{\mathrm{d}}{\mathrm{d}t}x_- = -\left(\tfrac{1}{2} - 2\right)x_- + x_-^{\mathrm{in}}, \qquad \frac{\mathrm{d}}{\mathrm{d}t}p_- = -\left(\tfrac{1}{2} + 2\right)p_- + p_-^{\mathrm{in}},$$

where $x_\pm^{\mathrm{in}}$, $p_\pm^{\mathrm{in}}$ denote appropriate noise contributions. These equations indicate that x_+ and p_- will become squeezed while x_- and p_+ will be anti-squeezed. This instability can be prevented by introducing the additional measurement (and feedback) channels; they will, however, also limit the generated squeezing and thus the amount of created entanglement.

6. This is equivalent to two-mode squeezing in the modes of S_1, S_2.

3.3 OPTOMECHANICAL TIME-CONTINUOUS TELEPORTATION

In section 3.2.1 we derived the constitutive equations of motion describing time-continuous teleportation (the conditional master equation and feedback master equation) for a generic system. In this section we will focus on the optomechanical implementation (see fig. 34). Technical details are discussed in appendix 3.A.2.

In order to successfully implement continuous teleportation in optomechanical systems we need to appropriately design our measurement setup. We saw that in the regime $g \ll \kappa \ll \omega_m$ and for a blue drive with $\Delta_c = \omega_m$ the optomechanical interaction essentially gives rise to a two-mode squeezing dynamics between the mechanical mode and the extracavity light field,[7] which is the required interaction for teleportation. Consequently the mechanical oscillator resonantly scatters photons into the lower sideband at $\omega_c = \omega_0 - \omega_m$; spectrally, the photons which are correlated with the mechanical motion are therefore located at this sideband frequency. We thus set up our Bell measurement in the following way: Firstly, we choose the centre frequency of the squeezed input light located at the sideband frequency ω_c. Secondly, we now use heterodyne detection to measure quadratures at the same frequency.

In appendix 3.A.2 we show that after adiabatic elimination of the cavity mode and a rotating-wave approximation, the evolution of the conditional mechanical state $\rho_c^{(m)}$ in a rotating frame with ω_m (neglecting the mechanical frequency shift by the optical-spring effect, see appendix 3.A.2) is described by the stochastic master equation[8]

$$
d\rho_c^{(m)} = \gamma_- \mathcal{D}[c_m]\rho_c^{(m)}\, dt + \gamma_+ \mathcal{D}[c_m^\dagger]\rho_c^{(m)}\, dt
$$

$$
- \sqrt{\frac{\eta g^2 \kappa}{2}} \left\{ \mathcal{H}[i\mu\eta_+ c_m^\dagger]\rho_c^{(m)}\, dW_+ - \mathcal{H}[\nu\eta_+ c_m^\dagger]\rho_c^{(m)}\, dW_- \right\}.
$$

$$(3.37)$$

The first row corresponds to the standard adiabatic master equation (1.55), while the second row describes the time-continuous Bell measurement, where the squeezing parameter M is encoded in $\mu = 1 - \alpha$ and $\nu = 1 + \alpha$, with $\alpha = (N + M)/(N + M^* + 1)$. η is the detection efficiency as before. The photo-currents resulting from the Bell measurement are

$$
I_+\, dt = -i\sqrt{\eta g^2 \kappa/2} \left\langle \eta_+ c_m^\dagger - \text{H.c.} \right\rangle dt + dW_+, \qquad (3.38a)
$$

$$
I_-\, dt = \sqrt{\eta g^2 \kappa/2} \left\langle \eta_+ c_m^\dagger + \text{H.c.} \right\rangle dt + dW_-, \qquad (3.38b)
$$

where $dW_\pm$ are correlated Wiener increments whose (co-)variances are given in eq. (3.9). For the choice $\Delta_c = \omega_m$ we have $\eta_+ = 2/\kappa$ and $\eta_- = 1/(\frac{\kappa}{2} + 2i\omega_m)$. Thus $I_\pm$ approximately correspond to measurements of the mechanical quadratures p_m and x_m respectively. We

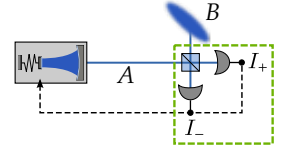FIG 34. Optomechanical time-continuous teleportation setup.

7. In this parameter regime we have an effective interaction Hamiltonian $H_{int} \propto c_m^\dagger a^\dagger(t) + c_m a(t)$

8. As a reminder, we defined:

$$\gamma_+ = \gamma\bar{n} + \Gamma_+$$

$$\gamma_- = \gamma(\bar{n} + 1) + \Gamma_-$$

$$\Gamma_\pm = 2g^2\,\text{Re}\,\eta_-$$

$$\eta_\pm = \frac{1}{\frac{\kappa}{2} - i(\Delta_c \mp \omega_m)}$$

model the feedback as instantaneous displacements of the mechanical oscillator in phase space, where the feedback strength is proportional to the heterodyne currents $I_\pm(t)$. This is described by Hamiltonian terms $I_\pm(t)F_\pm$, where $F_\pm = F_\pm^\dagger$ are generalized forces. The feedback operators we choose to be

$$F_+ = -\sqrt{2g^2\kappa}\,\eta_+\,x_\mathrm{m}, \tag{3.39a}$$

$$F_- = -\sqrt{2g^2\kappa}\,\eta_+\,p_\mathrm{m}, \tag{3.39b}$$

which generate a displacement in p_m and x_m respectively. The pre-factors of $F_\pm$ (i. e., the feedback gain) we chose such that they match the measurement strength of the Bell detection. The corresponding feedback master equation (in the same rotating frame) can be written as

$$\dot{\rho}^{(\mathrm{m})} = \gamma(\bar{n}+1)\mathcal{D}[c_\mathrm{m}]\rho^{(\mathrm{m})} + \gamma\bar{n}\mathcal{D}[c_\mathrm{m}^\dagger]\rho^{(\mathrm{m})}$$
$$+ (4g^2/\kappa)\left\{\lambda_1(\epsilon)\mathcal{D}[J_1(\epsilon)] + \lambda_2(\epsilon)\mathcal{D}[J_2(\epsilon)]\right\}\rho^{(\mathrm{m})}, \tag{3.40}$$

where $\epsilon = [1 + (4\omega_\mathrm{m}/\kappa)^2]^{-1}$ quantifies the suppression of the counter-rotating interaction terms (i. e., the optomechanical beam-splitter) as before. The effective Lindblad terms are determined by λ_i and J_i, which are obtained (see appendix 3.A.2) from the eigenvalue decomposition of the positive matrix

$$\mathbf{\Lambda} = \begin{pmatrix} \frac{w_2}{\eta} - \frac{1}{2}(1+\epsilon) & -\frac{w_3}{\eta} + \frac{i}{2}(1+\epsilon) \\ -\frac{w_3}{\eta} - \frac{i}{2}(1+\epsilon) & \frac{w_1}{\eta} - \frac{1}{2}(1+\epsilon) \end{pmatrix}.$$

For efficient detection ($\eta = 1$) we obtain $\lambda_1 = (2N+1) + O(\epsilon)$ and $\lambda_2 = O(\epsilon)$, which means that in the sideband-resolved regime the jump operator $J_2(\epsilon)$ contributes only weakly. In zeroth order in ϵ the dominating dissipative dynamics are generated by

$$J_1(0) \propto -i(2N+1-M-M^*)x_\mathrm{m} + (1+M-M^*)p_\mathrm{m}, \tag{3.41}$$

which is just the situation we already encountered in section 3.2.1. This means that $|M\rangle\langle M|$ is a dark state of $D[J_1(0)]$ and thus in the ideal limit of $\gamma = 0$, $\epsilon = 0$, $\eta = 1$ the steady state of (3.40) is

$$\lim_{t\to\infty}\rho^{(\mathrm{m})}(t) = |M\rangle\langle M|. \tag{3.42}$$

Hence, the optical input state is perfectly transferred to the mechanical mode.

Moving away from the ideal case, the protocol's performance is degraded by mechanical decoherence effects ($\gamma\bar{n} > 0$), counter-rotating terms of the optomechanical interaction which are suppressed by $\epsilon < 1$, and inefficient detection ($\eta < 1$) which leads to imperfect feedback. [All these effects are captured by the master equation (3.40).] Figure 35 shows the steady-state squeezing ζ transmitted to the mech-
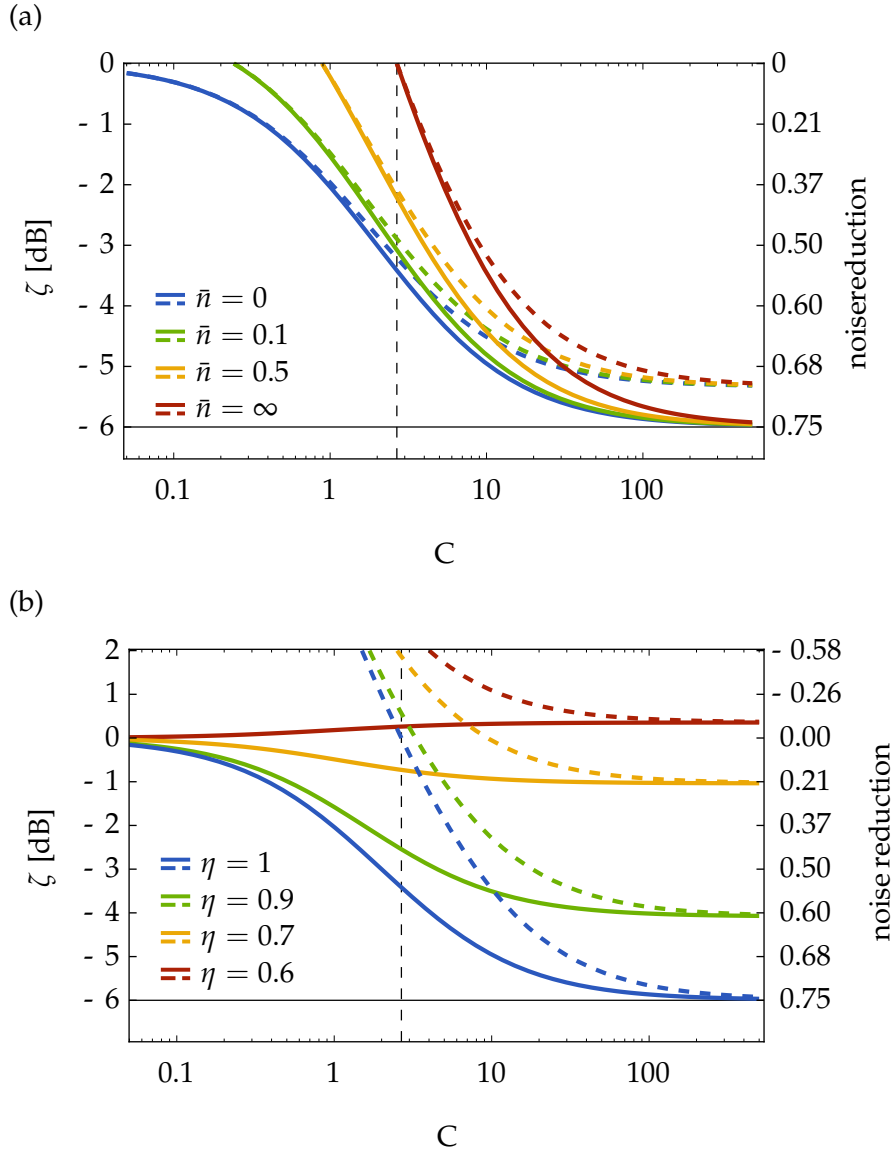
FIGURE 35. Mechanical squeezing ζ against cooperativity C: (a) Varying mechanical bath occupation $\bar{n} = 0, 1/10, 1/2, \infty$ (represented by different colours) and unit detection efficiency $\eta = 1$; The solid (dashed) lines represent a sideband resolution of $\kappa/\omega_{\mathrm{m}} = 1/10$ (1). (b) Different detection efficiencies $\eta = 1, 9/10, 7/10, 6/10$ (represented by different colours) and $\kappa = \omega_{\mathrm{m}}/10$; Here the solid (dashed) lines represent $\bar{n} = 0$ (∞). In both plots the horizontal solid line at $\zeta = -6$dB (corresponding to $N \approx 0.56$) shows the squeezing level of the input light and the vertical dashed line the critical cooperativity $C_{\mathrm{crit}} \approx 2.7$. Note that in (b) C_{crit} marks the value of C above which the blue dashed line ($n \to \infty$, $\eta = 1$) falls below 0 (i. e., squeezing is transferred).

anical mode for different parameters plotted against the optomechanical cooperativity $C = 4g^2/(\bar{n}+1)\gamma\kappa$. In the upper plot we assume perfect detection efficiency $\eta = 1$ and find that in this case there exists a critical value $C_{\text{crit}}(N) = 1/[\sqrt{N(N+1)}]$ determined by the input squeezing N above which the resulting mechanical state is squeezed for any thermal occupation number $\bar{n}$. The lower plot clearly shows that this is no longer true if we assume non-unit detection efficiency η. We find that below a certain critical value $\eta_{\text{crit}}(N,\bar{n})$ we can no longer transfer squeezing to the mechanical oscillator, but we rather heat it instead. (This is even true for a zero-temperature mechanical environment, as illustrated in the plot.) In this general case it can be beneficial to chose a modified feedback gain, i.e., use feedback operators $\tilde{F}_\pm = \sigma F_\pm$ with $\sigma \neq 1$. In the parameter regime we consider, however, the resulting improvements are negligible.
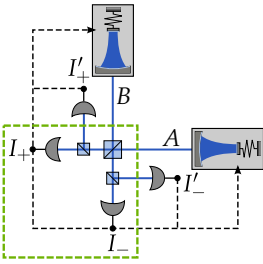
FIG 36. Schematic of optomechanical time-continuous entanglement swapping setup (green dashed boxes mark the time-continuous Bell measurement)

9. In the language of control theory this means that the complete system is not observable (see for example [WM09]).

3.4 OPTOMECHANICAL TIME-CONTINUOUS ENTANGLEMENT SWAPPING

We now replace the squeezed field mode with a second optomechanical cavity, as is depicted in fig. 36. The goal of this scheme is to generate stationary entanglement between the two mechanical subsystems. The implementation is akin to the teleportation protocol presented above: Both cavities are driven on the blue sideband to resonantly enhance the two-mode squeezing interaction, and their output light is sent to the Bell detection setup which operates at the cavity resonance frequency ω_c. Feeding back the Bell detection results $I_\pm$ corresponding to the x_+ and p_- quadratures of the optical fields to both mechanical systems dissipatively drives them towards an entangled state. There is a slight complication, however. A single Bell measurement only allows us to separately monitor two of the four variables $(x_{\text{m},1}, p_{\text{m},1}, x_{\text{m},2}, p_{\text{m},2})$ needed to describe the quantum state of the mechanical systems.[9] Combined with the fact that we drive the system on the blue side of the cavity resonance (and thus in an unstable regime) this means that we cannot actively stabilize the system and—depending on the driving strength and sideband resolution—no steady state may exist. To compensate for this we extend the setup by two additional heterodyne detectors, measuring x_- and p_+ with outcomes $I'_\mp$. The effective measurement strength of this stabilizing measurements with respect to the Bell measurement is set by the transmissivity v of the beam-splitter in front of the heterodyne setup (see fig. 36). Appropriate feedback of all measurement currents $I_\pm$, $I'_\pm$ (for simplicity libelled I_i, $i = 1,\dots,4$, below) to both mechanical systems finally allows us to stabilize them in an entangled state. Note that this setup effectively realizes two simultaneous Bell measurements of the pairs (x_+, p_-) and (x_-, p_+) with detection efficiencies v and $1-v$ respectively. In the rest of this section the two optomech-

anical systems are assumed to be identical and all detectors to have the same quantum detection efficiency η.

In appendix 3.A.3 we show that in an adiabatic approximation the conditional state of the two mechanical oscillators $\rho^{(m)}$ in a rotating frame can be described by the SME (setting $\Delta_c = \omega_m$)

$$
d\rho_c^{(m)} = \epsilon \frac{4g^2}{\kappa} \left\{ \mathcal{D}[c_{m,1}]\rho_c^{(m)} + \mathcal{D}[c_{m,2}]\rho_c^{(m)} \right\} dt
$$

$$
+ \sum_{i=1}^{2} \left\{ \gamma(\bar{n}+1)\mathcal{D}[c_{m,i}]\rho_c^{(m)} + \gamma\bar{n}\mathcal{D}[c_{m,i}^\dagger]\rho_c^{(m)} \right\} dt
$$

$$
+ \frac{2g^2}{\kappa} \sum_{i=1}^{4} \left\{ \mathcal{D}[J_i]\rho_c^{(m)} dt + \sqrt{\eta}\mathcal{H}[J_i]\rho_c^{(m)} dW_i \right\}, \quad (3.43)
$$

where we set $(J_1, J_2) = \sqrt{v}(c_{m,+}^\dagger, ic_{m,-}^\dagger)$, $(J_3, J_4) = \sqrt{1-v}(ic_{m,+}^\dagger, c_{m,-}^\dagger)$ and $c_{m,\pm} = c_{m,1} \pm c_{m,2}$. The Wiener processes W_i are uncorrelated and thus obey $dW_i\, dW_j = \delta_{ij}\, dt$, and correspond to the photo-currents

$$
I_i\, dt = \sqrt{4g^2/\kappa}\langle J_i + J_i^\dagger \rangle_c\, dt + dW_i. \quad (3.44)
$$

The final steady state of this protocol depends on the feedback operators $F_i = F_i^\dagger$ we apply. In analogy to the previous section we choose $(F_1, F_2) = \sqrt{v}\sigma(ic_+ - ic_+^\dagger, c_- + c_-^\dagger)$ and $(F_3, F_4) = \sqrt{1-v}(c_+ + c_+^\dagger, ic_- - ic_-^\dagger)$, which can realize independent displacements of all mechanical quadratures. This time we introduced an additional gain parameter σ which we can vary in order to optimize the amount of entanglement in the resulting steady state. With these choices the FME for optomechanical entanglement swapping takes the form

$$
\dot{\rho}_c^{(m)} = -i[H_{fb}, \rho_c^{(m)}] + \epsilon\frac{4g^2}{\kappa}\left(\mathcal{D}[c_{m,1}] + \mathcal{D}[c_{m,2}]\right)\rho_c^{(m)}
$$

$$
+ \sum_{i=1}^{2}\left\{\gamma(\bar{n}+1)\mathcal{D}[c_{m,i}]\rho_c^{(m)} + \gamma\bar{n}\mathcal{D}[c_{m,i}^\dagger]\rho_c^{(m)}\right\}
$$

$$
+ \frac{2g^2}{\kappa}\sum_{i=1}^{4}\left\{\mathcal{D}[J_i - iF_i]\rho_c^{(m)} + \frac{1-\eta}{\eta}\mathcal{D}[F_i]\right\}, \quad (3.45)
$$

where the dynamics generated by the feedback is described by

$$
H_{fb} = i\frac{2g^2}{\kappa}[(1+\sigma)v - 1](c_{m,+}^2 + c_{m,-}^2 - \text{H.c.}). \quad (3.46)
$$

We can now analyse the stability properties of the linear feedback system by evaluating the corresponding Routh–Hurwitz criterion. In the case of no stabilizing feedback ($v = 1$) we find that the admissible optomechanical coupling is limited from above by $4g^2/\kappa < 1/(1-\epsilon)$. This condition thus only allows appreciably values of $4g^2/\kappa$ for $\epsilon \approx 1$, and thus in the bad-cavity regime. The stabilization is caused by the

counter-rotating beam-splitter terms $c_{m,i}c^\dagger_{m,i} + \mathrm{H.c.}$ of the optomechanical Hamiltonian, which cool the mechanical systems. This cooling effect, however, diminishes the amount of generated steady-state entanglement. If we switch on the stabilizing feedback and thus choose $v < 1$, we can rewrite the Routh–Hurwitz criterion in the form

$$[3 + (4g^2/\kappa)^{-1} + \epsilon] > 4v > [(1 - \epsilon) - (4g^2/\kappa)^{-1}]/\sigma$$

(where we assumed $\epsilon < 1$). These inequalities are tightest in the limit $\epsilon \to 0$, $g^2/\kappa \to \infty$ where we have $3 > 4v > 1/\sigma$. For the rest of this section we choose $v = 3/4$ which ensures stability of the feedback system for any values of g^2/κ and ϵ—and consequently the sideband-resolution κ/ω_m—as long as the feedback gain fulfils $\sigma > 1/3$. In the stable regime and for $\epsilon = 0$, $\eta = 1$ we find a simple analytic expression for the steady-state logarithmic negativity,

$$E_\mathcal{N}^{ss} = \ln \left(\frac{\frac{1}{2}C(\bar{n} + 1)(3\sigma - 1)(4v - 1) + 1}{C(\bar{n} + 1)[3\sigma(\sigma - 1) + 1] + 2\bar{n} + 1} \right), \tag{3.47}$$

where we again introduced the cooperativity $C = 4g^2/(\bar{n} + 1)\gamma\kappa$. Generally we can—for a set of parameters $(C, \bar{n}, \epsilon, v, \eta)$—maximize the entanglement $E_\mathcal{N}$ with respect to the feedback gain σ. In fig. 37 we plot the resulting steady-state values in terms of logarithmic negativity $E_\mathcal{N}$ and EPR variance

$$\Delta_{EPR} = \min_{\phi_1, \phi_2} \left([\Delta(x_{m,1}^{\phi_1} - x_{m,2}^{\phi_2})]^2 + [\Delta(p_{m,1}^{\phi_1} + p_{m,2}^{\phi_2})]^2 \right), \tag{3.48}$$

where $x_{m,i}^\phi = (c_{m,i}e^{-i\phi} + c^\dagger_{m,i}e^{+i\phi})/\sqrt{2}$ and $p_{m,i}^\phi = x_{m,i}^{\phi+\pi/2}$ are rotated mechanical quadratures. [Again, the criterion for entanglement is $\Delta_{EPR} < 2$ [Dua+00; Sim00]]. In the first plot we assume a perfect detection efficiency $\eta = 1$ and consider different bath occupation numbers $\bar{n}$. We again see that there exists a critical cooperativity C_{crit} above which we are able to generate entanglement regardless of $\bar{n}$. From (3.47) we can deduce the expression

$$C_{crit}(v, \sigma) = 4/[3\sigma(1 + 4v - 2\sigma) - (1 + 4v)]. \tag{3.49}$$

(As is evident from the plot, the C_{crit} is independent of ϵ.) For the parameters used in the plot (taking into account the optimization with respect to σ) we find $C_{crit} = 2$. Again, counter-rotating terms decrease entanglement but are strongly suppressed by the sideband resolution. In fig. 37(b) we take into account losses and non-unit detection efficiency, $\eta < 1$, which drastically reduces the amount of achieved entanglement. As before we find a critical loss value $\eta_{crit}(\bar{n}, v)$ (for the parameters chosen in the plot slightly above 65%) below which entanglement creation is prohibited.

(a)

(b)
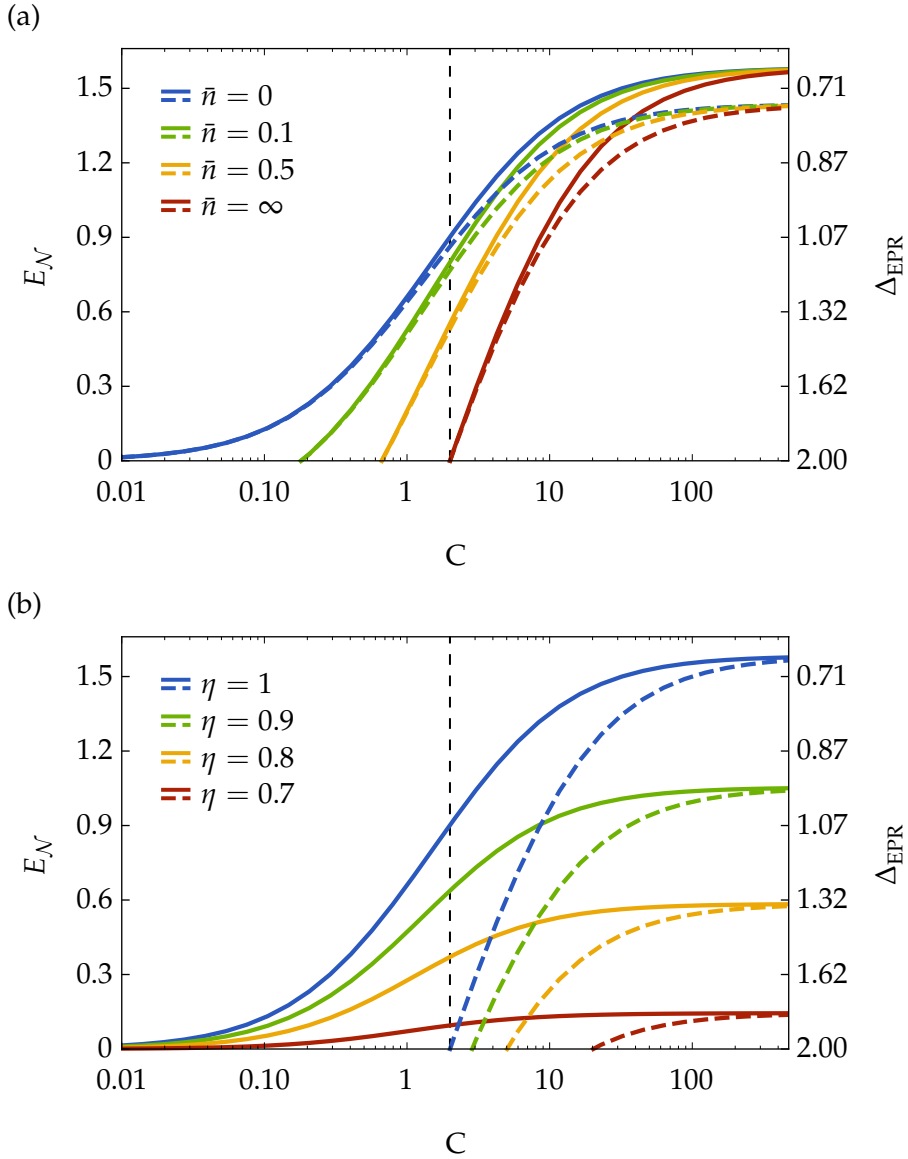
FIGURE 37. Two-mode mechanical steady-state entanglement in terms of $E_{\mathcal{N}}^{\mathrm{ss}}$ and Δ_{EPR} against cooperativity C, maximized with respect to feedback gain σ: (a) Varying mechanical bath occupation $\bar{n} = 0, 1/10, 1/2, \infty$ (represented by different colours) for unit detection efficiency $\eta = 1$; The solid (dashed) lines represent a sideband resolution of $\kappa/\omega_{\mathrm{m}} = 1$ $(1/10)$. (b) Different detection efficiencies $\eta = 1, 9/10, 7/10, 6/10$ (represented by different colours) and $\kappa = \omega_{\mathrm{m}}/10$; Here the solid (dashed) lines represent $\bar{n} = 0$ (∞). The black vertical line shows the critical cooperativity $C_{\mathrm{crit}} = 2$.

3.5 EXPERIMENTAL IMPLEMENTATION OF A KALMAN FILTER

In the previous chapters we have extensively discussed different stochastic master equations that describe the evolution of conditional quantum states, conditioned on the outcomes of different measurement setups. This section will be devoted to illustrating how conditional quantum states can be evaluated from experimental data.

3.5.1 *General Considerations*

The generic SME for homodyne detection (1.57) of a cavity's output field is typically written in a form such that the evolution is driven by a Wiener process $W(t)$. The connection to measured data in an experiment is given by the identity (1.59), which shows that the Wiener increment $\mathrm{d}W(t)$ is the difference between the expected measurement outcome [according to the conditional state $\rho_c(t)$] and the actual measurement result. In filtering theory $W(t)$ is called *innovation* *process* (or innovation sequence) [Ste94; Hei+05]. In order to evaluate the state $\rho_c(t)$ from a measurement trajectory $\{I(s) : s \leq t\}$ we thus have to integrate a nonlinear equation of the form (choosing to measure the amplitude quadrature and neglecting photon losses)

innovation process

$$\mathrm{d}\rho_c(t) = \mathcal{L}\rho_c(t)\,\mathrm{d}t + \sqrt{\kappa}[I(t) - \sqrt{\kappa}\langle c_\mathrm{c}(t) + c_\mathrm{c}^\dagger(t)\rangle_c]\,\mathcal{H}[c_\mathrm{c}]\rho_c(t)\,\mathrm{d}t.$$

$$(3.50)$$

We show in appendix B.3 that in the case of Gaussian systems and a linear measurement (such as homodyne detection), this equation can be mapped to the (stochastic) differential equations (1.67). In classical filtering theory equations (1.67) are known as the *Kalman filter* [Kal60; KB61], which presents the optimal estimator under a minimum-mean-square-error criterion [Ste94; Xio08]. Let us briefly discuss the interpretation of the classical Kalman filter in its continuous form. If we describe by X a state of a Gaussian system in a classical state space (e. g., the phase space of a harmonic oscillator), the Kalman filter ascribes to it an optimal estimate $\hat{X}$ and an estimation-error covariance matrix $\hat{\Sigma} = \mathbb{E}[(X - \hat{X})(X - \hat{X})^\mathrm{T}]$, where $\mathbb{E}[\cdot]$ denotes the expectation value with respect to the initial probability distribution describing the system. The estimate is chosen to minimize the mean-square error $\mathbb{E}[\|X - \hat{X}\|^2] = \mathrm{tr}(\hat{\Sigma})$. The true state X (a point in the state space) thus follows a Gaussian distribution with a covariance given by $\hat{\Sigma}$ centred at $\hat{X}$. The Kalman filter equations describe how the conditional state is iteratively updated (see fig. 38): First, the estimate $\hat{X}$ and the covariance $\hat{\Sigma}$ are propagated for an infinitesimal time interval $\mathrm{d}t$ according to the system dynamics. Second, the measurement outcome is incorporated as a Bayesian update that corrects the value of the estimate $\hat{X}$ and contracts the covariance ellipse. The updated values are again propagated by $\mathrm{d}t$ and the procedure is re-
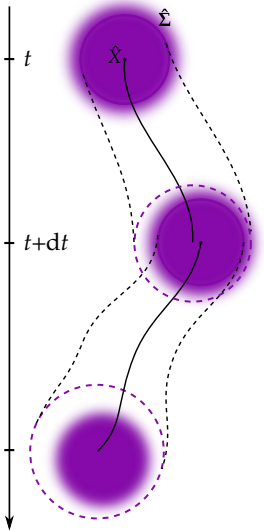

FIG 38. Schematic state-space representation of the Kalman evolution. The conditional state is depicted by a circle and evolves in time according to the system dynamics. After a time $\mathrm{d}t$ a Bayesian update is applied based on the measurement outcome to find the new conditional state.

peated. Note that of the Kalman equations only the one for $\hat{X}(t)$ actually depends on the measurement trajectory $I(t)$, while the evolution of $\hat{\Sigma}(t)$ solely depends on the linear dynamics of the underlying system. This has an important consequence: Given an initial state and a system's state-space model (i. e., the matrices $\mathbf{F}$, $\mathbf{H}$, $\mathbf{G}$, $\mathbf{N}$, and $\mathbf{M}$; see appendix B.3.1) all quantities that depend on $\hat{\Sigma}(t)$ only [e. g., the mean occupation number or the logarithmic negativity], are predetermined for the complete time evolution, and are independent of the observations made in the experiment. It is therefore crucial to build an accurate model of the experimental setup and verify its accuracy against the measured data. This can be achieved by testing that the (experimentally obtained) innovation process $W(t)$ is indeed a Wiener process, i. e., that for $t > s$ it obeys $W(t) - W(s) \sim \mathcal{N}(0, t - s)$, where $\mathcal{N}(\mu, \sigma^2)$ is the normal distribution with a mean μ and a variance σ^2 [Klo94]. How this can be implemented in practice will be discussed in the next section.

3.5.2 *Technical considerations*

Discrete Formulation

The filtering procedure described in the previous section is based on continuous measurements and continuous Bayesian updates. In any experiment measurements will always be made after discrete time steps of length Δt set by the sampling frequency $F_s = 1/\Delta t$ of the measurement equipment. In the same way a numeric integration of the stochastic master equation or the Kalman filter will also be conducted using a finite step size. Historically, the Kalman filter was first formulated for the discrete case [Kal60] and later extended to the continuous case—this extension commonly being called Kalman–Bucy filter [KB61]. Let us briefly review the discrete Kalman filter for a Gaussian time-invariant system described by a state vector $X_k \in \mathbb{R}^n$ at a time $t_k = k\Delta t$ and a state-space model

$$X_k = \bar{\mathbf{F}}X_{k-1} + \bar{\mathbf{G}}u_{k-1} + v_{k-1}, \tag{3.51a}$$

$$y_k = \mathbf{H}X_k + q_k, \tag{3.51b}$$

where $y_k \in \mathbb{R}^m$ describes the measurement process. $v_k \sim \mathcal{N}(0, \bar{\mathbf{N}})$ and $q_k \sim \mathcal{N}(0, \bar{\mathbf{R}})$ are Gaussian white-noise processes with covariance matrices $\bar{\mathbf{N}} \in \mathbb{R}^{n \times n}$ and $\bar{\mathbf{R}} \in \mathbb{R}^{m \times m}$ respectively. In general q and v are correlated, with a correlation matrix given by $\mathbb{E}[v_k q_k^{\mathrm{T}}] = \bar{\mathbf{M}} \in \mathbb{R}^{n \times m}$. Additionally we assume the initial state of the system to be given by $X_0 \sim \mathcal{N}(m_0, \Sigma_0)$. The corresponding Kalman filter is typically formulated in a two-step process, the two steps—state evolution and Bayesian update—corresponding to the procedure illustrated in fig. 38. We denote by $\mathcal{N}(\hat{X}_{k|k-1}, \hat{\Sigma}_{k|k-1})$ the *prior* state of the system at time t_k conditioned on measurements up to t_{k-1} (i. e.,

prior and posterior estimate

before the measurement update at t_k); by $\mathcal{N}(\hat{X}_k, \hat{\Sigma}_k)$ we denote the *posterior* state conditioned on measurements up to t_k (i.e., after the measurement update at t_k). The propagation step is described by the equations [Ste94, p 361f]

$$\hat{X}_{k|k-1} = \bar{\mathbf{F}}\hat{X}_{k-1} + \bar{\mathbf{G}}u_{k-1}, \tag{3.52a}$$

$$\hat{\Sigma}_{k|k-1} = \bar{\mathbf{F}}\hat{\Sigma}_k\bar{\mathbf{F}}^{\mathrm{T}} + \bar{\mathbf{N}}, \tag{3.52b}$$

and the Bayesian update is effected by

$$\hat{X}_k = \hat{X}_{k|k-1} + \mathbf{K}_k(y_k - \mathbf{H}\hat{X}_{k|k-1}), \tag{3.53a}$$

$$\hat{\Sigma}_k = (\mathbb{1} - \mathbf{H}\hat{\Sigma}_{k|k-1})\hat{\Sigma}_{k|k-1} - \mathbf{K}_k\bar{\mathbf{M}}^{\mathrm{T}}, \tag{3.53b}$$

$$\mathbf{K}_k = (\hat{\Sigma}_{k|k-1}\mathbf{H}^{\mathrm{T}} + \bar{\mathbf{M}})\times$$
$$(\mathbf{H}\hat{\Sigma}_{k|k-1}\mathbf{H}^{\mathrm{T}} + \mathbf{H}\hat{\Sigma}_{k|k-1}\mathbf{H}^{\mathrm{T}} + \mathbf{H}\bar{\mathbf{M}} + \bar{\mathbf{M}}^{\mathrm{T}}\mathbf{H}^{\mathrm{T}} + \bar{\mathbf{R}})^{-1}, \tag{3.53c}$$

Kalman gain   where $\mathbf{K}_k$ is the so-called *Kalman gain*. In the limit $\Delta t \to 0$ these equations lead to the differential Kalman filter equations (1.67) [where in (1.67) we considered the less general case $\bar{\mathbf{R}} = \mathbb{1}_m$ only]. The connection between the discrete and the continuous state-space model is found by the following procedure [Ste94; Sim06]: We start from the continuous (time-invariant) state-space model (B.38), slightly generalizing it to

$$\mathrm{d}X(t) = \big[\mathbf{F}X(t) + \mathbf{G}u(t) + v(t)\big]\mathrm{d}t, \tag{3.54a}$$

$$\mathrm{d}Y(t) = \big[\mathbf{H}X(t) + q(t)\big]\mathrm{d}t, \tag{3.54b}$$

where we introduced the measurement noise process $q(t)$ with $\mathbb{E}[q(t)q^{\mathrm{T}}(t')] = \mathbf{R}\delta(t - t')$, and $v(t)\,\mathrm{d}t = \mathrm{d}V$. We now integrate eq. (3.54a) for a time $\Delta t = t_k - t_{k-1}$, defining $X_k := X(t_k)$ and the fundamental solution $\mathbf{\Phi}(\tau) = \exp(\mathbf{F}\tau)$. We thus find

$$X_k = \mathbf{\Phi}(\Delta t)X_{k-1} + \int_{t_{k-1}}^{t_k} \mathrm{d}\tau\,\mathbf{\Phi}(t_k - \tau)[\mathbf{G}u(\tau) + v(\tau)]. \tag{3.55}$$

Assuming a piecewise continuous input which is constant over the sampling time Δt, i.e., $u(s) \equiv u_{k-1}$ for $s \in [t_{k-1}, t_k]$,[10] we can solve the first integral term, yielding

10. This is called zero-order hold in signal processing.

$$\int_{t_{k-1}}^{t_k} \mathrm{d}\tau\,\mathbf{\Phi}(t_k - \tau)\mathbf{G}u(\tau) = [\mathbf{\Phi}(\Delta t) - \mathbb{1}]\mathbf{F}^{-1}\mathbf{G}u_{k-1}. \tag{3.56}$$

The second integral we define as the discrete noise increment

$$v_{k-1} = \int_{t_{k-1}}^{t_k} \mathrm{d}\tau\,\mathbf{\Phi}(t_k - \tau)v(\tau). \tag{3.57}$$

Its covariance matrix $\bar{\mathbf{N}} = \mathbb{E}[v_k v_k^{\mathrm{T}}]$ can be readily calculated by evaluating

$$\mathbb{E}[v_k v_l^{\mathrm{T}}] = \int_{t_{k-1}}^{t_k} \mathrm{d}\tau \int_{t_{l-1}}^{t_l} \mathrm{d}\tau'\,\mathbf{\Phi}(t_k - \tau)\,\mathbb{E}[v(\tau)v^{\mathrm{T}}(\tau')]\mathbf{\Phi}^{\mathrm{T}}(t_k - \tau')$$

$$= \delta_{kl}\int_{t_{k-1}}^{t_k} \mathrm{d}\tau\,\mathbf{\Phi}(t_k - \tau)\mathbf{N}\mathbf{\Phi}^{\mathrm{T}}(t_k - \tau). \tag{3.58}$$

In the case that the sampling rate is much faster than the system's timescales, i.e., $\lambda_{\max}\Delta t \ll 1$ where $\lambda_{\max}$ is the largest eigenvalue of $\mathbf{F}$, we can neglect the time evolution in eq. (3.58) and approximate $\bar{\mathbf{N}} \approx \mathbf{N}\Delta t$. A computationally efficient method to evaluate the exact integrals involving $\mathbf{\Phi}$ is given in [Van78]. The measurement-noise covariance matrix $\bar{\mathbf{R}}$ and the correlation matrix $\bar{\mathbf{M}}$ on the other hand are chosen such, that by taking the limit $\Delta t \to 0$ one obtains from eqs. (3.52) and (3.53) the correct continuous form (1.61b). (In particular this means that $\hat{\mathbf{\Sigma}}_k$ must be independent of Δt.) This leads to $\bar{\mathbf{R}} = \mathbf{R}/\Delta t$ and $\bar{\mathbf{M}} = \mathbf{M}$ [Sim06, p 232].

Testing Model Consistency

The main tool to test the accuracy of an employed model in an experiment is the so-called innovation sequence [Hei+05, p 292f]

$$\nu_k = y_k - \mathbf{H}\hat{X}_{k|k-1} = \mathbf{H}(X_k - \hat{X}_{k|k-1}) + q_k, \qquad (3.59)$$

a white-noise Gaussian process. Due to the orthogonality relation (see appendix B.1.2) the estimation error and the measurement noise are uncorrelated, and the innovation sequence's correlation function is

$$\mathbb{E}[\nu_k \nu_l^{\mathrm{T}}] = \mathbf{S}\delta_{kl} := (\mathbf{H}\hat{\mathbf{\Sigma}}_{k|k-1}\mathbf{H}^{\mathrm{T}} + \bar{\mathbf{R}})\delta_{kl}. \qquad (3.60)$$

By virtue of the Cholesky decomposition we can write $\mathbf{S}^{-1} = \mathbf{L}\mathbf{L}^{\mathrm{T}}$, and introduce the normalized innovation sequence $\tilde{\nu}_k = \mathbf{L}^{\mathrm{T}}\nu_k$. The components of $\tilde{\nu}_k$ are independent Gaussian random variables with unit variance. The squared normalized innovation sequence $\tilde{\nu}_k^{\mathrm{T}}\tilde{\nu}_k = \nu_k^{\mathrm{T}}\mathbf{S}^{-1}\nu_k$ thus follows a χ_n^2-distribution [BLK01, p 59]. An optimally working Kalman filter thus fulfils the following conditions:

1 The squared innovation sequence $\tilde{\nu}_k^{\mathrm{T}}\tilde{\nu}_k$ follows a χ_n^2-distribution; a less strict alternative condition is that the components of $\tilde{\nu}_k$ are Gaussian random variables with unit variance.

2 The innovation sequence $\tilde{\nu}_k$ itself is white.

Condition 1 can for example be verified by applying the Kolmogorov–Smirnov test [Fra51], which quantifies the distance between an empirical and a hypothetical distribution function (here either a χ^2 or a normal distribution).

Condition 2 can either be tested by applying the Ljung–Box test [LB78] or by calculating the *periodogram* of the innovation sequence, which should be flat with a given variance for a white process [Hei+05]. Let us collect the central expressions involved in performing this test (for an extensive discussion of these results see, e.g., [Shi10]). We assume z is a (scalar) Gaussian white-noise process, i.e., $z_n \sim \mathcal{N}(0, \sigma^2)$ and $\mathbb{E}[z_n z_m] = \sigma^2 \delta_{nm}$. Its discrete Fourier transform can be written in the form

$$Z_k = \sum_{n=0}^{N-1} z_n e^{-i2\pi f_k t_n} = \sum_{n=0}^{N-1} z_n e^{-i2\pi \frac{kn}{N}}, \qquad (3.61)$$

where the frequency is sampled at discrete points $f_n = (n/N)F_s = n/(N\Delta t)$. Note that, as $z_n \in \mathbb{R}$ are Gaussian random variables, $Z_k = A_k + iB_k$ ($A_k, B_k \in \mathbb{R}$) are also Gaussian, with $\mathbb{E}[A_k^2] = \mathbb{E}[B_k^2] = N\sigma^2/2$. The power spectrum of z can be estimated by calculating its *periodogram* [Shi10, p 229f]

$$P_k = \frac{1}{MN} \sum_{m=1}^{M} |Z_k^m|^2 = \frac{1}{MN} \sum_{m=1}^{M} \left[(A_k^m)^2 + (B_k^m)^2 \right], \tag{3.62}$$

where we apply averaging over M independent samples in order to increase the signal-to-noise ratio of the periodogram.[11] Rescaling appropriately one can then see that the random variable

11. This technique is commonly called Bartlett's method.

$$\frac{2MP_k}{\sigma^2} = \frac{1}{N\sigma^2/2} \sum_{m=1}^{M} \left[(A_k^m)^2 + (B_k^m)^2 \right] \sim \chi_{2M}^2 \tag{3.63}$$

is χ^2-distributed with $2M$ degrees of freedom [Shi10, p 247].

To apply this as a test for the innovation sequence, we set z to one component of the normalized innovation sequence $\tilde{v}$, and consequently $\sigma = 1$. One can then calculate the rescaled periodogram as in eq. (3.63), and test the resulting empirical against the χ_{2M}^2 distribution.

Modelling Coloured Noise

The Kalman filter in the formulation presented here relies on a state-space model that is driven by Gaussian white noise processes. In many experiments, classical noise sources, such as amplitude and phase noise of a laser, have a coloured spectrum. To model this, one can extend the state-space model of the actual physical system to an equivalent larger model that is driven by a white noise process only. The Kalman filter can then be constructed based on this extended state-space model [Ste94, p 364].

Consider an n-dimensional coloured noise process ξ whose time evolution is described by $d\xi = \mathbf{F}_\xi \xi\, dt + d\zeta$, where ζ is white noise. Its spectrum is given by the rational function

$$\mathbf{S}_\xi(\omega) = \chi(\omega)\mathbf{N}_\zeta \chi(-\omega)^\mathsf{T}, \tag{3.64}$$

where $\chi(\omega) = -(i\omega \mathbb{1}_n + \mathbf{F}_\xi)^{-1}$ is the transfer function of the process and $\mathbf{N}_\zeta$ is the covariance matrix of ζ. Consider now a system described by $x(t)$ driven by the coloured noise process ξ, with an equation of motion of the form

$$dx = \mathbf{F}_x x\, dt + dv + d\xi. \tag{3.65}$$

We can now define $z = (x, \xi)$ and extend the state-space model (3.65) to

$$dz = \begin{pmatrix} \mathbf{F}_x & \mathbb{1}_n \\ 0 & \mathbf{F}_\xi \end{pmatrix} z + \begin{pmatrix} v \\ \zeta \end{pmatrix}, \tag{3.66}$$

which can be used as the basis for a Kalman filter.
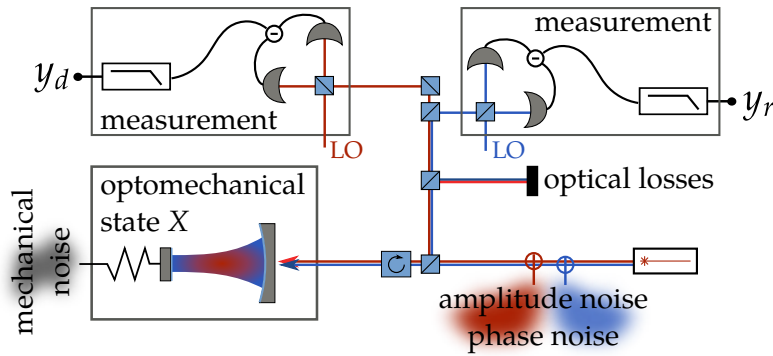
FIGURE 39. Schematic of experimental setup: The optomechanical cavity is driven by two laser fields, which are both subject to classical amplitude and phase noise. The output light is detected by two independent homodyne detectors, yielding measurement processes y_r and y_d.

Building a Model from Submodels

For practical applications the state-space model describing the complete experimental apparatus can quickly become large, making its construction by hand intractable. In order to handle increasingly large models, one can build them up from smaller submodels which describe single physical entities (such as beam-splitters, optical cavities, optomechanical systems, but also digital filters). These submodels can then conveniently be connected into a network using the framework described in [GJ09] which formalizes the concept of cascaded systems introduced by [Gar93; Car93a].

3.5.3   *The Experiment*

We now discuss the implementation of the Kalman filter for an optomechanical experiment, demonstrating optimal state estimation of the optomechanical quantum state. Although the system is currently operated in a classical regime, this experiment constitutes an important next step towards real-time quantum control of optomechanical systems. The experimental data presented in this section were taken by Jason Hölscher-Obermaier and Witlef Wieczorek [Wie+15].

The Experimental Setup

In this setup (as schematically depicted in fig. 39) we drive two independent optical modes of an optomechanical cavity with two laser beams, one of which (denoted by a subscript r) is resonant with the cavity (i.e., $\Delta_r = 0$), while the other one (subscript d) is tuned to the lower mechanical sideband at $\Delta_d = -\omega_m$. The resonant beam is used to monitor the cavity length to lock the laser frequency with respect to the cavity resonance; the detuned beam can be used as a control beam, for example, to cool the mechanical motion. The cavity is

double-sided, with a total decay rate $\kappa = \kappa_{\text{in}} + \bar{\kappa}$ (as discussed in section 1.1.2), which is the same for both optical modes. The fields reflected from the cavity are independently measured by two homodyne detection setups, yielding measurements of the generalized quadratures y_{r} and y_{d}. Both beams carry classical amplitude and phase noise, and suffer from passive beam-splitter losses. To incorporate the classical noise into our description, we extend the standard Langevin equations to [GV01; Rab+09; Abd+11; GBS11a]

$$\dot{x}_{\text{m}} = \quad \omega_{\text{m}} p_{\text{m}}, \tag{3.67a}$$

$$\dot{p}_{\text{m}} = -\omega_{\text{m}} x_{\text{m}} - \gamma_{\text{m}} p_{\text{m}} + \sum_{i=\text{r,d}} 2g_i[\cos\theta_i x_i - \sin\theta_i p_i] + f, \tag{3.67b}$$

$$\dot{x}_i = -\frac{\kappa}{2} x_i + \Delta_i p_i + g_i \sin(\theta_i) x_{\text{m}} + \sqrt{\kappa_{\text{in}}} x_{i,1}^{\text{in}}$$
$$+ \sqrt{\bar{\kappa}} x_{i,2}^{\text{in}} + \sqrt{2\kappa_{\text{in}}}\,\delta\beta_i + |\alpha_{0,i}| \sin\theta_i\,\dot{\phi}_i, \tag{3.67c}$$

$$\dot{p}_i = -\frac{\kappa}{2} p_i - \Delta_i x_i + 2g_i \cos(\theta_i) x_{\text{m}} + \sqrt{\kappa_{\text{in}}} p_{i,1}^{\text{in}}$$
$$+ \sqrt{\bar{\kappa}} p_{i,2}^{\text{in}} + |\alpha_{0,i}| \cos\theta_i\,\dot{\phi}_i, \tag{3.67d}$$

where x_i, p_i with $[x_i, p_j] = \mathrm{i}\delta_{ij}$ (for $i, j \in \{\text{r}, \text{d}\}$) describe the amplitude and phase quadrature of the two cavity modes. Vacuum noise entering through both cavity mirrors is denoted by x_i^{in}, y_i^{in}, with variances $\langle x_i^{\text{in}}(t) x_j^{\text{in}}(s)\rangle = \langle p_i^{\text{in}}(t) p_j^{\text{in}}(s)\rangle = \frac{1}{2}\delta_{ij}\delta(t - s)$ ($i, j \in \{1, 2\}$). The angles θ_i are determined by $\theta_i = \arctan(\Delta_i/\kappa)$. Terms proportional to $\delta\beta_i$ and $\dot{\phi}_i$ describe classical amplitude and phase noise of the driving lasers. The quadratures detected by the homodyne detectors are given by cavity input–output relations, yielding

$$y_i = \sqrt{1 - \eta}\left(\sqrt{\kappa_{\text{in}}}\, x_i + x_i^{\text{in}} + \delta\beta_i\right)\cos(\varphi_i)$$
$$+ \sqrt{1 - \eta}\left(\sqrt{\kappa_{\text{in}}}\, p_i + p_i^{\text{in}}\right)\sin(\varphi_i) + \sqrt{\eta} y_i^{\text{in}}, \tag{3.68}$$

where φ_i denotes the local-oscillator phases. Additionally we introduced the overall efficiency η (including losses and detector efficiency) and an independent vacuum noise process y_i^{in}. The classical noise processes $\delta\beta_i$ and $\dot{\phi}_i$ are modelled as Gaussian coloured noise, whose spectra has to be determined from experimental data.

Using the Langevin equations (3.67) as a basis, we can build a sophisticated state-space model of the complete experimental setup. The resulting Kalman filter can then be used to estimate the state of the mechanical and the optical subsystems, as well as their correlations.

Results

We apply the Kalman filter in post-processing to the recorded homodyne data to obtain estimates of the full optomechanical state vector

$X = (x_m, p_m, x_r, p_r, x_d, p_d)^T$, together with the corresponding estimation error. Short snippets of the resulting trajectories are shown in fig. 40, for two different values of the coupling strength g_d, while g_r is always fixed to $g_r = 0.2\kappa$. The left column shows results from the weak coupling regime ($g_d = 0.2\kappa$), nicely displaying the harmonic mechanical oscillation in the mechanical as well as in the optical quadratures—the latter being modulated via the optomechanical interaction. In the right column the system is operated in the strong coupling regime ($g_d = 1.68\kappa$); this leads to sideband cooling of the mechanical mode and a strong suppression of the mechanical oscillation. In both cases it is clear to see that only the phase quadrature of the resonant cavity couples to the mechanical motion, while the amplitude quadrature contains noise. Both quadratures of the detuned beam, on the other hand, are modulated by the mechanics.
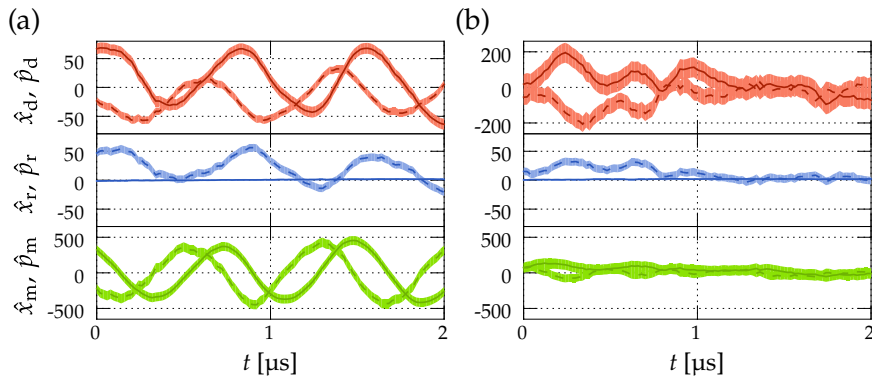
FIGURE 40. Estimated optomechanical quadratures in the (a) weak ($g_d = 0.2\kappa$) and (b) strong ($g_d = 1.68\kappa$) coupling regime. The solid lines show the amplitude (position) quadratures $\hat{x}_d$, $\hat{x}_r$ ($\hat{x}_m$), the dashed lines the phase (momentum) quadratures $\hat{p}_d$, $\hat{p}_r$ ($\hat{p}_m$). The shaded areas correspond to two times the estimation error (i.e., the 95% confidence interval). The experiment was performed at room temperature with a micromechanical oscillator of $\omega_m = 2\pi \times 1.278\,\text{MHz}$, $\gamma_m = 2\pi \times 265\,\text{Hz}$, and optomechanical parameters $\kappa = 0.34\,\omega_m$, $g_0 = 2\pi \times 7.7\,\text{Hz}$. For both coupling strengths g_d of the detuned beam we use $g_r = 0.2\,\kappa$, $\varphi_d \approx 0$, and $\varphi_r = \pi/2$.

Figure 41 shows a phase-space representation of the estimated optomechanical quadratures, similar to the schematic depiction in fig. 10. In the weak coupling regime the mechanical system—rotating in phase space—traces out a symmetric, thermal distribution [subfigure (a)]. The black dashed line shows the uncertainty ellipse of the unconditional state, which is here chosen to be the 95% confidence region. The area enclosed by it is proportional to the uncertainty product $\det(\Sigma_m)$ of the mechanical state (denoting by Σ_m the mechanical covariance matrix), and thus inversely proportional to the state's purity

$$\text{tr}(\rho_m^2) = \frac{1}{\sqrt{\det(\Sigma_m)}}. \tag{3.69}$$
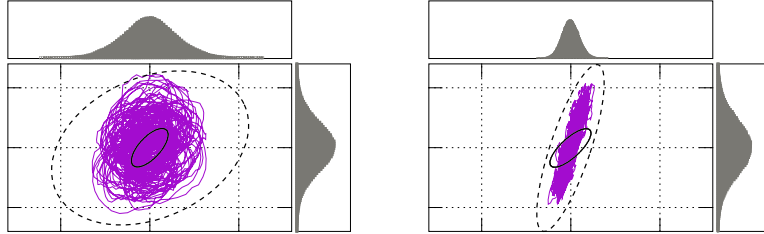
FIGURE 41. Phase-space picture of the estimated quadratures. The left column [(a), (c)] shows the weak coupling regime ($g_\mathrm{d} = 0.2\kappa$), the right column [(b), (d)] the strong coupling regime ($g_\mathrm{d} = 1.68\kappa$). (a) and (b) depict the phase space of the mechanical oscillator, (c) and (d) depict correlations between the phase quadrature of the resonantly driven cavity mode and the mechanical position. Each trajectory covers $100\,\mu$s. The dashed ellipses indicate the 95% confidence region (calculated from the unconditional covariance matrix Σ), the solid black ellipses show the corresponding extent of the conditional state (as determined by $\hat{\Sigma}$). Histograms over the estimated quadratures are shown as sidepanels (averaged over $100\,$ms).

Comparing it to the uncertainty ellipse of the conditional state (black solid line), we note a clear reduction in uncertainty due to the conditioning procedure. This effect—the conditional reduction of the occupation number—is sometimes referred to as *cooling by measurement* [Van+13]. In our case it leads to a reduction of the occupation by a factor of 27. In the strong coupling regime [subfigure (b)] one can observe the effects of sideband cooling, which heavily reduces the variance of the unconditional mechanical state. In addition, the strong optomechanical interaction introduces a notable asymmetry, which shows that the state is not thermal anymore and equipartition is violated. The marginals drawn along the phase space axes nicely demonstrate the Gaussian distribution of the optomechanical state.

Figures 41(c) and 41(d) show correlations between the mechanical position and the phase quadrature of the resonant beam. Analogous to the mechanical phase space, the uncertainty reduction due to sideband cooling is clearly visible in the shown correlations.

Finally we analyse the obtained innovation sequence to verify the consistency of our assumed model with the measured data. As discussed in section 3.5.2, in the ideal situation the innovation sequence should be white, and should therefore posses a flat noise
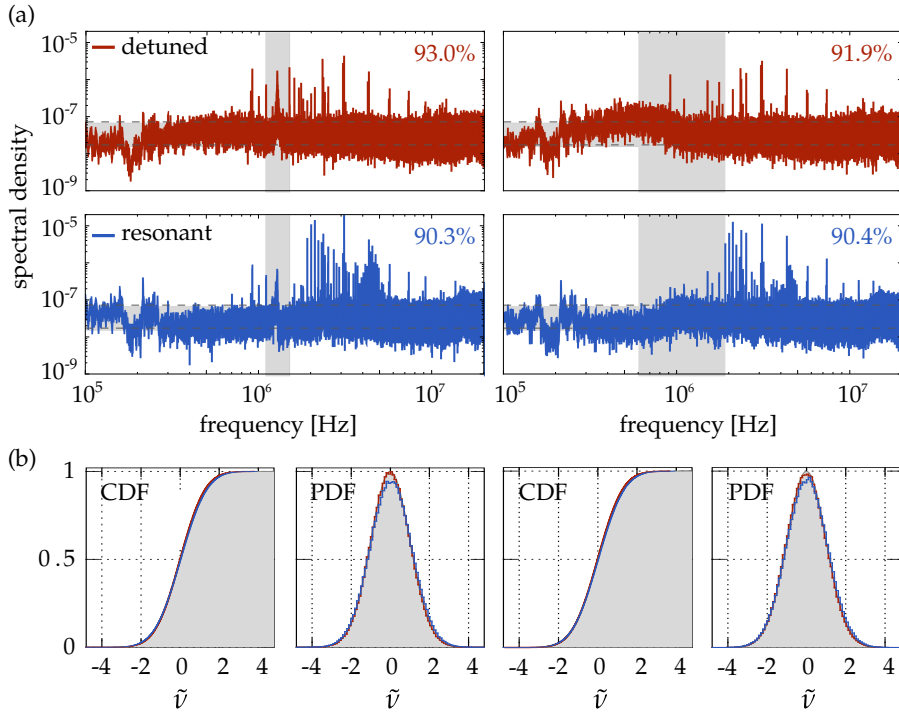
FIGURE 42. (a) Noise power spectrum of the normalized innovation sequence for the detuned beam (upper row) and the resonant beam (lower row). The left column shows the results for weak coupling, the right column for strong coupling. The 95% confidence region is shown by the dashed horizontal lines. The effective percentages of points in the confidence region are given in the plots. The vertical grey shaded area marks the fundamental mechanical mode. (b) Comparison of the empirical cumulative distribution function (CDF) and probability density function (PDF) (red and blue lines) with the theoretical form (grey shaded areas) for the weak (left) and strong (right) coupling regime.

power spectrum with a certain variance. Figure 42(a) shows the noise power spectrum of the normalized innovation sequence for both homodyne measurements in the weak and the strong coupling regime. The dashed lines indicate the confidence interval that 95% of the datapoints should fall into. The fractions of datapoints effectively contained in this region are given in the plots. We can see that we have a fairly good agreement with the hypothetical values, especially in the region around the mechanical frequency (indicated by the vertical grey-shaded areas). The deviations from the theoretical flat spectrum are mainly due to low-frequency noise at around $200\,\mathrm{kHz}$, caused by the spectral response of the photodetectors, and sharp piezo-resonances between $2-5\,\mathrm{MHz}$. Neither of these features is taken into account in the state-space model. Due to these reasons the whiteness test presented in section 3.5.2 does not succeed for this particular model. In Figure 42(b) we compare the empirical cumulative distribution function (CDF) [BLK01, p 33] and the corresponding

probability density function (PDF) to the hypothetical Gaussian distribution. We again find good overall agreement of our model with the measured data.

Although this experiment is conducted in a classical regime, it demonstrates the ability to evaluate the conditional quantum state of optomechanical systems via Kalman filtering. The estimation procedure was applied in post-processing, but can in principle be operated in real time. Combining the presented techniques with continuous measurements in the strong cooperativity regime (as demonstrated in [Wil+14]) enables measurement based feedback cooling of the mechanical motion into the ground state, as well as the realisation of the more sophisticated optomechanical quantum control protocols laid out in this thesis.

3.A APPENDIX: DETAILS ON THE OPTOMECHANICAL IMPLE-MENTATION

3.A.1 *Adiabatic Elimination under Continuous Observation*

As we discussed in appendix 2.C the adiabatic elimination of the cavity mode corresponds to a perturbative expansion in the small parameter $g/\kappa \ll 1$. At the same time it is important to keep κ/ω_m and $\Delta_\mathrm{c}/\omega_\mathrm{m}$ constant in order to capture the dynamical back-action effects of the cavity, which are crucial for a correct description of optomechanical systems. In appendix 2.C we discussed this adiabatic-elimination procedure on basis of a standard master equation. The method applied there cannot be applied to the stochastic master equation considered here, however, as the measurement operator $\mathcal{H}$ is nonlinear. Instead we follow the procedure described in [DJ99].

The conditional master equation for an optomechanical system whose output field is subject to a heterodyne measurement of a quadrature $a(t)\,\mathrm{e}^{-\mathrm{i}\Delta_\mathrm{lo}t} + a^\dagger(t)\,\mathrm{e}^{\mathrm{i}\Delta_\mathrm{lo}t}$ is given by

$$
\begin{aligned}
\mathrm{d}\tilde{\rho}_c = & -\mathrm{i}\sqrt{2}g\left[\left(c_\mathrm{c}\,\mathrm{e}^{\mathrm{i}\Delta_\mathrm{c}t} + c_\mathrm{c}^\dagger\,\mathrm{e}^{-\mathrm{i}\Delta_\mathrm{c}t}\right)\tilde{x}_\mathrm{m}, \tilde{\rho}_c\right]\mathrm{d}t \\
& + \kappa\left[c_\mathrm{c}\tilde{\rho}_c c_\mathrm{c}^\dagger - \tfrac{1}{2}\left(c_\mathrm{c}^\dagger c_\mathrm{c}\tilde{\rho}_c + \tilde{\rho}_c c_\mathrm{c}^\dagger c_\mathrm{c}\right)\right]\mathrm{d}t \\
& + \sqrt{\kappa}\left[\mathrm{e}^{\mathrm{i}(\Delta_\mathrm{c}+\Delta_0)t}(c_\mathrm{c} - \langle c_\mathrm{c}\rangle)\tilde{\rho}_c + \mathrm{e}^{-\mathrm{i}(\Delta_\mathrm{c}+\Delta_\mathrm{lo})t}\,\tilde{\rho}_c(c_\mathrm{c}^\dagger - \langle c_\mathrm{c}^\dagger\rangle)\right]\mathrm{d}W.
\end{aligned}
\tag{3.70}
$$

Δ_lo is the detuning of the LO with respect to the laser drive of the cavity. We are working in an interaction picture with respect to $\omega_\mathrm{m}c_\mathrm{m}^\dagger c_\mathrm{m} - \Delta_\mathrm{c}c_\mathrm{c}^\dagger c_\mathrm{c}$, indicated by the operators $\tilde{x}_\mathrm{m}$, $\tilde{\rho}_c$, etc. In order to eliminate the cavity we decompose $\tilde{\rho}_c$ as

$$
\tilde{\rho}_c \approx \tilde{\rho}_{00} \otimes |0\rangle\langle 0| + \tilde{\rho}_{10} \otimes |1\rangle\langle 0| + \tilde{\rho}_{01} \otimes |0\rangle\langle 1| + \tilde{\rho}_{11} \otimes |1\rangle\langle 1|, \tag{3.71}
$$

such that

$$
\langle c_\mathrm{c}\rangle = \mathrm{tr}(\tilde{\rho}_{10}), \tag{3.72a}
$$
$$
\langle c_\mathrm{c}^\dagger\rangle = \mathrm{tr}(\tilde{\rho}_{01}). \tag{3.72b}
$$

We can consider the matrix elements $\tilde{\rho}_{ij}$ to be of order $i + j$ in the small parameter g/κ; eq. (3.71) thus corresponds to a second-order expansion. For the components $\tilde{\rho}_{ij}$ we find

$$
\begin{aligned}
\mathrm{d}\tilde{\rho}_{00} = & -\mathrm{i}\sqrt{2}g\left(\mathrm{e}^{\mathrm{i}\Delta_\mathrm{c}t}\,\tilde{x}_\mathrm{m}\tilde{\rho}_{10} - \mathrm{H.c.}\right)\mathrm{d}t + \kappa\tilde{\rho}_{11}\,\mathrm{d}t \\
& + \sqrt{\kappa}\left\{\mathrm{e}^{\mathrm{i}(\Delta_\mathrm{c}+\Delta_\mathrm{lo})t}\left[\tilde{\rho}_{10} - \mathrm{tr}(\tilde{\rho}_{10})\tilde{\rho}_{00}\right] - \mathrm{H.c.}\right\}\mathrm{d}W, \\
\mathrm{d}\tilde{\rho}_{10} = & -\mathrm{i}\sqrt{2}g\left(\mathrm{e}^{-\mathrm{i}\Delta_\mathrm{c}t}\,\tilde{x}_\mathrm{m}\tilde{\rho}_{00} - \mathrm{e}^{-\mathrm{i}\Delta_\mathrm{c}t}\,\tilde{\rho}_{11}\tilde{x}_\mathrm{m}\right)\mathrm{d}t - \frac{1}{2}\kappa\tilde{\rho}_{10}\,\mathrm{d}t \\
& - \sqrt{\kappa}\,\mathrm{e}^{\mathrm{i}(\Delta_\mathrm{c}+\Delta_\mathrm{lo})t}\,\mathrm{tr}(\tilde{\rho}_{10})\tilde{\rho}_{10}\,\mathrm{d}W \\
& - \sqrt{\kappa}\,\mathrm{e}^{-\mathrm{i}(\Delta_\mathrm{c}+\Delta_\mathrm{lo})t}\left[\tilde{\rho}_{11} - \mathrm{tr}(\tilde{\rho}_{01})\tilde{\rho}_{10}\right]\mathrm{d}W,
\end{aligned}
$$

and

$$
\begin{aligned}
\mathrm{d}\tilde{\rho}_{11} = {}& -\mathrm{i}g\sqrt{2}\left(\mathrm{e}^{-\mathrm{i}\Delta_c t}\tilde{x}_{\mathrm{m}}\tilde{\rho}_{01} - \mathrm{e}^{\mathrm{i}\Delta_c t}\tilde{\rho}_{10}\tilde{x}_{\mathrm{m}}\right)\mathrm{d}t - \kappa\tilde{\rho}_{11}\,\mathrm{d}t \\
& - \sqrt{\kappa}\left\{\mathrm{e}^{\mathrm{i}(\Delta_c+\Delta_{\mathrm{lo}})t}\,\mathrm{tr}(\tilde{\rho}_{10})\tilde{\rho}_{11} + \mathrm{e}^{-\mathrm{i}(\Delta_c+\Delta_{\mathrm{lo}})t}\,\mathrm{tr}(\tilde{\rho}_{01})\tilde{\rho}_{11}\right\}\mathrm{d}W.
\end{aligned}
$$

The adiabatic solution for $\tilde{\rho}_{10}$ is [compare this to eq. (1.44)]

$$
\tilde{\rho}_{10} = -\mathrm{i}g\,\mathrm{e}^{-\mathrm{i}\Delta_c t}\left[\eta_-\tilde{c}_{\mathrm{m}} + \eta_+\tilde{c}_{\mathrm{m}}^\dagger\right]\tilde{\rho}_{00}, \tag{3.73}
$$

where we neglected terms of second and higher order in g/κ and introduced $\eta_\pm$ as given by eq. (1.45). We are interested in the effective equation of motion for the reduced density matrix of the mirror $\tilde{\rho}_c^{(\mathrm{m})} = \mathrm{tr}_c(\tilde{\rho}) \approx \tilde{\rho}_{00} + \tilde{\rho}_{11}$,

$$
\begin{aligned}
\mathrm{d}\tilde{\rho}_c^{(\mathrm{m})} = {}& -\mathrm{i}g\sqrt{2}\left[\tilde{x}_{\mathrm{m}}\left(\mathrm{e}^{\mathrm{i}\Delta_c t}\tilde{\rho}_{10} + \mathrm{e}^{-\mathrm{i}\Delta_c t}\tilde{\rho}_{01}\right) - \mathrm{H.\,c.}\right]\mathrm{d}t \\
& + \sqrt{\kappa}\left\{\mathrm{e}^{\mathrm{i}(\Delta_c+\Delta_{\mathrm{lo}})t}\left[\tilde{\rho}_{10} - \mathrm{tr}(\tilde{\rho}_{10})\tilde{\rho}_c^{(\mathrm{m})}\right] + \mathrm{H.\,c.}\right\}\mathrm{d}W. \tag{3.74}
\end{aligned}
$$

From the adiabatic solution for $\tilde{\rho}_{10}$ and $\tilde{\rho}_{01} = \tilde{\rho}_{10}^\dagger$ we find,

$$
\begin{aligned}
\mathrm{e}^{\mathrm{i}\Delta_c t}\tilde{\rho}_{10} + \mathrm{e}^{-\mathrm{i}\Delta_c t}\tilde{\rho}_{01} \approx {}& \\
& -\mathrm{i}g\left\{\left[\eta_-\tilde{c}_{\mathrm{m}} + \eta_+\tilde{c}_{\mathrm{m}}^\dagger\right]\tilde{\rho}_c^{(\mathrm{m})} - \tilde{\rho}_c^{(\mathrm{m})}\left[\eta_+^*\tilde{c}_{\mathrm{m}} + \eta_-^*\tilde{c}_{\mathrm{m}}^\dagger\right]\right\},
\end{aligned}
$$

where we used $\tilde{\rho}_{00} \approx \tilde{\rho}_c^{(\mathrm{m})}$ which is correct to the desired order. Correspondingly we find for

$$
\begin{aligned}
\mathrm{e}^{\mathrm{i}\Delta_c t}\left[\tilde{\rho}_{10} - \mathrm{tr}(\tilde{\rho}_{10})\tilde{\rho}_c^{(\mathrm{m})}\right] \approx {}& \\
& -\mathrm{i}g\left[\left(\eta_-\tilde{c}_{\mathrm{m}} + \eta_+\tilde{c}_{\mathrm{m}}^\dagger\right) - \langle\eta_-\tilde{c}_{\mathrm{m}} + \eta_+\tilde{c}_{\mathrm{m}}^\dagger\rangle\right]\tilde{\rho}_c^{(\mathrm{m})}.
\end{aligned}
$$

Plugging this into eq. (3.74) we end up with

$$
\mathrm{d}\tilde{\rho}_c^{(\mathrm{m})} = -\sqrt{2}g^2\left[\tilde{x}_{\mathrm{m}}, \tilde{y}\tilde{\rho}_c^{(\mathrm{m})} - \tilde{\rho}_c^{(\mathrm{m})}\tilde{y}^\dagger\right]\mathrm{d}t - g\sqrt{\kappa}\mathcal{H}[\mathrm{i}\tilde{y}\,\mathrm{e}^{\mathrm{i}\Delta_{\mathrm{lo}}t}]\tilde{\rho}_c^{(\mathrm{m})}\,\mathrm{d}W, \tag{3.75}
$$

where

$$
\tilde{y} = \eta_-c_{\mathrm{m}}\,\mathrm{e}^{-\mathrm{i}\omega_{\mathrm{m}}t} + \eta_+c_{\mathrm{m}}^\dagger\,\mathrm{e}^{\mathrm{i}\omega_{\mathrm{m}}t}. \tag{3.76}
$$

Equation (3.75) does not give rise to a valid Lindblad equation when averaged over all possible measurement trajectories as $\tilde{y}$ is not a Hermitian operator. In order to get a consistent equation we apply a RWA to both the dynamics generated by the first commutator term and the measurement term. Let us take a closer look at the first term in eq. (3.75): Plugging in the definitions of $\tilde{x}_{\mathrm{m}}$ and $\tilde{y}$ we find resonant terms of the form $c_{\mathrm{m}}\tilde{\rho}^{(\mathrm{m})}c_{\mathrm{m}}^\dagger$, $c_{\mathrm{m}}^\dagger c_{\mathrm{m}}\tilde{\rho}^{(\mathrm{m})}$, etc., and off-resonant terms oscillating at $\mathrm{e}^{\pm 2\mathrm{i}\omega_{\mathrm{m}}t}$. The resonant terms have two effects (see section 1.3.1): First they give rise to cooling and heating, and second to

a frequency shift of the mechanical resonance frequency to $\omega_{\mathrm{m}}^{\mathrm{eff}}$. We have to account for this frequency shift by changing to a different frame rotating at $\omega_{\mathrm{m}}^{\mathrm{eff}}$, which we still denote by $\tilde{\rho}^{(\mathrm{m})}$ for simplicity.

We can now introduce a time coarse graining in the form of $\mathrm{d}\rho_c^{(\mathrm{m})} = \int_t^{t+\delta t} \mathrm{d}\tilde{\rho}_c^{(\mathrm{m})}$ as we have done in appendix 2.C.2. We assume that it can be arranged such that $\tilde{\rho}_c^{(\mathrm{m})}$ varies slowly on the timescale δt (and can thus be pulled out from all time integrals), while we still average over many mechanical periods, i.e., $\delta t\, \omega_{\mathrm{m}}^{\mathrm{eff}} \gg 1$. In the adiabatic regime the relevant system timescales are given by g^2/κ and $\bar{n}\gamma$, the effective interaction strength and mechanical decoherence rate respectively. Hence we find that δt must fulfill $\omega_{\mathrm{m}}^{\mathrm{eff}} \gg 1/\delta t \gg g^2/\kappa, \bar{n}\gamma$.

Although equation (3.75) is valid for any Δ_{lo} and Δ_c, the form of the resulting equation in RWA depends on the choice of Δ_{lo}. Here we are only interested in the case $\Delta_{\mathrm{lo}} = \pm\omega_{\mathrm{m}}^{\mathrm{eff}}$. For the first term in (3.75) the RWA then simply amounts to dropping all terms oscillating with $\exp(\pm 2\mathrm{i}\omega_{\mathrm{m}}^{\mathrm{eff}}t)$ (as they are averaged out by the time coarse graining), which introduces an error of order $\mathcal{O}(1/\delta t\, \omega_{\mathrm{m}}^{\mathrm{eff}})$. To treat the heterodyne measurement we introduce the coarse-grained noise increment $\mathrm{d}W_0 = \int_t^{t+\delta t} \mathrm{d}W$ (see appendix B.1.1 for a more detailed treatment of heterodyne detection), which obeys $(\mathrm{d}W_0)^2 = \mathrm{d}t$. The averaged operator $\bar{\rho}_c^{(\mathrm{m})}$ for $\Delta_{\mathrm{lo}} = \omega_{\mathrm{m}}^{\mathrm{eff}}$ obeys

$$\mathrm{d}\bar{\rho}_c^{(\mathrm{m})} = \gamma_- \, \mathcal{D}[c_{\mathrm{m}}]\bar{\rho}_c^{(\mathrm{m})} \, \mathrm{d}t + \gamma_+ \, \mathcal{D}[c_{\mathrm{m}}^\dagger]\bar{\rho}_c^{(\mathrm{m})} \, \mathrm{d}t$$
$$- g\sqrt{\kappa}\mathcal{H}[\mathrm{i}\eta_- c_{\mathrm{m}}]\bar{\rho}_c^{(\mathrm{m})} \, \mathrm{d}W_0, \quad (3.77)$$

and for $\Delta_{\mathrm{lo}} = -\omega_{\mathrm{m}}^{\mathrm{eff}}$ we find

$$\mathrm{d}\bar{\rho}_c^{(\mathrm{m})} = \gamma_- \, \mathcal{D}[c_{\mathrm{m}}]\bar{\rho}_c^{(\mathrm{m})} \, \mathrm{d}t + \gamma_+ \, \mathcal{D}[c_{\mathrm{m}}^\dagger]\bar{\rho}_c^{(\mathrm{m})} \, \mathrm{d}t$$
$$- g\sqrt{\kappa}\mathcal{H}[\mathrm{i}\eta_+ c_{\mathrm{m}}^\dagger]\bar{\rho}_c^{(\mathrm{m})} \, \mathrm{d}W_0, \quad (3.78)$$

with $\gamma_- = \Gamma_- + \gamma_{\mathrm{m}}(\bar{n}+1)$ and $\gamma_+ = \Gamma_+ + \gamma_{\mathrm{m}}\bar{n}$. In principle there exist additional sideband modes centered at $\pm 2\omega_{\mathrm{m}}^{\mathrm{eff}}$, which in RWA are not correlated with W_0, and are not of interest for use here. We thus average over them.

3.A.2 *Time-continuous Teleporation*

Here we derive the stochastic and feedback master equations for the optomechanical teleportation setup presented in section 3.3, following the lines of section 3.2.1 with modifications accommodating the optomechanical implementation. The one-dimensional electromagnetic field A couples to the cavity via the linear interaction $H_{\mathrm{int}} = \mathrm{i}\sqrt{\kappa}[c_c a^\dagger(t) - c_c^\dagger a(t)]$. As before, A is assumed to be in the vaccuum state, while the second field B is in a pure squeezed state. In this section we refer to several different rotating frames: the frame

of the driving laser rotating at ω_0 (which is our standard frame of reference), the squeezing frame which defines the central frequency for the squeezed input light at ω_s, and the local oscillator frame at ω_{lo} in reference to which all measurements will be made. We therefore have the relations

$$a(t) = a_{\mathrm{lo}}(t)\, e^{-i\Delta_{\mathrm{lo}} t}, \tag{3.79a}$$

$$b(t) = b_s(t)\, e^{-i\Delta_s t} = b_{\mathrm{lo}}(t)\, e^{-i\Delta_{\mathrm{lo}} t}, \tag{3.79b}$$

with the definitions $\Delta_{\mathrm{lo}} = \omega_{\mathrm{lo}} - \omega_0$, $\Delta_s = \omega_s - \omega_0$. The squeezed input state is then, in the squeezing frame, defined by the eigenvalue equation $\left[b_s(t) - \alpha b_s^\dagger(t)\right]|M\rangle_B = 0$ with $\alpha = (N+M)/(N+M^*+1)$ and $N(N+1) = |M|^2$. The Schrödinger equation of the full system in the LO frame can be written as (neglecting for the moment the coupling to the mechanical bath as this can easily be added in the end, see discussion in appendix 2.C)

$$d|\Psi\rangle = -iH_{\mathrm{eff}}|\Psi\rangle\, dt + \sqrt{\kappa}\left(dA_{\mathrm{lo}}^\dagger + \alpha\, dA_{\mathrm{lo}}\right) e^{i\Delta_{\mathrm{lo}} t} c_{\mathrm{c}}|\Psi\rangle$$
$$+ \sqrt{\kappa}\left[dB_{\mathrm{lo}}\, e^{-i(\Delta_{\mathrm{lo}} - \Delta_s)t} - \alpha\, dB_{\mathrm{lo}}^\dagger\, e^{i(\Delta_{\mathrm{lo}} - \Delta_s)t}\right] e^{i\Delta_{\mathrm{lo}} t} c_{\mathrm{c}}|\Psi\rangle, \quad (3.80)$$

where $|\Psi\rangle$ is the state describing the complete system with an initial condition $|\Psi_0\rangle = |\psi_0\rangle_S \otimes |\mathrm{vac}\rangle_A \otimes |M\rangle_B$. If we now choose $\Delta_s = \Delta_{\mathrm{lo}}$, we can rewrite this as

$$d|\Psi\rangle = \left[-iH_{\mathrm{eff}}\, dt + \sqrt{\kappa/2}\,(\mu\, dX_+ + i\nu\, dP_-)\, c_{\mathrm{c}}\, e^{i\Delta_{\mathrm{lo}} t}\right]|\Psi\rangle,$$

where $dX_+ = \sqrt{1/2}(a_{\mathrm{lo}} + a_{\mathrm{lo}}^\dagger + b_{\mathrm{lo}} + b_{\mathrm{lo}}^\dagger)\, dt$ and $dP_- = i\sqrt{1/2}(a_{\mathrm{lo}} - a_{\mathrm{lo}}^\dagger - b_{\mathrm{lo}} + b_{\mathrm{lo}}^\dagger)\, dt$, and $\mu = 1 - \alpha$, $\nu = 1 + \alpha$ as before. By comparing this to Schrödinger equation (3.6) we can deduce that the heterodyne Bell measurement at ω_{lo} is described by SME (3.15) together with the expression for the measurement currents (3.8) if we set $s = c_{\mathrm{c}}\, e^{i\Delta_{\mathrm{lo}} t}$. Thus the master equation

$$d\rho_c = \mathcal{L}\rho_c\, dt + \sqrt{\kappa}\mathcal{H}[(\mu\, dW_+ + i\nu\, dW_-)c_{\mathrm{c}}\, e^{i\Delta_{\mathrm{lo}} t}]\rho_c \tag{3.81}$$

together with the output equations

$$I_+\, dt = \sqrt{1/2}\langle c_{\mathrm{c}}\, e^{i\Delta_{\mathrm{lo}} t} + \mathrm{H.c.}\rangle_c\, dt + dW_+, \tag{3.82a}$$

$$I_-\, dt = i\sqrt{1/2}\langle c_{\mathrm{c}}\, e^{i\Delta_{\mathrm{lo}} t} - \mathrm{H.c.}\rangle_c\, dt + dW_- \tag{3.82b}$$

provides us with a description of the conditional state of the full optomechanical system (including the cavity mode) conditioned on the heterodyne currents $I_\pm$. What we eventually seek to obtain is an effective description of the mechanical system only. Under the weak coupling assumption $g/\kappa \ll 1$ we can eliminate the cavity mode. It is straightforward to generalize the procedure from appendix 3.A.1 to the case of a time-continuous Bell measurement. To make the desired

expansion we must first transform (3.81) into the interaction picture defined by the free Hamiltonian $\omega_m c_m^\dagger c_m - \Delta_c c_c^\dagger c_c$,

$$d\tilde{\rho}_c = -ig\left[(c_c\, e^{i\Delta_c t} + \text{H.c.})(c_m\, e^{-i\omega_m t} + \text{H.c.}), \tilde{\rho}_c\right]dt$$
$$+ \sqrt{\kappa}\mathcal{H}[(\mu\, dW_+ + i\nu\, dW_-)c_c\, e^{i(\Delta_{lo}+\Delta_c)t}]\tilde{\rho}_c + \kappa\mathcal{D}[c_c]\tilde{\rho}_c\, dt. \quad (3.83)$$

(All operators marked with a tilde, e.g., $\tilde{\rho}$, are defined with respect to this rotating frame.) One can then show that the SME for the mechanical system (in the rotating frame at ω_m) can be written as

$$d\tilde{\rho}_c^{(m)} = -\sqrt{2}g^2\left[\tilde{x}_m, \tilde{y}\tilde{\rho}_c^{(m)} - \tilde{\rho}_c^{(m)}\tilde{y}^\dagger\right]dt$$
$$+ \sqrt{g^2\kappa}\mathcal{H}[(-i\mu\, dW_+ + \nu\, dW_-)\tilde{y}\, e^{i\Delta_{lo}t}]\tilde{\rho}_c^{(m)}, \quad (3.84)$$

where $\tilde{\rho}_c^{(m)}$ denotes the conditional state of the mechanical subsystem. As we illustrate in the main text we drive the optomechanical cavity on the blue sideband ($\omega_0 = \omega_c + \omega_m$), but want the LO to be resonant with the scattered photons ($\omega_{lo} = \omega_0 - \omega_m^{\text{eff}}$), and thus set $\Delta_{lo} = -\omega_m^{\text{eff}}$ (note the shifted resonance frequency; see appendix 3.A.1). As before we introduce the coarse-grained noise increments $dW_\pm^{(0)} = \int_t^{t+\delta t} dW_\pm$, which obey (3.9). We end up with an effective SME for the mechanical system,

$$d\tilde{\rho}_c^{(m)} = \gamma_- \mathcal{D}[c_m]\tilde{\rho}_c^{(m)}\, dt + \gamma_+ \mathcal{D}[c_m^\dagger]\tilde{\rho}_c^{(m)}\, dt$$
$$+ \sqrt{g^2\kappa/2}\,\mathcal{H}[(-i\mu\, dW_+^{(0)} + \nu\, dW_-^{(0)})\eta_+ c_m^\dagger]\tilde{\rho}_c^{(m)}, \quad (3.85)$$

where we added mechanical decoherence terms.

To apply feedback we have to extract the modes corresponding to the filtered noise processes $W_\pm^{(0)}$ from the heterodyne currents $I_\pm$. This can be achieved by applying the coarse-graining procedure from above to (3.82a) and (3.82b), i.e., $I_\pm^{(0)} = \int_t^{t+\delta t} I_\pm\, dt$. Together with $\langle c_c \rangle_c = -ig\langle y \rangle_c$, which results from the adiabatic elimination [see eqs. (3.72) and (3.73)], we find

$$I_+^{(0)}\, dt \approx -ig\sqrt{\kappa/2}\langle \eta_+ c_m^\dagger - \text{H.c.} \rangle\, dt + dW_+^{(0)}, \quad (3.86a)$$
$$I_-^{(0)}\, dt \approx g\sqrt{\kappa/2}\langle \eta_+ c_m^\dagger + \text{H.c.} \rangle\, dt + dW_-^{(0)}, \quad (3.86b)$$

where we neglected contributions from higher sidebands, introducing corrections on the order $\mathcal{O}(1/\delta t\, \omega_m^{\text{eff}})$. With the identification $s = -ig\sqrt{\kappa}\,\eta_+ c_m^\dagger$ the set of equations (3.85), (3.86) is equivalent to the generic case discussed before. However, equation (3.85) additionally contains decoherence terms due to the coupling to the mechanical environment ($\gamma\bar{n}\mathcal{D}[c_m^\dagger] + \gamma(\bar{n}+1)\mathcal{D}[c_m]$) and due to optomechanical back-action ($2g^2\,\text{Re}(\eta_-)\mathcal{D}[c_m]$). For the choice

$$F_+ = -g\sqrt{\kappa}\eta_+(c_m + c_m^\dagger), \quad (3.87a)$$
$$F_- = ig\sqrt{\kappa}\eta_+(c_m - c_m^\dagger), \quad (3.87b)$$

(where the prefactors are chosen to match the operator s), and after adding the appropriate decoherence terms, the FME for optomechanical teleportation can be written as

$$\dot{\rho}^{(\mathrm{m})} = \left\{ \gamma(\bar{n} + 1)\mathcal{D}[c_{\mathrm{m}}] + \gamma\bar{n}\mathcal{D}[c_{\mathrm{m}}^{\dagger}] \right\} \tilde{\rho}^{(\mathrm{m})}$$

$$+ \frac{4g^2}{\kappa} \left\{ (1 + \epsilon)\mathcal{D}[c_{\mathrm{m}}] + \frac{w_3}{\eta}\mathcal{D}[x_{\mathrm{m}} + p_{\mathrm{m}}] \right.$$

$$\left. + \left(\frac{w_1 - w_3}{\eta} - 1 \right)\mathcal{D}[p_{\mathrm{m}}] + \left(\frac{w_2 - w_3}{\eta} - 1 \right)\mathcal{D}[x_{\mathrm{m}}] \right\} \tilde{\rho}^{(\mathrm{m})},$$

$$(3.88)$$

where $\epsilon = [1 + (4\omega_{\mathrm{m}}/\kappa)^2]^{-1}$ and we finally set $\Delta_c = \omega_{\mathrm{m}}$. Note that this equation is not necessarily in Lindblad form, as the decoherence terms' prefactors may in general be negative. To fix this we can apply the following diagonalisation procedure. We parametrise the jump operators in terms of $X_{\mathrm{m}} = (x_{\mathrm{m}}, p_{\mathrm{m}})^{\mathrm{T}}$ as $s = \tilde{\Lambda}X$ and rewrite the master equation as

$$\dot{\rho} = \sum_k l_k \mathcal{D}[s_k] = \sum_i l_k \left[s_k \rho s_k^{\dagger} - \tfrac{1}{2}\rho s_k^{\dagger} s_k - \tfrac{1}{2}s_k^{\dagger} s_k \rho \right]$$

$$= \sum_{ijk} l_k \tilde{\Lambda}_{ki}\tilde{\Lambda}_{kj}^{*} \left[X_i \rho X_j - \tfrac{1}{2}\rho X_j X_i - \tfrac{1}{2}X_j X_i \rho \right]$$

$$= \sum_{ijm} \lambda_m O_{im} O_{mj}^{\mathrm{T}} \left[X_i \rho X_j - \tfrac{1}{2}\rho X_j X_i - \tfrac{1}{2}X_j X_i \rho \right] \qquad (3.89)$$

$$= \sum_m \lambda_m \left[J_m \rho J_m - \tfrac{1}{2}\rho J_m J_m - \tfrac{1}{2}J_m J_m \rho \right] = \sum_m \lambda_m \mathcal{D}[J_m]\rho.$$

This shows that by virtue of the eigenvalue decomposition of the (2×2) Hermitian matrix Λ, $\Lambda_{ij} = \sum_k l_k \tilde{\Lambda}_{ki}\tilde{\Lambda}_{kj}^{*}$, we can write $\dot{\rho} = \sum_i \lambda_i \mathcal{D}[J_i]\rho$ with $J_i = v_i \cdot X$, where λ_i and v_i ($i = 1, 2$) are the eigenvalues and eigenvectors of Λ respectively. In all cases considered in this thesis, Λ is positive definite and thus $\lambda_i > 0$; we can therefore bring the corresponding master equations into Lindblad form.

3.A.3 *Time-continuous Entanglement Swapping*

In this section we derive the SME (3.43) and FME (3.45) which specify the generic case in section 3.2.2 for the optomechanical implementation. Again, the goal is to derive equations for the mechanical systems, which we obtain by adiabatic elimination of the cavity and subsequent application of a RWA. As before, the Bell detection operates at the cavity frequency ω_c detuned by $\Delta_{\mathrm{lo}} = \omega_{\mathrm{lo}} - \omega_0$ with respect to the driving laser, and relations (3.79) still apply. Following the logic from appendix 3.A.2 we thus define $s_i = \sqrt{\kappa}\,\mathrm{e}^{\mathrm{i}\Delta_{\mathrm{lo}}t}c_{\mathrm{m},i}$, which we use together with the generic entanglement SME (3.35) and FME (3.36) as the starting point for our approximations. Going to the rotat-

ing frame with $\sum_i (\omega_m c_{m,i}^\dagger c_{m,i} - \Delta_c c_{m,i}^\dagger c_{m,i})$ and applying the adiabatic approximation procedure to (3.35) leaves us with

$$
\begin{aligned}
d\tilde{\rho}_c^{(m)} = &-\sqrt{2}g^2 \sum_{i=1,2} \left[\tilde{x}_{m,i}, \tilde{y}_i \tilde{\rho}_c^{(m)} - \tilde{\rho}_c^{(m)} \tilde{y}_i^\dagger \right] dt \\
&+ \sqrt{g^2 \kappa v/2}\, \mathcal{H}[(\tilde{y}_+ \, dW_+ + i\tilde{y}_- \, dW_-)\, e^{i\Delta_{lo}t}] \tilde{\rho}_c^{(m)} \\
&+ \sqrt{g^2 \kappa (1-v)/2}\, \mathcal{H}[(i\tilde{y}_+ \, dV_+ + \tilde{y}_- \, dV_-)\, e^{i\Delta_{lo}t}] \tilde{\rho}_c^{(m)}, \quad (3.90)
\end{aligned}
$$

where $\tilde{y}_\pm = \tilde{y}_1 \pm \tilde{y}_2$ with $\tilde{y}_i = \eta_- c_{m,i}\, e^{-i\omega_m t} + \eta_+ c_{m,i}^\dagger\, e^{i\omega_m t}$. To apply a time coarse graining $\delta\rho_c^{(m)} = \int_t^{t+\delta t} d\rho_c^{(m)}$ we first change to the frame rotating with ω_m^{eff} (taking into account the optical spring effect). If we choose $\Delta_{lo} = -\omega_m^{eff}$ we can drop the fast rotating terms in the first line of (3.90). For the measurement terms (second and third line) we again introduce $\delta W_\pm^{(0)}$ and average over any sideband modes. After taking the limit $\delta t \to dt$ we end up with

$$
\begin{aligned}
d\tilde{\rho}_c^{(m)} = &\, \gamma_- \{\mathcal{D}[c_{m,1}] + \mathcal{D}[c_{m,2}]\} \tilde{\rho}_c^{(m)} \, dt \\
&+ \gamma_+ \{\mathcal{D}[c_{m,1}^\dagger] + \mathcal{D}[c_{m,2}^\dagger]\} \tilde{\rho}_c^{(m)} \, dt \\
&+ \sqrt{g^2 \kappa v/2}\, \eta_+ \mathcal{H}[c_{m,+}^\dagger \, dW_+^{(0)} + i c_{m,-}^\dagger \, dW_-^{(0)}] \tilde{\rho}_c^{(m)} \\
&+ \sqrt{g^2 \kappa (1-v)/2}\, \eta_+ \mathcal{H}[i c_{m,+}^\dagger \, dV_+^{(0)} + c_{m,-}^\dagger \, dV_-^{(0)}] \tilde{\rho}_c^{(m)} \quad (3.91)
\end{aligned}
$$

where we introduced $c_{m,\pm} = c_{m,1} \pm c_{m,2}$ and we added mechanical decoherence terms. We apply the same coarse graining to the measurement currents (3.34) and find, by using $s_i = \sqrt{\kappa}\, e^{i\Delta_{lo}t} c_{m,i}$ and $\langle c_{m,i} \rangle_c = -ig\langle y_i \rangle_c$,

$$
I_+^{(0)} \, dt = -i\sqrt{g^2 \kappa v/2}\, \langle \eta_+ c_{m,+}^\dagger - \mathrm{H.c.} \rangle_c + dW_+^{(0)}, \quad (3.92a)
$$

$$
I_-^{(0)} \, dt = \sqrt{g^2 \kappa v/2}\, \langle \eta_+ c_{m,-}^\dagger + \mathrm{H.c.} \rangle_c + dW_-^{(0)}, \quad (3.92b)
$$

$$
I_+'^{(0)} \, dt = \sqrt{g^2 \kappa (1-v)/2}\, \langle \eta_+ c_{m,+}^\dagger + \mathrm{H.c.} \rangle_c + dV_+^{(0)}, \quad (3.92c)
$$

$$
I_-'^{(0)} \, dt = -i\sqrt{g^2 \kappa (1-v)/2}\, \langle \eta_+ c_{m,-}^\dagger - \mathrm{H.c.} \rangle_c + dV_-^{(0)}. \quad (3.92d)
$$

One can clearly see that equations (3.91) and (3.92) are equivalent to SME (3.35) and measurement currents (3.34) if we set $s_\pm = \sqrt{g^2 \kappa}\, \eta_+ c_{m,\pm}^\dagger$ and add appropriate decoherence terms. We can therefore use FME (3.36) directly, and together with the choice $(F_1, F_2) = \sqrt{v}\sigma(i c_{m,+} - i c_{m,+}^\dagger, c_{m,-} + c_{m,-}^\dagger)$, $(F_3, F_4) = \sqrt{1-v}(c_{m,+} + c_{m,+}^\dagger, i c_{m,-} - i c_{m,-}^\dagger)$ we find equation (3.45).

QUANTUM STOCHASTIC CALCULUS

A.1 QUANTUM-OPTICAL MODEL

In this section we briefly review the quantum-optical model of an open quantum system coupling to the electromagnetic field, following the presentation in [GC85]. A detailed discussion of this topic can for example be found in [GZ04; ZG97; Bar06].

We consider a quantum system S described by some Hamiltonian H_{sys} which couples to a 1d electromagnetic field A, consisting of a continuum of harmonic oscillators. The environment (or bath) is described in the Schrödinger picture by the creation and annihilation operators $a_0^\dagger(\omega)$ and $a_0(\omega)$, which fulfil the canonical commutation relations

$$[a_0(\omega), a_0^\dagger(\omega')] = \delta(\omega - \omega'). \tag{A.1}$$

The bath is thus described by the free Hamiltonian[1]

$$H_{bath} = \int_{-\infty}^{\infty} d\omega\, \omega a_0^\dagger(\omega) a_0(\omega), \tag{A.2}$$

1. setting (here and in the rest of the section) $\hbar = 1$ for simplicity

and in a RWA we assume the coupling to the system to be described by

$$H_{int} = \int_{-\infty}^{\infty} d\omega\, k(\omega) [s a_0^\dagger(\omega) + s^\dagger a_0(\omega)] \tag{A.3}$$

with a frequency dependent coupling constant $k(\omega)$. The system operator s we often call *jump operator*. Note that both operators s and $a(t)$ have a dimension[2] $[s] = [a(t)] = \sqrt{Hz}$. Typically, the system will evolve on a time scale $1/\omega_0$ set by the large optical frequency ω_0 (e. g., the cavity resonance frequency), which we eliminate by moving to the corresponding rotating frame; This amounts to the replacement $s \rightarrow s\, e^{-i\omega_0 t}$. Similarly, we move into an interaction picture with the free bath Hamiltonian H_{bath} generated by the unitary[3]

2. Using the conventions of this section a leaky cavity is, e. g., described by $s = \sqrt{\kappa} c_c$

$$\Theta(t) = \exp(-i H_{bath} t), \tag{A.4}$$

and thus substitute $a_0(\omega) \rightarrow a_0(\omega)\, e^{-i\omega t}$. In a Markov approximation which consists of taking the limit of a flat coupling, i. e., $k(\omega) \equiv 1$, we can then write

3. Note that $\Theta(t)$ forms a unitary one-parameter group, i. e., $\Theta^\dagger(t)\Theta(t) = \mathbb{1}$ and $\Theta(t + t') = \Theta(t)\Theta(t')$.

$$H_{int} = s a_{in}^\dagger(t) + s^\dagger a_{in}(t) \tag{A.5}$$

where we introduced the field operators

$$a_{in}(t) = \frac{1}{\sqrt{2\pi}} \int_{-\infty}^{\infty} d\omega\, a_0(\omega)\, e^{-i(\omega-\omega_0)t}. \tag{A.6}$$

Due to the Markov approximation they obey the singular commutation relation

$$[a_{\mathrm{in}}(t), a_{\mathrm{in}}^{\dagger}(t')] = \delta(t - t'). \tag{A.7}$$

The system dynamics are then typically described in terms of QLEs in the Stratonovich form for an arbitrary system operator X

$$(\mathbf{S}) \quad \dot{X} = -\mathrm{i}[X, H_{\mathrm{sys}}] - \frac{1}{2}([X, s^{\dagger}]s - s^{\dagger}[X, s])$$
$$- [X, s^{\dagger}]a_{\mathrm{in}}(t) + [X, s]a_{\mathrm{in}}^{\dagger}(t) \tag{A.8}$$

The field operator a_{in} acts as a driving term for the equations of motion of the system S and thus be regarded as an input channel. Note that a_{in} is defined in terms of Schrödinger bath operators at the initial time. Its time argument thus does not denote a time dependence in the sense of the Heisenberg picture, but should rather be interpreted as the time the initial input interacts with the system. Depending on the state of the bath at this initial time, this input can either be a noise term (e. g., for a thermal state of the bath), a classical drive (for a coherent state), or something more general such as a single-photon input. In order to interpret a_{in} as quantum white-noise, we need to assume it to be δ-correlated, e. g.,

$$\langle a_{\mathrm{in}}^{\dagger}(t) a_{\mathrm{in}}(t') \rangle := \mathrm{tr}(a_{\mathrm{in}}^{\dagger}(t) a_{\mathrm{in}}(t') \sigma_0) = N\delta(t - t'), \tag{A.9a}$$

$$\langle a_{\mathrm{in}}(t) a_{\mathrm{in}}^{\dagger}(t') \rangle := \mathrm{tr}(a_{\mathrm{in}}(t) a_{\mathrm{in}}^{\dagger}(t') \sigma_0) = (N + 1)\delta(t - t'), \tag{A.9b}$$

where σ_0 is the initial state of the system + bath (here in a thermal state with mean occupation number N). This does not correspond to a thermal state where the photon number follows the Bose–Einstein distribution $n_{\mathrm{B}}(\omega)$, but rather an ensemble with a constant number of photons per unit bandwidth. In this sense quantum white-noise is an approximation that is valid in a certain (small) bandwith only. In principle quantum stochastic differential equation (QSDE) in Stratonovich form can also be formulated for non-white noise terms, as is the case for mechanical oscillators (see section 1.3.1).

Similar to the input field a_{in} we can define the output field a_{out} of the system S, which is related to the input field via the *input–output* relations [GC85]

$$a_{\mathrm{out}}(t) = s(t) + a_{\mathrm{in}}(t). \tag{A.10}$$

Note that $s(t)$ denotes the Heisenberg operator given by the corresponding QLE, see appendix A.3. The outgoing field at time t thus consists of a reflected part of the input field and a contribution from the internal system modes (which in turn contain contributions from the input field at earlier times).

In the white-noise limit of the Markov approximation (including an appropriate state of the bath) and in the interaction picture introduced above, one can develop a non-commutative quantum analogue of the classical stochastic Itō-calculus to describe the joint unitary evolution of the system S and the white-noise field A [HP84]. This leads to the so-called *Hudson–Parthasarathy equation*, an Itō QSDE for the evolution operator U given by

$$dU(t) = \left[-i \left(H_{\text{sys}} - i\frac{1}{2}s^\dagger s \right) dt + s\, dA^\dagger(t) - s^\dagger\, dA(t) \right] U(t) \quad \text{(A.11)}$$

with the initial condition $U(0) = \mathbb{1}$. Here we introduced the *quantum Wiener process $A(t)$* (analogue to a classical complex Wiener process) and its (forward-pointing) Itō-increments

quantum Wiener process

$$dA(t) = A(t + dt) - A(t), \quad \text{(A.12a)}$$
$$dA^\dagger(t) = A^\dagger(t + dt) - A^\dagger(t). \quad \text{(A.12b)}$$

Formally the quantum Wiener process (A.12) is related to the field operators from the previous section by

$$A(t) = \int_0^t ds\, a_{\text{in}}(s), \qquad A^\dagger(t) = \int_0^t ds\, a_{\text{in}}^\dagger(s). \quad \text{(A.13)}$$

For the electromagnetic field initially in the vacuum state the Itō-increments obey the following multiplication rules:

Itō-calculus

$$
\begin{array}{c|ccc}
\times & dA & dA^\dagger & dt \\
\hline
dA & 0 & dt & 0 \\
dA^\dagger & 0 & 0 & 0 \\
dt & 0 & 0 & 0
\end{array}
\quad \text{(A.14)}
$$

More generally two quantum stochastic processes $X(t), Y(t)$ obey the Itō product rule

$$d[X(t)Y(t)] = [dX(t)]Y(t) + X(t)\, dY(t) + dX(t)\, dY(t), \quad \text{(A.15)}$$

again with $dX(t) := X(t + dt) - X(t)$, etc. The standard chain rule is modified in a similar way: For a differentiable function f, we have

$$df(X(t)) = f'(X(t))\, dX(t) + \frac{1}{2}f''(X(t))\, dX(t)^2, \quad \text{(A.16)}$$

which in particular leads to

$$f(X(t+dt)) = f(X(t)) + f'(X(t))\, dX(t) + \tfrac{1}{2}f''(X(t))\, dX(t)^2. \quad \text{(A.17)}$$

Due to the forward-pointing definition of the Itō-increments (non-anticipating) functions such as X commute with the increments at equal times, i.e.,

$$[X(t), dA(t)] = [X(t), dA^\dagger(t)] = 0. \quad \text{(A.18)}$$

effective Hamiltonian   In particular this property also holds for the evolution operator U. It will be convenient to introduce the non-Hermitian, effective Hamiltonian

$$H_{\text{eff}} = H_{\text{sys}} - \text{i}\frac{1}{2}s^\dagger s, \tag{A.19}$$

which contains the so-called Itō-correction $-\text{i}s^\dagger s/2$ (compare this to appendix A.6).

unitarity of U   Using Itō-calculus one can show that $\text{d}[U(t)U^\dagger(t)] = \text{d}[U^\dagger(t)U(t)] = 0$, i.e., $U(t)$ is unitary for all t as expected for the solution of a Schrödinger equation. $U(t)$ does not form a group, however, but *cocycle property*   rather fulfils the *cocycle* property [Bar06]

$$U(t + t') = \Theta^\dagger(t')U(t)\Theta(t')U(t') \qquad \forall t, t' > 0 \tag{A.20}$$

with respect to the free evolution of the electromagnetic bath Θ. Moving out of the interaction picture we can define

$$V(t) = \begin{cases} \Theta(t)U(t) & t \geq 0 \\ U^\dagger(|t|)\Theta(t) & t \leq 0 \end{cases}, \tag{A.21}$$

which form a unitary group, and thus $V^\dagger(t) = V(-t)$ and $V(t + t') = V(t)V(t')$, etc.

A.3   HEISENBERG–LANGEVIN EQUATIONS

For a given QSDE defining U, the Heisenberg equations of motion of an arbitrary system operator X can be found by applying the formalism introduced above. We first transform to the Heisenberg picture using the map (also called quantum flow)

$$j_t(X) = U^\dagger(t)(X \otimes \mathbb{1}_{\text{field}})U(t), \tag{A.22}$$

and then use Itō-calculus to deduce the equation for $\text{d}j_t(X)$. For a vacuum field we find (introducing $\bar{X} = X \otimes \mathbb{1}_{\text{field}}$ for notational convenience)

$$\begin{aligned} \text{d}j_t(X) &= \text{d}U^\dagger(t)\bar{X}U(t) + U^\dagger(t)\bar{X}\,\text{d}U(t) + \text{d}U^\dagger(t)\bar{X}\,\text{d}U(t) \\ &= \text{i}U^\dagger(t)(H_{\text{eff}}^\dagger\bar{X} - \bar{X}H_{\text{eff}})U(t)\,\text{d}t \\ &\quad + U^\dagger(t)\bar{X}[s\,\text{d}A^\dagger(t) - s^\dagger\,\text{d}A(t)]U(t) \\ &\quad + U^\dagger(t)[s^\dagger\,\text{d}A(t) - s\,\text{d}A^\dagger(t)]\bar{X}U(t) \\ &\quad + U^\dagger(t)[s^\dagger\,\text{d}A(t) - s\,\text{d}A^\dagger(t)]\bar{X}[s\,\text{d}A^\dagger(t) - s^\dagger\,\text{d}A(t)]U(t) \\ &= U^\dagger(t)[\text{i}H_{\text{eff}}^\dagger\bar{X} - \text{i}\bar{X}H_{\text{eff}} + s^\dagger\bar{X}s]U(t)\,\text{d}t \\ &\quad + U^\dagger(t)[\bar{X}, s\,\text{d}A^\dagger(t)]U(t) - U^\dagger(t)[s^\dagger\,\text{d}A(t), \bar{X}]U(t) \\ &= U^\dagger(t)\left\{\text{i}[H, \bar{X}] + [s^\dagger\bar{X}s - \tfrac{1}{2}(s^\dagger s\bar{X} + \bar{X}s^\dagger s)]\right\}U(t)\,\text{d}t \\ &\quad + U^\dagger(t)[\bar{X}, s]U(t)\,\text{d}A^\dagger(t) - U^\dagger(t)[s^\dagger, \bar{X}]U(t)\,\text{d}A(t). \end{aligned}$$

We thus obtain the Itō QLE [Bar06]

$$dj_t(X) = j_t(\mathcal{L}^\dagger X)\,dt + j_t([X,s])\,dA^\dagger(t) + j_t([s^\dagger, X])\,dA(t), \quad (A.23)$$

where $\mathcal{L}^\dagger$ is the adjoint of the Liouvillian introduced in (A.31) given by

$$\mathcal{L}^\dagger X = -i[X, H_{sys}] + \mathcal{D}^\dagger[s]X, \quad (A.24a)$$

$$\mathcal{D}^\dagger[s]X = s^\dagger X s - \tfrac{1}{2}(s^\dagger s X + X s^\dagger s). \quad (A.24b)$$

Following the usual notation used in quantum optics we often denote the Heisenberg-picture operators by $X(t) := j_t(X)$.

The evolution of the output field is obtained in a similar way. We define $A_{out}(t)$ by moving to the Heisenberg picture, i.e.,

$$A_{out}(t) = U^\dagger(t)[\mathbb{1}_{sys} \otimes A(t)]U(t). \quad (A.25)$$

We can easily obtain the corresponding QSDE [Bar86]

$$dA_{out}(t) = j_t(s)\,dt + dA(t), \quad (A.26)$$

which corresponds to the input–output relations (A.10).

A.4 STOCHASTIC EVOLUTION OF THE QUANTUM STATE

The time-evolution of the state vector $|\Psi\rangle$ (describing system + field) is just given by $|\Psi(t)\rangle = U(t)|\Psi_0\rangle$ with an initial state $|\Psi_0\rangle = |\psi_0\rangle \otimes |vac\rangle$. The vacuum state $|vac\rangle$ of the field obeys[4] $dA(t)|vac\rangle = 0$. As we have established that $[U(t), dA(t)] = 0$ we can write the resulting equation in the form

4. In the same way we have $a_{in}(t)|vac\rangle = a_0(\omega)|vac\rangle = 0$.

$$d|\Psi(t)\rangle = \left[-iH_{eff}\,dt + s\,dA^\dagger(t) \right]|\Psi(t)\rangle. \quad (A.27)$$

If we define the stochastic density operator $\sigma(t) = |\Psi(t)\rangle\langle\Psi(t)|$ we readily find the generalisation of the von-Neuman equation [GZ04, p 349]

$$d\sigma(t) = -i[H_{eff}\sigma(t) - \sigma(t)H_{eff}^\dagger]\,dt$$
$$+ dA^\dagger(t)s\sigma(t)s^\dagger\,dA(t) + dA^\dagger(t)s\sigma(t) + \sigma(t)\,dA(t)s^\dagger. \quad (A.28)$$

A.5 MASTER EQUATION

If we are exclusively interested in the evolution of the system we can trace-out the bath variables and define the system state by

$$\rho(t) = tr_{field}\big(U(t)\rho_0 \otimes |vac\rangle\langle vac|U^\dagger(t)\big). \quad (A.29)$$

We then find (by evaluating $d\rho$ in Itō-calculus and dividing by dt afterwards)

$$\dot{\rho}(t) = \mathcal{L}\rho(t) := -i[H_{eff}\rho(t) - \rho(t)H_{eff}^\dagger] + s\rho(t)s^\dagger, \quad (A.30)$$

which shows a clear similarity to (A.28). The Liouvillian $\mathcal{L}$ in its expanded form reads

$$\mathcal{L}\rho = -\mathrm{i}[H_{\mathrm{sys}}, \rho] + \mathcal{D}[s]\rho, \tag{A.31a}$$

$$\mathcal{D}[s]\rho = s\rho s^\dagger - \tfrac{1}{2}(s^\dagger s\rho + \rho s^\dagger s). \tag{A.31b}$$

Note that we have the identity[5]

$$\mathrm{tr}(X\mathcal{L}\rho) = \mathrm{tr}(\rho\mathcal{L}^\dagger X) \tag{A.32}$$

with the adjoint Liouvillian $\mathcal{L}^\dagger$ defined in (A.24).

A.6 STOCHASTIC EQUATIONS IN STRATONOVICH FORM

To convert between the Itō and Stratonovich formulation of quantum-stochastic processes we can for *linear* equations use the following approach [GZ04, p 346f]. Consider the Stratonovich stochastic differential equation

$$(\mathbf{S}) \qquad \mathrm{d}X(t) = [\mathcal{A}\,\mathrm{d}t + \mathcal{B}\,\mathrm{d}A(t) + \mathcal{C}\,\mathrm{d}A^\dagger(t)]X(t), \tag{A.33}$$

with linear operators $\mathcal{A}$, $\mathcal{B}$, $\mathcal{C}$ and a given initial condition $X(0)$. This equation has the formal solution

$$X(t) = \mathcal{T}_+ \exp\left\{\int_0^t [\mathcal{A}\,\mathrm{d}t + \mathcal{B}\,\mathrm{d}A(t) + \mathcal{C}\,\mathrm{d}A^\dagger(t)]\right\} X(0), \tag{A.34}$$

where $\mathcal{T}_+$ denotes the time-ordered product. We can now calculate the Itō increment $\mathrm{d}X(t) = X(t + \mathrm{d}t) - X(t)$ by using the rules of Itō-calculus outlined in the previous section and find

$$
\begin{aligned}
\mathrm{d}X(t) &= \left\{\exp[\mathcal{A}\,\mathrm{d}t + \mathcal{B}\,\mathrm{d}A(t) + \mathcal{C}\,\mathrm{d}A^\dagger(t)] - 1\right\} X(t) \\
&= \left\{[\mathcal{A} + \tfrac{1}{2}\mathcal{B}\mathcal{C}]\,\mathrm{d}t + \mathcal{B}\,\mathrm{d}A(t) + \mathcal{C}\,\mathrm{d}A^\dagger(t)\right\} X(t),
\end{aligned}
\tag{A.35}
$$

where we assumed the field to be in vacuum and thus $\mathrm{d}A\,\mathrm{d}A^\dagger = \mathrm{d}t$ to be the only non-vanishing quadratic term. Applying this to the Hudson–Parthasarathy equation (A.11) we find the corresponding Stratonovich equation to be

$$(\mathbf{S}) \qquad \mathrm{d}U(t) = \left[-\mathrm{i}H_{\mathrm{sys}}\,\mathrm{d}t + s\,\mathrm{d}A^\dagger(t) - s^\dagger\,\mathrm{d}A(t)\right] U(t). \tag{A.36}$$

Using eq. (A.34) this has the formal solution

$$U(t) = \mathcal{T}_+ \exp\left\{\int_0^t [-\mathrm{i}H_{\mathrm{sys}}\,\mathrm{d}t + s\,\mathrm{d}A^\dagger(t) - s^\dagger\,\mathrm{d}A(t)]\right\} \mathbb{1}. \tag{A.37}$$

As it is conventional in quantum optics, in this thesis stochastic differential equations started by a fluxion of the form $\dot{X}$ are written in Stratonovich form without explicit denotation by ($\mathbf{S}$). Equations starting with an increment $\mathrm{d}X$ are to be read as of Itō-type, if not stated otherwise.

A.7 NON-VACUUM FIELD STATES

For a general (squeezed) Gaussian initial state of the electromagnetic field the field operators obey the correlation function

$$\langle a_{\mathrm{in}}^\dagger(t) a_{\mathrm{in}}(t') \rangle_{(N,M)} = N \delta(t - t'), \tag{A.38a}$$

$$\langle a_{\mathrm{in}}(t) a_{\mathrm{in}}(t') \rangle_{(N,M)} = M \delta(t - t'), \tag{A.38b}$$

with parameters $M \in \mathbb{C}$, $N \geq 0$, and $|M|^2 \leq N(N+1)$, where equality is attained for a pure state. The vacuum multiplication table (A.14) is thus modified to

$$
\begin{array}{c|ccc}
\times & \mathrm{d}A & \mathrm{d}A^\dagger & \mathrm{d}t \\
\hline
\mathrm{d}A & M\,\mathrm{d}t & (N+1)\,\mathrm{d}t & 0 \\
\mathrm{d}A^\dagger & N\,\mathrm{d}t & M^*\,\mathrm{d}t & 0 \\
\mathrm{d}t & 0 & 0 & 0
\end{array}
\tag{A.39}
$$

Note that while the Stratonovich form of the corresponding QSDEs does not change, the Itō-form has to be modified accordingly [Bar86]. We find instead of (A.11) [GZ04, p 350f]

$$\mathrm{d}U(t) = -\mathrm{i}H_{\mathrm{sys}}U(t)\,\mathrm{d}t$$
$$- \frac{1}{2}\left[ss^\dagger N + s^\dagger s(N+1) - ssM^* - s^\dagger s^\dagger M \right] U(t)\,\mathrm{d}t$$
$$+ \left[s\,\mathrm{d}A^\dagger(t) - s^\dagger\,\mathrm{d}A(t) \right] U(t). \tag{A.40}$$

Similar modification are found for the corresponding Langevin and master equation.

In this section we briefly review the most important results from the theory of quantum filtering and (linear–quadratic–Gaussian) control. Quantum filtering—the extraction of information about the quantum state from noisy measurements—was developed in the mathematical physics community [Bel80; Bel92] and later in the context of quantum optics [Car93b].

B.1 THE BELAVKIN EQUATION

B.1.1 *Quantum Optical Derivation*

Here we discuss a derivation of the stochastic Schrödinger equation and the corresponding stochastic master equation for homodyne detection from a quantum-optics perspective (see [Car93b] and [GZ04] for a in-depth discussion). We consider the situation depicted in fig. 43, where a system S couples to the one-dimensional electromagnetic field A, which is initially in vacuum and is subject to homodyne detection. Homodyne detection is realized by a strong local oscillator (LO) which is mixed with the field A on a (balanced) beam splitter and subsequent detection by photo detectors. We first assume unit detection efficiency, but will discuss the case of inefficient detection at the end of the section.

We start from the Schrödinger equation (A.27) which describes the full system $(S + A)$ and we assume an initial state $|\Psi_0\rangle = |\psi_0\rangle_S \otimes |vac\rangle_A$. Equation (A.27) can then be written in the form

$$d|\Psi(t)\rangle = \left\{ -iH_{\text{eff}}\, dt + s\left[dA^\dagger(t) + dA(t)\right] \right\} |\Psi(t)\rangle, \quad (B.1)$$

where we used the fact that $dA(t)|\Psi(t)\rangle = dA(t)|\Psi_0\rangle = dA(t)|vac\rangle = 0$ [GZ04, p 375]. A homodyne measurement of an electromagnetic quadrature $x = a + a^\dagger$ with a result $I_x \in \mathbb{R}$ effectively projects the state of the light field onto the eigenstate $|I_x\rangle_A$ of x, where $x|I_x\rangle_A = I_x|I_x\rangle_A$. Projecting (B.1) onto $|I_x\rangle$ results in [GG94]

$$\langle I_x|\Psi(t + dt)\rangle \otimes |I_x\rangle = [\mathbb{1} - iH_{\text{eff}}\, dt + s\, I_x\, dt] \langle I_x|\Psi(t)\rangle \otimes |I_x\rangle.$$

Defining $|\tilde{\psi}_c(t + dt)\rangle := \langle I_x|\Psi(t + dt)\rangle$ as the state *after the measuremet* and factoring off the bath state thus leads to the linear stochastic Schrödinger equation [Car93b]

$$d|\tilde{\psi}_c(t)\rangle = [-iH_{\text{eff}}\, dt + s\, I_x(t)\, dt] |\psi_c(t)\rangle, \quad (B.2)$$
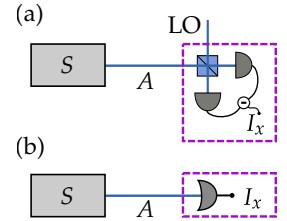

FIG 43. (a) Physical realisation of homodyne detection and (b) its equivalent depiction as it is used throughout the thesis.

linear stochastic Schrödinger equation

with the forward pointing Itō-increment $d|\tilde{\psi}_c(t)\rangle = |\tilde{\psi}_c(t+dt)\rangle - |\psi_c(t)\rangle$. $|\tilde{\psi}_c\rangle$ is the unnormalised system state which is conditioned on the homodyne photo-current I_x, which is a Gaussian random variable with a probability distribution $Y_t(I_x) = |\langle I_x|\Psi(t+dt)\rangle|^2$. One obtains [BP96; GG94; WM09]

$$Y_t(I_x)\,dI_x = \sqrt{\frac{dt}{2\pi}}\exp\left(-\frac{dt}{2}[I_x - \langle s+s^\dagger\rangle_c]^2\right)dI_x, \tag{B.3}$$

where the conditional expectation value is defined with respect to the normalised conditional state, i.e., $\langle s\rangle_c = \langle\psi_c(t)|s|\psi_c(t)\rangle$. Using this, I_x can be written as

$$I_x\,dt = \langle s+s^\dagger\rangle_c\,dt + dW, \tag{B.4}$$

where W is a classical Wiener process with $dW(t)^2 = dt$ and zero mean. We can introduce the classical stochastic process $\tilde{X}$ defined by $d\tilde{X}(t) = I_x(t)\,dt$, which is statistically equivalent to $dX(t) = dA_{\mathrm{out}}(t) + dA_{\mathrm{out}}^\dagger(t)$.[1] This is due to non-demolition properties of the measurement operator, see appendix B.1.2 and [BVJ07]. It obeys $d\tilde{X}(t)^2 = dt$.

From the stochastic Schrödinger equation (B.2) we can obtain a stochastic master equation for the conditional density operator in the following way. We first find the equation of motion for the unnormalized conditional state $\tilde{\rho}_c = |\tilde{\psi}_c\rangle\langle\tilde{\psi}_c|$ by multiplying out (B.2). We obtain

$$\begin{aligned}
d\tilde{\rho}_c(t) &= \tilde{\rho}_c(t+dt) - \rho_c(t)\\
&= |\psi_c(t)\rangle\,[d\langle\tilde{\psi}_c(t)|] + [d|\tilde{\psi}_c(t)\rangle]\,\langle\psi_c(t)| + [d|\tilde{\psi}_c(t)\rangle]\,[d\langle\tilde{\psi}_c(t)|]\\
&= \mathcal{L}\rho_c(t)\,dt + \left[s\rho_c(t) + \rho_c(t)s^\dagger\right]d\tilde{X}(t).
\end{aligned} \tag{B.5}$$

Equation (B.5) is the quantum analog to the classical Zakai equation [Xio08]. Note that although the Liouvillian is trace-preserving [i.e., $\mathrm{tr}(\mathcal{L}\rho) = 0$], the second term in (B.5) does not possess this property. The equation for the normalized state $\rho_c(t) = \tilde{\rho}_c(t)/\mathrm{tr}(\tilde{\rho}_c(t))$ is then found by noting that

$$\begin{aligned}
\mathrm{tr}(\tilde{\rho}_c(t+dt)) &= \mathrm{tr}(\rho_c(t) + d\tilde{\rho}_c(t))\\
&= 1 + \langle s+s^\dagger\rangle_c\,d\tilde{X} - i\langle H_{\mathrm{eff}} - H_{\mathrm{eff}}^\dagger\rangle_c\,dt + \langle ss^\dagger\rangle_c\,dt \quad \text{(B.6)}\\
&= 1 + \langle s+s^\dagger\rangle_c\,d\tilde{X},
\end{aligned}$$

where now $\langle A\rangle_c = \mathrm{tr}(\rho_c(t)A)$ and we used $\mathrm{tr}(\rho_c(t)) = 1$. Thus we find

$$\mathrm{tr}(\tilde{\rho}_c(t+dt))^{-1} = 1 - \langle s+s^\dagger\rangle_c\,d\tilde{X} + \langle s+s^\dagger\rangle_c^2\,dt, \tag{B.7}$$

---

1. Typically one does not distinguish between dX and $d\tilde{X}$ and just defines $dX = I_x\,dt$.

which is obtained by expanding $\text{tr}(\tilde{\rho}_c(t + dt))^{-1}$ to *second order* in $d\widetilde{X}$ (leading to a first-order expansion in dt). Using Itō multiplication rules this leads to

$$d\rho_c(t) = \frac{\tilde{\rho}_c(t + dt)}{\text{tr}(\tilde{\rho}_c(t + dt))} - \rho_c(t)$$
$$= \mathcal{L}\rho_c(t)\,dt + \mathcal{H}[s]\rho_c(t)\,dW(t), \qquad (B.8)$$

which is the desired result (see [GZ04, p 375] and [WM09, p 161]). The (nonlinear) measurement term is given by

$$\mathcal{H}[s]\rho_c = [s - \text{tr}(\rho_c s)]\rho_c + \rho_c[s - \text{tr}(\rho_c s)]^\dagger. \qquad (B.9)$$

It is clear from the derivation that under made assumptions the SSE (B.2) is equivalent to the SME (B.8). The stochastic master equation is more general, however, as it can accommodate for additional, unobserved decay channels (such as photon losses/inefficient detection or coupling of a mechanical oscillator to a heat bath), as well as for mixed initial states.

We can generalize the homodyne master equation in several ways: Above we assumed a measurement of a specific light quadrature $x = a + a^\dagger$. To measure a rotated quadrature $x^\phi = a\,e^{-i\phi} + a^\dagger e^{+i\phi}$ we have to make the replacement $s \to e^{i\phi} s$, which simply follows from replacing $a \to e^{-i\phi} a$. We can as easily obtain the SME corresponding to heterodyne detection at a LO frequency $\omega_{\text{lo}} \neq \omega_0$ by substituting $s \to e^{i\Delta_{\text{lo}}t} s$, where $\Delta_{\text{lo}} = \omega_{\text{lo}} - \omega_0$. Below we will discuss the situation where we split up the field with a beam-splitter (with a splitting ration $\eta : 1 - \eta, 0 \leq \eta \leq 1$) and perform two simultaneous homodyne measurements on its outputs. The measured modes A', B after the beam-splitter (see fig. 44) are related to A before the beam-splitter via [GJ09] $a(t) = \sqrt{\eta}\,a'(t) + \sqrt{1 - \eta}\,b(t)$, where A' and B are both initially in vacuum and are uncorrelated such that $dA(t)\,dB^\dagger(t) = 0$, etc. Plugging this relation into (B.1) and projecting onto the quadratures $e^{-i\phi_1} a' + e^{i\phi_1} a'^\dagger$, $e^{-i\phi_2} b + e^{i\phi_2} b^\dagger$ one can repeat above steps and find

$$d\rho_c = \mathcal{L}\rho_c\,dt + \sqrt{\eta}\,\mathcal{H}[e^{i\phi_1} s]\rho_c\,dW_1$$
$$+ \sqrt{1 - \eta}\,\mathcal{H}[e^{i\phi_2} s]\rho_c\,dW_2, \quad (B.10)$$

FIG 44. Dual homodyne detection

with uncorrelated Wiener processes W_i, i.e., $dW_i\,dW_j = \delta_{ij}\,dt$. To model photon losses or inefficient photo-detectors, we average over, say, the second measurement process, and thus discard all information obtained from it. Due to the fact that W_2 is a Wiener process and thus has zero mean, the equation of motion for the resulting conditional state—which is now conditioned on the measurement results of the first channel only—is obtained by averaging, and thus dropping, the last term in (B.10). The beam-splitter transmissivity is then identified with the efficiency of the photo-detection. Formally we can
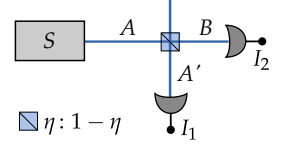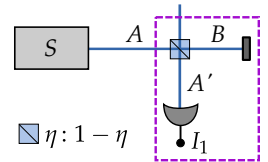

FIG 45. Effective description of inefficient homodyne detection

obtain the same result from (B.8) by replacing $s \to \sqrt{\eta} s$ in the measurement term, while keeping the Liouvillian unchanged. The general SME for heterodyne detection at a LO frequency $\omega_{\mathrm{lo}} = \omega_0 + \Delta_{\mathrm{lo}}$, at a phase ϕ, and with a detection efficiency η thus is

$$d\rho_c = \mathcal{L}\rho_c \, dt + \sqrt{\eta} \, \mathcal{H}[e^{i(\Delta_{\mathrm{lo}}t + \phi)} s]\rho_c \, dW. \tag{B.11}$$

Often we will be faced with the situation where the LO detuning is large on the typical frequencies of the system. In this case, a time coarse-grained description of the heterodyne measurement is appropriate [WM09, p 166f]. To this end we choose a time interval δt which is large compared to $\Delta_{\mathrm{lo}}^{-1}$ but short on all system timescales, and define the time-averaged density matrix $\bar{\rho}$ by

$$\int_t^{t+\delta t} d\rho = \rho(t + \delta t) - \rho(t) =: d\bar{\rho}(t). \tag{B.12}$$

At the same time we have to assume that $\rho(t)$ is slowly varying on the timescale δt and we can consequently make the approximation

$$\int_t^{t+\delta t} d\tau \rho(\tau) \approx \rho(t)\delta t =: \bar{\rho}(t) \, dt. \tag{B.13}$$

This leads us to define the Fourier cosine and sine components of the Wiener process $W(t)$ by

$$\sqrt{2} \int_t^{t+\delta t} dW(\tau) \, e^{-i\Delta_{\mathrm{lo}}\tau} =: dW_{\mathrm{c}} + i \, dW_{\mathrm{s}}, \tag{B.14}$$

where dW_{s} and dW_{s} are both real. Calculating their variances we find

$$dW_{\mathrm{c}}(t)^2 = 2 \int_t^{t+\delta t} \int_t^{t+\delta t} dW(\tau) \, dW(\tau') \cos(\Delta_{\mathrm{lo}}\tau) \cos(\Delta_{\mathrm{lo}}\tau')$$
$$= \int_t^{t+\delta t} dW(\tau)[1 + \cos(2\Delta_{\mathrm{lo}}\tau)] = [1 + \mathcal{O}(\Delta_{\mathrm{lo}}\delta t)^{-1}]\delta t,$$

and in a similar way $dW_{\mathrm{s}}(t)^2 = [1 + \mathcal{O}(\Delta_{\mathrm{lo}}\delta t)^{-1}]\delta t$. For the cross-correlations we have

$$dW_{\mathrm{s}}(t) \, dW_{\mathrm{c}}(t) = 2 \int_t^{t+\delta t} \int_t^{t+\delta t} dW(\tau) \, dW(\tau') \cos(\Delta_{\mathrm{lo}}\tau) \sin(\Delta_{\mathrm{lo}}\tau')$$
$$= \int_t^{t+\delta t} dW(\tau) \sin(2\Delta_{\mathrm{lo}}\tau) = \mathcal{O}(\Delta_{\mathrm{lo}}\delta t)^{-1}\delta t.$$

We thus see that W_{c}, W_{s} are Wiener processes which are (approximately) uncorrelated. On timescales much longer than δt we can make the replacement $\delta t \to dt$ and can thus use the Itō table

$$dW_{\mathrm{c}}^2 = dW_{\mathrm{s}}^2 = dt, \tag{B.15a}$$
$$dW_{\mathrm{c}} \, dW_{\mathrm{s}} = 0. \tag{B.15b}$$

We therefore find an effective stochastic master equation for heterodyne detection, reading

$$\mathrm{d}\bar{\rho}_c = \mathcal{L}\bar{\rho}_c\,\mathrm{d}t + \sqrt{\frac{\eta}{2}}\,\mathcal{H}[\mathrm{e}^{\mathrm{i}\phi}\,s]\bar{\rho}_c\,\mathrm{d}W_c + \sqrt{\frac{\eta}{2}}\,\mathcal{H}[-\mathrm{i}\,\mathrm{e}^{\mathrm{i}\phi}\,s]\bar{\rho}_c\,\mathrm{d}W_s. \quad \text{(B.16)}$$

We thus see that in this limit a heterodyne measurement is equivalent to simultaneous homodyne measurements of two conjugate quadratures, each with half efficiency (as is depicted in fig. 44).

More generally we can describe an open quantum system coupling to m vacuum field channels, $m' \leq m$ of which are subject to homodyne detection, by the equation

$$\mathrm{d}\rho_c = -\mathrm{i}[H,\rho_c]\,\mathrm{d}t + \sum_{i=1}^{m}\mathcal{D}[s_i]\rho_c\,\mathrm{d}t + \sum_{i=1}^{m'}\mathcal{H}[s_i]\rho_c\,\mathrm{d}W_i. \quad \text{(B.17)}$$

The case $m' < m$ can be used to describe inefficient photo-detection, as we just demonstrated in the discussion above, or decoherence channels which cannot be observed at all, e. g., phonon losses of a mechanical oscillator. Equations of this form are often called Belavkin equations [Bel92].

B.1.2 *Derivation by Nonlinear Filtering*

In this section we derive the stochastic master equation for homodyne detection from the perspective of classical nonlinear filtering. In our derivation we will follow the technique laid out in [GK10]. First we briefly review the most important properties of the conditional expectation value (see, e. g., [BVJ07]). In the following we denote by $\mathbb{E}[A]$ the expectation value of a random variable A with respect to some probability space. For a quantum observable A and a quantum state ρ we identify $\mathbb{E}[A] = \mathrm{tr}(A\rho)$. The following construction works independently of this specific choice, however.

Conditional Expectation Value

Let $\mathcal{A}$ be a (von-Neumann) algebra of operators and $\mathcal{A}' = \{B : [B, A] = 0, \forall A \in \mathcal{A}\}$ its *commutant*. We then call the map $\mathbb{E}[\cdot|\mathcal{A}] :$ *commutant* $\mathcal{A}' \to \mathcal{A}$ the *conditional expectation* from $\mathcal{A}$ onto $\mathcal{A}'$ if

$$\mathbb{E}[\mathbb{E}[B|\mathcal{A}]g(A)] = \mathbb{E}[Bg(A)] \quad \text{(B.18)}$$

for all $A \in \mathcal{A}$, $B \in \mathcal{A}'$ and some measureable function g (in particular $g = \mathrm{id}$ and $g(A) \equiv 1$). The conditional expectation has the following useful properties:

$$\mathbb{E}[B|\mathcal{A}] = B \text{ for all } B \in \mathcal{A} \quad \text{(B.19a)}$$

$$\mathbb{E}[\mathbb{E}[B|\mathcal{A}]|\mathcal{C}] = \mathbb{E}[B|\mathcal{C}] \text{ for } \mathcal{C} \subset \mathcal{A} \quad \text{(B.19b)}$$

$$\mathbb{E}[AB|\mathcal{C}] = A\,\mathbb{E}[B|\mathcal{C}] \text{ for } A \in \mathcal{C} \quad \text{(B.19c)}$$

The expectation $\mathbb{E}$ defines a scalar product $\langle A, B \rangle_{\mathbb{E}} := \mathbb{E}[A^{\dagger}B]$, which induces the norm $\|A\|_{\mathbb{E}} := \langle A, A \rangle_{\mathbb{E}}^{1/2}$. From the definition (B.18) then directly follows the orthogonality relation

$$\langle \mathbb{E}[B|A] - B, g(A) \rangle_{\mathbb{E}} = 0 \tag{B.20}$$

for all $A \in \mathcal{A}$, $B \in \mathcal{A}'$. The conditional expectation thus also satisfies the least-squares property [BVJ07]

$$\|B - \mathbb{E}[B|\mathcal{A}]\|_{\mathbb{E}} \leq \|B - A\|_{\mathbb{E}}. \tag{B.21}$$

This means that $\mathbb{E}[\cdot|\mathcal{A}]$ is the orthogonal projection from $\mathcal{A}'$ onto $\mathcal{A}$.

Characteristic Function Technique

Suppose we continuously monitor the output of a quantum system whose evolution is described by eq. (A.11) via homodyne detection, yielding a measurement of the field quadrature $Y(t) = A_{\text{out}}(t) + A_{\text{out}}^{\dagger}(t)$ [where A_{out} is defined in (A.25)]. We denote by $\mathcal{Y}_t = \{Y(t') : 0 \leq t' \leq t\}$ the algebra generated by the observation process Y and by $\mathcal{Y}_t'$ its commutant, $\mathcal{Y}_t' = \{A : [A, Y] = 0, \forall Y \in \mathcal{Y}_t\}$. For $0 \leq t' \leq t$ we then have the *non-demolition* property [BVJ07]

$$[j_t(X), Y(t')] = 0 \tag{B.22}$$

[such that $j_t(X) \in \mathcal{Y}_t$] and the *self non-demolition* property

$$[Y(t), Y(t')] = 0. \tag{B.23}$$

This allows us to map the quantum filtering problem to a classical filtering problem which we can tackle by methods from classical non-linear filtering theory.

We define the quantum state $\mathbb{E}[\cdot] = \text{tr}(\rho_0 \otimes \rho_{\text{vac}} \cdot)$ and seek to find an estimate[2] $\pi_t(X) \in \mathcal{Y}_t$ for the Heisenberg operator $X(t) = j_t(X)$ which minimizes the quadratic error $\mathbb{E}[(\pi_t(X) - j_t(X))^2]$ based on the observations $Y(t)$. As this requirement is equivalent to eq. (B.21) we directly find

2. π_t is often called the quantum filter

$$\pi_t(X) = \mathbb{E}[j_t(X)|\mathcal{Y}_t]. \tag{B.24}$$

We will now show how to calculate $\pi_t(X)$ explicitly using the characteristic function technique [GK10], for the case of a single vacuum input. Due to the orthogonality property (B.20) of the conditional expectation we have the identity $\mathbb{E}[(\pi_t(X) - j_t(X))C_t] = 0$ for all $C_t \in \mathcal{Y}_t$. We can thus make the following Ansatz

$$dC_t = g_t C_t \, dY(t), \tag{B.25a}$$

$$d\pi_t(X) = \alpha_t \, dt + \beta_t \, dY(t), \tag{B.25b}$$

for adapted stochastic processes α_t, $\beta_t \in \mathcal{Y}_t$. This implies $C_t, \pi_t(X) \in \mathcal{Y}_t$ [while on the other hand $j_t(X) \notin \mathcal{Y}_t$]. We can then use $d\mathbb{E}[(\pi_t(X) -$

$j_t(X))C_t] = 0$, which, due to Itō-rules consists of three terms. We find for the first term[3]

$$I = \mathbb{E}[(\mathrm{d}\pi_t(X) - \mathrm{d}j_t(X))C_t]$$
$$= \mathbb{E}[\alpha_t C_t]\,\mathrm{d}t + \mathbb{E}[\beta_t\,\mathrm{d}Y(t)C_t] - \mathbb{E}[\mathrm{d}j_t(X)C_t]$$
$$= \mathbb{E}[\alpha_t C_t]\,\mathrm{d}t + \mathbb{E}[\beta_t j_t(s + s^\dagger)C_t]\,\mathrm{d}t - \mathbb{E}[j_t(\mathcal{L}^* X)C_t]\,\mathrm{d}t$$
$$= \mathbb{E}[\alpha_t C_t]\,\mathrm{d}t + \mathbb{E}[\beta_t \pi_t(s + s^\dagger)C_t]\,\mathrm{d}t - \mathbb{E}[\pi_t(\mathcal{L}^* X)C_t]\,\mathrm{d}t,$$

where to go from the second to the third line we used (i) the fact that Y is generated by a Wiener process and therefore the increments $\mathrm{d}Y(t)$ are independent of $Y(t)$ at equal times, i.e., $\mathbb{E}[\mathrm{d}Y(t)f(Y(t))] = \mathbb{E}[\mathbb{E}[\mathrm{d}Y(t)]f(Y(t))]$ for a measureable function f, (ii) $\mathbb{E}[\mathrm{d}Y(t)] = \mathbb{E}[j_t(s + s^\dagger)]\,\mathrm{d}t$, and (iii) for the field initially in vacuum we have $\mathbb{E}[\mathrm{d}A(t)] = 0$ and $\mathbb{E}[\mathrm{d}A^\dagger(t)] = 0$. In particular this means that $\mathbb{E}[\beta_t\,\mathrm{d}A(t)C_t] = \mathbb{E}[\beta_t\,\mathrm{d}A^\dagger(t)C_t] = 0$. To go to the fourth line we used the orthogonality property, thus $\mathbb{E}[j_t(X)C_t] = \mathbb{E}[\pi_t(X)C_t]$. For the second term we find

$$II = \mathbb{E}[(\pi_t(X) - j_t(X))\,\mathrm{d}C_t]$$
$$= \mathbb{E}[(\pi_t(X) - j_t(X))g_t C_t j_t(s + s^\dagger)]\,\mathrm{d}t$$
$$= \mathbb{E}[\pi_t(X)\pi_t(s + s^\dagger)g_t C_t]\,\mathrm{d}t - \mathbb{E}[\pi_t(X(s + s^\dagger))g_t C_t]\,\mathrm{d}t$$

by the same reasoning as above. Going from the second to the third line we used (B.19c), which implies $\pi_t(\pi_t(X)j_t(s)) = \pi_t(X)\pi_t(s)$, and $j_t(XY) = j_t(X)j_t(Y)$. For the third term we obtain by using the Itō table (A.14)

$$III = \mathbb{E}[(\mathrm{d}\pi_t(X) - \mathrm{d}j_t(X))\,\mathrm{d}C_t]$$
$$= \mathbb{E}[(\beta_t(X)\,\mathrm{d}Y(t) - \mathrm{d}j_t(X))g_t C_t\,\mathrm{d}Y(t)]$$
$$= \mathbb{E}[\beta_t(X)g_t C_t]\,\mathrm{d}t - \mathbb{E}[j_t([s^\dagger, X])g_t C_t]\,\mathrm{d}t$$
$$= \mathbb{E}[\beta_t(X)g_t C_t]\,\mathrm{d}t - \mathbb{E}[\pi_t([s^\dagger, X])g_t C_t]\,\mathrm{d}t.$$

As g_t is an arbitrary function we can deduce from $I + II + III = 0$ by equating the coefficients of g_t and $g_t C_t$ that

$$0 = \alpha_t + \beta_t \pi_t(s + s^\dagger) - \pi_t(\mathcal{L}^* X),$$
$$0 = \pi_t(X)\pi_t(s + s^\dagger) - \pi_t(X(s + s^\dagger)) + \beta_t - \pi_t([s^\dagger, X])$$
$$= \pi_t(X)\pi_t(s + s^\dagger) - \pi_t(Xs + s^\dagger X) + \beta_t,$$

where both equalities hold almost surely with respect to $\mathbb{E}$. Solving this for α_t and β_t, and using the ansatz (B.25b) we find for the quantum filter

$$\mathrm{d}\pi_t(X) = \pi_t(\mathcal{L}^* X)\,\mathrm{d}t + [\pi_t(Xs + s^\dagger X) - \pi_t(X)\pi_t(s + s^\dagger)]\,\mathrm{d}W, \quad \text{(B.26)}$$

where

$$\mathrm{d}W(t) = \mathrm{d}Y(t) - \pi_t(s + s^\dagger)\,\mathrm{d}t \quad \text{(B.27)}$$

is the *innovations process*. $W(t)$ is a Wiener process with $\mathbb{E}[dW] = 0$, $dW^2 = dt$ and therefore $\mathbb{E}[\pi_s(X) \, dW(t)] = 0$ for $0 \le s \le t$. The innovations process can be interpreted as the difference between the observed changed $dY(t)$ and the expected change $\pi_t(s + s^\dagger) \, dt$ of the field. We can obtain the adjoint equation for the conditional density matrix ρ_c by identifying $\pi_t(X) = \text{tr}(\rho_c(t)X)$. This leads to the SME (B.8).

B.2 MARKOVIAN HOMODYNE FEEDBACK

In this section we discuss how to describe Markovian (i.e., instant-aneous) homodyne feedback in a framework developed in [Wis94]. The setup is basically the one from fig. 28, where the photo-current $I_x(t)$ is fed back to the system. Markovian feedback dynamics can be described by the expression

$$(\mathbf{S}) \qquad [d\rho_c]_{\text{fb}} = \mathcal{K}[F]\rho_c \, d\widetilde{X}, \qquad (\text{B.28})$$

the strength of the feedback being proportional to $d\widetilde{X} = I_x(t) \, dt$. The feedback is assumed to be described by a Hamiltonian evolution and we thus write the linear operator $\mathcal{K}$ as

$$\mathcal{K}[F]\rho = -\mathrm{i}[F, \rho], \qquad (\text{B.29})$$

where the Hermitian operator $F = F^\dagger$ describes a generalised force. As explicitly stated, eq. (B.28) has to be interpreted as a Stratonovich equation [Wis94]. In order to reconcile this with a master equation in the Itō-formalism [e.g., eq. (B.8)] we first have to convert it to Itō form. For a general master equation (with generic linear operators $\mathcal{L}$ and $\mathcal{K}$, and a nonlinear operator $\mathcal{H}$) this procedure yields the following:

- We start from a conditional Itō master equation

$$d\rho_c = \mathcal{L}\rho_c \, dt + \mathcal{H}\rho_c \, dW$$

- We convert eq. (B.28) to the Itō form by applying the relations from appendix A.6,

$$(\mathbf{I}) \qquad [d\rho_c]_{\text{fb}} = \frac{1}{2}\mathcal{K}[F]^2\rho_c \, dt + \mathcal{K}[F]\rho_c \, d\widetilde{X}$$

- As analysed in [Wis94], Markovian feedback can be described by al-ternately applying the generators of the conditional and the feedback evolution, applying feedback *after* the measurement, i.e.,

$$\rho_c(t + dt) = \exp\left(\tfrac{1}{2}\mathcal{K}^2 \, dt + \mathcal{K} \, d\widetilde{X}\right) \exp\left(\mathcal{L} \, dt + \mathcal{H} \, dW\right)\rho_c(t).$$

Expanding each exponential to first order in dt yields

$$\begin{aligned} \rho_c(t + dt) &= \left(1 + \tfrac{1}{2}\mathcal{K}^2 \, dt + \mathcal{K} \, d\widetilde{X}\right)\left(1 + \mathcal{L} \, dt + \mathcal{H} \, dW\right)\rho_c(t) \\ &= \left(1 + \mathcal{L} + \tfrac{1}{2}\mathcal{K}^2 + \mathcal{K}\mathcal{H}\right)\rho_c \, dt + \left(\mathcal{H} \, dW + \mathcal{K} \, d\widetilde{X}\right)\rho_c. \end{aligned}$$

Using the definitions of $\mathcal{K} := \mathcal{K}[F]$ and $\mathcal{H} := \mathcal{H}[s]$ [with eqs. (B.9) and (B.29)], and the expression of the homodyne current $\mathrm{d}\widetilde{X}$ [eq. (B.4)] we can show

$$\mathcal{K}\mathcal{H}\rho\,\mathrm{d}t + \mathcal{K}\rho\,\mathrm{d}\widetilde{X} = \mathcal{K}(\mathcal{H} + \langle s + s^\dagger\rangle_c)\rho\,\mathrm{d}t + \mathcal{K}\rho\,\mathrm{d}W$$
$$= \mathcal{K}(s\rho + \rho s^\dagger)\rho\,\mathrm{d}t + \mathcal{K}\rho\,\mathrm{d}W.$$

Additionally we note that

$$\frac{1}{2}\mathcal{K}^2\rho = -\frac{1}{2}[F,[F,\rho]] = \mathcal{D}[F]\rho. \tag{B.30}$$

Plugging in these two relations we can then take the classical average over the measurement results (dropping all terms proportional to $\mathrm{d}W$) to obtain an unconditional master equation,

$$\dot{\rho} = \mathcal{L}\rho + \mathcal{D}[F]\rho + \mathcal{K}(s\rho + \rho s^\dagger).$$

Finally, using the identity

$$\mathcal{D}[s - \mathrm{i}F]\rho = \mathcal{D}[s]\rho + \mathcal{D}[F]\rho - \mathrm{i}[F, s\rho + \rho s^\dagger] - \frac{\mathrm{i}}{2}[\rho, Fs + s^\dagger F], \tag{B.31}$$

this can be transformed to

$$\dot{\rho} = \mathcal{L}\rho - \mathcal{D}[s]\rho + \mathcal{D}[s - \mathrm{i}F]\rho - \mathrm{i}[\tfrac{1}{2}(Fs + s^\dagger F), \rho]. \tag{B.32}$$

If we now use the form (A.31) of the Lindblad operator we end up with

$$\dot{\rho} = -\mathrm{i}[H_{\mathrm{sys}}, \rho] + \mathcal{D}[s - \mathrm{i}F]\rho - \mathrm{i}[\tfrac{1}{2}(Fs + s^\dagger F), \rho]. \tag{B.33}$$

Let us discuss a two-fold generalization of this equation: First, we consider m independent measurement and feedback channels that are described by the operators s_i and F_i ($i = 1, \ldots, m$) respectively. This generalisation is immediate in the light of equation (B.17). Second, we take into account a non-unit detection efficiency $0 < \eta < 1$. We know from appendix B.1.1 that we can obtain the corresponding SME by rescaling the jump operator $s \to \sqrt{\eta}s$, but *only in the measurement terms* $\mathcal{H}[s]$, while the decoherence terms $\mathcal{D}[s]$ are unchanged. We use eq. (B.32) as our starting point and rescale $s \to \sqrt{\eta}s$ in *the feedback terms only* and at the same time adjust the feedback gain to $F \to F/\sqrt{\eta}$. This yields

$$\dot{\rho} = -\mathrm{i}[H, \rho] + \sum_i \left\{ \mathcal{D}[s_i]\rho + \frac{1}{\eta}\mathcal{D}[F_i]\rho - \mathrm{i}[F_i, s_i\rho + \rho s_i^\dagger] \right\}$$
$$= -\mathrm{i}[H, \rho] + \sum_i \left\{ \mathcal{D}[s_i - \mathrm{i}F_i]\rho + \frac{1-\eta}{\eta}\mathcal{D}[F_i]\rho - \mathrm{i}\frac{1}{2}[s_i^\dagger F_i + F_i s_i, \rho] \right\}, \tag{B.34}$$

which agrees with [WM09, p 246f].

B.3 QUANTUM FILTERING IN LINEAR SYSTEMS

In this section we briefly review the most important equations of quantum LQG control, following closely the presentation in [EB05]. We start by deriving the Gaussian quantum filter—the so-called Kalman-Bucy filter—and afterwards discuss how its output can be combined with optimal control techniques.

B.3.1 *Kalman Filtering*

Consider a Gaussian n-dimensional open quantum system coupling to m vacuum field channels, $m' \leq m$ of which are subject to homodyne detection, yielding the measurement outputs $Y_i = A_{i,\text{out}} + A_{i,\text{out}}$. The system's state conditioned on the outcomes of the homodyne measurements is described by the Belavkin equation (B.17) or equivalently by a slightly generalised version of the quantum filter (B.26)

$$
\mathrm{d}\pi_t(X) = -\mathrm{i}\pi_t([X, H])\,\mathrm{d}t + \sum_{i=1}^{m} \pi_t(\mathcal{D}^\dagger[s_i]X)\,\mathrm{d}t
$$
$$
+ \sum_{i=1}^{m'} [\pi_t(Xs_i + s_i^\dagger X) - \pi_t(X)\pi_t(s_i + s_i^\dagger)]\,\mathrm{d}W_i. \quad \text{(B.35)}
$$

W_i are Wiener processes with $\mathrm{d}W_i\,\mathrm{d}W_j = \delta_{ij}\,\mathrm{d}t$ and the Hamiltonian is at most quadratic in the system's quadratures, which we collect into a column vector $\boldsymbol{X} = (X_1, \ldots, X_{2n})^{\mathsf{T}}$. The canonical commutation relations can then be written as $[X_i, X_j] = \mathrm{i}J_{ij}$, where $\mathbf{J}$ is a skew-symmetric real matrix. Similarly we define $\boldsymbol{Y} = (Y_i, \ldots, Y_{m'})$. We can parametrize the jump operators $\boldsymbol{s} = (s_1, \ldots, s_m)^{\mathsf{T}}$, and the Hamiltonian H as

$$
\boldsymbol{s} = \boldsymbol{\Lambda X}, \tag{B.36}
$$
$$
H = \tfrac{1}{2}\boldsymbol{X}^T \mathbf{R}\boldsymbol{X} + [\boldsymbol{X}^\mathsf{T}\tilde{\mathbf{R}}\boldsymbol{u}(t) + \text{H.c.}], \tag{B.37}
$$

where $\mathbf{R} \in \mathbb{R}^{2n \times 2n}$ is symmetric, $\tilde{\mathbf{R}} \in \mathbb{C}^{2n \times m}$, and $\boldsymbol{u}(t)$ is a m-dimensional input signal, which will later be used as a control input. The system can then be described in terms of a linear vector quantum Langevin equation and an output equation (see the subsection below for a derivation)

$$
\mathrm{d}\boldsymbol{X}(t) = [\mathbf{F}\boldsymbol{X}(t) + \mathbf{G}\boldsymbol{u}(t)]\,\mathrm{d}t + \mathrm{d}\boldsymbol{V}(t), \tag{B.38a}
$$
$$
\mathrm{d}\boldsymbol{Y}(t) = \mathbf{H}\boldsymbol{X}(t)\,\mathrm{d}t + [\mathrm{d}\boldsymbol{A}(t) + \mathrm{d}\boldsymbol{A}(t)^\dagger], \tag{B.38b}
$$

with the real matrices

$$
\mathbf{F} = \mathbf{J}[\mathbf{R} + \text{Im}(\boldsymbol{\Lambda}^\dagger\boldsymbol{\Lambda})], \tag{B.39a}
$$
$$
\mathbf{H} = 2\,\text{Re}\,(\boldsymbol{\Lambda}), \tag{B.39b}
$$
$$
\mathbf{G} = \mathbf{J}(\tilde{\mathbf{R}} + \tilde{\mathbf{R}}^*), \tag{B.39c}
$$

and the real, vector valued noise process

$$d\mathbf{V} = i\mathbf{J}(\mathbf{\Lambda}^T d\mathbf{A}^\dagger - \mathbf{\Lambda}^\dagger d\mathbf{A}), \tag{B.40}$$

where $d\mathbf{A} = (dA_1, \ldots, dA_m)^T$. We assume the field is in the vacuum state ρ_{vac}, such that $dA_i(t) dA_j(t) = \delta_{ij} dt$. The (co)variances of $d\mathbf{V}$ are thus determined by

$$\mathbf{N} dt = \text{Re}(d\mathbf{V} d\mathbf{V}^T) = \mathbf{J} \text{Re}(\mathbf{\Lambda}^\dagger \mathbf{\Lambda}) \mathbf{J}^T dt, \tag{B.41a}$$

$$\mathbf{M} dt = \text{Re}(d\mathbf{V}[d\mathbf{A} + d\mathbf{A}^\dagger]^T) = -\mathbf{J} \text{Im}(\mathbf{\Lambda}^T) dt. \tag{B.41b}$$

From the quantum filter equations we can deduce the equations of motion for the conditional mean values $\hat{X}_i = \pi_t(X_i)$ and symmetric covariance matrix $\hat{\Sigma}_{ij} = \frac{1}{2}\pi_t(X_i X_j + X_j X_i) - \hat{X}_i \hat{X}_j$. We find

$$d\hat{\mathbf{X}}(t) = \left[\mathbf{F}\hat{\mathbf{X}}(t) + \mathbf{G}\mathbf{u}(t)\right] dt \\ + \mathbf{K}(t)\left[d\mathbf{Y}(t) - \mathbf{H}\hat{\mathbf{X}}(t) dt\right], \tag{B.42a}$$

$$\frac{d}{dt}\hat{\mathbf{\Sigma}}(t) = \mathbf{F}\hat{\mathbf{\Sigma}}(t) + \hat{\mathbf{\Sigma}}(t)\mathbf{F}^T + \mathbf{N} \\ - \left[\hat{\mathbf{\Sigma}}(t)\mathbf{H}^T + \mathbf{M}\right]\left[\hat{\mathbf{\Sigma}}(t)\mathbf{H}^T + \mathbf{M}\right]^T, \tag{B.42b}$$

where

$$\mathbf{K}(t) = \hat{\mathbf{\Sigma}}(t)\mathbf{H}^T + \mathbf{M}. \tag{B.43}$$

Equations (B.42) together with (B.43) are known as the *Kalman–Bucy* filter in classical estimation theory [KB61]. Presuming certain stability conditions [WM09, p 292f], the steady-state solution of the conditional covariance matrix $\hat{\mathbf{\Sigma}}$ can be found by setting the right-hand side of (B.42b) to zero, and solving the resulting algebraic Riccati equation. If instead we are interested in the properties of the unconditional state, we can solve the Lyapunov equation obtained from (B.42b) by dropping the last term. [The resulting equation can also be obtained from (B.38a) by application of Itō calculus.]

Derivation of the Linear Langevin Equations

We can derive the linear vector Langevin equation (B.38a) from the general form (A.23) by using the definition of the Liouville operator (A.24) together with eqs. (B.36) and (B.37). In the following we are using a sum convention where repeated indices are summed over. For the unitary evolution we find

$$-i[X_k, H] = -\tfrac{i}{2}R_{ij}[X_k, X_i X_j] - i(\tilde{R}_{ij}u_j[X_k, X_i] - \text{H. c.}) \\ = -\tfrac{i}{2}R_{ij}([X_k, X_i]X_j + X_i[X_k, X_j]) + (\tilde{R}_{ij} + \tilde{R}_{ij}^*)u_j J_{ki} \\ = \tfrac{1}{2}R_{ij}(J_{ki}X_j + X_i J_{kj}) + (\tilde{R}_{ij} + \tilde{R}_{ij}^*)u_j J_{ki} \\ = J_{ki}[R_{ij}X_j + (\tilde{R}_{ij} + \tilde{R}_{ij}^*)u_j],$$

where in the second to last line we used $\mathbf{R} = \mathbf{R}^{\mathrm{T}}$. The Lindblad term yields

$$
\begin{aligned}
\sum_l \mathcal{D}^\dagger[s_l]X_k &= s_l^\dagger X_k s_l - \tfrac{1}{2}[s_l^\dagger s_l X_k + X_k s_l^\dagger s_l] \\
&= \Lambda_{li}^* \Lambda_{lj}\big(X_i^\dagger X_k X_j - \tfrac{1}{2}[X_i^\dagger X_j X_k + X_k X_i^\dagger X_j]\big) \\
&= \tfrac{1}{2}\Lambda_{li}^* \Lambda_{lj}\big(X_i[X_k, X_j] + [X_i, X_k]X_j\big) \\
&= \tfrac{\mathrm{i}}{2}\Lambda_{li}^* \Lambda_{lj}[J_{kj}X_i - J_{ki}X_j] \\
&= \tfrac{\mathrm{i}}{2}J_{kj}(\Lambda_{li}^* \Lambda_{lj} - \Lambda_{lj}^* \Lambda_{li})X_i = -J_{kj}\,\mathrm{Im}(\Lambda_{lj}\Lambda_{li}^*)X_i,
\end{aligned}
$$

while the noise terms result in

$$
\begin{aligned}
[X_k, s_l]\,\mathrm{d}A_l^\dagger &= \Lambda_{li}[X_k, X_i]\,\mathrm{d}A_l^\dagger = \mathrm{i}\Lambda_{li}J_{ki}\,\mathrm{d}A_l^\dagger, \\
[s_l^\dagger, X_k]\,\mathrm{d}A_l &= \Lambda_{li}^*[X_i, X_k]\,\mathrm{d}A_l = \mathrm{i}\Lambda_{li}^* J_{ik}\,\mathrm{d}A_l.
\end{aligned}
$$

Putting this in vector form we immediately find eq. (B.38a). The output equation eq. (B.38b) follows directly from the input–output relations eq. (A.26) and the definition of the jump operators.

Derivation of the Kalman Filter Equations

The Kalman filter equations can be derived starting from the quantum filter equation (B.35) by using Itō-calculus. The derivation is very similar to the one of the classical Kalman filter, see, e. g., [Xio08]. We start with the conditional mean and find an explicit expression for $\mathrm{d}\hat{X}(t) = \mathrm{d}\pi_t(X)$. The result contains the three terms: The terms generated by the Hamiltonian evolution and the diffusive dynamics we can copy from above, thus

$$
\begin{aligned}
-\mathrm{i}\pi_t([X_k, H]) &= J_{ki}[R_{ij}\pi_t(X_j) + (\tilde{R}_{ij} + \tilde{R}_{ij}^*)u_j], \\
\sum_l \pi_t(\mathcal{D}^\dagger[s_l]X_k) &= -J_{kj}\,\mathrm{Im}(\Lambda_{lj}\Lambda_{li}^*)\pi_t(X_i).
\end{aligned}
$$

Introducing the shorthand notation $\tilde{s}_i = s_i - \pi_t(s_i)$ and $\tilde{X}_i = X_i - \pi_t(X_i)$, the measurement term (without the noise increment) can be written as

$$
\begin{aligned}
\pi_t(X_k \tilde{s}_l &+ \tilde{s}_l X_k) \\
&= \Lambda_{li}\pi_t(X_k \tilde{X}_i) + \Lambda_{li}^* \pi_t(\tilde{X}_i X_k) \\
&= \Lambda_{li}\pi_t(\tilde{X}_k \tilde{X}_i) + \Lambda_{li}^* \pi_t(\tilde{X}_i \tilde{X}_k) + (\Lambda_{li} + \Lambda_{li}^*)\pi_t(X_k)\pi_t(\tilde{X}_i) \\
&= \mathrm{Re}\,(\Lambda_{li})[\pi_t(\tilde{X}_k \tilde{X}_i + \tilde{X}_i \tilde{X}_k)] + \mathrm{i}\,\mathrm{Im}\,(\Lambda_{li})\pi_t([\tilde{X}_k, \tilde{X}_i]) \\
&= 2\,\mathrm{Re}\,(\Lambda_{li})\hat{\Sigma}_{ki} - \mathrm{Im}\,(\Lambda_{li})J_{ki},
\end{aligned}
$$

where we used $\pi_t(\tilde{s}_i) = \pi_t(\tilde{X}) = 0$ and $\hat{\Sigma}_{ij} = \pi_t(\tilde{X}_i \tilde{X}_j + \tilde{X}_j \tilde{X}_i)$.

Adding up the resulting expressions and casting them into vector form leaves us with

$$d\pi_t(\boldsymbol{X}) = \boldsymbol{J}[\boldsymbol{R} + \mathrm{Im}\,(\boldsymbol{\Lambda}^\dagger\boldsymbol{\Lambda})]\pi_t(\boldsymbol{X})\,dt + \boldsymbol{J}(\boldsymbol{R} + \boldsymbol{R}^*)\boldsymbol{u}(t)\,dt$$
$$+ [2\hat{\boldsymbol{\Sigma}}(t)\,\mathrm{Re}(\boldsymbol{\Lambda})^\mathrm{T} - \boldsymbol{J}\,\mathrm{Im}(\boldsymbol{\Lambda})^\mathrm{T}]\,d\boldsymbol{W}(t). \quad \text{(B.44)}$$

It remains to show that

$$dW_i = dY_i - \pi_t(s_i + s_i^\dagger)\,dt = dY_i - (\Lambda_{ij} + \Lambda_{ij}^*)\pi_t(X_j)\,dt. \quad \text{(B.45)}$$

This leads to eq. (B.42a). The evolution of the corresponding covariance is determined by

$$d\hat{\Sigma}_{lk} = \frac{1}{2}\,d\pi_t(X_lX_k + X_kX_l) - d[\pi_t(X_l)\pi_t(X_k)]. \quad \text{(B.46)}$$

For simplicity we here neglect the deterministic input and thus set $\tilde{\boldsymbol{R}} = 0$; it is, however, straightforward to extend the presented derivation to the more general case $\tilde{\boldsymbol{R}} \neq 0$. The second term in eq. (B.46) can be directly obtained from eq. (B.44) by using Itō-rules. It is made up of the terms

$$\pi_t(X_k)\,d\pi_t(X_l) = [F_{ki}\pi_t(X_i)\,dt + K_{ki}\,dW_i]\pi_t(X_l), \quad \text{(B.47a)}$$
$$d\pi_t(X_k)\,d\pi_t(X_l) = K_{ki}K_{il}\,dt, \quad \text{(B.47b)}$$

plus the corresponding expression for $\pi_t(X_l)\,d\pi_t(X_k)$. The expressions for the first term in eq. (B.46) are more involved. For the Hamiltonian evolution we find

$$-\,\mathrm{i}\pi_t([X_lX_k, H]) = -\tfrac{\mathrm{i}}{2}R_{mn}\pi_t([X_lX_k, X_mX_n])$$
$$= \tfrac{1}{2}R_{mn}\pi_t(X_lX_mJ_{ln} + X_lX_nJ_{km} + X_mX_kJ_{ln} + X_nX_kJ_{lm})$$
$$= R_{mn}\pi_t(X_lX_nJ_{km} + X_nX_kJ_{lm}),$$

and after symmetrisation

$$-\,\mathrm{i}\pi_t([X_kX_l + X_lX_k, H])$$
$$= J_{lm}R_{mn}\pi_t([X_n, X_k]_+) + J_{km}R_{mn}\pi_t([X_n, X_l]_+)$$
$$= 2J_{lm}R_{mn}[\hat{\Sigma}_{nk} + \pi_t(X_n)\pi_t(X_k)]$$
$$+ 2J_{km}R_{mn}[\hat{\Sigma}_{nl} + \pi_t(X_n)\pi_t(X_l)].$$

We now note that we can write the Lindblad term $\mathcal{D}^\dagger[s]X = \frac{1}{2}(s^\dagger[X, s] + [s^\dagger, X]s)$. Together with the definition[4] $\lambda_{nm} = (\boldsymbol{\Lambda}^\dagger\boldsymbol{\Lambda})_{nm}$ this leads to

$$\sum_j \pi_t(\mathcal{D}^\dagger[s_j]X_lX_k) = \tfrac{1}{2}\Lambda_{jn}^*\Lambda_{jm}\pi_t(X_n[X_lX_k, X_m] + [X_n, X_lX_k]X_m)$$
$$= \tfrac{\mathrm{i}}{2}\Lambda_{jn}^*\Lambda_{jm}\pi_t(X_n[J_{km}X_l + J_{lm}X_k] + [J_{nl}X_k + J_{nk}X_l]X_m)$$
$$= \tfrac{\mathrm{i}}{4}\lambda_{nm}\pi_t(J_{km}X_nX_l + J_{lm}X_nX_k + J_{nl}X_kX_m + J_{nk}X_lX_m)$$
$$- \tfrac{\mathrm{i}}{4}\lambda_{nm}^*\pi_t(J_{km}X_lX_n + J_{lm}X_kX_n + J_{nl}X_mX_k + J_{nk}X_mX_l).$$

4. Note that $\lambda_{mn} = (\boldsymbol{\Lambda}^\mathrm{T}\boldsymbol{\Lambda}^*)_{nm} = \lambda_{nm}^*$

We now decompose $\lambda_{nm} = \text{Re}(\lambda_{nm}) + \text{i}\,\text{Im}(\lambda_{nm})$ into its real and imaginary part, and observe that $\text{Re}(\lambda_{nm}) = \text{Re}(\lambda_{mn})$ and $\text{Im}(\lambda_{nm}) = -\text{Im}(\lambda_{mn})$. Above expression can thus be written as the sum of the two terms

$$\frac{\text{i}}{4}\text{Re}(\lambda_{nm})\pi_t(J_{km}[X_n, X_l] + J_{lm}[X_n, X_k])$$
$$+ \frac{\text{i}}{4}\text{Re}(\lambda_{nm})\pi_t(J_{nl}[X_k, X_m] + J_{nk}[X_l, X_m])$$
$$= \frac{\text{i}}{2}\text{Re}(\lambda_{nm})\pi_t(J_{km}[X_n, X_l] + J_{lm}[X_n, X_k])$$
$$= -\frac{1}{2}\text{Re}(\lambda_{nm})(J_{km}J_{nl} + J_{lm}J_{nk}) = -J_{ln}\text{Re}(\lambda_{nm})J_{mk}$$

and

$$-\frac{1}{4}\text{Im}(\lambda_{nm})\pi_t(J_{km}[X_l, X_n]_+ + J_{nk}[X_m, X_l]_+)$$
$$-\frac{1}{4}\text{Im}(\lambda_{nm})\pi_t(J_{nl}[X_m, X_k]_+ + J_{lm}[X_k, X_n]_+)$$
$$= -\frac{1}{2}\text{Im}(\lambda_{nm})\pi_t(J_{km}[X_l, X_n]_+ + J_{nl}[X_m, X_k]_+)$$
$$= [\hat{\Sigma}_{ln} + \pi_t(X_l)\pi_t(X_n)]\,\text{Im}(\lambda_{nm})J_{mk}$$
$$+ J_{ln}\text{Im}(\lambda_{nm})[\hat{\Sigma}_{mk} + \pi_t(X_m)\pi_t(X_k)].$$

Note that both expressions are symmetric under the substitution $k \leftrightarrow l$. For the measurement term we obtain

$$\pi_t(X_l X_k \tilde{s}_i + \tilde{s}_i^\dagger X_l X_k)$$
$$= \Lambda_{ij}\pi_t(X_l X_k \tilde{X}_j) + \Lambda_{ij}^*\pi_t(\tilde{X}_j X_l X_k)$$
$$= \Lambda_{ij}\pi_t([\tilde{X}_l + \pi_t(X_l)][\tilde{X}_k + \pi_t(X_k)]\tilde{X}_j)$$
$$+ \Lambda_{ij}^*\pi_t(\tilde{X}_j[\tilde{X}_l + \pi_t(X_l)][\tilde{X}_k + \pi_t(X_k)])$$
$$= \Lambda_{ij}[\pi_t(X_k)\pi_t(\tilde{X}_l \tilde{X}_j) + \pi_t(X_l)\pi_t(\tilde{X}_k \tilde{X}_j)]$$
$$+ \Lambda_{ij}^*[\pi_t(X_k)\pi_t(\tilde{X}_j \tilde{X}_l) + \pi_t(X_l)\pi_t(\tilde{X}_j \tilde{X}_k)]$$
$$= \text{Re}(\Lambda_{ij})[\pi_t(X_k)\pi_t([\tilde{X}_l, \tilde{X}_j]_+) + \pi_t(X_l)\pi_t([\tilde{X}_k, \tilde{X}_j]_+)]$$
$$- \text{i}\,\text{Im}(\Lambda_{ij})[\pi_t(X_k)\pi_t([\tilde{X}_j, \tilde{X}_l]) + \pi_t(X_l)\pi_t([\tilde{X}_j, \tilde{X}_k])]$$
$$= 2\,\text{Re}\,(\Lambda_{ij})[\pi_t(X_k)\hat{\Sigma}_{lj} + \pi_t(X_l)\hat{\Sigma}_{kj}]$$
$$+ \text{Im}\,(\Lambda_{ij})[\pi_t(X_k)J_{jl} + \pi_t(X_l)J_{jk}],$$

where we used that for Gaussian states central moments of odd order must vanish, i.e., $\pi_t(\tilde{X}_i \tilde{X}_j \tilde{X}_k) = 0$ for all i, j, k. Combining these expressions yields

$$\frac{1}{2}\,\text{d}\pi_t(X_l X_k + X_k X_l) = F_{lj}\hat{\Sigma}_{jk} + \hat{\Sigma}_{lj}F_{kj} + N_{lk}$$
$$+ F_{lj}\hat{X}_j\hat{X}_k + \hat{X}_l\hat{X}_j F_{kj} + K_{lj}\,\text{d}W_j\hat{X}_k + \hat{X}_l\,\text{d}W_j K_{kj}. \quad \text{(B.48)}$$

The first line corresponds to the standard Lyapunov equation. Plugging eqs. (B.47) and (B.48) into (B.46), the second line of (B.48) cancels with eq. (B.47a) and the corresponding term for $\pi_t(X_l)\,\text{d}\pi_t(X_k)$. We eventually obtain the Riccati equation (B.42b).

B.3.2 *Quantum LQG control*

Linear–quadratic–gaussian control concerns the control of linear systems subject to additive Gaussian noise such that a quadratic cost function is minimised. The LQG controller turns out to be a combination of the system's Kalman filter plus a quadratic regulator, where the control signal $u(t)$ depends on a set of observations $\{Y(s) : 0 \leq s \leq t\}$. In this thesis we only deal with the asymptotic control problem for $t \to \infty$ as we are interested in the steady state of our systems. We therefore want to find a feedback strategy which minimizes the total cost [BH08]

$$\int_0^\infty \mathbb{E}[h(X(t), u(t))]\, dt. \tag{B.49}$$

We choose h to be of the form

$$h(X, u) = X^T P X + u^T Q u, \tag{B.50}$$

where $\mathbf{P} \geq 0$ and $\mathbf{Q} > 0$ are both real, symmetric matrices of appropriate dimensions. Under the assumption of certain stability conditions [WM09, p 298] the optimal feedback signal is given by [EB05]

$$u(t) = -\mathbf{C}(t)\hat{X}(t), \tag{B.51}$$

$$\mathbf{C} = \mathbf{Q}^{-1}\mathbf{G}^T\mathbf{\Omega}^{ss}, \tag{B.52}$$

with $\mathbf{\Omega}^{ss}$ the solution of the algebraic Riccati equation

$$\mathbf{F}^T\mathbf{\Omega}^{ss} + \mathbf{\Omega}^{ss}\mathbf{F} + \mathbf{P} - \mathbf{\Omega}^{ss}\mathbf{G}\mathbf{Q}^{-1}\mathbf{G}^T\mathbf{\Omega}^{ss} = 0. \tag{B.53}$$

In section 3.1 we need to calculate the steady-state covariance matrix of a linear system including optimal feedback. This can be achieved by first noting that (due to the separation principle [BH08]) we can write (B.42a) as

$$d\hat{X}(t) = (\mathbf{F} - \mathbf{G}\mathbf{C})\hat{X}(t)\, dt + \mathbf{K}\, dW, \tag{B.54}$$

where W is a Wiener process with $dW(t)\, dW(t)^T = \mathbb{1}_m\, dt$ (the innovations process). We also need that [EB03; BVJ07]

$$\mathrm{Re}\big(\mathbb{E}[(X(t) - \hat{X}(t))(X(t) - \hat{X}(t))^T]\big) = \hat{\mathbf{\Sigma}}(t), \tag{B.55}$$

$$\mathbb{E}[(X(t) - \hat{X}(t))\hat{X}(t)^T] = 0, \tag{B.56}$$

where the first relation follows from the definition of $\hat{X}$ and $\hat{\mathbf{\Sigma}}$, and the second from the orthogonality principle (B.20). We therefore find

$$\mathrm{Re}\big(\mathbb{E}[X(t)X(t)^T]\big) = \hat{\mathbf{\Sigma}}(t) + \mathbb{E}[\hat{X}(t)\hat{X}(t)^T], \tag{B.57}$$

where the equation of motion for the last term on the right-hand side $\Xi(t) = \mathbb{E}[\hat{X}(t)\hat{X}(t)^T]$ can be deduced from (B.54). The steady-state solution Ξ^{ss} which fulfills

$$(\mathbf{F} - \mathbf{G}\mathbf{C})\Xi^{ss} + \Xi^{ss}(\mathbf{F} - \mathbf{G}\mathbf{C})^T + \mathbf{K}\mathbf{K}^T = 0. \tag{B.58}$$

The steady-state solution of the symmetric covariance matrix of the controlled quantum system is thus given by

$$\lim_{t \to \infty} \text{Re} \left(\mathbb{E}[\boldsymbol{X}(t)\boldsymbol{X}(t)^{\text{T}}] \right) = \hat{\boldsymbol{\Sigma}}^{\text{ss}} + \boldsymbol{\Xi}^{\text{ss}}. \tag{B.59}$$

Finally, we want to estimate the magnitude of the expected feedback signal. We quantify this by $\mathbb{E}[\boldsymbol{u}^{\text{T}}(t)\boldsymbol{u}(t)]$. In the steady state we find

$$\mathbb{E}[\boldsymbol{u}^{\text{T}}(t)\boldsymbol{u}(t)] = \mathbb{E}[\hat{\boldsymbol{X}}^{\text{T}}\boldsymbol{C}^{\text{T}}\boldsymbol{C}\hat{\boldsymbol{X}}] = \text{tr}(\boldsymbol{C}\boldsymbol{\Xi}^{\text{ss}}\boldsymbol{C}^{\text{T}}). \tag{B.60}$$

B.4 ROUTH–HURWITZ CRITERION

Consider the characteristic polynomial of a matrix $\boldsymbol{M} \in \mathbb{R}^{n \times n}$

$$h_n(\lambda) = \det(\boldsymbol{M} - \lambda \mathbb{1}_n) = a_0 \lambda^n + a_1 \lambda^{n-1} + \cdots + a_{n-1}\lambda + a_n, \tag{B.61}$$

with real coefficients a_i $(i = 1, \dots, n)$ and $a_0 \neq 0$. All roots of h_n then have negative real part if and only if the determinants of all Hurwitz matrices are positive [Ilo7, p. 1086], i.e.,

$$\det \boldsymbol{H}_j > 0, \qquad j = 1, \dots, n. \tag{B.62}$$

The Hurwitz matrices $\boldsymbol{H}_j \in \mathbb{R}^{j \times j}$ are defined by

$$(H_j)_{nm} = a_{2n-m}, \qquad 1 \leq n, m \leq j \tag{B.63}$$

with $a_i := 0$ for $i < 0$ and $n < i$. This yields, explicitly written in matrix form,

$$\boldsymbol{H}_j = \begin{pmatrix} a_1 & a_0 & 0 & \dots & 0 \\ a_3 & a_2 & a_1 & \dots & 0 \\ a_5 & a_4 & a_3 & \dots & 0 \\ \vdots & \vdots & \vdots & \ddots & \vdots \\ a_{2j-1} & a_{2j-2} & a_{2j-3} & \dots & a_j \end{pmatrix}. \tag{B.64}$$

As an example, for $n = 3$ this gives the following matrices:

$$\boldsymbol{H}_1 = \begin{pmatrix} a_1 \end{pmatrix}, \quad \boldsymbol{H}_2 = \begin{pmatrix} a_1 & a_0 \\ a_3 & a_2 \end{pmatrix}, \quad \boldsymbol{H}_3 = \begin{pmatrix} a_1 & a_0 & 0 \\ a_3 & a_2 & a_1 \\ 0 & 0 & a_3 \end{pmatrix}; \tag{B.65}$$

B.5 EVALUATING INTEGRALS OF RATIONAL FUNCTIONS

The presented method is useful for finding analytic solutions to a Lyapunov equation. Consider an integral of the form

$$\int_{-\infty}^{\infty} \mathrm{d}x \frac{g_n(x)}{h_n(x)h_n(-x)}, \tag{B.66}$$

where

$$h_n(x) = a_0 x^n + a_1 x^{n-1} + \cdots + a_{n-1}x + a_n, \tag{B.67a}$$

$$g_n(x) = b_0 x^{2n-2} + b_1 x^{2n-4} + \cdots + b_{n-2}x^2 + b_{n-1}, \tag{B.67b}$$

with $a_0 \neq 0$. The polynomials h_n and g_n are therefore determined by $n + 1$ and n coefficients respectively. We assume that all roots of h_n lie in the *upper half-plane*. The solution of (B.66) is then given by [IIo7, p. 253][5]

$$\int_{-\infty}^{\infty} \mathrm{d}x \frac{g_n(x)}{h_n(x)h_n(-x)} = \mathrm{i}(-1)^{n+1}\frac{\pi}{a_0}\frac{\Lambda_n}{\Delta_n}, \tag{B.68}$$

5. Note that the factor $(-1)^{n+1}$ is wrongly missing in the reference.

where $\Delta_n = \det \mathbf{H}_n$ is the determinant of the Hurwitz matrix $\mathbf{H}_n$ defined in appendix B.4 and $\Lambda_n = \det \mathbf{M}_n$, with

$$\mathbf{M}_n = \begin{pmatrix} b_0 & a_0 & 0 & 0 & 0 \\ b_1 & a_2 & a_1 & a_0 & 0 \\ b_2 & a_4 & a_3 & a_2 & 0 \\ \vdots & \vdots & \vdots & \ddots & \vdots \\ b_{n-1} & a_{2n-2} & a_{2n-3} & \cdots & a_n \end{pmatrix}, \tag{B.69}$$

which is a $n \times n$ matrix obtained from $\mathbf{H}_n$ by replacing the first column with the coefficients $(b_0, b_1, \ldots, b_{n-1})$ of g_n. Note that formula (B.68) is also valid when g_n includes odd powers of x, as their contribution averages to zero over the $(-\infty, \infty)$.

[Abd+11]   M. Abdi et al., 'Effect of phase noise on the generation of stationary entanglement in cavity optomechanics', *Physical Review A* 84, 032325 (2011), DOI: `10.1103/PhysRevA.84.032325` (pp 37, 108).

[ADR82]   A. Aspect, J. Dalibard and G. Roger, 'Experimental Test of Bell's Inequalities Using Time- Varying Analyzers', *Physical Review Letters* 49, 1804 (1982), DOI: `10.1103/PhysRevLett.49.1804` (p 63).

[AI07]   G. Adesso and F. Illuminati, 'Entanglement in continuous-variable systems: recent advances and current perspectives', *Journal of Physics A: Mathematical and Theoretical* 40, 7821 (2007), DOI: `10.1088/1751-8113/40/28/S01` (p 42).

[AK02]   J. R. Anglin and W. Ketterle, 'Bose–Einstein condensation of atomic gases', *Nature* 416, 211 (2002), DOI: `10.1038/416211a` (p 1).

[AKM14]   M. Aspelmeyer, T. J. Kippenberg and F. Marquardt, 'Cavity optomechanics', *Reviews of Modern Physics* 86, 1391 (2014), DOI: `10.1103/RevModPhys.86.1391` (pp 7, 11, 15, 20, 29, 46).

[Ang+13]   S. Z. Ang et al., 'Optomechanical parameter estimation', *New Journal of Physics* 15, 103028 (2013), DOI: `10.1088/1367-2630/15/10/103028` (p 1).

[Ans+09]   M. Ansmann et al., 'Violation of Bell's inequality in Josephson phase qubits', *Nature* 461, 504 (2009), DOI: `10.1038/nature08363` (p 63).

[Arc+06]   O. Arcizet et al., 'Radiation-pressure cooling and optomechanical instability of a micromirror', *Nature* 444, 71 (2006), DOI: `10.1038/nature05244` (p 2).

[Ase+13]   P. Asenbaum et al., 'Cavity cooling of free silicon nanoparticles in high vacuum', *Nature Communications* 4 (2013), DOI: `10.1038/ncomms3743` (p 2).

[Bar+04]   M. D. Barrett et al., 'Deterministic quantum teleportation of atomic qubits', *Nature* 429, 737 (2004), DOI: `10.1038/nature02608` (p 86).

[Bar06]   A. Barchielli, 'Continual Measurements in Quantum Mechanics and Quantum Stochastic Calculus', in: *Open Quantum Systems III*, ed. by S. Attal, A. Joye and C.-A. Pillet, vol. 1882, Berlin/Heidelberg: Springer-Verlag, 2006, 207 (pp 121, 124, 125).

[Bar86] A. Barchielli, 'Measurement theory and stochastic differential equations in quantum mechanics', *Physical Review A* 34, 1642 (1986), DOI: 10.1103/PhysRevA.34.1642 (pp 125, 127).

[BC12] J. B. Brask and R. Chaves, 'Robust nonlocality tests with displacement-based measurements', *Physical Review A* 86, 010103 (2012), DOI: 10.1103/PhysRevA.86.010103 (p 64).

[Bel64] J. Bell, 'On the Einstein-Podolsky-Rosen Paradox', *Physics* 1, 195 (1964) (p 63).

[Bel66] J. S. Bell, 'On the Problem of Hidden Variables in Quantum Mechanics', *Reviews of Modern Physics* 38, 447 (1966), DOI: 10.1103/RevModPhys.38.447 (p 63).

[Bel80] V. Belavkin, 'Optimal filtering of Markov signals with quantum white noise', *Radio Eng Electron Physics* 25, 1445 (1980) (pp 1, 26, 129).

[Bel92] V. P. Belavkin, 'Quantum stochastic calculus and quantum nonlinear filtering', *Journal of Multivariate Analysis* 42, 171 (1992), DOI: 10.1016/0047-259X(92)90042-E (pp 89, 129, 133).

[Bel99] V. Belavkin, 'Measurement, filtering and control in quantum open dynamical systems', *Reports on Mathematical Physics* 43, A405 (1999), DOI: 10.1016/S0034-4877(00)86386-7 (p 82).

[Ben+93] C. H. Bennett et al., 'Teleporting an unknown quantum state via dual classical and Einstein-Podolsky-Rosen channels', *Physical Review Letters* 70, 1895 (1993), DOI: 10.1103/PhysRevLett.70.1895 (p 2).

[BG08] V. P. Belavkin and M. Guta, *Quantum Stochastics and Information: Statistics, Filtering and Control*, Singapore: World Scientific, 2008 (p 1).

[BGK97] V. B. Braginsky, M. L. Gorodetsky and F. Y. Khalili, 'Optical bars in gravitational wave antennas', *Physics Letters A* 232, 340 (1997), DOI: 10.1016/S0375-9601(97)00413-1 (p 23).

[BH08] L. Bouten and R. van Handel, 'On the separation principle of quantum control', in: *Quantum Stochastics and Information: Statistics, Filtering and Control*, ed. by V. P. Belavkin and M. I. Guta, Singapore: World Scientific, 2008 (p 143).

[BJK97] S. Bose, K. Jacobs and P. L. Knight, 'Preparation of nonclassical states in cavities with a moving mirror', *Physical Review A* 56, 4175 (1997), DOI: 10.1103/PhysRevA.56.4175 (pp 2, 52).

[BJW01]   J. C. Bergquist, S. R. Jefferts and D. J. Wineland, 'Time measurement at the millennium', *Physics Today* 54, 37 (2001), DOI: 10.1063/1.1366066 (p 1).

[BK81]   R. Benguria and M. Kac, 'Quantum Langevin Equation', *Physical Review Letters* 46, 1 (1981), DOI: 10.1103/PhysRevLett.46.1 (p 17).

[BK96]   V. B. Braginsky and F. Y. Khalili, 'Quantum nondemolition measurements: the route from toys to tools', *Reviews of Modern Physics* 68, 1 (1996), DOI: 10.1103/RevModPhys.68.1 (p 14).

[BK98]   S. L. Braunstein and H. J. Kimble, 'Teleportation of Continuous Quantum Variables', *Physical Review Letters* 80, 869 (1998), DOI: 10.1103/PhysRevLett.80.869 (p 42).

[BL05]   S. L. Braunstein and P. van Loock, 'Quantum information with continuous variables', *Reviews of Modern Physics* 77, 513 (2005), DOI: 10.1103/RevModPhys.77.513 (pp 42, 43, 59).

[Bla+04]   A. Blais et al., 'Cavity quantum electrodynamics for superconducting electrical circuits: An architecture for quantum computation', *Physical Review A* 69, 062320 (2004), DOI: 10.1103/PhysRevA.69.062320 (p 53).

[BLK01]   Y. Bar-Shalom, X. R. Li and T. Kirubarajan, *Estimation with Applications to Tracking and Navigation: Theory Algorithms and Software*, John Wiley & Sons, 2001 (pp 105, 111).

[BM67]   V. B. Braginskii and A. B. Manukin, 'Ponderomotive Effects of Electromagnetic Radiation', *Soviet Journal of Experimental and Theoretical Physics* 25, 653 (1967) (pp 1, 11).

[BMT70]   V. B. Braginskii, A. B. Manukin and M. Y. Tikhonov, 'Investigation of Dissipative Ponderomotive Effects of Electromagnetic Radiation', *Soviet Journal of Experimental and Theoretical Physics* 31, 829 (1970) (pp 1, 11).

[Bou+97]   D. Bouwmeester et al., 'Experimental quantum teleportation', *Nature* 390, 575 (1997), DOI: 10.1038/37539 (pp 43, 86).

[BP02]   H.-P. Breuer and F. Petruccione, *The Theory of Open Quantum Systems*, Oxford University Press, 2002 (p 73).

[BP96]   A. Barchielli and A. M. Paganoni, 'Detection theory in quantum optics: stochastic representation', *Quantum and Semiclassical Optics: Journal of the European Optical Society Part B* 8, 133 (1996), DOI: 10.1088/1355-5111/8/1/011 (p 130).

[Bre+08]   F. Brennecke et al., 'Cavity Optomechanics with a Bose-Einstein Condensate', *Science* 322, 235 (2008), DOI: `10.1126/science.1163218` (p 2).

[Bro+12]   D. W. C. Brooks et al., 'Non-classical light generated by quantum-noise-driven cavity optomechanics', *Nature* 488, 476 (2012), DOI: `10.1038/nature11325` (pp 2, 14).

[BS10]   P. F. Barker and M. N. Shneider, 'Cavity cooling of an optically trapped nanoparticle', *Physical Review A* 81, 023826 (2010), DOI: `10.1103/PhysRevA.81.023826` (p 11).

[BV02]   V. B. Braginsky and S. P. Vyatchanin, 'Low quantum noise tranquilizer for Fabry–Perot interferometer', *Physics Letters A* 293, 228 (2002), DOI: `10.1016/S0375-9601(02)00020-8` (p 23).

[BVJ07]   L. Bouten, R. Van Handel and M. R. James, 'An Introduction to Quantum Filtering', *SIAM Journal on Control and Optimization* 46, 2199 (2007), DOI: `10.1137/060651239` (pp 1, 130, 133, 134, 143).

[BVT80]   V. B. Braginsky, Y. I. Vorontsov and K. S. Thorne, 'Quantum Nondemolition Measurements', *Science* 209, 547 (1980), DOI: `10.1126/science.209.4456.547` (p 14).

[BW98]   K. Banaszek and K. Wódkiewicz, 'Nonlocality of the Einstein-Podolsky-Rosen state in the Wigner representation', *Physical Review A* 58, 4345 (1998), DOI: `10.1103/PhysRevA.58.4345` (p 64).

[BW99]   K. Banaszek and K. Wódkiewicz, 'Testing Quantum Nonlocality in Phase Space', *Physical Review Letters* 82, 2009 (1999), DOI: `10.1103/PhysRevLett.82.2009` (p 64).

[Car93a]   H. J. Carmichael, 'Quantum trajectory theory for cascaded open systems', *Physical Review Letters* 70, 2273 (1993), DOI: `10.1103/PhysRevLett.70.2273` (pp 53, 107).

[Car93b]   H. Carmichael, *An open systems approach to quantum optics*, Berlin: Springer, 1993 (p 129).

[Cer+11]   J. Cerrillo et al., 'Pulsed Laser Cooling for Cavity-Optomechanical Resonators', *1104.5448* (2011) (p 43).

[CG69]   K. E. Cahill and R. J. Glauber, 'Density Operators and Quasiprobability Distributions', *Physical Review* 177, 1882 (1969), DOI: `10.1103/PhysRev.177.1882` (p 67).

[Cha+10]   D. E. Chang et al., 'Cavity opto-mechanics using an optically levitated nanosphere', *Proceedings of the National Academy of Sciences* 107, 1005 (2010), DOI: `10.1073/pnas.0912969107` (p 11).

[Cha+11]   J. Chan et al., 'Laser cooling of a nanomechanical os-
            cillator into its quantum ground state', *Nature* 478, 89
            (2011), DOI: `10.1038/nature10461` (p 2).

[Che+14]   Y. Chen et al., 'Qubit Architecture with High Coherence
            and Fast Tunable Coupling', *Physical Review Letters* 113,
            220502 (2014), DOI: `10.1103/PhysRevLett.113.220502`
            (p 53).

[CHP01]   J.-M. Courty, A. Heidmann and M. Pinard, 'Quantum
            limits of cold damping with optomechanical coupling',
            *The European Physical Journal D - Atomic, Molecular, Op-
            tical and Plasma Physics* 17, 399 (2001), DOI: `10.1007/`
            `s100530170014` (pp 14, 81).

[CHP03]   J.-M. Courty, A. Heidmann and M. Pinard, 'Quantum
            Locking of Mirrors in Interferometers', *Physical Review
            Letters* 90, 083601 (2003), DOI: `10.1103/PhysRevLett.90.`
            `083601` (p 2).

[CHP99]   P. F. Cohadon, A. Heidmann and M. Pinard, 'Cooling of
            a Mirror by Radiation Pressure', *Physical Review Letters*
            83, 3174 (1999), DOI: `10.1103/PhysRevLett.83.3174`
            (pp 2, 84).

[Chu02]   S. Chu, 'Cold atoms and quantum control', *Nature* 416,
            206 (2002), DOI: `10.1038/416206a` (p 1).

[Cir+92]   J. I. Cirac et al., 'Laser cooling of trapped ions in a
            standing wave', *Physical Review A* 46, 2668 (1992), DOI:
            `10.1103/PhysRevA.46.2668` (p 28).

[Cir80]   B. S. Cirel'son, 'Quantum generalizations of Bell's in-
            equality', *Letters in Mathematical Physics* 4, 93 (1980), DOI:
            `10.1007/BF00417500` (p 64).

[CL83]   A. O. Caldeira and A. J. Leggett, 'Path integral ap-
            proach to quantum Brownian motion', *Physica A:
            Statistical Mechanics and its Applications* 121, 587 (1983),
            DOI: `10.1016/0378-4371(83)90013-4` (pp 8, 17).

[Cla+69]   J. F. Clauser et al., 'Proposed Experiment to Test Local
            Hidden-Variable Theories', *Physical Review Letters* 23,
            880 (1969), DOI: `10.1103/PhysRevLett.23.880` (p 64).

[CMJ08]   A. A. Clerk, F. Marquardt and K. Jacobs, 'Back-action
            evasion and squeezing of a mechanical resonator us-
            ing a cavity detector', *New Journal of Physics* 10, 095010
            (2008), DOI: `10.1088/1367-2630/10/9/095010` (p 2).

[Col+11]   G. D. Cole et al., 'Phonon-tunnelling dissipation in
            mechanical resonators', *Nature Communications* 2, 231
            (2011), DOI: `10.1038/ncomms1212` (p 9).

[Cor+07]   T. Corbitt et al., 'An All-Optical Trap for a Gram-Scale Mirror', *Physical Review Letters* 98, 150802 (2007), DOI: `10.1103/PhysRevLett.98.150802` (p 23).

[CS79]   S. Chaturvedi and F. Shibata, 'Time-convolutionless projection operator formalism for elimination of fast variables. Applications to Brownian motion', *Zeitschrift für Physik B Condensed Matter* 35, 297 (1979), DOI: `10.1007/BF01319852` (pp 72, 73).

[Cub+03]   T. S. Cubitt et al., 'Separable States Can Be Used To Distribute Entanglement', *Physical Review Letters* 91, 037902 (2003), DOI: `10.1103/PhysRevLett.91.037902` (p 37).

[DG14]   A. Dabrowska and J. Gough, 'Belavkin Filtering with Squeezed Light Sources', *arXiv:1405.7795 [quant-ph]* (2014) (p 87).

[DJ99]   A. C. Doherty and K. Jacobs, 'Feedback control of quantum systems using continuous state estimation', *Physical Review A* 60, 2700 (1999), DOI: `10.1103/PhysRevA.60.2700` (pp 81, 113).

[Dol+14]   F. Dolde et al., 'High-fidelity spin entanglement using optimal control', *Nature Communications* 5 (2014), DOI: `10.1038/ncomms4371` (p 2).

[Don+14]   G. Donati et al., 'Observing optical coherence across Fock layers with weak-field homodyne detectors', *Nature Communications* 5 (2014), DOI: `10.1038/ncomms6584` (p 64).

[Dor+83]   A. Dorsel et al., 'Optical Bistability and Mirror Confinement Induced by Radiation Pressure', *Physical Review Letters* 51, 1550 (1983), DOI: `10.1103/PhysRevLett.51.1550` (pp 1, 18).

[DP10]   D. Dong and I. R. Petersen, 'Quantum control theory and applications: a survey', *IET Control Theory & Applications* 4, 2651 (2010), DOI: `10.1049/iet-cta.2009.0508` (p 1).

[Dua+00]   L. M. Duan et al., 'Inseparability Criterion for Continuous Variable Systems', *Physical Review Letters* 84, 2722 (2000), DOI: `10.1103/PhysRevLett.84.2722` (pp 40, 56, 100).

[EB03]   S. Edwards and V. Belavkin, 'On the duality of quantum filtering and optimal feedback control in quantum open linear dynamical systems', in: *Physics and Control, 2003. Proceedings. 2003 International Conference*, vol. 3, 2003, 768, DOI: `10.1109/PHYCON.2003.1237001` (p 143).

[EB05]   S. C. Edwards and V. P. Belavkin, 'Optimal Quantum Filtering and Quantum Feedback Control', *arXiv:quant-ph/0506018* (2005) (pp 138, 143).

[EF07]   R. Estrada and S. A. Fulling, 'Functions and Distributions in Spaces with Thick Points', *International Journal of Applied Mathematics and Statistics*™ 10, 25 (2007) (p 35).

[EGC09]   F. Elste, S. M. Girvin and A. A. Clerk, 'Quantum Noise Interference and Backaction Cooling in Cavity Nanomechanics', *Physical Review Letters* 102, 207209 (2009), DOI: `10.1103/PhysRevLett.102.207209` (p 11).

[Eic+09]   M. Eichenfield et al., 'Optomechanical crystals', *Nature* 462, 78 (2009), DOI: `10.1038/nature08524` (p 2).

[Ein09]   A. Einstein, 'Zum gegenwärtigen Stande des Strahlungsproblems', *Physikalische Zeitschrift*, 185 (1909) (p 11).

[EPR35]   A. Einstein, B. Podolsky and N. Rosen, 'Can Quantum-Mechanical Description of Physical Reality Be Considered Complete?', *Physical Review* 47, 777 (1935), DOI: `10.1103/PhysRev.47.777` (pp 59, 63).

[Fab+94]   C. Fabre et al., 'Quantum-noise reduction using a cavity with a movable mirror', *Physical Review A* 49, 1337 (1994), DOI: `10.1103/PhysRevA.49.1337` (pp 1, 20).

[FC72]   S. J. Freedman and J. F. Clauser, 'Experimental Test of Local Hidden-Variable Theories', *Physical Review Letters* 28, 938 (1972), DOI: `10.1103/PhysRevLett.28.938` (p 63).

[Flu+15]   E. Flurin et al., 'Superconducting Quantum Node for Entanglement and Storage of Microwave Radiation', *Physical Review Letters* 114, 090503 (2015), DOI: `10.1103/PhysRevLett.114.090503` (p 66).

[Fra51]   Frank J. Massey, 'The Kolmogorov-Smirnov Test for Goodness of Fit', *Journal of the American Statistical Association* 46, 68 (1951), DOI: `10.1080/01621459.1951.10500769` (p 105).

[FSW14]   I. Favero, J. Sankey and E. M. Weig, 'Mechanical Resonators in the Middle of an Optical Cavity', in: *Cavity Optomechanics*, ed. by M. Aspelmeyer, T. J. Kippenberg and F. Marquardt, Quantum Science and Technology, Springer Berlin Heidelberg, 2014, 83 (p 9).

[Fur+98]   A. Furusawa et al., 'Unconditional Quantum Teleportation', *Science* 282, 706 (1998), DOI: `10.1126/science.282.5389.706` (p 43).

[Gal+14] C. Galland et al., 'Heralded Single-Phonon Preparation, Storage, and Readout in Cavity Optomechanics', *Physical Review Letters* 112, 143602 (2014), DOI: `10.1103/PhysRevLett.112.143602` (p 52).

[Gar+04] R. García-Patrón et al., 'Proposal for a Loophole-Free Bell Test Using Homodyne Detection', *Physical Review Letters* 93, 130409 (2004), DOI: `10.1103/PhysRevLett.93.130409` (p 69).

[Gar84] C. W. Gardiner, 'Adiabatic elimination in stochastic systems. I. Formulation of methods and application to few-variable systems', *Physical Review A* 29, 2814 (1984), DOI: `10.1103/PhysRevA.29.2814` (p 73).

[Gar93] C. W. Gardiner, 'Driving a quantum system with the output field from another driven quantum system', *Physical Review Letters* 70, 2269 (1993), DOI: `10.1103/PhysRevLett.70.2269` (pp 53, 107).

[GBS11a] R. Ghobadi, A. R. Bahrampour and C. Simon, 'Optomechanical entanglement in the presence of laser phase noise', *Physical Review A* 84, 063827 (2011), DOI: `10.1103/PhysRevA.84.063827` (p 108).

[GBS11b] R. Ghobadi, A. R. Bahrampour and C. Simon, 'Quantum optomechanics in the bistable regime', *Physical Review A* 84, 033846 (2011), DOI: `10.1103/PhysRevA.84.033846` (p 37).

[GC85] C. W. Gardiner and M. J. Collett, 'Input and output in damped quantum systems: Quantum stochastic differential equations and the master equation', *Physical Review A* 31, 3761 (1985), DOI: `10.1103/PhysRevA.31.3761` (pp 16, 121, 122).

[Gen+08a] C. Genes et al., 'Ground-state cooling of a micromechanical oscillator: Comparing cold damping and cavity-assisted cooling schemes', *Physical Review A* 77, 033804 (2008), DOI: `10.1103/PhysRevA.77.033804` (pp 14, 81).

[Gen+08b] C. Genes et al., 'Robust entanglement of a micromechanical resonator with output optical fields', *Physical Review A* 78, 032316 (2008), DOI: `10.1103/PhysRevA.78.032316` (pp 26, 29, 37).

[Ger+03] J. Geremia et al., 'Quantum Kalman Filtering and the Heisenberg Limit in Atomic Magnetometry', *Physical Review Letters* 91, 250801 (2003), DOI: `10.1103/PhysRevLett.91.250801` (p 1).

[GG94]   P. Goetsch and R. Graham, 'Linear stochastic wave
           equations for continuously measured quantum sys-
           tems', *Physical Review A* 50, 5242 (1994), DOI: 10.1103/
           PhysRevA.50.5242 (pp 129, 130).

[Gig+06]   S. Gigan et al., 'Self-cooling of a micromirror by radi-
           ation pressure', *Nature* 444, 67 (2006), DOI: 10.1038/
           nature05273 (p 2).

[GJ09]   J. Gough and M. James, 'The Series Product and Its Ap-
           plication to Quantum Feedforward and Feedback Net-
           works', *Automatic Control, IEEE Transactions on* 54, 2530
           (2009), DOI: 10.1109/TAC.2009.2031205 (pp 94, 107,
           131).

[GJM13]   S. Gammelmark, B. Julsgaard and K. Mølmer, 'Past
           Quantum States of a Monitored System', *Physical
           Review Letters* 111, 160401 (2013), DOI: 10.1103/
           PhysRevLett.111.160401 (p 1).

[GK10]   J. Gough and C. Kostler, 'Quantum Filtering in Coher-
           ent States', *Communications on Stochastic analysis* 4, 505
           (2010) (pp 133, 134).

[Gou12]   J. E. Gough, 'Principles and applications of quantum
           control engineering', *Philosophical Transactions of the
           Royal Society A: Mathematical, Physical and Engineering
           Sciences* 370, 5239 (2012), DOI: 10.1098/rsta.2012.0331
           (p 1).

[GPZ10]   F. Galve, L. A. Pachón and D. Zueco, 'Bringing En-
           tanglement to the High Temperature Limit', *Phys-
           ical Review Letters* 105, 180501 (2010), DOI: 10.1103/
           PhysRevLett.105.180501 (p 37).

[Grö+09]   S. Gröblacher et al., 'Demonstration of an ultracold
           micro-optomechanical oscillator in a cryogenic cavity',
           Nature Physics 5, 485 (2009), DOI: 10.1038/nphys1301
           (p 8).

[Grö+15]   S. Gröblacher et al., 'Observation of non-Markovian mi-
           cromechanical Brownian motion', *Nature Communica-
           tions* 6 (2015), DOI: 10.1038/ncomms8606 (p 9).

[GV01]   V. Giovannetti and D. Vitali, 'Phase-noise measurement
           in a cavity with a movable mirror undergoing quantum
           Brownian motion', *Physical Review A* 63, 023812 (2001),
           DOI: 10.1103/PhysRevA.63.023812 (pp 17, 108).

[GZ04]   C. W. Gardiner and P. Zoller, *Quantum Noise*, 3rd ed.,
           Berlin: Springer, 2004 (pp 15, 17, 24, 25, 61, 121, 125–
           127, 129, 131).

[HA09]   S. Huang and G. S. Agarwal, 'Entangling nanomech-
           anical oscillators in a ring cavity by feeding squeezed
           light', *New Journal of Physics* 11, 103044 (2009), DOI: `10.`
           `1088/1367-2630/11/10/103044` (p 37).

[Ham+05]   K. Hammerer et al., 'Quantum Benchmark for Storage
           and Transmission of Coherent States', *Physical Review
           Letters* 94, 150503 (2005), DOI: `10.1103/PhysRevLett.94.`
           `150503` (p 44).

[Har94]   L. Hardy, 'Nonlocality of a Single Photon Revisited',
           Physical Review Letters 73, 2279 (1994), DOI: `10.1103/`
           `PhysRevLett.73.2279` (p 64).

[Hei+05]   F. v. d. Heijden et al., *Classification, Parameter Estima-
           tion and State Estimation: An Engineering Approach Using
           MATLAB*, John Wiley & Sons, 2005 (pp 102, 105).

[Hel69]   C. W. Helstrom, 'Quantum detection and estimation
           theory', *Journal of Statistical Physics* 1, 231 (1969), DOI:
           `10.1007/BF01007479` (p 1).

[Hes+04]   B. Hessmo et al., 'Experimental Demonstration of
           Single Photon Nonlocality', *Physical Review Letters* 92,
           180401 (2004), DOI: `10.1103/PhysRevLett.92.180401`
           (p 64).

[Hil+84]   M. Hillery et al., 'Distribution functions in physics:
           Fundamentals', *Physics Reports* 106, 121 (1984), DOI:
           `10.1016/0370-1573(84)90160-1` (p 70).

[HM13]   R. Hamerly and H. Mabuchi, 'Coherent controllers for
           optical-feedback cooling of quantum oscillators', *Phys-
           ical Review A* 87, 013815 (2013), DOI: `10.1103/PhysRevA.`
           `87.013815` (p 81).

[Hof+11]   A. J. Hoffman et al., 'Coherent control of a supercon-
           ducting qubit with dynamically tunable qubit-cavity
           coupling', *Physical Review B* 84, 184515 (2011), DOI: `10.`
           `1103/PhysRevB.84.184515` (p 53).

[HP08]   M. J. Hartmann and M. B. Plenio, 'Steady State Entan-
           glement in the Mechanical Vibrations of Two Dielectric
           Membranes', *Physical Review Letters* 101, 200503 (2008),
           DOI: `10.1103/PhysRevLett.101.200503` (p 37).

[HP84]   R. L. Hudson and K. R. Parthasarathy, 'Quantum Ito's
           formula and stochastic evolutions', *Communications
           in Mathematical Physics* 93, 301 (1984), DOI: `10.1007/`
           `BF01258530` (p 123).

[HPC05]   K. Hammerer, E. S. Polzik and J. I. Cirac, 'Teleportation
           and spin squeezing utilizing multimode entanglement
           of light with atoms', *Physical Review A* 72, 052313 (2005),
           DOI: `10.1103/PhysRevA.72.052313` (pp 37, 42).

[HR06]   S. Haroche and J.-M. Raimond, *Exploring the Quantum: Atoms, Cavities, and Photons*, OUP Oxford, 2006 (p 1).

[II07]   I.S. Gradshteyn and I.M. Ryshik, *Table of Integrals, Series, and Products*, 7 edition, Amsterdam: Academic Press, 2007 (pp 18, 21, 72, 144, 145).

[Iwa+13]   K. Iwasawa et al., 'Quantum-Limited Mirror-Motion Estimation', *Physical Review Letters* 111, 163602 (2013), DOI: 10.1103/PhysRevLett.111.163602 (p 1).

[Jia+09]   X. Jiang et al., 'High-Q double-disk microcavities for cavity optomechanics', *Optics Express* 17, 20911 (2009), DOI: 10.1364/OE.17.020911 (p 2).

[Joh+14]   J. R. Johansson et al., 'Entangled-state generation and Bell inequality violations in nanomechanical resonators', *Physical Review B* 90, 174307 (2014), DOI: 10.1103/PhysRevB.90.174307 (p 64).

[Kal60]   R. E. Kalman, 'A New Approach to Linear Filtering and Prediction Problems', *Journal of Basic Engineering* 82, 35 (1960), DOI: 10.1115/1.3662552 (pp 102, 103).

[KB61]   R. E. Kalman and R. S. Bucy, 'New Results in Linear Filtering and Prediction Theory', *Journal of Fluids Engineering* 83, 95 (1961), DOI: 10.1115/1.3658902 (pp 102, 103, 139).

[Ker+13]   J. Kerckhoff et al., 'Tunable Coupling to a Mechanical Oscillator Circuit Using a Coherent Feedback Network', *Physical Review X* 3, 021013 (2013), DOI: 10.1103/PhysRevX.3.021013 (p 66).

[Kha+10]   F. Khalili et al., 'Preparing a Mechanical Oscillator in Non-Gaussian Quantum States', *Physical Review Letters* 105, 070403 (2010), DOI: 10.1103/PhysRevLett.105.070403 (p 52).

[Kie+13]   N. Kiesel et al., 'Cavity cooling of an optically levitated submicron particle', *Proceedings of the National Academy of Sciences* 110, 14180 (2013), DOI: 10.1073/pnas.1309167110 (p 2).

[Kip+05]   T. J. Kippenberg et al., 'Analysis of Radiation-Pressure Induced Mechanical Oscillation of an Optical Microcavity', *Physical Review Letters* 95, 033901 (2005), DOI: 10.1103/PhysRevLett.95.033901 (p 2).

[Klo94]   P. E. Kloeden, *Numerical Solution of Sde Through Computer Experiments*, Springer, 1994 (p 103).

[KMB00]   A. Kuzmich, L. Mandel and N. P. Bigelow, 'Genera-
           tion of Spin Squeezing via Continuous Quantum Non-
           demolition Measurement', *Physical Review Letters* 85,
           1594 (2000), DOI: `10.1103/PhysRevLett.85.1594` (p 1).

[KPM97]   C. Kurtsiefer, T. Pfau and J. Mlynek, 'Measurement of
           the Wigner function of an ensemble of helium atoms',
           Nature 386, 150 (1997), DOI: `10.1038/386150a0` (p 52).

[Kra+11]   H. Krauter et al., 'Entanglement Generated by Dis-
           sipation and Steady State Entanglement of Two Mac-
           roscopic Objects', *Physical Review Letters* 107, 080503
           (2011), DOI: `10.1103/PhysRevLett.107.080503` (p 1).

[KŻ04]   A. Kenfack and K. Życzkowski, 'Negativity of the
           Wigner function as an indicator of non-classicality',
           Journal of Optics B: Quantum and Semiclassical Optics 6,
           396 (2004), DOI: `10.1088/1464-4266/6/10/003` (p 52).

[Law95]   C. K. Law, 'Interaction between a moving mirror and
           radiation pressure: A Hamiltonian formulation', *Phys-
           ical Review A* 51, 2537 (1995), DOI: `10.1103/PhysRevA.51.`
           `2537` (p 12).

[LB78]   G. M. Ljung and G. E. P. Box, 'On a measure of lack of
           fit in time series models', *Biometrika* 65, 297 (1978), DOI:
           `10.1093/biomet/65.2.297` (p 105).

[LHM10]   M. Ludwig, K. Hammerer and F. Marquardt, 'Entangle-
           ment of mechanical oscillators coupled to a nonequilib-
           rium environment', *Physical Review A* 82, 012333 (2010),
           DOI: `10.1103/PhysRevA.82.012333` (p 37).

[Lin76]   G. Lindblad, 'On the generators of quantum dynamical
           semigroups', *Communications in Mathematical Physics* 48,
           119 (1976), DOI: `10.1007/BF01608499` (p 24).

[LJJ09]   S.-W. Lee, H. Jeong and D. Jaksch, 'Testing quantum
           nonlocality by generalized quasiprobability functions',
           Physical Review A 80, 022104 (2009), DOI: `10.1103/`
           `PhysRevA.80.022104` (p 64).

[Man+02]   S. Mancini et al., 'Entangling Macroscopic Oscillators
           Exploiting Radiation Pressure', *Physical Review Letters*
           88, 120401 (2002), DOI: `10.1103/PhysRevLett.88.120401`
           (p 37).

[Mar+07]   F. Marquardt et al., 'Quantum Theory of Cavity-
           Assisted Sideband Cooling of Mechanical Motion',
           Physical Review Letters 99, 093902 (2007), DOI: `10.1103/`
           `PhysRevLett.99.093902` (pp 14, 23, 24).

[MDC10]   H. Miao, S. Danilishin and Y. Chen, 'Universal quantum entanglement between an oscillator and continuous fields', *Physical Review A* 81, 052307 (2010), DOI: `10.1103/PhysRevA.81.052307` (p 37).

[ME09]   A. Mari and J. Eisert, 'Gently Modulating Optomechanical Systems', *Physical Review Letters* 103, 213603 (2009), DOI: `10.1103/PhysRevLett.103.213603` (p 37).

[Mee+96]   D. M. Meekhof et al., 'Generation of Nonclassical Motional States of a Trapped Atom', *Physical Review Letters* 76, 1796 (1996), DOI: `10.1103/PhysRevLett.76.1796` (p 52).

[Mey+85]   P. Meystre et al., 'Theory of radiation-pressure-driven interferometers', *Journal of the Optical Society of America B* 2, 1830 (1985), DOI: `10.1364/JOSAB.2.001830` (p 18).

[MG09]   F. Marquardt and S. Girvin, 'Optomechanics', *Physics* 2, 40 (2009), DOI: `10.1103/Physics.2.40` (p 11).

[Mil+15]   J. Millen et al., 'Cavity Cooling a Single Charged Levitated Nanosphere', *Physical Review Letters* 114, 123602 (2015), DOI: `10.1103/PhysRevLett.114.123602` (p 2).

[MK09]   L. Mišta and N. Korolkova, 'Improving continuous-variable entanglement distribution by separable states', *Physical Review A* 80, 032310 (2009), DOI: `10.1103/PhysRevA.80.032310` (p 37).

[MM12]   P. Marian and T. A. Marian, 'Uhlmann fidelity between two-mode Gaussian states', *Physical Review A* 86, 022340 (2012), DOI: `10.1103/PhysRevA.86.022340` (p 67).

[MMT97]   S. Mancini, V. I. Man'ko and P. Tombesi, 'Ponderomotive control of quantum macroscopic coherence', *Physical Review A* 55, 3042 (1997), DOI: `10.1103/PhysRevA.55.3042` (pp 1, 2).

[MT94]   S. Mancini and P. Tombesi, 'Quantum noise reduction by radiation pressure', *Physical Review A* 49, 4055 (1994), DOI: `10.1103/PhysRevA.49.4055` (pp 20, 21).

[Mur+08]   K. W. Murch et al., 'Observation of quantum-measurement backaction with an ultracold atomic gas', *Nature Physics* 4, 561 (2008), DOI: `10.1038/nphys965` (p 2).

[MVT98]   S. Mancini, D. Vitali and P. Tombesi, 'Optomechanical Cooling of a Macroscopic Oscillator by Homodyne Feedback', *Physical Review Letters* 80, 688 (1998), DOI: `10.1103/PhysRevLett.80.688` (pp 2, 81).

[NC04]   H. Nha and H. J. Carmichael, 'Proposed Test of Quantum Nonlocality for Continuous Variables', *Physical Review Letters* 93, 020401 (2004), DOI: `10.1103/PhysRevLett.93.020401` (p 69).

[Nee+06]   J. S. Neergaard-Nielsen et al., 'Generation of a Superposition of Odd Photon Number States for Quantum Information Networks', *Physical Review Letters* 97, 083604 (2006), DOI: `10.1103/PhysRevLett.97.083604` (p 59).

[OCo+10]   A. D. O'Connell et al., 'Quantum ground state and single-phonon control of a mechanical resonator', *Nature* 464, 697 (2010), DOI: `10.1038/nature08967` (pp 2, 3).

[Our+06]   A. Ourjoumtsev et al., 'Generating Optical Schrödinger Kittens for Quantum Information Processing', *Science* 312, 83 (2006), DOI: `10.1126/science.1122858` (p 59).

[Pai+11]   H. Paik et al., 'Observation of High Coherence in Josephson Junction Qubits Measured in a Three-Dimensional Circuit QED Architecture', *Physical Review Letters* 107, 240501 (2011), DOI: `10.1103/PhysRevLett.107.240501` (p 57).

[Pal+13]   T. A. Palomaki et al., 'Entangling Mechanical Motion with Microwave Fields', *Science* 342, 710 (2013), DOI: `10.1126/science.1244563` (pp 2, 3, 37, 40, 46, 49, 56, 62, 67).

[Par09]   M. G. A. Paris, 'Quantum estimation for quantum technology', *International Journal of Quantum Information* 07, 125 (2009), DOI: `10.1142/S0219749909004839` (p 1).

[Pat+07]   M. Paternostro et al., 'Creating and Probing Multipartite Macroscopic Entanglement with Light', *Physical Review Letters* 99, 250401 (2007), DOI: `10.1103/PhysRevLett.99.250401` (p 37).

[Pec+14]   M. Pechal et al., 'Microwave-Controlled Generation of Shaped Single Photons in Circuit Quantum Electrodynamics', *Physical Review X* 4, 041010 (2014), DOI: `10.1103/PhysRevX.4.041010` (p 66).

[PHH99]   M. Pinard, Y. Hadjar and A. Heidmann, 'Effective mass in quantum effects of radiation pressure', *The European Physical Journal D - Atomic, Molecular, Optical and Plasma Physics* 7, 107 (1999), DOI: `10.1007/s100530050354` (p 7).

[Pie+14]   M. Pierre et al., 'Storage and on-demand release of microwaves using superconducting resonators with tunable coupling', *Applied Physics Letters* 104, 232604 (2014), DOI: `10.1063/1.4882646` (p 66).

[Pin+05]   M. Pinard et al., 'Entangling movable mirrors in a double-cavity system', *Europhysics Letters* 72, 747 (2005), DOI: `10.1209/epl/i2005-10317-6` (p 37).

[Pir+06]   S. Pirandola et al., 'Macroscopic Entanglement by Entanglement Swapping', *Physical Review Letters* 97, 150403 (2006), DOI: `10.1103/PhysRevLett.97.150403` (p 37).

[Ple05]   M. B. Plenio, 'Logarithmic Negativity: A Full Entanglement Monotone That is not Convex', *Physical Review Letters* 95, 090503 (2005), DOI: `10.1103/PhysRevLett.95.090503` (p 28).

[Pog+07]   M. Poggio et al., 'Feedback Cooling of a Cantilever's Fundamental Mode below 5 mK', *Physical Review Letters* 99, 017201 (2007), DOI: `10.1103/PhysRevLett.99.017201` (p 82).

[PPR13]   T. P. Purdy, R. W. Peterson and C. A. Regal, 'Observation of Radiation Pressure Shot Noise on a Macroscopic Object', *Science* 339, 801 (2013), DOI: `10.1126/science.1231282` (p 2).

[Pur+13]   T. P. Purdy et al., 'Strong Optomechanical Squeezing of Light', *Physical Review X* 3, 031012 (2013), DOI: `10.1103/PhysRevX.3.031012` (pp 2, 14).

[Rab+09]   P. Rabl et al., 'Phase-noise induced limitations on cooling and coherent evolution in optomechanical systems', *Physical Review A* 80, 063819 (2009), DOI: `10.1103/PhysRevA.80.063819` (p 108).

[Rie+04]   M. Riebe et al., 'Deterministic quantum teleportation with atoms', *Nature* 429, 734 (2004), DOI: `10.1038/nature02570` (p 86).

[Ris+12a]   D. Ristè et al., 'Feedback Control of a Solid-State Qubit Using High-Fidelity Projective Measurement', *Physical Review Letters* 109, 240502 (2012), DOI: `10.1103/PhysRevLett.109.240502` (p 54).

[Ris+12b]   D. Ristè et al., 'Initialization by Measurement of a Superconducting Quantum Bit Circuit', *Physical Review Letters* 109, 050507 (2012), DOI: `10.1103/PhysRevLett.109.050507` (p 54).

[RL11]   C. A. Regal and K. W. Lehnert, 'From cavity electromechanics to cavity optomechanics', *Journal of Physics: Conference Series* 264, 012025 (2011), DOI: `10.1088/1742-6596/264/1/012025` (p 2).

[Rom+10]   O. Romero-Isart et al., 'Toward quantum superposition of living organisms', *New Journal of Physics* 12, 033015 (2010), DOI: `10.1088/1367-2630/12/3/033015` (p 11).

[Rom+11] O. Romero-Isart et al., 'Optically levitating dielectrics in the quantum regime: Theory and protocols', *Physical Review A* 83, 013803 (2011), DOI: `10.1103/PhysRevA.83.013803` (pp 37, 42).

[Row+01] M. A. Rowe et al., 'Experimental violation of a Bell's inequality with efficient detection', *Nature* 409, 791 (2001), DOI: `10.1038/35057215` (p 63).

[Saf+13] A. H. Safavi-Naeini et al., 'Squeezed light from a silicon micromechanical resonator', *Nature* 500, 185 (2013), DOI: `10.1038/nature12307` (pp 2, 14).

[Sau90] P. R. Saulson, 'Thermal noise in mechanical experiments', *Physical Review D* 42, 2437 (1990), DOI: `10.1103/PhysRevD.42.2437` (p 9).

[Saw+15] A. Sawadsky et al., 'Observation of Generalized Optomechanical Coupling and Cooling on Cavity Resonance', *Physical Review Letters* 114, 043601 (2015), DOI: `10.1103/PhysRevLett.114.043601` (p 11).

[Sch+06] A. Schliesser et al., 'Radiation Pressure Cooling of a Micromechanical Oscillator Using Dynamical Backaction', *Physical Review Letters* 97, 243905 (2006), DOI: `10.1103/PhysRevLett.97.243905` (p 2).

[Sch+11] M. H. Schleier-Smith et al., 'Optomechanical Cavity Cooling of an Atomic Ensemble', *Physical Review Letters* 107, 143005 (2011), DOI: `10.1103/PhysRevLett.107.143005` (p 2).

[She+06] J. F. Sherson et al., 'Quantum teleportation between light and matter', *Nature* 443, 557 (2006), DOI: `10.1038/nature05136` (pp 42, 86).

[Shi10] R. Shiavi, *Introduction to Applied Statistical Signal Analysis: Guide to Biomedical and Electrical Engineering Applications*, Academic Press, 2010 (pp 105, 106).

[Sim00] R. Simon, 'Peres-Horodecki Separability Criterion for Continuous Variable Systems', *Physical Review Letters* 84, 2726 (2000), DOI: `10.1103/PhysRevLett.84.2726` (pp 40, 56, 100).

[Sim06] D. Simon, *Optimal State Estimation: Kalman, H Infinity, and Nonlinear Approaches*, John Wiley & Sons, 2006 (pp 104, 105).

[Sri+14] S. J. Srinivasan et al., 'Time-reversal symmetrization of spontaneous emission for quantum state transfer', *Physical Review A* 89, 033857 (2014), DOI: `10.1103/PhysRevA.89.033857` (p 66).

[Ste94]   R. F. Stengel, *Optimal Control and Estimation*, Reissue edition, New York: Dover Publications, 1994 (pp 102, 104, 106).

[Stro8]   S. H. Strogatz, *Nonlinear Dynamics And Chaos*, Westview Press, 2008 (p 18).

[Szo+12]   A. Szorkovszky et al., 'Position estimation of a parametrically driven optomechanical system', *New Journal of Physics* 14, 095026 (2012), DOI: `10.1088/1367-2630/14/9/095026` (p 1).

[Tab89]   M. Tabor, *Chaos and integrability in nonlinear dynamics: an introduction*, Wiley, 1989 (p 18).

[Teu+11]   J. D. Teufel et al., 'Sideband cooling of micromechanical motion to the quantum ground state', *Nature* 475, 359 (2011), DOI: `10.1038/nature10261` (p 2).

[Tho+08]   J. D. Thompson et al., 'Strong dispersive coupling of a high-finesse cavity to a micromechanical membrane', *Nature* 452, 72 (2008), DOI: `10.1038/nature06715` (pp 2, 11).

[Tho+78]   K. S. Thorne et al., 'Quantum Nondemolition Measurements of Harmonic Oscillators', *Physical Review Letters* 40, 667 (1978), DOI: `10.1103/PhysRevLett.40.667` (p 14).

[Tsa09]   M. Tsang, 'Time-Symmetric Quantum Theory of Smoothing', *Physical Review Letters* 102, ' (2009), DOI: `10.1103/PhysRevLett.102.250403` (p 1).

[TWC11]   M. Tsang, H. M. Wiseman and C. M. Caves, 'Fundamental Quantum Limit to Waveform Estimation', *Physical Review Letters* 106, 090401 (2011), DOI: `10.1103/PhysRevLett.106.090401` (p 1).

[TWC91]   S. M. Tan, D. F. Walls and M. J. Collett, 'Nonlocality of a single photon', *Physical Review Letters* 66, 252 (1991), DOI: `10.1103/PhysRevLett.66.252` (p 64).

[Vac+08]   G. Vacanti et al., 'Optomechanical to mechanical entanglement transformation', *New Journal of Physics* 10, 095014 (2008), DOI: `10.1088/1367-2630/10/9/095014` (p 37).

[Vac00]   B. Vacchini, 'Completely Positive Quantum Dissipation', *Physical Review Letters* 84, 1374 (2000), DOI: `10.1103/PhysRevLett.84.1374` (p 17).

[Vai94]   L. Vaidman, 'Teleportation of quantum states', *Physical Review A* 49, 1473 (1994), DOI: `10.1103/PhysRevA.49.1473` (p 42).

[VAK13]   M. R. Vanner, M. Aspelmeyer and M. S. Kim, 'Quantum State Orthogonalization and a Toolset for Quantum Optomechanical Phonon Control', *Physical Review Letters* 110, 010504 (2013), DOI: `10.1103/PhysRevLett.110.010504` (p 52).

[Van+11]   M. R. Vanner et al., 'Pulsed quantum optomechanics', *Proceedings of the National Academy of Sciences* 108, 16182 (2011), DOI: `10.1073/pnas.1105098108` (pp 38, 43).

[Van+13]   M. R. Vanner et al., 'Cooling-by-measurement and mechanical state tomography via pulsed optomechanics', *Nature Communications* 4 (2013), DOI: `10.1038/ncomms3295` (p 110).

[Van78]   C. Van Loan, 'Computing integrals involving the matrix exponential', *IEEE Transactions on Automatic Control* 23, 395 (1978), DOI: `10.1109/TAC.1978.1101743` (p 105).

[Vit+02]   D. Vitali et al., 'Mirror quiescence and high-sensitivity position measurements with feedback', *Physical Review A* 65, 063803 (2002), DOI: `10.1103/PhysRevA.65.063803` (pp 14, 81).

[Vit+07a]   D. Vitali et al., 'Entangling a nanomechanical resonator and a superconducting microwave cavity', *Physical Review A* 76, 042336 (2007), DOI: `10.1103/PhysRevA.76.042336` (p 37).

[Vit+07b]   D. Vitali et al., 'Optomechanical Entanglement between a Movable Mirror and a Cavity Field', *Physical Review Letters* 98, 030405 (2007), DOI: `10.1103/PhysRevLett.98.030405` (p 37).

[VMH13]   D. V. Vasilyev, C. A. Muschik and K. Hammerer, 'Dissipative versus conditional generation of Gaussian entanglement and spin squeezing', *Physical Review A* 87, 053820 (2013), DOI: `10.1103/PhysRevA.87.053820` (p 92).

[VMT07]   D. Vitali, S. Mancini and P. Tombesi, 'Stationary entanglement between two movable mirrors in a classically driven Fabry–Perot cavity', *Journal of Physics A: Mathematical and Theoretical* 40, 8055 (2007), DOI: `10.1088/1751-8113/40/28/S14` (p 37).

[VW02]   G. Vidal and R. F. Werner, 'Computable measure of entanglement', *Physical Review A* 65, 032314 (2002), DOI: `10.1103/PhysRevA.65.032314` (p 28).

[VW06]   W. Vogel and D.-G. Welsch, *Quantum Optics*, John Wiley & Sons, 2006 (p 9).

[Wal+04]   A. Wallraff et al., 'Strong coupling of a single photon to a superconducting qubit using circuit quantum electrodynamics', *Nature* 431, 162 (2004), DOI: `10.1038/nature02851` (p 53).

[WC13]   M. J. Woolley and A. A. Clerk, 'Two-mode back-action-evading measurements in cavity optomechanics', *Physical Review A* 87, 063846 (2013), DOI: `10.1103/PhysRevA.87.063846` (p 2).

[Wei+98]   G. Weihs et al., 'Violation of Bell's Inequality under Strict Einstein Locality Conditions', *Physical Review Letters* 81, 5039 (1998), DOI: `10.1103/PhysRevLett.81.5039` (p 63).

[Wie+15]   W. Wieczorek et al., 'Optimal State Estimation for Cavity Optomechanical Systems', *Physical Review Letters* 114, 223601 (2015), DOI: `10.1103/PhysRevLett.114.223601` (p 107).

[Wil+07]   I. Wilson-Rae et al., 'Theory of Ground State Cooling of a Mechanical Oscillator Using Dynamical Backaction', *Physical Review Letters* 99, 093901 (2007), DOI: `10.1103/PhysRevLett.99.093901` (pp 14, 23, 24).

[Wil+08]   I. Wilson-Rae et al., 'Cavity-assisted backaction cooling of mechanical resonators', *New Journal of Physics* 10, 095007 (2008), DOI: `10.1088/1367-2630/10/9/095007` (p 76).

[Wil+14]   D. J. Wilson et al., 'Measurement and control of a mechanical oscillator at its thermal decoherence rate', *arXiv:1410.6191 [quant-ph]* (2014) (pp 3, 84, 112).

[Win13]   D. J. Wineland, 'Nobel Lecture: Superposition, entanglement, and raising Schrödinger's cat', *Reviews of Modern Physics* 85, 1103 (2013), DOI: `10.1103/RevModPhys.85.1103` (p 1).

[Wis94]   H. M. Wiseman, 'Quantum theory of continuous feedback', *Physical Review A* 49, 2133 (1994), DOI: `10.1103/PhysRevA.49.2133` (pp 89, 90, 136).

[Wis95]   H. M. Wiseman, 'Using feedback to eliminate backaction in quantum measurements', *Physical Review A* 51, 2459 (1995), DOI: `10.1103/PhysRevA.51.2459` (p 2).

[WM08]   D. Walls and G. J. Milburn, *Quantum optics*, Berlin: Springer, 2008 (p 10).

[WM09]   H. M. Wiseman and G. J. Milburn, *Quantum Measurement and Control*, Cambridge: Cambridge University Press, 2009 (pp 3, 25, 27, 82, 84, 88, 98, 130–132, 137, 139, 143).

[WM93]   H. M. Wiseman and G. J. Milburn, 'Quantum theory of optical feedback via homodyne detection', *Physical Review Letters* 70, 548 (1993), DOI: `10.1103/PhysRevLett.70.548` (p 90).

[Woo+08] M. J. Woolley et al., 'Nanomechanical squeezing with detection via a microwave cavity', *Physical Review A* 78, 062303 (2008), DOI: `10.1103/PhysRevA.78.062303` (p 2).

[WV96]   S. Wallentowitz and W. Vogel, 'Unbalanced homodyning for quantum state measurements', *Physical Review A* 53, 4528 (1996), DOI: `10.1103/PhysRevA.53.4528` (p 64).

[Xio08]   J. Xiong, *An Introduction to Stochastic Filtering Theory*, OUP Oxford, 2008 (pp 102, 130, 140).

[XSH11]   A. Xuereb, R. Schnabel and K. Hammerer, 'Dissipative Optomechanics in a Michelson-Sagnac Interferometer', *Physical Review Letters* 107, 213604 (2011), DOI: `10.1103/PhysRevLett.107.213604` (p 11).

[Yin+13] Y. Yin et al., 'Catch and Release of Microwave Photon States', *Physical Review Letters* 110, 107001 (2013), DOI: `10.1103/PhysRevLett.110.107001` (p 66).

[Yur87]   B. Yurke, 'Squeezed-state generation using a Josephson parametric amplifier', *Journal of the Optical Society of America B* 4, 1551 (1987), DOI: `10.1364/JOSAB.4.001551` (p 52).

[ZG97]   P. Zoller and C. W. Gardiner, 'Quantum Noise in Quantum Optics: the Stochastic Schrödinger Equation', in: *Quantum Fluctuations, Volume 63*, ed. by S. Reynaud, E. Giacobino and F. David, 1st ed., Amsterdam: North Holland, 1997 (p 121).

[ZPB03]   J. Zhang, K. Peng and S. L. Braunstein, 'Quantum-state transfer from light to macroscopic oscillators', *Physical Review A* 68, 013808 (2003), DOI: `10.1103/PhysRevA.68.013808` (p 37).

Curriculum Vitæ

Sebastian Hofer

Personal Details

Date/Place of Birth: 22 January 1984, Rum, Austria
Citizenship: Austrian

Education

since 2009	**Doctoral Studies** Faculty of Physics, University of Vienna Supervised by Prof. Markus Aspelmeyer and Prof. Klemens Hammerer (University of Hannover)
since 2010	**CoQuS Doctoral Program** Vienna Doctoral Program on Complex Quantum Systems Austrian Science Fund (FWF)
2008–2009	**Diploma Thesis** Institute for Theoretical Physics, University of Innsbruck Supervised by Prof. Peter Zoller and Dr. Klemens Hammerer Title: *Creation and Verification of Optomechanical Correlations* received Mag. rer. nat. August 2009
2003	**Civillian Service** Österreichischer Alpenverein
2002–2009	**Graduate Studies of Physics** University of Innsbruck
1994–2002	**Secondary School** Bundesrealgymnasium Adolf-Pichler-Platz, Innsbruck Matura with honors July 2002 Participation in Physics Olympiad 1999–2002

Publications

2015	**Violation of Bell's Inequality in Electromechanics** Sebastian G. Hofer, Konrad W. Lehnert, and Klemens Hammerer *arXiv:1506.08097 [quant-ph]* (2015)
2015	**Optimal state estimation for cavity optomechanical systems** Witlef Wieczorek, Sebastian G. Hofer, Jason Hölscher-Obermaier, Ralf Riedinger, Klemens Hammerer, and Markus Aspelmeyer *Physical Review Letters* 114, 223601 (2015)

2014   Entanglement-enhanced time-continuous quantum control in optomechanics
Sebastian G. Hofer, and Klemens Hammerer
Physical Review A 91, 033822 (2014)

2013   Time-continuous Bell measurements
Sebastian G. Hofer, Denis V. Vasilyev, Markus Aspelmeyer, and Klemens Hammerer
Physical Review Letters 111, 170404 (2013)

2011   Optomechanical entanglement and teleportation in the pulsed regime
Sebastian G. Hofer, Witlef Wieczorek, Markus Aspelmeyer, and Klemens Hammerer
Physical Review A 84, 052327 (2011)

schools and conferences

March 2015   Photons Beyond Qubits
Olomouc, Czech Republic
Invited Talk: *Quantum Control in Cavity Optomechanics: Theory and Experiment*

March 2015   Spring Meeting of the German Physical Society
Heidelberg, Germany
Talk: *Entanglement-enhanced quantum control in cavity optomechanics*

July 2014   Workshop on Quantum Science: Implementations
Benasque, Spain

March 2014   Gordon Research Conference: Mechanical systems in the quantum regime
Ventura CA, United States of America
Poster: *Time-continuous Bell measurements*

March 2014   APS March Meeting 2014
Denver CO, United States of America
Talk: *Time-continuous Bell measurements*

January 2014   Winter School on Quantum Physics and Quantum Information
Olomouc, Czech Republic
Invited Lecture: *Continuous Wave Quantum Optomechanics*

March 2013   Spring Meeting of the German Physical Society
Hannover, Germany
Talk: *Time-continuous Bell measurements*

May 2012   Singapore School of Physics
Singapore
Poster: *Optimal optomechanical feedback cooling*

February 2012	**Quantumoptics Conference Obergurgl** Obergurgl, Austria Poster: *Optomechanical entanglement and teleportation in the pulsed regime*

| September 2011 | **Conference on Quantum Information Processing and Communication (QIPC)**
 Zürich, Switzerland
 Poster: *Optomechanical entanglement and teleportation in the pulsed regime* |

| March 2011 | **Spring Meeting of the German Physical Society**
 Dresden, Germany
 Talk: *Optomechanical entanglement and teleportation in the pulsed regime* |

| August 2010 | **Summer School on Quantum and Non-Linear Optics**
 Sonderborg, Denmark
 Poster: *Optomechanical entanglement and teleportation in the pulsed regime* |

| March 2010 | **Spring Meeting of the German Physical Society**
 Hannover, Germany
 Talk: *Optomechanics beyond the RWA: Towards optomechanical entanglement* |

| February 2010 | **Quantumoptics Conference Obergurgl**
 Obergurgl, Austria
 Poster: *Optomechanics beyond the RWA: Towards optomechanical entanglement* |

| September 2008 | **Summer School on Cold Atoms and Optical Lattices**
 Oxford, United Kingdom |

TEACHING EXPERIENCE

2008	**Tutorial** for "Einführung in die Theoretische Physik" (Classical Mechanics), University of Innsbruck

| 2007 | **Tutorial** for "Theoretische Physik 3" (Statistical Mechanics), University of Innsbruck |

| 2006 | **Tutorial** for "Theoretische Physik 2" (Quantum Mechanics), University of Innsbruck |

INTERNSHIPS AND RESEARCH VISITS

March 2014	**Research Visit** Group of Prof. Konrad W. Lehnert JILA, University of Colorado Boulder

November 2013	**Research Visit** Group of Prof. Gerard Milburn Centre for Engineered Quantum Systems, The University of Queensland
Summer 2007	**Internship** Quantum Optics Group of Prof. Tilmann Esslinger Institute for Quantumelectrodynamics, ETH Zürich
Summer 2003	**Internship** Ultracold Atoms and Quantum Gases Group of Prof. Rudolf Grimm Institute for Experimental Physics, University of Innsbruck

computer skills

Scientific Software: Mathematica, Matlab, LaTeX
Programming Languages: C, Python, PHP
Operating Systems: MacOS, Linux, Windows

language skills

German (native)
English (fluently written and spoken)
French (basic skills)